Zeitschrift: IABSE reports = Rapports AIPC = IVBH Berichte
Band: 62 (1991)

Rubrik: Sub-Theme 2.5: Reliance upon concrete tensile strength

Reliance upon Concrete Tensile Strength

Prise en compte de la résistance à la traction du béton

Inanspruchnahme der Betonzugfestigkeit

Arne HILLERBORG
Prof. Emeritus
Lund Inst. of Technology
Lund, Sweden

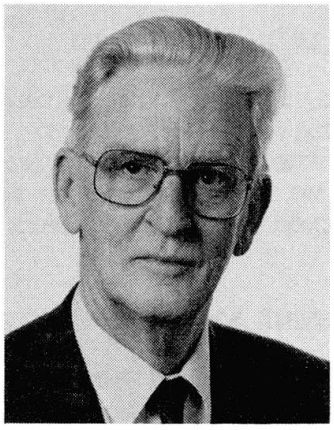

Arne Hillerborg, born in 1923, earned his Ph.D. in Stockholm in 1951. He was appointed Associate Professor of Structural Mechanics in 1968 and Professor of Building Materials in 1973.

SUMMARY

In designing concrete structures we rely on concrete tensile strength, although this is not clearly stated in the design rules. Examples of this are given. The tensile fracture process is described, the importance of toughness is demonstrated and the definition of toughness is discussed. Examples of analytical results are given. These show that there is a size dependency, in that the formal strength of a structure decreases as the size increases. Further analyses may lead to better design rules, resulting in a more constant safety factor.

RÉSUMÉ

Dans le cadre du dimensionnement des structures en béton, on tient compte de sa résistance à la traction bien que ceci ne soit pas clairement établi dans les règlementations le concernant. A titre d'illustration, des exemples sont présentés. Le processus de rupture en traction est décrit; on démontre l'importance de la ténacité du béton dont on discute la définition. Des résultats analytiques sont présentés: ils montrent que la taille de la structure est importante, car sa résistance formelle diminue lorsque ses dimensions augmentent. Des analyses futures peuvent mener à de meilleures règlementations aboutissant à un facteur de sécurité plus uniforme.

ZUSAMMENFASSUNG

Bei der Bemessung von Stahlbetontragwerken verlassen wir uns auf die Betonzugfestigkeit, obwohl dies aus den Bemessungsregeln nicht deutlich hervorgeht. Hierfür werden Beispiele gegeben. Es wird das Tragverhalten beim Zugbruch beschrieben, die Bedeutung der Zähigkeit demonstriert und ihre Definition diskutiert. Die Berechnungen einiger Beispiele zeigen, dass es einen Massstabseinfluss gibt, indem die Tragfähigkeit eines Tragwerks mit zunehmender Grösse abnimmt. Weitere Analysen können zu verbesserten Bemessungsregeln führen, die ein ausgeglicheneres Sicherheitsniveau ergeben.

1. CASES WHERE WE RELY ON CONCRETE TENSILE STRENGTH

When we teach the design of concrete structures, we often state that one basic assumption is that concrete does not carry tensile stresses, but that all tensile stresses have to be absorbed by reinforcement. As a matter of fact, this only applies to the design of tensile reinforcement.

The following are examples of cases where we rely on concrete tensile strength:

1.1 Bond and anchorage of reinforcing bars

Anchorage of deformed bars is to a large extent due to compressive forces between the lugs and the surrounding concrete. These forces act in a skew direction with respect to the bar and thus cause splitting tensile stresses in the concrete; see Fig. 1. We have to rely on the tensile strength of concrete for the anchorage of deformed reinforcing bars, and maybe also for plain bars.

1.2 Shear and punching without shear reinforcement

Shear stresses cause tensile stresses. When these stresses exceed the tensile strength, skew cracks appear. We rely on the tensile strength for preventing the formation of these skew cracks, or for preventing their growth from causing shear failure. In the latter case, the toughness associated with tensile fracture is important. The importance of toughness will be discussed later.

1.3 Splitting caused by dowel action

In connection with the formation of shear cracks, a rotation of the two parts of the beam or slab in relation to each other takes place around the compression zone above the crack; Fig. 2. This results in a vertical relative movement at the level of the tensile reinforcement. This movement is counteracted by dowel forces between reinforcement and concrete, which give rise to large local splitting stresses, tending to spall off the concrete cover. This type of failure may be of particular importance for punching failure. In this case the toughness is very important, as it may help in distributing the high local stresses over a larger area.

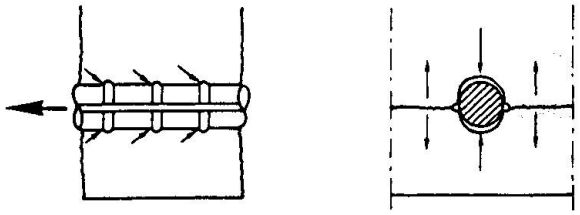

Fig.1 Splitting forces from reinforcement and possible tensile cracks

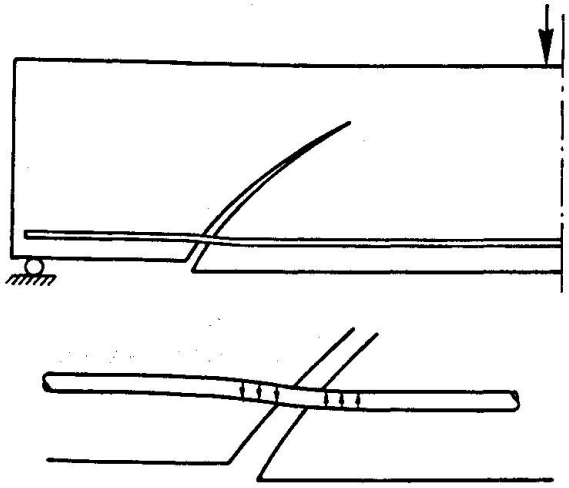

Fig.2 Dowel action causing risk of spalling of concrete cover.

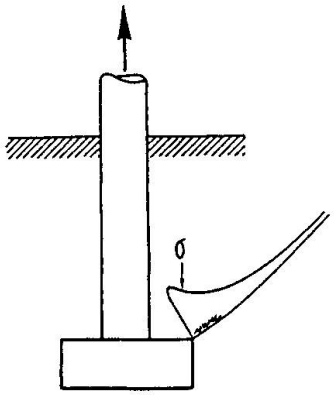

Fig.3 Stress concentration and possible formation of a crack where a bolt is anchored in concrete

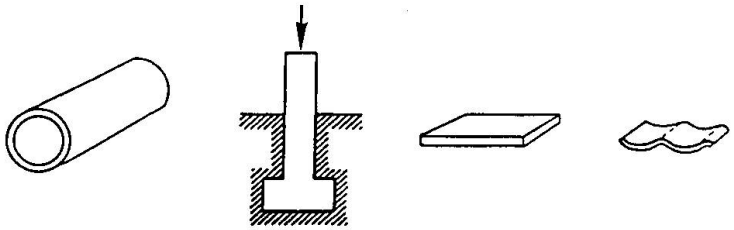

Fig.4 Examples of the use of unreinforced concrete

1.4 Anchorage of bolts

When a bolt is anchored in concrete, e.g. as in Fig. 3, a tensile force in the bolt causes tensile stresses in the surrounding concrete. It is not possible to anchor a bolt in concrete unless we rely on tensile strength.

1.5 Unreinforced concrete pipes, footings etc

Where unreinforced concrete is used in structures exposed to bending, it is quite obvious that we rely on tensile strength. Examples of such structures are concrete pipes of a moderate diameter, footings, prefabricated pavement slabs and concrete tiles; Fig. 4.

2. BRITTLENESS AND TOUGHNESS

Severe tensile stress concentrations may occur at, for example, the tip of shear cracks, near the crack surface in dowel action (Fig. 2), and near the bolt head at the anchorage of bolts (Fig. 3).

There are also stress concentrations in concrete due to internal cracking, which is always present. These cracks may e.g. be due to chemical shrinkage during the cement hydration. These cracks are small, but they nevertheless give rise to high theoretical stress concentrations at the crack tips.

Whenever the stress at a point exceeds the tensile strength, there is a risk that a crack may form, which has a tendency to propagate, as cracks in their turn give rise to stress concentrations. If the crack propagation is not prevented, it will lead to failure of the structure. As high stress concentrations are often present, it is of primary importance that mechanisms which prevent crack propagation exist.

There are two main mechanisms for the prevention of crack propagation. One is the possibility that the crack may propagate into a region where the tensile stress concentration at the tip disappears. The other is that the toughness of the material is great enough to absorb the released energy.

A bending crack in a reinforced beam is a typical point where an unstable crack may form and propagate as soon as the tensile strength is exceeded, but where it will be arrested and stay stable after the crack tip has reached the compression zone. This corresponds to the normal assumption for the design of a bent beam. In this case we may disregard the toughness of concrete in tension, even though it may have some influence on the beam stiffness and on the ultimate moment.

In many other cases, the formation of a crack and its propagation are only prevented by the toughness of concrete. If concrete were a perfectly brittle material, the stress concentrations would often lead to sudden brittle failures already at low external loads. Such concrete could hardly be used as a structural material. Toughness is therefore a very essential material property. For many structures it may be of the same importance as the strength.

In order to be able to take the toughness into account, it must be possible to quantify this property. This can be done by means of a suitable material model describing the tensile fracture behaviour.

3. TENSILE FRACTURE BEHAVIOUR

The tensile fracture behaviour can be described by means of a hypothetical tensile test on a plain bar of a constant cross section; Fig. 5. The test is made in deformation control, so that the total length of the specimen is slowly increased.

At first the stress increases as the deformation increases. At that stage the strains are the same all along the bar, provided that the material is homogeneous. Microcracks develop and grow, but in a stable way.

When the stress reaches the tensile strength, it cannot be increased any further. Instead, fracture phenomena start to develop at some section along the bar. A fracture zone starts to develop.

What happens at the fracture zone is that microcracks grow faster than at other points in the bar, and the microcracks also coalesce. These cracks would be unstable under constant stress conditions, but they may grow in a stable way in deformation control. As the cracks grow, the stress that can be transferred through this section decreases. The stress in the bar decreases as the deformation increases. The stress decrease outside the fracture zone corresponds to an unloading, with a corresponding strain decrease according to an unloading curve.

The fracture zone starts developing when the peak of the stress-deformation curve is passed. The part of the curve before the peak is reached is often called the pre-peak region or the ascending branch, whereas the part after the peak has been passed is called the post-peak region or the descending branch.

The pre-peak region can be described by a stress-strain curve, as the strain is equal all along the bar. This is not possible in the post-peak region, as we now have increasing deformations within the fracture zone, but decreasing deformations outside this zone. As there are two different types of behaviour, we need two different relations to describe the stress-deformation properties. This statement has general validity. Thus it is not possible to find a unique stress-strain curve which is also valid for the descending branch, either for tension or for compression.

The total deformation ΔL on a gauge length L in the post-peak part can be

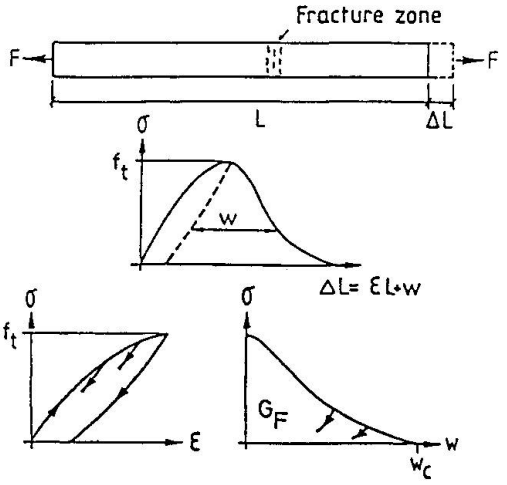

Fig.5 A tensile test and the description of the total elongation by means of two relations

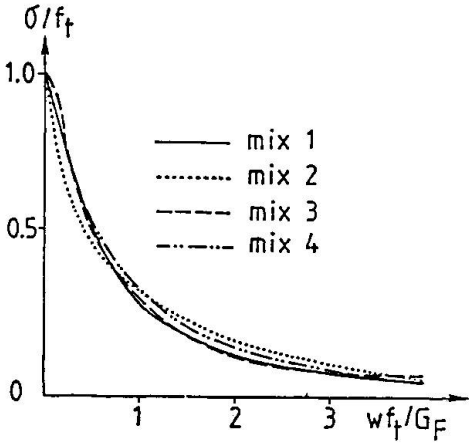

Fig.6 The shape of the σ-w-curve in a dimensionless form according to Petersson [6]

described by means of the following formula, referring to the two curves in Fig. 5

$$\Delta L = \epsilon L + w \qquad (1)$$

For the descending branch of the total curve the value of ϵ should be taken from the unloading branch, starting from the peak in the σ-ϵ-diagram. The value w is the additional deformation within the fracture zone. It should be observed that w is a displacement, not a strain.

Equation (1) may be used as a general material description for stress-deformation properties in tension, and not only for the bar in Fig. 5. In the general case, the value of ϵ should be taken as the relevant value, which may be on the ascending branch or on an unloading curve starting from any point on the ascending branch. The value of w is zero if the peak has not been passed; otherwise it is taken from the σ-w-diagram, in some cases from an unloading branch in this diagram.

Concrete in a structure is exposed to a more complicated stress and strain situation than the bar in Fig. 5. There may be stresses and strains in directions perpendicular to the main tensile stress direction. If these are large compared to the strength at the moment when the peak is reached, they may influence the peak value and the shapes of the curves. Thus Eq. (1) can only be assumed to be a good approximation of the stress-deformation properties in tension if the stresses - tensile or compressive - in lateral directions are much lower than the correponding strengths.

One important property in this connection is the way in which the non-elastic deformations take place in the material. The non-elastic deformations in concrete are due to the opening of micro-cracks before the peak and of larger cracks after the peak. This type of deformation does not cause any major lateral stresses or strains. This is an important reason for assuming that Eq. (1) can be used as a general description for concrete. For metals, large non-elastic deformations are due to yielding, which causes high lateral deformations and stresses. Thus Eq. (1) with the corresponding diagrams in Fig. 5 may not be assumed to give a valid general description of the stress-deformation properties in tension for metals.

The toughness is due to the non-linear deformations. For concrete in tension, the non-linearity of the pre-peak curve is rather insignificant and does not contribute substantially to the toughness. The non-linear deformations and the toughness are mainly due to the post-peak part of the curve, which, in its turn, mainly depends on the σ-w-curve. As a reasonable simplification, the toughness of concrete in tension may be assumed to depend only on the properties of the σ-w-curve.

One important property of the σ-w-curve is the area below the curve. This area is denoted by G_F and it is defined as

$$G_F = \int_0^{w_c} \sigma dw \qquad (2)$$

From this formula it can be seen that G_F represents the amount of energy absorbed in one unit area of the fracture zone during the complete fracture process. G_F is thus the fracture energy per unit area. It is, as a rule, simply called fracture energy.

The properties of the σ-w-curve may be divided into three parts:

f_t

G_F

the shape, expressed in a dimensionless form

According to Petersson [6], Fig. 6 shows the shapes of the σ-w-curves for three different concrete mixes expressed in a dimensionless form. Petersson drew the conclusion that this shape is approximately the same for different concrete mixes. Later many σ-w-curves have been measured by different laboratories, and the results do not seem to contradict Petersson's conclusion. Thus as a reasonable approximation it will here be assumed that the shape is constant. This simplifies the analyses very much, as - in comparing different concrete qualities - the properties of the σ-w-curve are defined by only two values, f_t and G_F. The tensile strength f_t is a conventional property, and it may be assumed to be known. The only non-conventional value that has to be determined is G_F.

Of course it has to be remembered that the assumption that the shape of the σ-w-curve is constant is an approximation, which may be too rough for some types of concrete. It cannot, for example, be used for fibre-reinforced concrete. It is also possible that in some cases the slope of the first part of the curve is more important than the value of G_F. In the discussion below it is, however, assumed that the shape is constant.

The toughness of the material may be characterized by a ratio between non-elastic and elastic deformations. G_F/f_t may be taken as a value for the non-elastic deformation; see Fig. 6. As a value for the elastic deformation, the strain at the tensile strength, f_t/E, where E is the modulus of elasticity, may be taken. The ratio between G_F/f_t and f_t/E is a length which is called the characteristic length l_{ch}

$$l_{ch} = EG_F/f_t^2 \qquad (3)$$

For ordinary concrete the value of l_{ch} is of the order 0.1-1.0 m, with an average value around 0.4 m.

The best way of measuring G_F has been much discussed. Since it is difficult to perform a stable tensile test in principle according to Fig. 5, this is not a

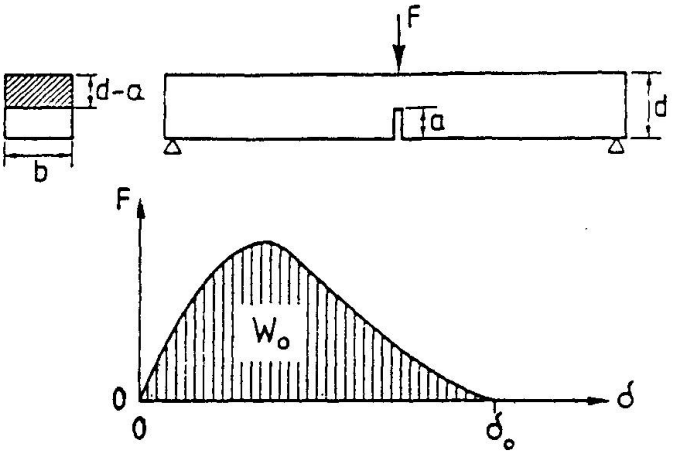

Fig.7 A stable bending test on a notched beam with registration of the load-deflection relation for the determination of G_F according to RILEM [7]

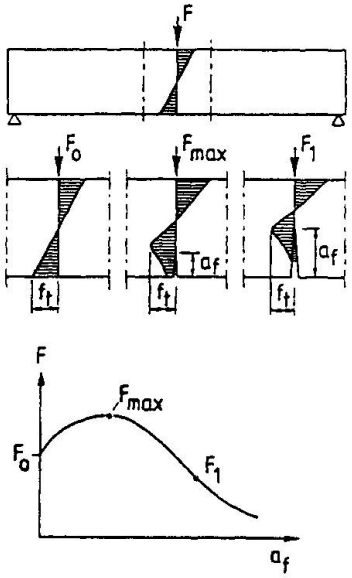

Fig.8 The principles of a numerical analysis of the formation and growth of a fracture zone

suitable standard test. A much simpler test is a stable bending test on a notched beam; Fig. 7. This type of test has therefore been proposed as a RILEM Recommendation [7]. It is assumed that all the energy released during the test is absorbed as fracture energy in the zone above the notch. The problems associated with the measurement of G_F will not be further discussed here.

The fracture energy G_F is a material property which has no direct connection with other properties, such as the compressive strength. It is quite possible that a change in concrete composition may lead to an increased strength but a decreased fracture energy. So far, we have too limited experience to know how to design a concrete mix in order to get a high fracture energy. We have some indications, e.g. that an increased maximum aggregate size may increase G_F, and that lightweight aggregates decrease G_F.

The characteristic length l_{ch} is a material property which can be said to define the toughness of the material. What is often more interesting is to have a value which characterizes the toughness of a structure. It can be shown that such a value is the ratio between l_{ch} and the size of the structure, defined e.g. by the depth of a beam. If the chosen size of the structure is denoted by d, the toughness is characterized by l_{ch}/d. As a rule, the inverse value d/l_{ch}, often called "brittleness number" [1] is used. It must be noted that the value of the brittleness number for a structure depends on the definition of d, which can be chosen arbitrarily, e.g. as beam depth, beam width, span, concrete cover, etc.

4. EXAMPLES OF RESULTS OF THEORETICAL ANALYSES

The description of tensile fracture given above can be used for analysing the behaviour of a structure which fails due to tensile stresses. Before failure, a fracture zone develops where the final failure takes place. Within the fracture zone, the σ-w-curve is valid for the relation between the transferred stress and the additional deformation. The σ-ϵ-curve is valid for all the material.

The fracture zone may be modelled as a zone which starts with zero width and takes all the displacement w, which means that its width is equal to w. It can then be looked upon as a "fictitious crack" with a width w, which transfers stresses σ according to the σ-w-curve. The model has therefore become known as the "fictitious crack model", although any reasonable small width of the fracure zone may be assumed in the numerical analyses without any noticeable influence on the results.

The analysis has to be numerically performed, as a rule by means of the finite element method. Fig. 8 demonstrates the principle of the analysis. When the tensile stress at the bottom of the beam reaches the tensile strength f_t, a fracture zone starts forming. When the beam deflection is increased, this fracture zone grows. At the same time, the stresses decrease close to the bottom of the beam, whereas they increase higher up in the beam. The stress at the tip of the fracture zone is constantly equal to f_t. As the fracture zone grows, the moment capacity, i.e. the load, at first increases due to a favourable redistribution of tensile stresses. At a later stage, it starts to decrease due to the decrease in tensile stresses at the bottom, associated with the increasing displacement w within the fracture zone. The moment capacity has a maximum, defining the flexural strength of the beam (modulus of rupture). In this way, the ratio between the flexural strength and the tensile strength can be determined; see below.

A number of structures have been numerically analysed by means of this method. Most of these analyses have been reported in [1]. Some significant examples will be discussed below.

All the analyses are based on the simplifying assumption that the σ-ϵ-relation is a straight line. The shape of the σ-w-curve is simplified to either a straight line or a bi-linear relation; see Fig. 9. These simplifications do not have any appreciable influence on the general conclusions drawn from the analyses.

4.1 Bending of a plain unreinforced beam

Fig. 9 shows the theoretical ratio between the flexural strength f_f and the tensile strength f_t for a beam with a rectangular section. Two different assumptions are used for the shape of the σ-w-curve. It can be seen that the assumed shape of this curve does not significantly influence the result. The scale in mm corresponds to an assumed value l_{ch}=250 mm.

It should be observed that the ratio f_f/f_t is uniquely defined by the ratio d/l_{ch} if the shape of the σ-w-curve is known. This type of uniqueness can be shown to have a general validity for any ratio f/f_t, where f is the formal strength value for a structure.

It should also be noted that logarithmic scales are used in Fig. 9. This is convenient for many reasons. One such reason is that it facilitates the judgement of the sensitivity of the results to variations of different properties, as will be shown below.

In Fig. 9, a dashed curve shows how an assumed distribution of shrinkage strains influences the flexural strength. The distribution has been assumed to be parabolic in the vertical direction. The maximum value is of the order which can be expected in normal indoor conditions. Although the assumptions are rather approximate, the general conclusion can be drawn that beams with small depths are rather insensitive to the influence of shrinkage, whereas deep beams are very sensitive.

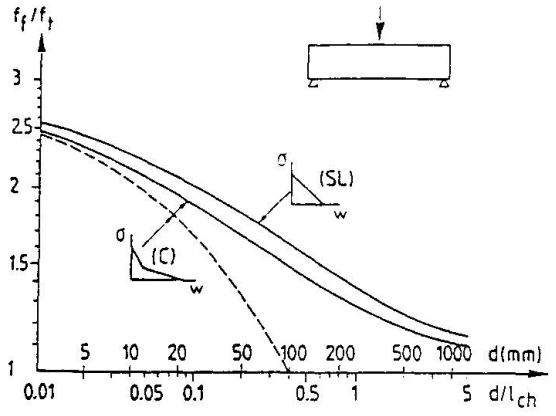

Fig.9 Theoretical ratio between flexural strength and tensile strength. The dashed curve includes influence of shrinkage

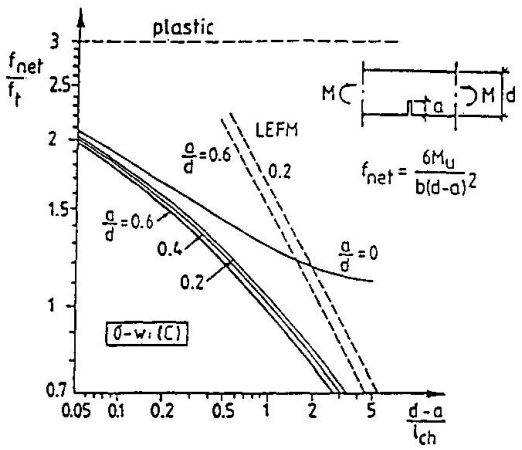

Fig 10 Theoretical ratio between net flexural strength and tensile strength for a notched beam

4.2 Bending of a notched beam

Fig. 10 shows how the net bending strength for the net area above a notch varies with the depth of the net section and with the relative notch depth a/d. A curve is also shown for a=0, i.e. a beam without a notch, the same as in Fig. 9. It can be seen that the relative notch depth has no significant influence as long as the notch is not very small. What is very interesting is that there is no major difference between the net bending strength of a notched beam and the strength of an unnotched beam for small beams, up to $(d-a)/l_{ch}$ about 0.5, which on an average corresponds to (d-a) about 0.2 m. Such small beams are said not to be "notch sensitive". The deeper the beams, the higher the notch sensitivity. It must be noted that the notch sensitivity depends both on the size of the structure and on a material property, l_{ch}. It is thus not a pure material property, which is sometimes claimed.

The dashed lines in Fig. 10 correspond to pure linear elastic fracture mechanics (LEFM), which can be seen not to be applicable to small beams, but to indicate the limiting case for large notched beams.

4.3 Unreinforced concrete pipes

Fig. 11 shows the results of an analysis of failure of unreinforced concrete pipes. Two different types of failure have been analysed. One type is a bending failure, with the pipe acting as a beam. The other type is called a crushing failure, with the forces acting along two opposite generatrices and the structure acting as a ring. In both cases, the formal flexural strength value is the maximum tensile stress at maximum load, calculated according to the theory of elasticity.

It can be seen from Fig. 11 that the formal flexural strength in crushing failure is higher than that in bending failure and that the size dependency is greater in crushing failure. One reason for these differences is that the active depth in the crushing failure is the wall thickness t, whereas in the bending failure it is the outer diameter. Another reason is that the structure is statically determinate in the bending failure, whereas in the crushing failure it is statically indeterminate, with a possible redistribution of moments before final failure. The ability to redistribute moments increases with a decreasing wall thickness.

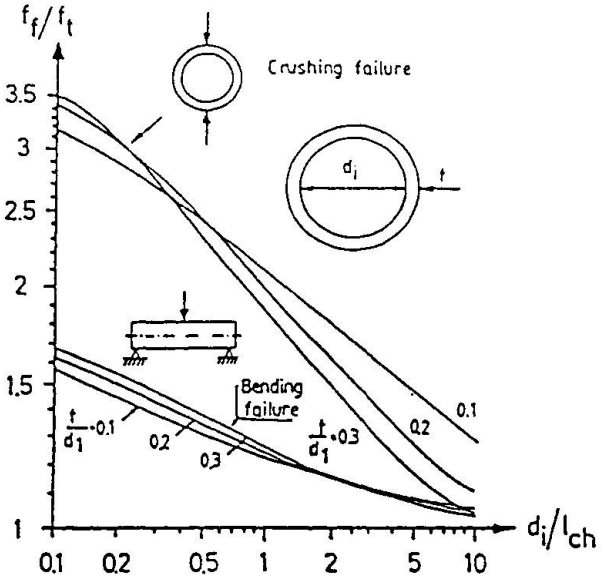

Fig.11 Theoretical ratio between a formal flexural strength and the tensile strength for two different types of failure of an unreinforced concrete pipe

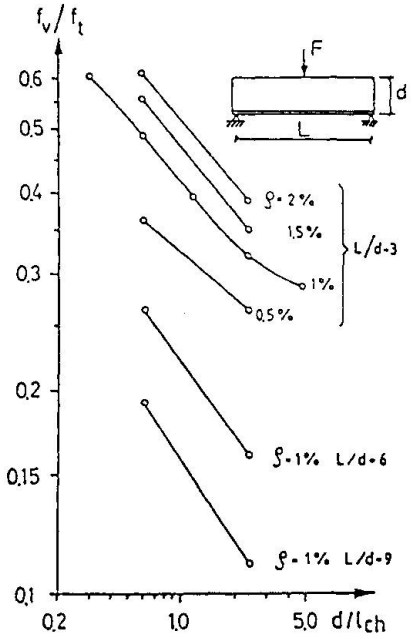

Fig.12 Theoretical ratio between a formal shear strength and the tensile strength of a beam with a tensile reinforcement ratio ρ

4.4 Shear failure

Gustafsson [2] performed an analysis of the shear failure of a beam with tension reinforcement, but without shear reinforcement. A number of assumptions and approximations had to be introduced in order to make the very laborious numerical analysis possible. No details will be given here, but the results alone, which are believed to give a reasonably accurate idea of the influence of different parameters. As the finite element programs develop, someone will hopefully perform a more advanced analysis. So far this is to the author's knowledge the only systematic analysis of shear failure which has been performed.

Fig. 12 summarizes the results. The points show calculated values: f_v is the formal shear strength, ρ is the percentage of reinforcement. The variables studied are the beam depth (d/l_{ch}), the reinforcement ratio and the span to depth ratio (L/d).

One thing which was not taken into account was the dowel action and the resulting possible splitting failure along the reinforcement. Nor were the shear stresses in the fracture zone ("aggregate interlock") taken into account in a realistic way.

5. INFLUENCING FACTORS

The formal strength f of a structure, expressed as e.g. a flexural strength or as a shear strength, is a function of the ratio d/l_{ch}, where d is a typical size of the structure. This function can be expressed in the general form (see

Figs. 9-12)

$$f/f_t = \varphi(d/l_{ch}) \quad (4)$$

In the diagrams, logarithmic scales are used. If we wish to study the sensitivity of f to small changes in other variables at a certain point in such a diagram, we may replace the curve by its tangent at this point. The equation of this tangent may be written in the following way:

$$\ln(f/f_t) = A - B\ln(d/l_{ch}) \quad (5)$$

Introducing $l_{ch}=EG_F/f_t^2$, the equation can be transformed into:

$$\ln f = A - B\ln d + B\ln E + B\ln G_F + (1-2B)\ln f_t \quad (6)$$

A differentiation of this equation gives:

$$df/f = -Bdd/d + BdE/E + BdG_F/G_F + (1-2B)df_t/f_t \quad (7)$$

This equation shows how the relative change in f is dependent on the relative change in each of the other variables. Thus an increase of G_F by 10% increases f by 10B%, and an increase of f_t by 10% increases f by 10(1-2B)%, where B is the negative slope of the tangent to the curve at the point in question.

The sensitivity of f with respect to changes in E or G_F can be said to be equal to B, and the sensitivity with respect to changes in f_t to (1-2B).

If different logarithmic scales are used on the axis, this has to be taken into account in the determination of B if Eq. (5) is to be fulfilled. In the diagrams above, the scale on the vertical axis is 4 times larger than that on the horizontal axis, which means that the slopes measured in the diagrams have to be divided by 4.

As to the flexural strength f_f according to Fig. 9, we find that, for ordinary beam sizes, B is approximately 0.15. The sensitivity with respect to changes in G_F is thus 0.15, and the sensivitity with respect to changes in f_t 0.7. With all other factors unchanged, an increase in the tensile strength by 10% will only increase the flexural strength by 7%.

From the dashed curve in Fig. 9 it is evident that the value of the slope B is much higher when the beam is exposed to shrinkage. It may then easily reach values above 0.3, particularly for large beams. In that case the sensitivity of f_f with respect to changes in G_F becomes very important, at the same time as the sensitivity with respect to changes in f_t is reduced. In order to increase the flexural strength of large beams exposed to shrinkage, it may be important to try to increase G_F rather than f_t.

According to Fig. 10, the value of B is higher for a notched beam than for an unnotched beam. It is typically of the order 0.25, which means that the sensitivity of f_{net} with respect to changes in G_F is about 0.25 and with respect to changes in f_t about 0.5. With all other factors unchanged, an increase in the tensile strength by 10% will only increase the net bending strength by about 5%.

According to Fig. 11, the value of B for unreinforced concrete pipes is about 0.1 for bending failure and about 0.3 for crushing failure. This means that for crushing failure the sensitivity of f_f with respect to changes in G_F is about 0.3, and with respect to changes in f_t about 0.4. In order to increase the crushing strength, it may thus be more important to increase G_F, if this can be

easily achieved, than to increase the tensile strength. For bending failure on the other hand, f_t is more important than G_F.

For shear failure according to Fig. 12 the average slope of all the lines corresponds to a value of B of about 0.25. The sensitivity of the shear strength with respect to changes in G_F is about 0.25, and with respect to changes in f_t about 0.5. The fracture energy is evidently an important factor for the shear strength of beams and slabs.

With B=0.25, the shear strength is inversely proportional to $d^{0.25}$, where d is the beam depth.

6. COMPARISONS WITH TEST RESULTS

6.1 Bending of plain unreinforced beams

Already in the very first published paper [3] on what later became known as the fictitious crack model, a comparison was made between the results of the theoretical analysis and of tests on the influence of the beam depth on the flexural strength. For beams without shrinkage, comparisons could be made with test results summarized by Meyer [5]. This comparison showed a good agreement, which encouraged a further development of the model. A comparison was also made with a small series of beams of different sizes with and without exposure to drying. In this case as well, a good agreement was found between theory and tests.

6.2 Unreinforced concrete pipes

Gustafsson [2] made a comparison of a few series of tests where equal pipes had been tested both for bending failure and for crushing failure. He was then able to show that the different formal flexural strengths calculated according to conventional formulae corresponded to the same tensile strength when the diagram in Fig. 11 was applied. As a matter of fact, the reason for his analysis was that the producers had difficulties in explaining why the formal bending strength calculated from a crushing test was more than 50% higher than that calculated from a bending test.

6.3 Shear failure

The analysis performed by Gustafsson [2] is the first purely theoretical analysis of shear failure. All design formulae have hitherto been based on extensive tests, often interpreted by means of some physical model, e.g. a strut and tie model, where empirical constants have been adjusted in order to achieve agreement with tests. A basic theoretical understanding of shear failure has been lacking. The analysis performed by Gustafsson is an important breakthrough, as it is the first time that some real theoretical understanding of shear fracture has been achieved. However, much more work remains to be done before shear fracture can be analysed and understood in detail.

One important factor which has been explained by means of theoretical analysis is the influence of beam depth. This influence has long been known from tests, and it is taken into account in concrete codes, e.g.according to CEB. No one has been able to explain it earlier by means of a theoretical analysis. From the test results the conclusion has been drawn that the shear strength is approximately inversely proportional to $d^{0.25}$ [4]. This is in agreement with

the theoretical analysis.

As a basis for concrete codes, a great number of test results have been summarized regarding the influences of different factors: in the first place beam depth, reinforcment ratio and span to depth ratio. The theoretical relative influences of these factors can be estimated approximately by means of Fig. 12. In all cases, a reasonable agreement between the analytic and the empirical results has been found; see [1] or [2].

6.4 Fracture mechanics test specimens

A great number of fracture mechanics tests, i.e. tests on differently shaped notched or precracked specimens, have been theoretically analysed. In particular, Gustafsson [2] has reported many such analyses. As a rule, they show good agreement between tests and analyses.

6.5 Summary

The comparisons which have been made between theoretical analyses and tests all show that the fictitious crack model according to Fig. 5 gives a realistic description of tensile failure, and that it can be expected to give much more reliable predictions of failure loads than the conventional methods. A systematic study by means of this model of cases where we rely on tensile strength will lead to a safer basis for concrete design. The resulting consequences from the points of view of safety and economy motivate a strong support for this type of research.

7. SOME PRACTICAL CONCLUSIONS

Some practical conclusions can be drawn from the systematic analyses. A number of these will be commented upon.

Starting with Fig. 9, we can see that the flexural strength decreases with an increasing beam depth. The increase is particularly important where the structure is exposed to drying shrinkage. One consequence is that the flexural stress which causes cracking is lower for large beams than for small beams. This is also the case for reinforced beams, as the reinforcement has only a small influence on the cracking load. The influence of size ought to be taken into account when the cracking moment is used in connection with the calculation of the stiffness of a beam.

Another consequence is that the flexural strength should only be relied upon for structures with either a very small depth or with negligible drying shrinkage within the tensile zone. Examples of very thin structures are pavement slabs of about 50 mm thickness and concrete tiles. Footings are an example of a case with a negligible drying shrinkage. Fig. 9 thus explains why we may rely on concrete flexural strength in these cases.

Fig. 11 is already used by manufacturers for the design of unreinforced pipes. It is a good example of the practical applicability of the model for tensile fracture. As the wall thickness of these pipes is limited, stresses due to drying shrinkage can be estimated to have a limited influence, although some increasing influence with an increasing size may be expected.

The analysis of shear failure in Fig. 12 supports the empirical findings upon which the concrete codes are based, e.g. regarding the influence of beam depth.

The analysis may support some changes in concrete codes, resulting in a more even safety factor and a better economy.

As the analytic results according to Fig. 12 are supported by test results regarding the influence of the beam depth, it may be assumed that the following general relation is valid:

$$f_v/f_t \sim (d/l_{ch})^{-0.25} \quad (8)$$

Introducing $l_{ch} = EG_F/f_t^2$ and rearranging gives:

$$f_v \sim (EG_F f_t^2/d)^{0.25} \quad (9)$$

As an approximation, it is often assumed that the tensile strength f_t is proportional to the square root of the compressive strength f_c. If we accept this assumption, we find:

$$f_v \sim (EG_F f_c/d)^{0.25} \quad (10)$$

From this relation the conclusion can be drawn that the fracture energy G_F is of about the same importance as the compressive strength f_c for the shear strength of a reinforced beam. When shear tests on beams are performed, the concrete quality should be given, not only as a concrete strength f_c, but also as a fracture energy G_F.

From Eq (10) it may be expected that the shear strength of lightweight concrete beams is lower than that of normal concrete beams with the same tensile strength, as E and G_F are lower for lightweight concrete than for normal concrete.

Creep under long-term loading causes a reduction in the formal E-value by a factor $1/(1+\Phi)$, where Φ is the creep factor. Thus e.g. with $\Phi=2$, the shear strength may be expected to be reduced by a factor of $(1/3)^{0.25}=0.76$, provided that G_F and f_t are not time-dependent.

8. POSSIBLE FURTHER APPLICATIONS

In principle, the model for tensile fracture can be applied in analysing all the cases where we need to rely on the tensile strength of concrete. We are still far from a sufficient understanding of all types of tensile-induced structural failures. Some of them are very complicated to analyse. This is the case with, for example, shear and punching failure, including the dowel action in combination with spalling forces from the bond stresses between reinforcing steel and concrete. A major research effort is needed within this area in order to achieve better guidelines for design rules. Such a research effort may be expected to lead to a more even safety factor and large savings.

The anchorage of bolts is a case which can be theoretically analysed, although it is rather complicated, because not only tension, but also shear stresses act in the fracture zone, and several fracture zones may have to be taken into account. Test results [1] show that the fracture energy in this case is an important concrete property, whereas the tensile strength has a limited influence. In terms of sensitivity, it seems that in this case the value of B is close to 0.5. One consequence of this is also that the formal stress associated with pull out of a bolt is very size-dependent.

Anchoring reinforcing bars always gives splitting tensile stresses, which may cause tensile-induced failure in a structure. A number of different situations

may be distinguished, depending on the type of anchorage, e.g. by bond or by end anchors, deformed or plain bars, prestressed or non-prestressed reinforcement, dowel action due to shear cracks etc. These different situations may all be theoretically analysed.

In order to obtain valid results for practical design purposes, the influence of shrinkage should also be analysed, as shrinkage may sometimes have an important unfavourable influence on the strength of a structure; see e.g. Fig.9.

9. CONCLUSIONS

The model for tensile fracture according to Fig. 5 (the "fictitious crack model") gives realistic predictions compared to test results. By means of this model it is possible to analyse tension-induced failures and to estimate to what extent the tensile strength of concrete may be relied upon.

From the analyses performed so far, the following general conclusions regarding tensile-induced structural failures may be drawn:

1. The formal strength (a formal stress value at maximum load) is size-dependent. The strength is proportional to d^{-B}, where d is a typical size of a structure and B normally varies between 0.15 and 0.5.

2. The formal strength depends on the tensile toughness of concrete. A material property closely connected with toughness is the fracture energy G_F. This material property should be determined and taken into account in the evaluation of test results and in design, particularly for less common types of concrete, such as high strength concrete and concrete with weak aggregates. The strength is proportional to G_F^B, with B as above.

3. The formal strength is proportional to E^B, where E is the elastic modulus and B has values as above. The ratio between long-term and short-term strength can be estimated from the formal reduction of E due to creep.

4. The formal strength is proportional to $f_t^{(1-2B)}$, where f_t is the tensile strength and B has values as above. In cases of high B values, the tensile strength may be a less important material property than G_F and E for a tension-induced failure.

5. Shrinkage may decrease the formal strength appreciably, particularly where the failure already has a brittle character.

6. Toughness (ductility) in tension is a property of the utmost importance for the reliance upon concrete tensile strength.

REFERENCES

1. ELFGREN L. (editor), Fracture mechanics of concrete structures. RILEM Report, Chapman and Hall, 1989.

2. GUSTAFSSON P J., Fracture mechanics studies of non-yielding materials like concrete. Report TVBM-1007, Div. of Building Materials, Lund Institute of Technology, 1985.

3. HILLERBORG A., MODÉER M., and PETERSSON P-E., Analysis of crack formation and crack growth in concrete by means of fracture mechanics and finite elements. Cement and Concrete Research, Vol 6 (1976), pp. 773-782.

4. LEONHARDT F., Shear in concrete structures. Bulletin d'information CEB No. 126, Shear and torsion, Paris 1978, pp. 66-124.

5. MAYER H., Die Berechnung von Durchbiegung von Stahlbetongbauteilen. Deutscher Ausschuss für Stahlbeton, H 194, 1967, W Ernst & Sohn, Berlin.

6. PETERSSON P-E., Crack growth and development of fracture zones in plain concrete and similar materials. Report TVBM-1006, Div. of Building Materials, Lund Institute of Technology, 1981.

7. RILEM, Determination of the fracture energy of mortar and concrete by means of three-point bend tests on notched beams. Materials and Structures, Vol 18 (1985) pp. 285-290.

Basic Concept for Using Concrete Tensile Strength

Concept de base visant l'utilisation de la résistance en traction du béton

Überlegungen zur Ausnutzung der Betonzugfestigkeit

Gert KÖNIG
Professor
Techn. Hochschule
Darmstadt, Germany

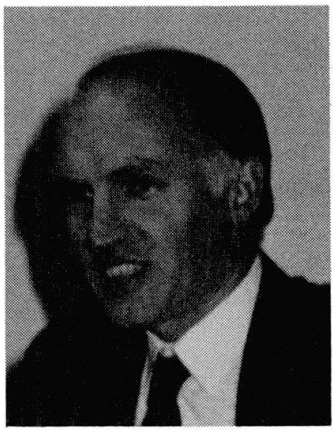

Gert König, born 1934. Since 1970 partner in a consulting office. Since 1975 Professor in the faculty of civil engineering at the Technische Hochschule of Darmstadt.

Herbert DUDA
Civil Eng.
Techn. Hochschule
Darmstadt, Germany

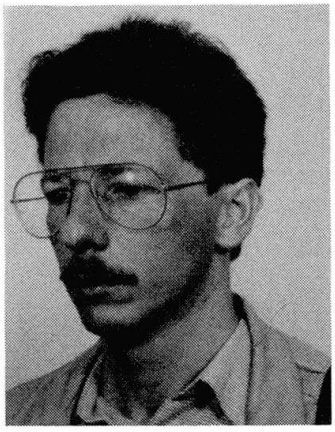

Herbert Duda, born 1958, obtained his civil engineering degree at the Technische Hochschule Darmstadt, he is currently an assistant at the Institut für Massivbau.

SUMMARY

A mechanical model is presented which is able to predict strain softening of concrete in tension. An arbitrary loading history can be described. Scale effects are taken into account. The report includes a critical review of test set-ups to study the material properties of concrete in tension. Finally, a basic concept for using concrete tensile strength in design is described.

RÉSUMÉ

Un modèle mécanique est présenté qui permet de relever la baisse de la résistance à la traction d'un béton mis en tension. L'évolution de la mise en charge est décrite, de même que l'on tient compte des effets de l'échelle de mesure. L'article présente également un rapport critique sur les installations utilisées dans l'étude de la résistance à la traction du béton. Finalement, un concept de base est donné pour utiliser à bon escient cette résistance lors du dimensionnement de structures.

ZUSAMMENFASSUNG

Es wird ein mechanisches Modell vorgestellt, das das Verformungsvermögen von Beton unter Zugbeanspruchung mit den wesentlichen Abhängigkeiten beschreibt. Eine beliebige Lastgeschichte kann damit verfolgt werden. Es können Massstabseffekte beschrieben und Versuchsaufbauten zur Bestimmung des Verhaltens von Beton auf Zug kritisch diskutiert werden. Schliesslich werden Aussagen zur Ausnutzung des Betons auf Zug bei der Dimensionierung der Tragwerke gemacht.

1. INTRODUCTION

In general, concrete is considered to be a brittle material. Especially in the case of tensile loaded concrete a very brittle behavior is expected, but in some cases, e.g. anchorage, tensile loaded concrete exhibits a very ductile behavior, also. In the case of pure bending, concrete may exhibit a ductile behavior. Figure 1 shows three load-crack-mouth-opening displacement curves (Load-CMOD-curve) [16]. The test specimen were notched beams under three point bending. They were made of HSC (C80) which is normally judged to be brittle; nevertheless, the behavior was ductile. The brittleness or ductility of concrete is not only governed by the material behavior but to the same extend by the size and the loading conditions.

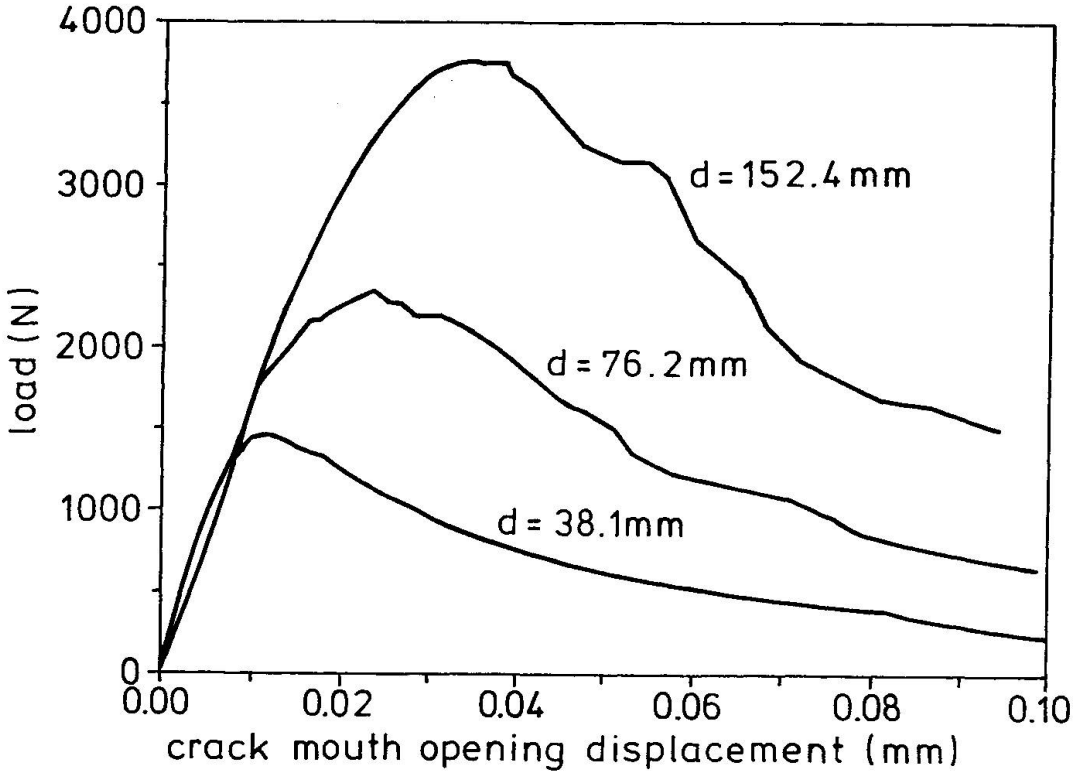

Fig. 1: Load - CMOD - curve for different depths d

2. MODELING OF STRAIN SOFTENING

The ductility or brittleness of concrete depends on the strain-softening behavior of concrete. There is a big difference in strain softening of concrete and e.g. steel. Having passed the yield point, steel first shows a strain hardening and after reaching the tensile strength, a strain softening behavior. Concrete shows no – or almost no – strain hardening. The strain softening starts immediately after the elastic limit is reached, it occurs due to cracking and not due to yielding as in steel.

The tensile behavior of concrete may be explained by Figure 2. A deformation controlled centric tension test may be undertaken at the specimen shown in Figure 2 left. The specimen is loaded with the force P. The total deformation is measured over the length l. On the left side of Figure 2 the specimen is plotted for the load steps A, B and C. The load steps are marked also at the load-deformation-curve on the right side. Load step A is before peak load; load step B at peak load and load step C after peak load, at the descending branch of the load displacement curve.

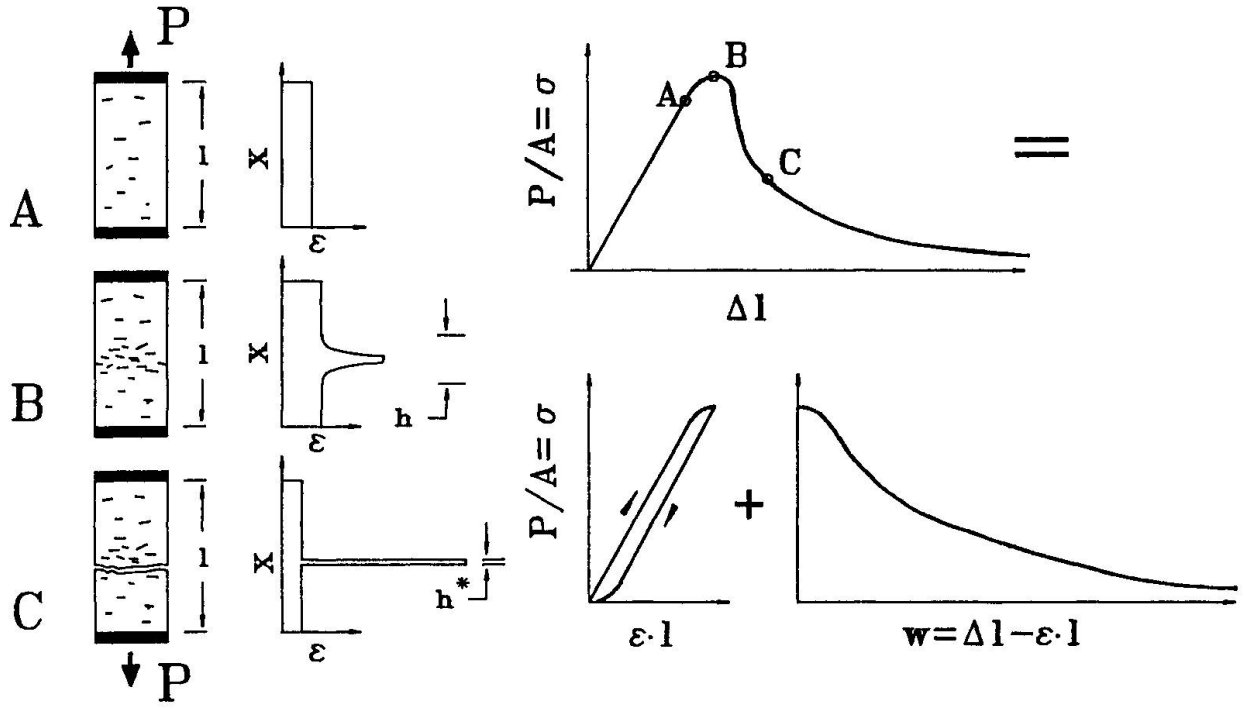

Fig. 2: Tensile behavior of concrete

Even before the peak load is reached, some micro-cracking occurs (Fig. 2A). As the micro-cracking is uniformly distributed on the macro level, a uniform strain over the length of the specimen may be assumed. The strain ε is plotted over the length of the specimen in Fig. 2, next to the specimen.
Immediately before the peak load an accumulation of micro-cracking occurs at the weakest part of the specimen. On the macro level this leads to an additional strain over the length h of this weak part. A crack band with the crack-band width h develops (see Fig. 2B).

Having passed the peak load the crack band localizes. The crack band width diminishes and the deformation within the crack band increases. The final failure occurs due to one single crack.
The total deformation of the specimen may be split up into the bulk deformation and the deformation of the crack band. The deformation of the crack band may be described either as an additional strain of a crack band with a fixed length h^* or as the crack width of a single crack. In the case of a single crack the crack band width diminishes to zero.

For most applications the crack band model and the single crack model are equivalent, but occasionally, the assumption concerning the crack band width (equals zero or greater zero and constant) may influence the result of a calculation. To create new crack surfaces the crack propagation criteria must be fulfilled over the crack band width. A crack starts propagating if the stress is equal to the tensile strength: either at one point (single crack) or over the crack band width (crack band).
In the case of, for instance, a three point bending test this leads to a dependency of the crack load from the crack band width (See Fig. 3).

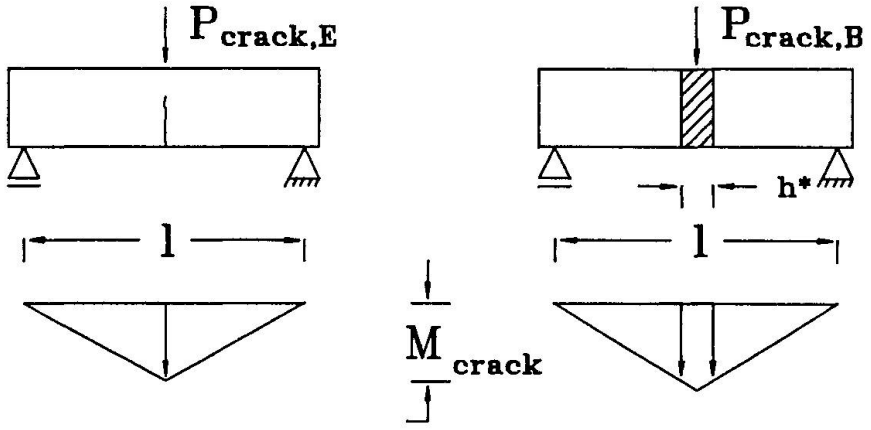

Fig. 3: Crack load of a three point bending test

As mentioned the micro crack accumulation starts within a crack band. The width of this crack band diminishes with increasing deformation. This leads at last to one single crack. The crack band width is not constant.
In this sense any assumption of a constant crack band width – equal or unequal zero – is arbitrary.

Hillerborg introduced the fictitious crack model, where he collected the deformation of the crack band to the crack-width w of one single 'fictitious' crack. The relation between the crack width of the 'fictitious' crack and the stress is the σ-w-relation. Two mechanisms contribute to the stress transfer over the crack. At the beginning of cracking it is merely a 'fictitious' crack. The crack width is the collected deformation of a band of micro-cracks. Within this crack band material bridges transfer the load. After the formation of a real single crack the stress transfer is possible due to aggregate interlock. In most cases a crack will run along the interfaces between the aggregate grains and the cement paste. The grains are pulled out of the paste. Due to this, friction forces between grains and matrix occur. The grains act like friction blocks and transfer friction forces over the crack.

Many experimental results are available for the σ-w-relation in the case of monotonic loading. Fig. 4 shows some suggestions taken from [1,2,3,4,5]. With the exception of the linear model, which is often chosen because of its simplicity, all σ-w-relations show the same behavior. The first branch of the relation is very steep, whereas the second branch is more flat. Most practical applications are unsensitive to the exact shape of the σ-w-relation. It makes no difference which of these suggestions is chosen.

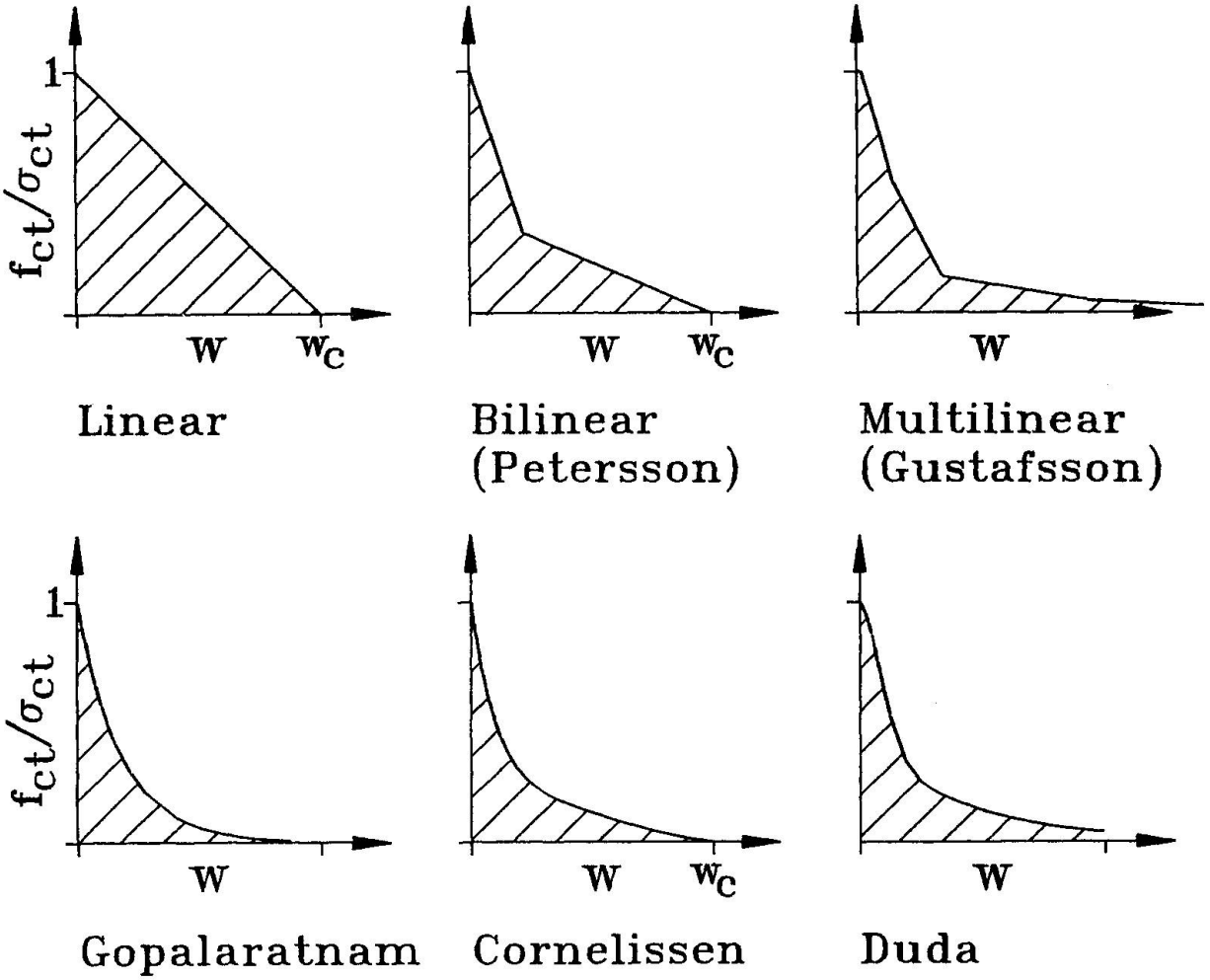

Fig. 4: σ-w-relations

Contrary to the monotonic loading, only few models are available for the case of cyclic loading. Figure 5 shows the models of Rots [6], Gylltoft [7], Reinhardt [8] and Duda [5]. The first three models use polygonal courses for the description of the hysteresis loop and an additional model for the envelope curve. The model of Duda is a rheological material model and describes both the envelope curve and the hysteresis loops.

The bulk behavior is described by a σ-ε-relation (see Figure 2). This relation is linear almost up to the peak load. The modulus of elasticity is equal to the initial tangential modulus of elasticity of the pressure part of the material behavior. The Poisson's ratio is in the order of $\mu = 0.15$ .. 0.25. Just before the peak load is reached, the σ-ε-relation bends of from the linear behavior. For the state of loading where the nonlinearity starts very different experimental results are available. In some experiments the nonlinearity starts at about half of the peak load, in other experiments the curve is linear up to the peak load. These differences in the experimental results are caused by the different boundary conditions. Any kind of unsystematic loading, like internal bending due to non-uniform cracking, residual stresses due to differential shrinkage, notch effects, etc. causes nonlinearities. Theoretical considerations [5] show that even when the material behaves linear-elastic up to the tensile strength, a specimen may behave non-linear before the peak load is reached (see Fig. 10). The nonlinear behavior of test specimens is more a specimen behavior than a material behavior. Because of this, it seems to be fair to assume linear elastic bulk material behavior up to the tensile strength, for the loading and unloading path.

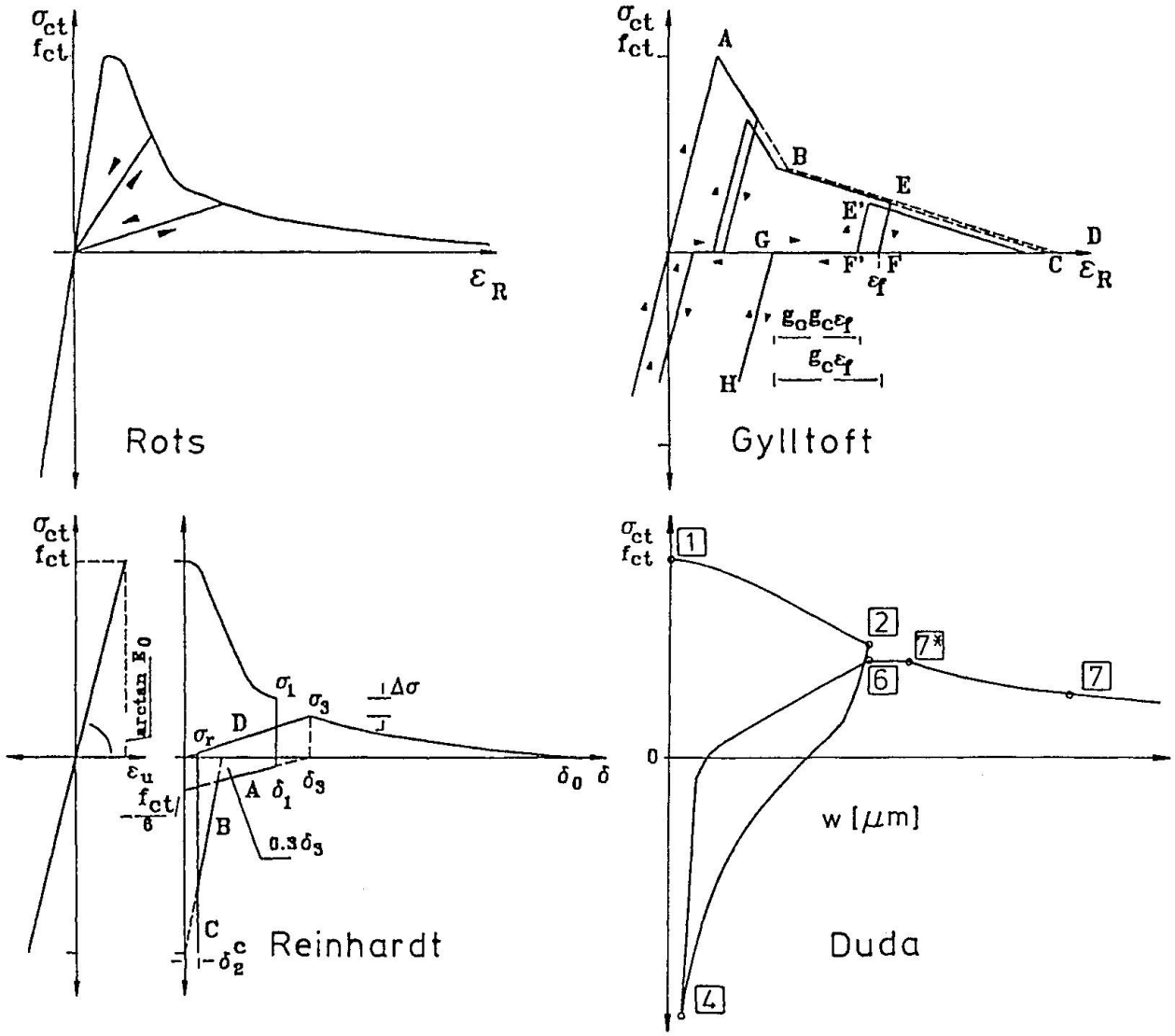

Fig. 5: Material models for cyclic loading

3. MAIN PARAMETER INFLUENCING STRAIN-SOFTENING

The strain-softening behavior of tensile loaded concrete can be described with the σ-w-relation. The parameters of the σ-w-relation are:

- tensile strength f_{ct}
- fracture energy G_F
- the shape of the curve

The tensile strength is a generaly accepted material parameter of concrete. There are standard tests (axial tensile test, bending test, brazilian test) for the determination of f_{ct}. The tensile strength of concrete is influenced by the same parameters as the compressive strength. These parameters are water/cement ratio, strength of cement, the strength and the kind of aggregate. The tensile strength can be approximated from the compressive strength e.g. Rüsch [9]:

$$f_{ct} = c \cdot \sqrt[3]{f_c^2}$$

The factor c is a empirical constant. For the 5% fractil c = 0.17, for the mean c = 0.24 and for the 95% fractil c = 0.32 is valid.

The fracture energy is the energy needed for the creation and complete opening of one unit new crack surface. It is equal to the area under the σ-w-relation (hatched areas in Fig. 4). This leads to

$$G_F = \int_0^{w_c} \sigma_{ct}(w) \cdot dw$$

The upper limit of integration w_c is equal to the crack width in which the crack is stress free. For models without such an ultimate crack width the upper limit is infinity. The fracture energy depends on:

- aggregate
  - * grading curve
  - * maximum aggregate size
  - * aggregate surface (rough or smooth)
  - * aggregate strength
- concrete strength
- water/cement ratio
- age
- curing
- temperature
- loading rate
- workability, consistence

One of the most important influencing factors is the percentage of coarse aggregate grains. The coarse grains are the bridges between the crack interfaces. Therefore, G_F increases both with the percentage of coarse grains and with the maximum grain size (d_{max}). In Figure 6 experimental results from Mihashi [10], Petersson [1], Wolinski [11], Kleinschrodt [12] Roelfsta [13], Wittmann [14], Carpinteri [15] and Duda [5] and a theoretical model introduced in Duda [5] are shown. The increase of G_F (y - axes) with the maximum grain size (x - axes) is obvious. There is a big scatter in the results of the different sources. The fracture energy depends not only on d_{max} but also on the other parameters as mentioned above.
These other parameters are different for different sources, what explains the big scatter. Furthermore it is impossible to change only one parameter (e.g. d_{max}) without changing also at least one of the others.

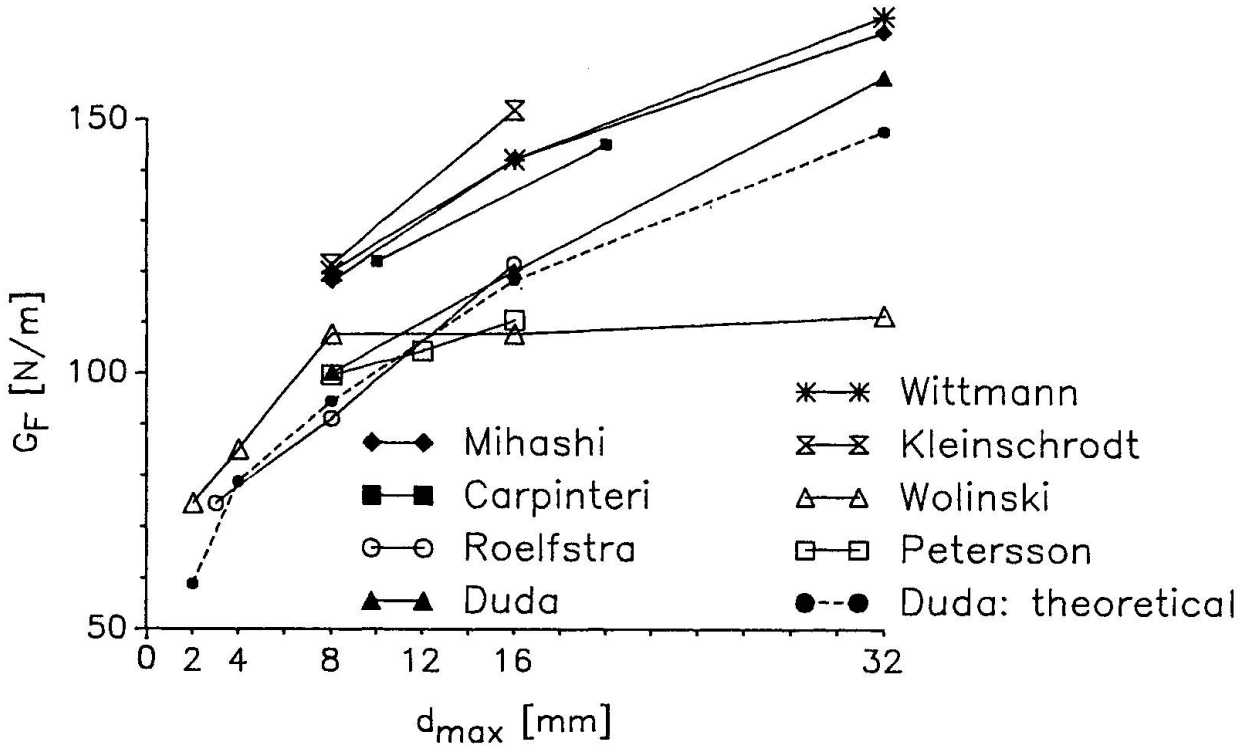

Fig. 6: Fracture energy over maximum aggregate size

Crushed aggregate with rough surfaces causes an increase in G_F compared with water-worn gravel with a smooth surface. The relation between the strength of the aggregate and the cement paste influences also the shape of the σ-w-relation. Figure 7 shows typical σ-w-relations of normal-, high strength- and light weight-concrete. In the case of comparatively weak cement paste and strong aggregate grains the crack runs through the paste and at the interfaces between the grains and the paste. The grains are pulled out of the cement matrix, transferring friction forces over the crack. When the cement paste reaches the strength of the aggregates, either due to the increased strength of the cement paste in the case of high strength concrete or due to the relative weak aggregates in the case of light-weight concrete, the crack will split most of the grains. The stress transferring capacity for greater crack width decreases rapidly. Due to this high-strength and light-weight concrete behaves much more brittle than normal concrete.

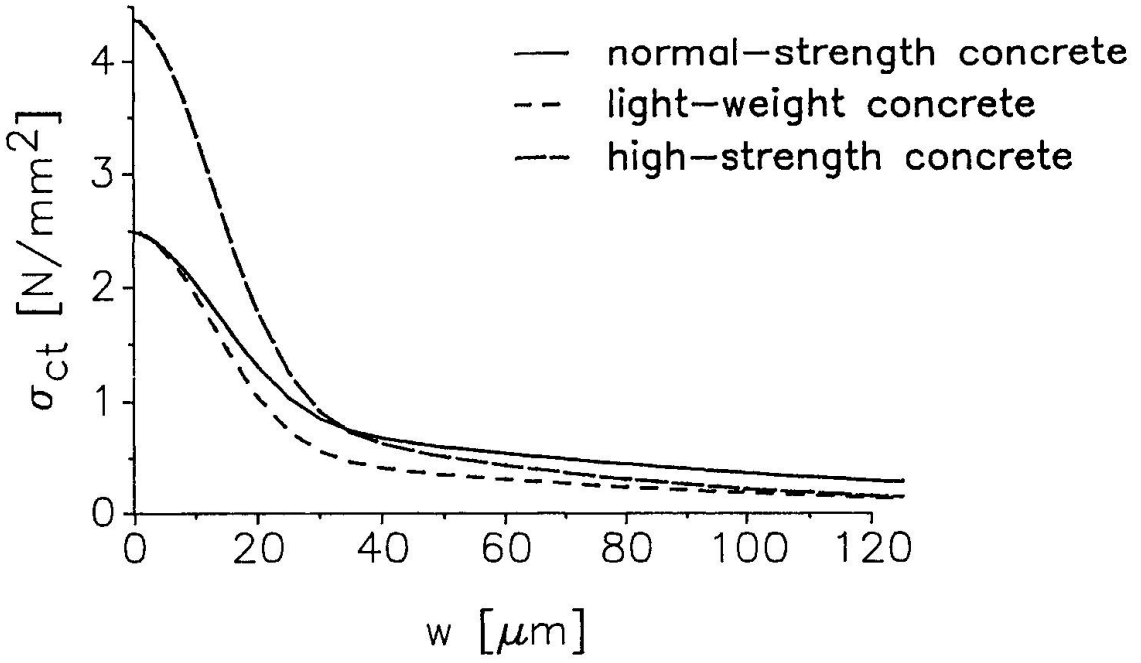

Fig. 7: σ-w-relation of normal-, lightweight- and high strength-concrete

The water/cement ratio influences G_F similar to its effect on the strength (See also Hordijk [17]). The maximum will be reached with W/C = 0.4. Higher and lower values lead to a decrease in G_F.

4. CRITICAL REVIEW OF TEST SETUPS

Various test setups are used to study the material properties of tensile loaded concrete. Some of these will be introduced and discussed.

4.1 Notched and un-notched centric tension test

It is self-evident to study the tension behavior of concrete with centric tension tests. A test setup may be as shown in Figure 8 at the left side. Loading plates are glued to both ends of the specimen. A test including also the descending path of the load deflection curve is feasible under deformation-control only. In the case of a cylinder (length = 300 mm) made of normal concrete the outcome of this test will be approximate as plotted on the right side in figure 8. The total deformation (Δl) is the sum of the bulk deformation ($\varepsilon \cdot l$) and the crack width (w). Due to the elastic unloading of the bulk there will be a snap-back in the load-deformation curve. As the test is controlled by increasing the total deformation, it is impossible to control the test between point A and B. Due to the elastic unloading of the testing machine, the test fails between the points A and $\tilde{B}$ in an unstable manner. As the distance between point A and $\tilde{B}$ represents about two third of the peak load, it is not reasonable to study the post peak response of concrete with such a kind of test.

To avoid the unstable failure the test must be controlled by a deformation which does not exhibit any snap-back. This is possible by using notched specimens. The crack-mouth-opening displacement of the notch can be used to control the test. From the theoretical point of view it is easy to run such a test, but in reality, there are still problems with the stability of the test and with the non-uniform crack opening.

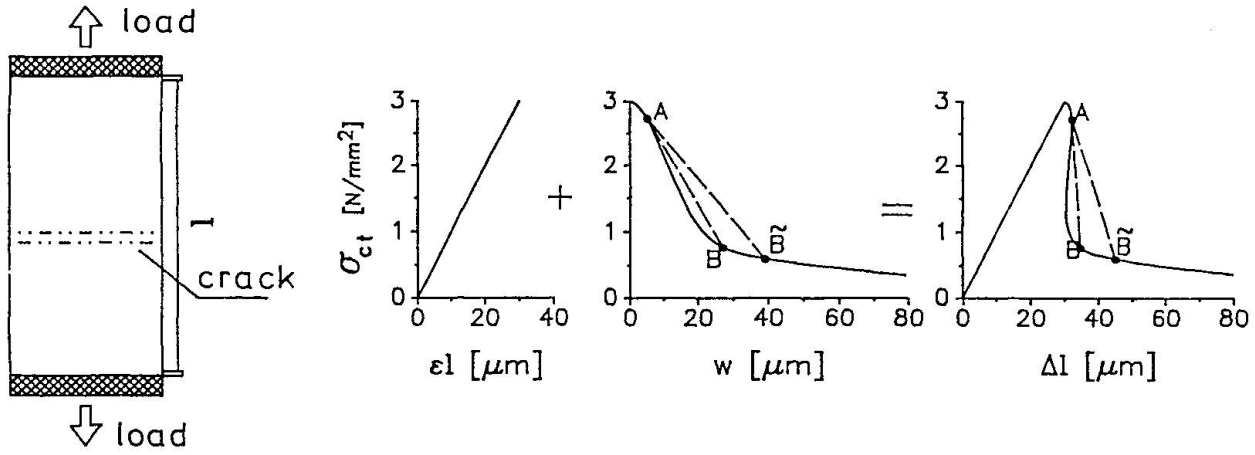

Fig. 8: Test setup for centric tension test

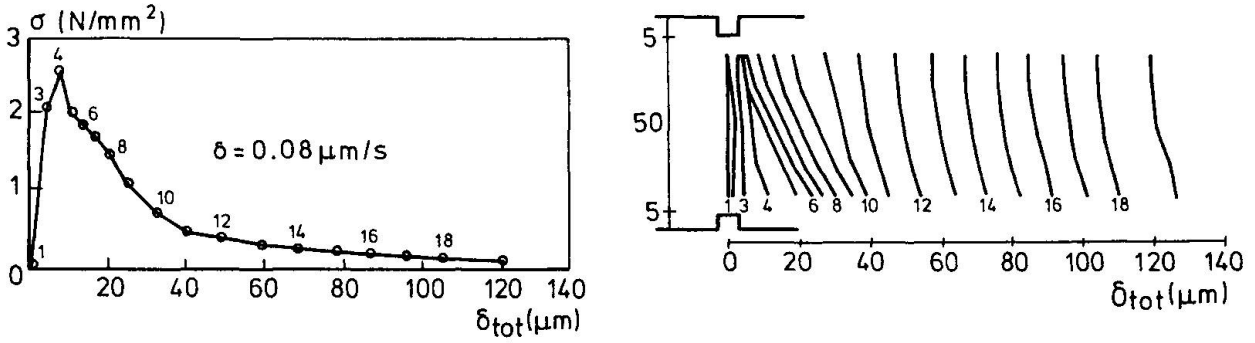

Fig. 9: Centric tension test

Figure 9 shows the results of a centric tension test with a notched specimen (Cornelissen [4]): on the left side the average stress over the average deformation of the crack-band, at the right side the crack profile for different load steps. The crack opening is non uniform. As the stress depends on the crack width the stress distribution is also non-uniform. Consideration of only the average stress and the average deformation is a pure approximation for the real σ-w-relation. Figure 10 shows the average σ-w-relation and the recalculated 'real' σ-w-relation of this test. The difference in the tensile strength is about 12%.

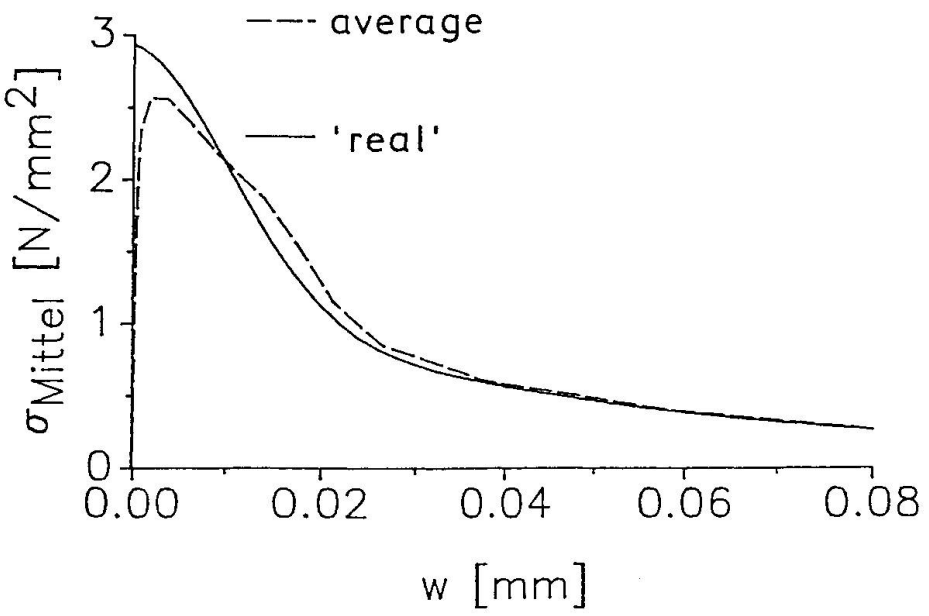

Fig. 10: Average and 'real' σ-w-relation

4.2 The brazilian test (splitting test).

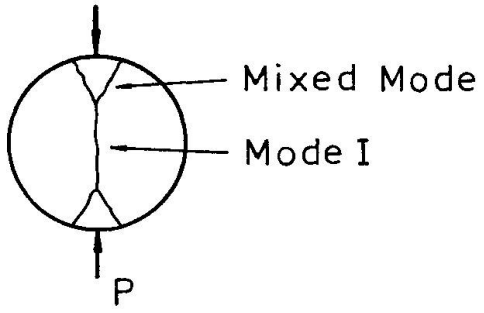

Fig. 11: Brazilian test

The splitting test is widely used to determine the tensile strength of concrete. A concrete cylinder or prism is loaded between two edges. The specimen fails due to a tension crack parallel with the load direction (see Figure 11). It is a reasonable test for the determination of the tensile strength, but there is no way of getting a reasonable post peak response with this test. At peak load wedge-shaped concrete pieces develop next to the edges. The post peak response is governed by the mixed mode (tension and shear) behavior at the interface between the wedges and the bulk.

Mode I (tension) occurs only in the center of the specimen. It seems to be impossible to extract the mode I material behavior from of the complicated mixed mode behavior of a brazilian test.

4.3 Three and four point bending tests

Bending tests are much easier to perform than centric tension tests. There is no need to glue load plates at the specimen. Because of the redistribution of stress, the descending part of the load deformation curve is less steep than in the case of pure tension.

Most bending tests are performed with notched beams because the place of cracking is fixed by the notch. Depending on the geometry and the material properties, the snap-back problems already mentioned may also occur with bending tests. Four point bending tests are advantageous as there is no shear-force between the loading points. With three point bending

tests there is always a shear force acting between the crack-interfaces (See Fig. 12). This may disturb the test-results.

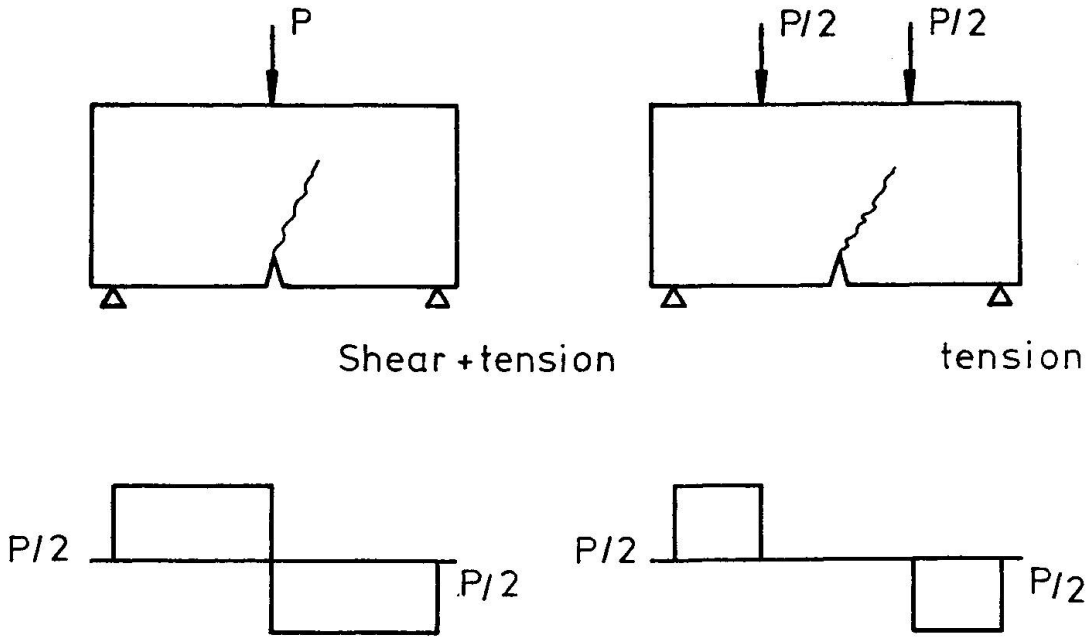

Fig. 12: Shear forces in three and four point bending

In order to extract the material behavior from the specimen behavior a recalculation is necessary. Depending on the available soft- and hardware equipment this recalculation procedure may be considerable time consuming.

4.4 Compact tension testes

Two different types of compact tension tests are shown in Figure 13. The compact tension specimens have the same fracture surface as other specimens, however, they are smaller in dimension. This may be advantageous for casting and handling the specimen. The crack interface is under pure tension. A recalculation equivalent to the recalculation of bending tests is necessary.

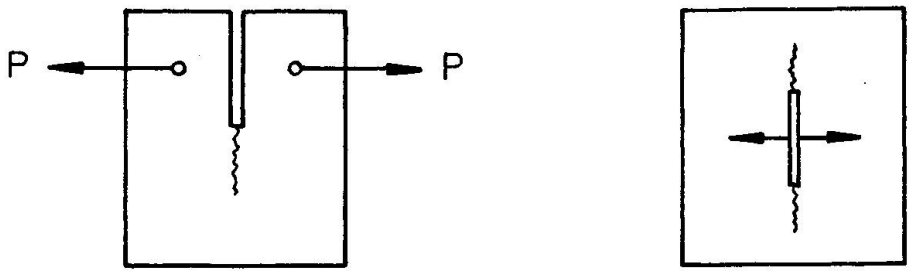

Fig. 13: Compact tension test

4.5 Conclusions

A lot of different test setups are in use. Depending on the aim of the test, the available test machine, the hard- and software equipment, etc. any of these may be advantageous or disadvantageous.

5. SCALE EFFECTS

When geometrical similar specimens do not behave similar for different sizes, we are dealing with a scale or size effect. Size effects occur anywhere in concrete. They are most significant in the case of tensile or shear load and less significant in the case of compression. A very well-known size effect is the dependence of the flexural strength of plain concrete on the depth of the beam. The increase in flexural strength is caused by the strain-softening behavior of concrete. The dependence of the flexural strength on the depth, the eccentricity, and the σ-w-relation was analyzed using finite elements. The depth was varied between 5 cm and 2 m, the eccentricity between zero (tension) and infinity (bending). The four different σ-w-relations plotted in Figure 14 where assumed.

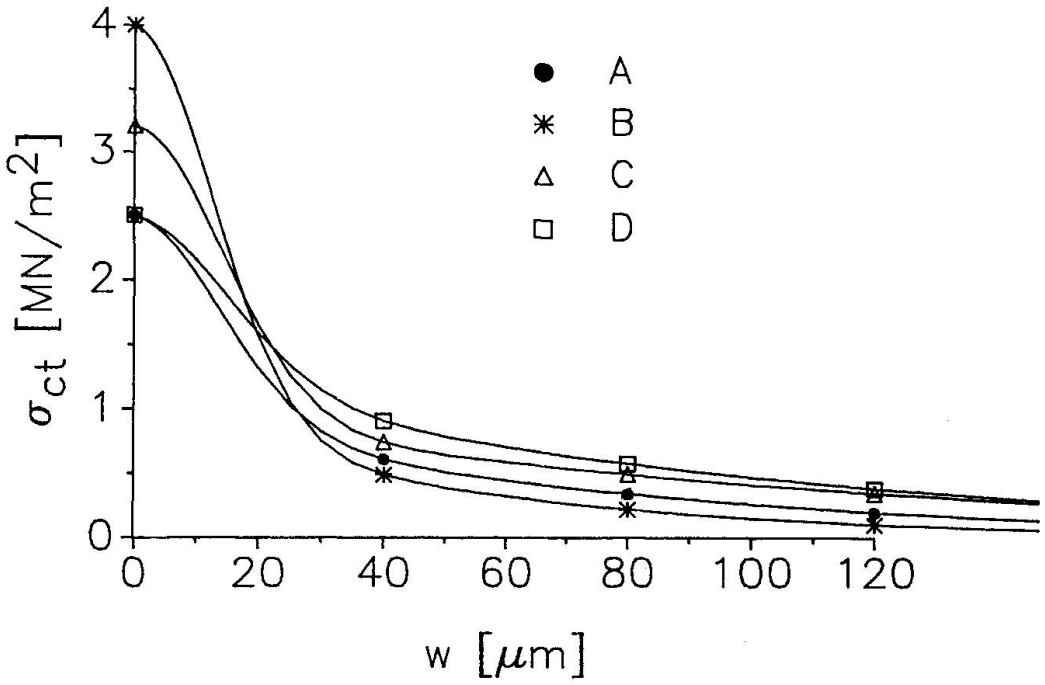

Fig. 14: σ-w-relations

Type A: normal concrete, C25, gravel, d_{max} = 8 mm
Type B: high strength concrete, C80, crushed limestone, d_{max} = 8 mm
Type C: normal concrete, C35, gravel, d_{max} = 32 mm
Type D: normal concrete, C25 crushed basalt, d_{max} = 16 mm

The flexural strength f_{cf} is defined as the ratio between the ultimate bending moment M_u and the moment of resistance.

$$f_{cf} = \frac{M_u \cdot 6}{b \cdot d^2}$$

The ratio of flexural strength f_{cf} and tensile strength f_{ct} is plotted in Figure 15 over the depth of the beam. It is obvious that the increase in flexural strength depends on the depth and on the kind of σ-w-relation.

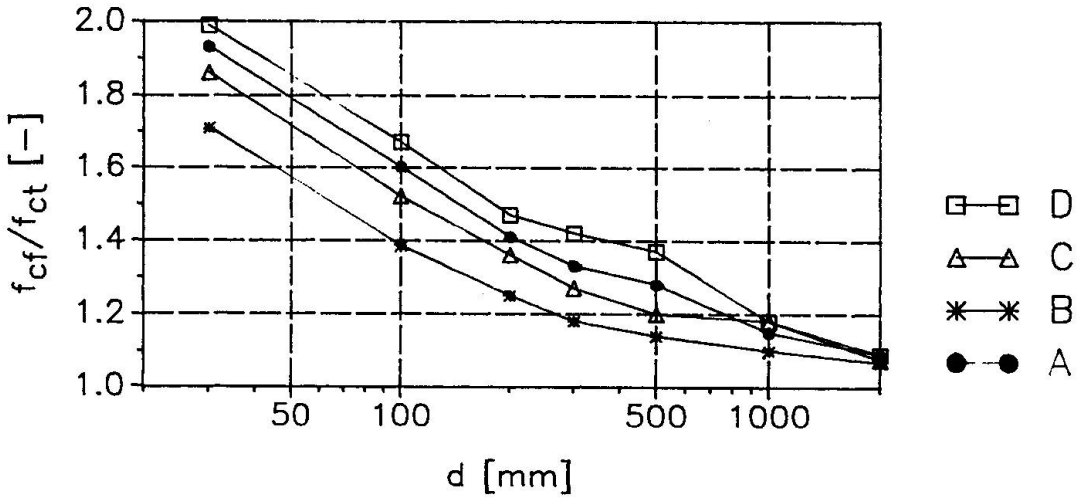

Fig. 15: Relative flexural strength of concrete under pure bending

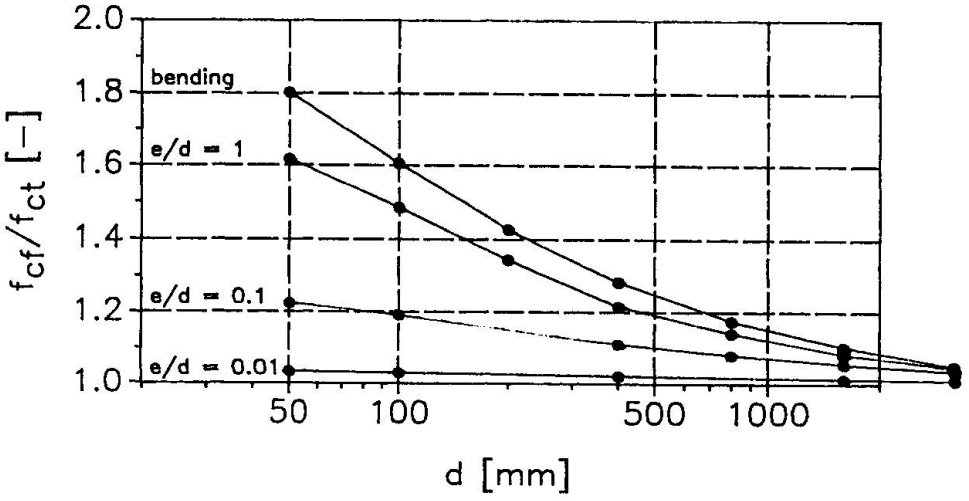

Fig. 16: Relative flexural strength of concrete under bending and normal force

A normal force action simultaneously with a bending moment influences the increase in flexural strength. In Figure 16 the relative flexural strength is plotted over the depth for different relative eccentricities e/d. The flexural strength for normal force N_u and bending moment $M_u = e \cdot N_u$ is defined as:

$$f_{cf} = \frac{N_u}{b \cdot d}\left(\frac{e \cdot 6}{d} + 1\right)$$

The increase in flexural strength occurs due to the redistribution of the tensile stress. The stress distribution under ultimate bending moment is plotted in Figure 17 for depth d = 10cm, d = 40cm and d $\rightarrow \infty$.

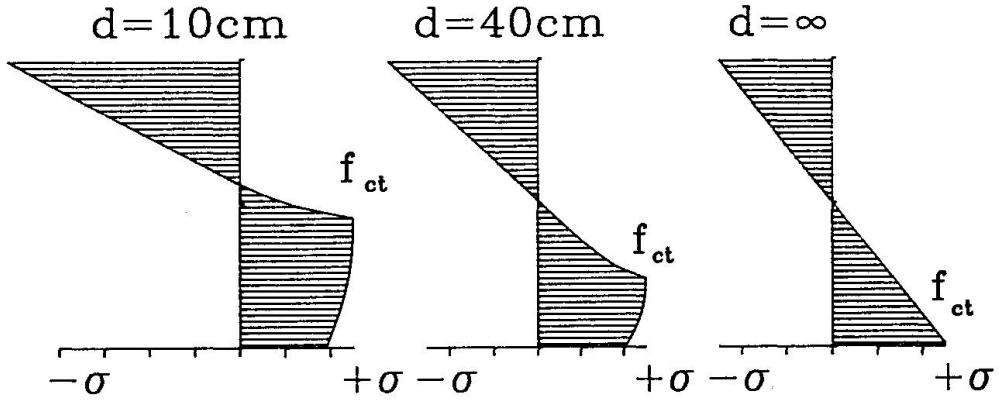

Fig. 17: Stress distribution for different beam depth

The extension of the redistribution zone depends on the σ-w-relation. The relative size of this zone is small for big beam depth and for small eccentricities.

The increase in flexural strength depends not only on the depth but to the same extend on the eccentricity and on the material properties. Even in this very simple case it is impossible to describe the size effect by a simple equation depending only on a geometrical parameter e.g. the depth of the beam. Generalized for other cases it must be concluded that any equation describing the size effect only with ageometrical parameter is a pure approximation of the real behavior.

6. BASIC CONCEPT FOR USING CONCRETE TENSILE STRENGTH

Whether the concrete tensile strength can be used or not depends essentially on the post peak response of the structural member. It must be distinguished between a pre-announced and an abrupt failure without any warning. In most cases the pre-announcements are visible cracking or unusually increasing deformations. In the first case one can hardly trust in the concrete tensile strength. In the second case the tensile strength may be used.
To decide whether there will be a gradual or sudden drop in bearing capacity the deformation behavior of concrete has to be calculated. In the case of pure tension this can be done using the material models as described in this paper.

There are some cases where the tensile strength of concrete is already used. It is known from experience that we can trust in the tensile strength, for instance in the case of very thin slabs or anchorage of reinforcement bars. The analysis of these cases shows that the redistribution zone is large compared to the total loaded area.

Large stress redistribution capacity leads to a large deformation before and after the peak load is reached. In this case tensile strength of concrete may be used. The redistribution zone may be large due to the geometry and/or due to the material behavior.
In cases where the redistribution zone is large due to the geometry, the tensile strength is often unwittingly made use of. Here, the advanced material models may be used for better understanding.

The other application - and perhaps the most interesting one - is whether or not one can predict a small or large redistribution zone in a given situation and whether or not one can rely on the tensile strength in said situation.

There is a very steep decay in the first branch of the σ-w-relation. In many cases this also leads to a steep decay in the load deformation curves of structural members made of plain concrete.

With the knowledge of the reason of sudden or gradual failure new advanced concrete mixtures can be found which exhibit a less steep decay in the bearing capacity after the first cracking (e.g. the admixture of fibers).

7. CONCLUSIONS

To describe the behavior of tension loaded members both the tensile strength and the deformation capacity is needed. In most cases it is much more important how the concrete behaves after cracking than to know the stress at which the first crack occurs. A concrete should not be judged by his strength only. The ductility represented by the fracture energy is as important as the strength, in some cases even more important.

References

[1] Petersson P.-E.:Crack growth and development of fracture zones in plain concrete and similar Materials. Report TVBM-1006, Thesis, Div. of Building Materials, Univ. of Lund Sweden, 1981.

[2] Gustafsson, P.J.: Fracture Mechanics Studies of nonyielding materials like concrete. Report TVBM-1007, Thesis, Div. of Building Materials, Univ. of Lund Sweden, 1985.

[3] Gopalaratnam, V.S.; Shah, S.P.: Softening response of plain concrete in direct tension. ACI Journal, 82-27, pp. 310-323, 1985.

[4] Cornelissen, H.A.W.; Hordijk, D.A.; Reinhardt, H.W.: Experiments and theory for the application of fracture mechanics to normal and lightweight concrete. Contributions international conference on fracture mechanics of concrete, Lausane, 1-3 October, 1985.

[5] Duda, H.: Bruchmechanisches Verhalten von Beton unter monotoner und zyklischer Zugbeanspruchung. Thesis, Institut fur Massivbau, TH Darmstadt, 1990.

[6] Rots, J.G.; Nauta, P.; Kusteres, G.M.A.; Blaauwendraad, J.: Smeared crack approach and fracture localization in concrete. Heron 30(1), Delft, 1985.

[7] Gylltoft, K.: Fracture mechanics model for fatigue in concrete. RILEM Materials and Structures, 17(97), pp. 55-58, 1984.

[8] Reinhardt, H.W.; Cornelissen, H.A.W.; Hordijk, D.A.: Tensile test and failure analysis of concrete. Journal of Structural Engineering, 112(11), 1986.

[9] Rüsch, H.: Die Ableitung der charakteristischen Werte der Betonzugfestigkeit. Beton (2), pp.55-58, 1975.

[10] Mihashi, H.; Wittmann, F.H.; Simonin, P.: Rokugo, K.: Fracture energy evaluation of concrete with compact tension testes. Proc. 9th Ann. Meeting of Japan Concrete Institut, Vol. 9-2, pp. 657-662, 1987.

[11] Wolinski, S.; Hordijk, D.A.; Reinhardt, H.W.; Cornelissen, H.A.W.: Influence of aggregate size of fracture mechanics parameter of concrete. Int. J. Cement Composites and Lightweight Concrete, 9(2), pp. 95-103, 1987.

[12] Kleinschrodt, H.D.; Winkler, H.: The influence of the maximum aggregate size and the size of specimen on fracture mechanics parameter. Fracture Toughness and Fracture Energy, F.H. Wittmann (editor), pp. 137-148, Elsevier, 1986.

[13] Roelfsta, P.E.; Wittmann, F.H.: Numerical method to link strain softening with failure of concrete. Fracture Toughness and Fracture Energy, F.H. Wittmann (editor), pp.163-175, Elsevier, 1986.

[14] Wittmann, F.H.; Rokugo, K.; Bruhwiler, E. Mihashi, H.; Simonin, P.: Fracture energy and strain softening of concrete as determined by means of compact tension specimens. Materials and Structures, (21), pp. 21-32, 1987.

[15] Carpinteri, A.; Gerrara, G.; Melchiorri, G.: Single edge notched specimen subjected to four point shear. Fracture of Concrete and Rock, S.P. Shah and S.E. Swartz (editor), pp. 605-614, Elsevier, 1989.

[16] Getto, R.; Bažant, Z.P.; Karr, M.E.: Fracture Properties and Brittleness of High Strength Concrete. Report No.89-10/B627f, Center for Advanced Cement-Based Materials, Northwestern University, Evanston, 1989

[17] Hordjik, D.A.; Van Mier, J.G.M.; Reinhardt, H.W.: Material Properties. RILEM Report, Fracture Mechanics of Concrete, L. Elfgren (editor), pp. 67-127 Chapman and Hall, 1989.

Leere Seite
Blank page
Page vide

Strain Softening under Bi-Axial Tension and Compression

Résistance du béton en cas de traction bi-axiale et de compression

Zweiaxiale Druck-Zug-Festigkeit gerissenen Betons

Tada-aki TANABE
Professor
Nagoya Univ.
Nagoya, Japan

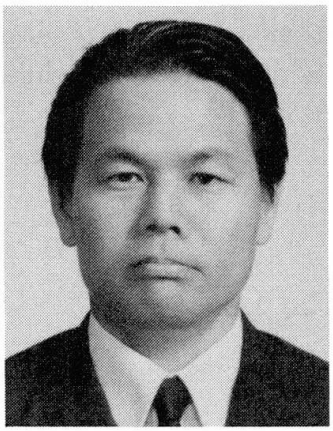

Since 1971, senior researcher at the Central Research Institute of Electric Power Industry. Since 1984, Professor in the Department of Civil Engineering, Nagoya University.

Zhishen WU
Res. Assoc.
Nagoya Univ.
Nagoya, Japan

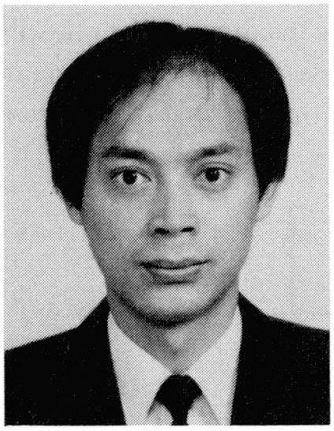

Obtained Dr. of Engineering degree at Nagoya University in 1990. Since then, research associate in the Department of Civil Engineering, Nagoya University.

SUMMARY

Strength criteria of concrete exhibiting strain softening have been derived based on a simple constitutive equation with much emphasis on the compressive strength reduction due to the tensile damage in the direction orthogonal to the compressive axis. The main experiments performed in Japan relating to the problem are described. Comparison of the theoretical reduction of the strength with the experimental data is made.

RÉSUMÉ

Les critères de résistance du béton dans le cadre du champ d'affaiblissement des contraintes ont dérivé d'une équation constitutive simple, où le point est mis sur l'abaissement de la résistance en compression. Celle-ci est due aux effets des efforts de traction dans la direction perpendiculaire à la direction de compression. Les expériences principalement effectuées au Japon à ce sujet sont présentées. Les données expérimentales obtenues sont comparées à la réduction théorique de la résistance.

ZUSAMMENFASSUNG

Es wurden einfache konstitutive Gleichungen für die Festigkeitskriterien von Beton gegeben, die besonders die Abnahme der Betondruckfesigkeit infolge Querzug und Rissbildung berücksichtigen. Die wichtigsten der in Japan durchgeführten Versuche zu diesem Problem werden vorgestellt, und es wird über die Vergleiche mit den theoretisch ermittelten Festigkeitsanwendungen berichtet.

1. INTRODUCTION

The research works related to the strength criteria or the failure surfaces in multi-axial stress states have advanced today to a substantial extent. However, most of these works are focused on the stress condition up until concrete reaches the maximum strength whether the stress may be in compression or in tension. Unlike the metallic material to which theoretical consideration for concrete constitutive equation owes to a great extent, the concrete material experiences strain softening after reaching its maximum point. The situation is same both for the compression failure and for tension failure.

It is well known that once concrete gets into the strain softening region, the stress strain relation becomes size dependent due to the strain localization. In the above situation, we naturally consider that the maximum strength will be different for the same amount of constraining stress to the transverse direction when one of the constraining stress is in elastic range while the other is in the softening range. The stress situation is shown in Fig.1.

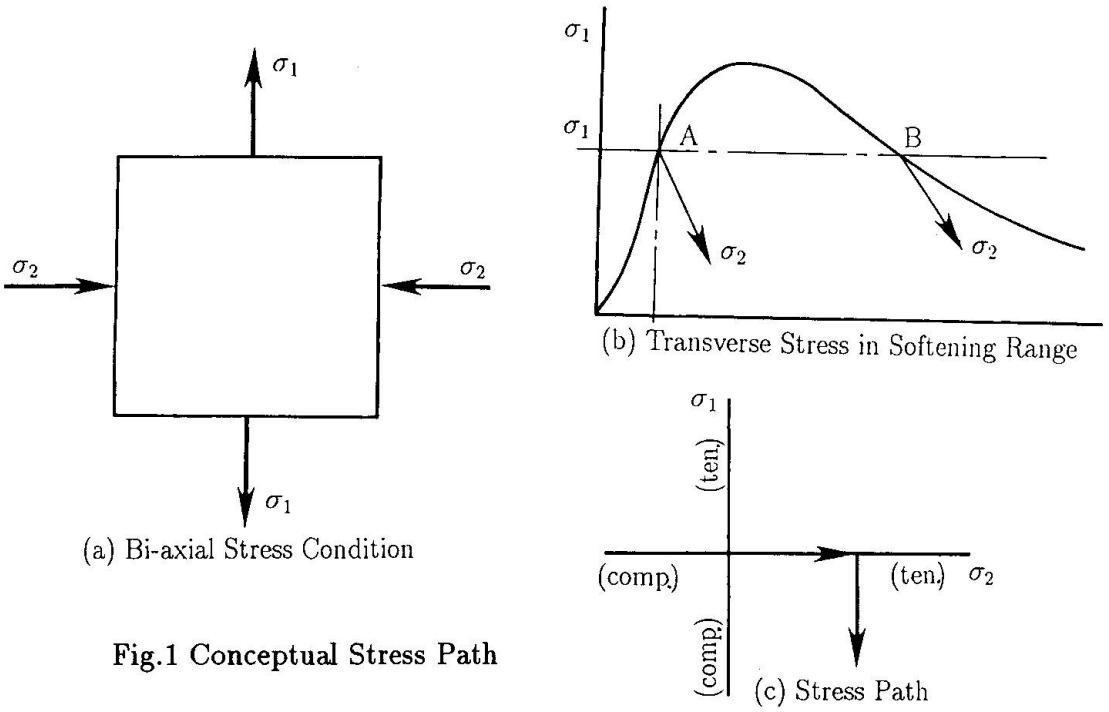

(a) Bi-axial Stress Condition

(b) Transverse Stress in Softening Range

(c) Stress Path

Fig.1 Conceptual Stress Path

The stress distribution of this kind is often encountered in shear problems of beams, walls and so on and it is generally recognized that the strength criteria for this situation is vitally important for the estimation of load bearing capacity. At present moment, the strength criteria for bi-axial tension and compression stress field in the softening zone is represented in terms of tensile strain in the transverse direction basing on the experimental results[1],[7],[8],[9],10]. However, it is desirable that the same characteristics may be expressed in more consistent way.

The current models proposed in CEB code[2] for the constitutive equation are essentially either homogeneous isotropic or orthotropic nonlinear elastic and they refer to the maximum stress point and do not refer to the strength reduction when the orthogonal stress is on the softening branch.

In other words, maintaining tensile stress σ_1 at point A in Fig.1-b and let require the maximum compressive strength of σ_2. The current constitutive equation can predict it rather accurately. However, σ_1 is maintained at point B in Fig.1-b and let require the maximum compressive strength of σ_2. It may not be altogether so well predictable.

With these reasons, they are not considered to fit for expressing above mentioned physical properties of concrete.

To cope with this problem, the adoption of work hardening and strain softening plasticity may be fitted[3]. However, the most rigorous work hardening and strain softening plasticity model which takes into account the strain localization may again have a difficulty for the adoption in this case since the tensile strain induced by the extension of buried-in reinforcement becomes appreciable amount, for example, 5000×10^{-6}, and the situation is different from simple tension. It is obvious that the strain softening and the strain localization in this case have been so much dispersed. With these reasons, the fracture energy based plasticity formulation is not applicable when we try to treat it in an average way.

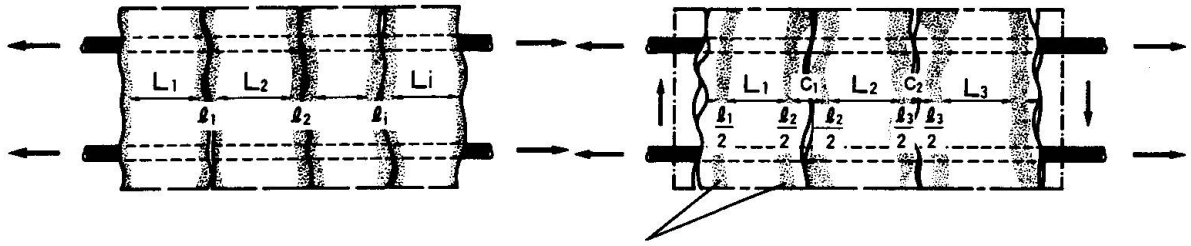

(a) Pure Tension (b) Tension and Shear

Fig.2 Reinforcement Induced Strain Fields of Concrete

Suppose,we have a uniaxial tension member as shown in Fig.2-a. It is clear that we have several zones which are in strain softening fields and the same number of zones which are in elastic fields. The average tensile strain there, then, are written as

$$\varepsilon_n = \frac{1}{\ell}\left[\sum_i \int_0^{Li} \varepsilon_e dx + \sum_j \int_0^{\ell j} \varepsilon_p dx + \sum_k w_k\right] \tag{1}$$

where ε_e and ε_p denote tensile strains in elastic regions and in softening regions respectively. The term w_k denotes kth crack width.

In the practical purpose of expressing concrete strength in the softening region,the averaged strain of the first and second term of Eq.(1) are important except for those cases when the detailed stress analysis which distinguishes the tensile strain in the softening zone and the strain in other zones are carried out.

When shear transfer occurs at a crack, the strain softening region is forced back to the central portion by the compression zone which has been induced by shear friction and the elastic tensile zone may be occupying the central portion. More detailed discussion will be found in the reference[4]. In consequence, the tensile strain distribution is considered to be more uniform, localization being less effective due to the existence of reinforcement. In this sense, we may be

able to adopt the simpler work hardening and softening plasticity model.

In this report, we will try to express the strength criteria in these situation by hardening and softening plasticity so that the simple and more consistent strain and stress relation may become possible without considering the strain localization.

2. Theoretical Consideration

2.1 Plastic Strain Formulation

The present formulation follows essentially the basic concept of the classical theory of hardening plasticity for the sake of its simplicity. The position of the subsequent failure surface is assumed to change its size continuously depending on the damage accumulated in the concrete material, i,e. the failure surface is a function of the plastic work $\omega(W^p)$.

$$f = f(\sigma_{ij}, \omega(W^p)) = 0 \tag{2}$$

where W^p denotes the plastic work accumulated after the initial failure, and σ_{ij} denotes the Cauchy's stress tensor. An independent function, i.e. plastic potential function g is defined as

$$g = g(\sigma_{ij}, \omega(W^p)) = 0 \tag{3}$$

Generally, the application of the classical plasticity theory implies that the total strain rate is composed of the elastic and the plastic part

$$\dot{\varepsilon}_{kl} = \dot{\varepsilon}^e_{kl} + \dot{\varepsilon}^p_{kl} \tag{4}$$

The plastic strain rate tensor then, is assumed to be from the plastic potential g as

$$\dot{\varepsilon}^p_{kl} = \lambda \frac{\partial g}{\partial \sigma_{kl}} \tag{5}$$

while the elastic strain rate tensor ε^e_{kl} is assumed to be related to the stress rate tensor via the elasticity tensor D^e_{ijkl}

$$\dot{\sigma}_{ij} = D^e_{ijkl}\dot{\varepsilon}^e_{kl} \tag{6}$$

where λ is a non-negative multiplier which can be determined from the consistency condition during loading.

Consequently, the consistency condition $\dot{f} = 0$ can be expressed as

$$\dot{f} = \frac{\partial f}{\partial \sigma_{ij}}\dot{\sigma}_{ij} + \frac{\partial f}{\partial W^p}\dot{W}^p \tag{7}$$

where $\dot{W}^p$ can be written as

$$\dot{W}^p = \sigma_{ij}\dot{\varepsilon}^p_{ij} \tag{8}$$

Substituting Eqs.(4),(5),(6) and (8) into Eq.(7) and solving for λ , yields

$$\lambda = \frac{\frac{\partial f}{\partial \sigma_{ij}} D^e_{ijkl} \dot{\varepsilon}_{kl}}{\frac{\partial f}{\partial \sigma_{mn}} D^e_{mnpq} \frac{\partial g}{\partial \sigma_{pq}} + h} \tag{9}$$

with a definition of

$$h = -\frac{\partial f}{\partial W^p} \sigma_{ij} \frac{\partial g}{\partial \sigma_{ij}} \tag{10}$$

Note that $\partial f/\partial W^p$ in Eq.(7) and Eq.(10) will be a negative value for the hardening behavior and a positive value for the softening behavior. As in the classical theory of plasticity, the subsequent yield surface can be expressed with multiparameter $\xi_1, \xi_2, \ldots, \xi_i, \ldots$

$$f(\sigma_{ij}, \xi_1(\omega), \xi_2(\omega), \cdots, \xi_i(\omega), \cdots) = 0 \tag{11}$$

Here, a series of these parameters are assumed to be unique functions of the damage parameter ω and defined to characterize the shape and size of the yield surfaces. The initial loading surface is assumed to coincide with the elastic limit surface. The subsequent yield surface expands with the increase of inelastic strains in hardening. After a state of stress reaches the ultimate condition named as the initial failure surface, the subsequent yield surface will begin to reduce its size continuously until it reaches the final failure state named as the final failure surface.

The function $\partial f/\partial W_p$ can be elaborated, then as

$$\frac{\partial f}{\partial W^p} = \left(\frac{\partial f}{\partial \xi_1}\frac{\partial \xi_1}{\partial \omega} + \frac{\partial f}{\partial \xi_2}\frac{\partial \xi_2}{\partial \omega} + \cdots + \frac{\partial f}{\partial \xi_i}\frac{\partial \xi_i}{\partial \omega} + \cdots\right)\frac{\partial \omega}{\partial W^p} \tag{12}$$

2.2 Definition of the Damage Parameter

Before discussing the damage parameter, let recall the concept of effective stress σ_e and effective plastic strain ε_p[5]. An effective plastic strain rate $\dot{\varepsilon}_p$ is defined in relation with the plastic work rate $\dot{W}_p$ as

$$\dot{W}^p = \sigma_{ij}\dot{\varepsilon}^p_{ij} = \sigma_e \dot{\varepsilon}_p \qquad (\dot{\varepsilon}_p > 0) \tag{13}$$

It is easily found that the single effective stress- effective plastic strain curve should preferably be reduced to a uniaxial stress-strain curve for a uniaxial stress test.

The damage parameter defines the damage of the material accumulated due to the progressive growth of the micro cracks etc., which is defined for convenience, in the form of

$$\omega = \frac{\beta}{\sigma_e \varepsilon_0} \int dW^p \tag{14}$$

where, β is a material constant, and

$$\varepsilon_0 = \frac{f'_c}{E_c} \tag{15}$$

Here, E_c denotes the modules of elasticity of concrete, and f'_c is the uniaxial compressive strength. Substituting Eq.(12) into Eq.(13), we have

$$\omega = \beta \int d\varepsilon_p/\varepsilon_0 \tag{16}$$

2.3 Application of Drucker-Prager Type Failure Surface

Although more sophisticated criteria may be preferable for simplicity, the following Drucker-Prager type yield criterion is employed for its simplicity.

$$f = \sqrt{J_2} + \alpha_f I_1 - k_f = 0 \tag{17}$$

Besides, a similar expression for the plastic potential function is assumed as

$$g = \sqrt{J_2} + \alpha_g I_1 - k_g = 0 \tag{18}$$

where $I_1 = \sigma_{kk}$ and $J_2 = \frac{1}{2} s_{ij} s_{ij}$ are the first invariant of stress tensor σ_{ij} , and the second invariant of deviatoric stress tensor s_{ij}, respectively, and α_f ,k_f, α_g and k_g are material constants.

Since it is known that the Mohr-Coulomb criterion is simple with constants of a clear physical meaning which are related to the uniaxial strength straightforwardly, the Drucker-Prager cone is matched with it such that two surfaces are made to agree along the compressive meridian. In this case, the two sets of material constant are related by

$$\alpha_f = \frac{2sin\phi^*}{\sqrt{3}(3 - sin\phi^*)}, k_f = \frac{6c^* cos\phi^*}{\sqrt{3}(3 - sin\phi^*)} \tag{19}$$

where ϕ^* and c^* are two strength parameters in the Mohr-Coulomb criterion, namely the so-called mobilized friction angle and mobilized cohesion [6], and the notation '*' is introduced to indicate that ϕ^* and c^* are not constant but depend on the plastic strain history through the damage parameter ω. In spite of the paucity of experimental data to support the definition of the damage parameter ω , we are able to say something about the dependence of ϕ^* and c^* on ω . The value of ϕ^* generally should be an ascending function of ω, while c^* may be expected to be a descending function of ω. Possible relations for the hardening and softening model are suggested as follows

$$c^* = cexp[-(m\omega)^2] \tag{20}$$

$$\begin{cases} \phi^* = \phi_0 + (\phi - \phi_0)\sqrt{2\omega - \omega^2} & \omega \leq 1 \\ \phi^* = \phi & \omega > 1 \end{cases} \tag{21}$$

where, m is a material parameter. The notations c and ϕ denote the cohesion and the internal-friction angle of the concrete respectively. All of these relations are shown in Fig.3.

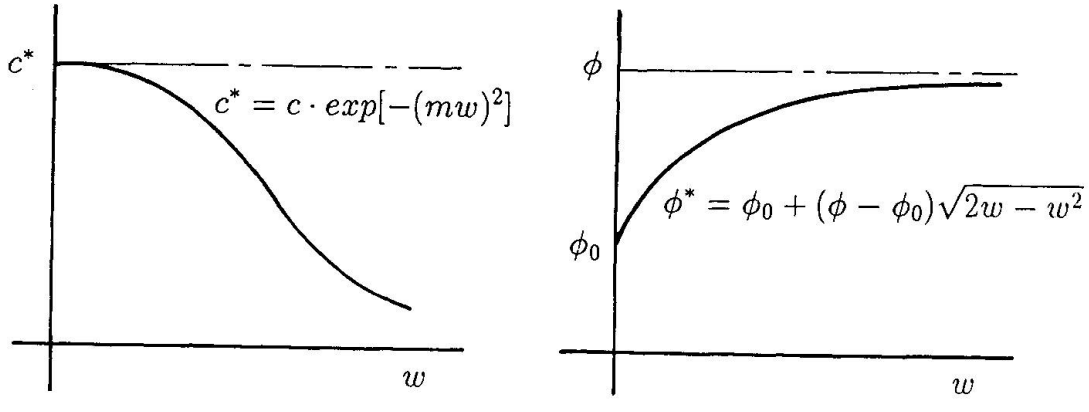

Fig.3 Possible Relations of $c^* - w$ and $\phi^* - w$

Similarly, we defined

$$\alpha_g = \frac{2sin\psi^*}{\sqrt{3}(3 - sin\psi^*)}, k_g = \frac{6c^*cos\psi^*}{\sqrt{3}(3 - sin\psi^*)} \tag{22}$$

with a defined mobilized dilatancy angle ψ^* . It is noted that for $\psi^* = \phi^*$, we have $f = g$ and the classical associated flow rule is recovered.

2.4 Flow Rule

The associated flow rule is applied predominantly for practical reasons, since no experiments have been conducted on subsequent loading surfaces for concrete materials. For associated flow rule, it is interesting to note the plastic work rate is

$$\dot{W}^p = \sigma_{ij}\dot{\varepsilon}^p_{ij} = \lambda\sigma_{ij}\frac{\partial f}{\partial \sigma_{ij}} = \lambda\sigma_{ij}\frac{\partial F}{\partial \sigma_{ij}} = \lambda nF \tag{23}$$

when $F(F = f + k)$ is homogeneous of degree n in the stresses, as it is for many cases in plasticity theories. The scalar function λ can be obtained by squaring each of the terms in Eq.(5) and adding as

$$\dot{\varepsilon}^p_{ij}\dot{\varepsilon}^p_{ij} = \lambda^2\frac{\partial F}{\partial \sigma_{ij}}\frac{\partial F}{\partial \sigma_{ij}} \tag{24}$$

Taking the square root of both sides and substituting λ into Eq.(23) shows that $\dot{\varepsilon}_p$ must be a function of F and $\sqrt{\dot{\varepsilon}^p_{ij}\dot{\varepsilon}^p_{ij}}$

$$\dot{\varepsilon}_p = \frac{\dot{W}^p}{\sigma_e} = \frac{\sqrt{\dot{\varepsilon}^p_{ij}\dot{\varepsilon}^p_{ij}}nF}{\sqrt{(\frac{\partial F}{\partial \sigma_{mn}})(\frac{\partial F}{\partial \sigma_{mn}})}\sigma_e} \tag{25}$$

where we have used the definition of plastic work(Eq.(13)) for defining the effective plastic strain ε_p. For the Drucker-Prager failure surface, the effective stress for the failure function can be obtained by substituting the uniaxial compressive stress condition into the function

$$\sigma_e = \frac{\sqrt{J_2} + \alpha_f I_1}{(\sqrt{1/3} - \alpha_f)} = \frac{k_f}{(\sqrt{1/3} - \alpha_f)} \tag{26}$$

By substituting Eq.(26) into Eq.(25), Eq.(25) can be reduced to

$$\dot{\varepsilon}_p = \frac{(-\alpha_f + 1/\sqrt{3})}{\sqrt{3\alpha_f^2 + 1/2}}\sqrt{\dot{\varepsilon}^p_{ij}\dot{\varepsilon}^p_{ij}} \tag{27}$$

Depending on the preceding discussion, $\partial f/\partial W^p$ in Eq.(12) for the Drucker-Prager criterion can be rewritten as

$$\frac{\partial f}{\partial W^p} = (\frac{\partial f}{\partial \alpha_f}\frac{\partial \alpha_f}{\partial \omega} + \frac{\partial f}{\partial k_f}\frac{\partial k_f}{\partial \omega})\frac{\partial \omega}{\partial W_p} = (I_1\frac{\partial \alpha_f}{\partial \omega} - \frac{\partial k_f}{\partial \omega})\frac{\partial \omega}{\partial W^p} \tag{28}$$

Here,

$$\frac{\partial \alpha_f}{\partial \omega} = \frac{2\sqrt{3}cos\phi^*}{(3-sin\phi^*)^2}\frac{\partial \phi^*}{\partial \omega} \tag{29}$$

$$\frac{\partial k_f}{\partial \omega} = \frac{6c^*(1-3sin\phi^*)}{\sqrt{3}(3-sin\phi^*)^2}\frac{\partial \phi^*}{\partial \omega} - \frac{12cm^2\omega}{\sqrt{3}(3-sin\phi^*)}e^{-(m\omega)^2}cos\phi^* \tag{30}$$

and

$$\frac{\partial \phi^*}{\partial \omega} = \begin{cases} \frac{(1-\omega)(\phi-\phi_0)}{\sqrt{2\omega-\omega^2}} & \omega \leq 1 \\ 0 & \omega > 1 \end{cases} \tag{31}$$

Moreover,

$$\frac{\partial \omega}{\partial W^p} = \frac{\beta}{\varepsilon_0 \sigma_e} \tag{32}$$

2.5 The c and ϕ Factors Affected by The Damage Parameter ω

The relation between the damage parameter ω and the c, ϕ will not be set in a unique way. At present study,however, we adopted the above mentioned equation. In these formulations, ω and c, ϕ change as shown in Fig.3 depending on the value of ω. The movement of failure surface with the increase of damage ω is shown in Fig.4 conceptually.

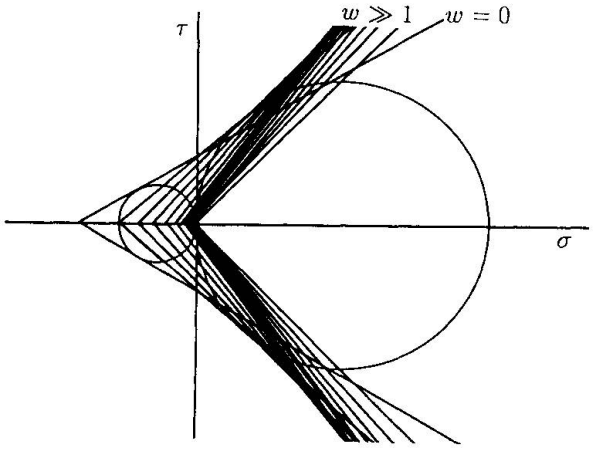

Fig.4 The Movement of Failure Surface

Looking at the figure, it may be understood that the maximum uniaxial compressive strength will be given by the circle which will make tangential contact with one of the lines with the maximum radii.

It is possible to select other relations between the damage parameter and failure parameter of c, and ϕ. As an example, several of the experimental data are compared in Fig.5 with the above mentioned criteria and reasonable agreement will be seen in the comparison for different loading paths.

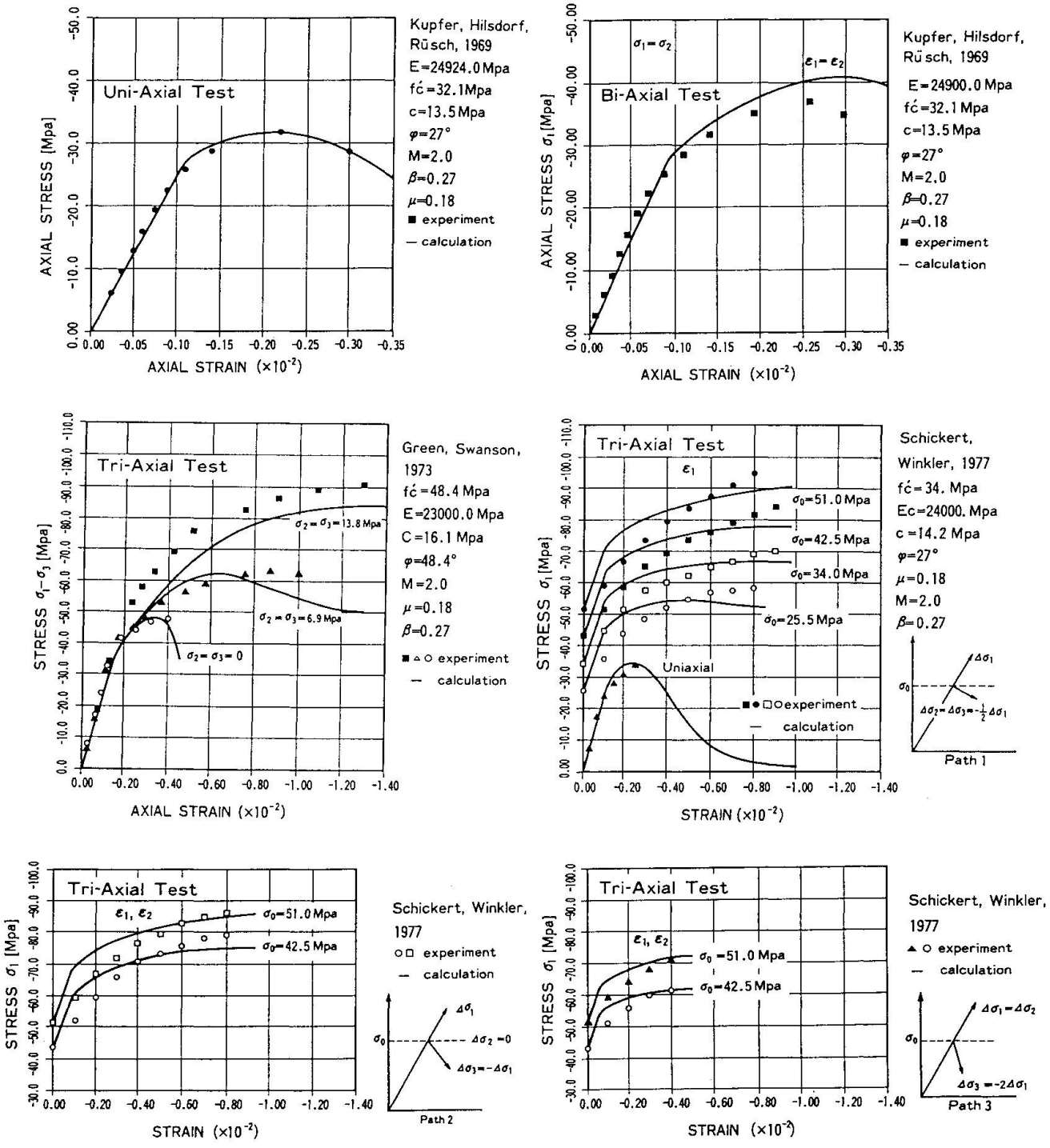

Fig.5 Comparison of Calculation and Experiments of Various Stress Paths

3. Experimental Results for The Bi-axial Tension and Compression

3.1 Vecchio and Collins' Test

In the beginning, it should be mentioned that those test results which are treated in this section are by no means bi-axial tension and compression test in its true sense. However,as mentioned in previous section, we try to utilize the results in the average sense and apply the theoretical criteria for those experimental results. At present moment, we have several experimental results for the stress field where one principal stress is in tension of the strain softening zone and the other principal stress is in compression, since the appearance of Vecchio and Collins reports[1] on the load carrying capacity of the panels subjected to in-plane shearing load. In that argument, treating the concrete element between the parallel cracks in uniformly stressed condition, he proposed the compressive strength reduction according to the amount of tensile strain to the transverse direction. The strength reduction was found to be the vital material characteristic which should be clarified to the detail since the strength of the member in shear depends upon the strength to such an extent. His proposal of strength reduction was as such that

$$\lambda = \frac{1}{0.80 + 0.34\left(\frac{\varepsilon_{1u}}{\varepsilon_0}\right)} \tag{33}$$

where ε_0 denotes the uniaxial compressive strain corresponding to the uniaxial compression strength of cylinder and ε_{1u} denotes the transverse tensile strain occurring.

3.2 Maekawa and Okamura's Test

In Japan, several experiments relating on this problem have been performed. Maekawa and Okamura[7] performed bi-axial tension and compression test using the cylindrical specimen. Inside the cylinder, water pressure was generated and ring tension was induced. The compressive strength,then obtained by the axial compression. They proposed the compressive strength reduction in the following form,

$$\begin{aligned} \lambda &= 1.0 && (\varepsilon_1 < \varepsilon_a) \\ &= 1.0 - 0.4\tfrac{\varepsilon_1 - \varepsilon_a}{\varepsilon_b - \varepsilon_a} && (\varepsilon_a \le \varepsilon_1 \le \varepsilon_b) \\ &= 0.6 && (\varepsilon_0 < \varepsilon_1) \\ \varepsilon_a &= 0.0012 \\ \varepsilon_b &= 0.0044 \end{aligned} \tag{34}$$

where ε_1 is the transverse tensile strain.

3.3 Sumi and Kawamata's Test

Sumi and Kawamata[8] has performed the most comprehensive experiment on the stress strain relation of cracked reinforced concrete panel elements using the specimens and the loading apparatus shown in Fig.6. For the equal reinforcement ratio in two orthogonal directions, they obtained the relation in the form of Eq.(35). They could measure the strain directly which corresponds to the first and second term of the Eq.(1) and the stress was calculated from the equivalence of the force to two directions.

$$\frac{\sigma_1}{f'_c} = f(\varepsilon_1)\left(1.5 + \frac{\varepsilon_{cr}}{\varepsilon_0}\right) - \left(\frac{\varepsilon_1}{\varepsilon_0}\right)^2 \tag{35}$$

where f'_c: uniaxial compressive strength of cylinder, ε_0: compressive strain which corresponds to f'_c, σ_1: compressive stress of cracked element, ε_1: compressive strain which corresponds to σ_1, and ε_{cr}: compressive strain of cracked element when transverse cracking initiated.

For the panels of unequal reinforcement ratio, the shear stress is transferred across the crack surfaces which add another factor for the stress strain relation in the cracked concrete element. With the similar method, they calculated the stress and strain. Finally, they proposed for this case the following equation.

$$\frac{\sigma_1}{f'_c} = \lambda f(\varepsilon_1)$$

$$\lambda = \frac{\left(4\frac{\sigma_2}{f'_c} + \frac{\sigma 1-max}{f'_c}\right)}{\left(\frac{\sigma_{1-max}}{f'_c}\right)} \tag{36}$$

where σ_2 denotes the stress in transverse direction while other notations appeared in Eq.(35).

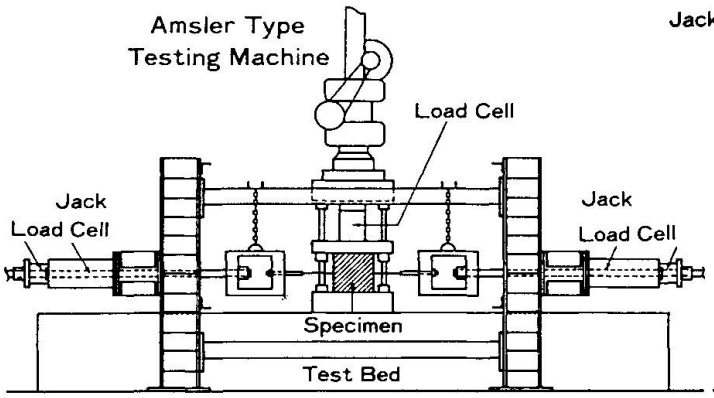

Fig.7 Shirai's Testing Method

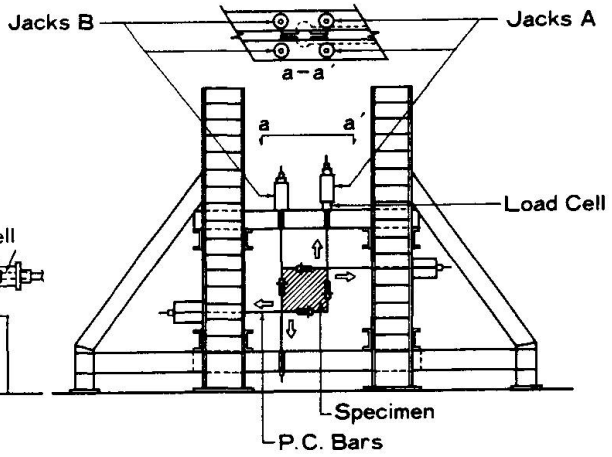

Fig.6 Sumi's Testing Method

The equation, however, gives higher strength when the orthogonal stress is in higher tension. In other word, this is contrary to the tendency reported in the past that the strain get larger, the stress is more reduced in the softening range and the strength in compression get smaller.

3.4 Shirai's Test

Shirai[9] performed experiment with the small specimen shown in Fig.7 and proposed the following equation.

$$\lambda_1 = -\left(\frac{0.31}{pi}\right) tan^{-1}\left[4820\varepsilon_1 - 11.82\right] + 0.84$$

$$\lambda_2 = -5.9\frac{f_{c1}}{f'_c} + 1.0$$

$$\lambda = \lambda_1 \cdot \lambda_2 \tag{37}$$

where f'_{c1} denotes the tensile stress working to the orthogonal direction.

3.5 Noguchi's Test

Noguchi[10] performed similar experiment and concluded the strength reduction in the form of

$$\lambda = \frac{1}{0.27 + 0.96(\frac{\varepsilon_{1u}}{\varepsilon_0})^{0.167}} \tag{38}$$

where ε_{1u} denotes average tensile strain to the transverse direction when the element fails in compression and ε_0 denotes the compressive strain of cylinder which corresponds to the uniaxial compressive strength of cylinder.

3.6 Comparison of the Theoretical Calculation and Results

All the experiments mentioned in the previous section showed that the failure surface shrink with the increase of tensile strain as shown in the Fig.8. It is also expected that the same strength reduction may occur in the softening compression and compression range though there have not been reported any experimental results so far.

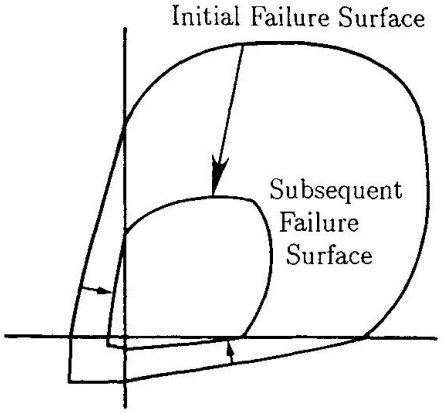

Fig.8 Shrinking Failure Surface

For those experimental results, the plasticity model mentioned in the previous section is applied. The concrete with uniaxial compression strength of 30 Mpa. has been loaded in various loading path. The one which has been the main topics of the present study is to load in uniaxial tension over the maximum point then stop the loading at some point in the softening range and starts to load it in compression to orthogonal direction keeping the damage which has been accumulated in previous loading path.

In this study, the accumulated damage ω was continued though the loading direction has changed 90 degrees and the maximum compression strength was calculated. Strength reduction which depend on the ratio are obtained and shown in Fig.9 in comparison with the experimental results which is the reproduction of Shirai's experimental results, however, being recalculated so that the strain of the coordinate be the 1st and second term of Eq.(1).

It may be seen that the reduction is in accordance with those proposed in the strain range

of 0 to 5000 $\times$ 10^{-6}. This is the numerical simulation for the purpose to show that the simple model proposed enable to trace the post peak strength reduction in reasonable way. However,it is true yet that we need more detailed study to relate modeling parameter with the actual condition of cracked reinforced concrete.

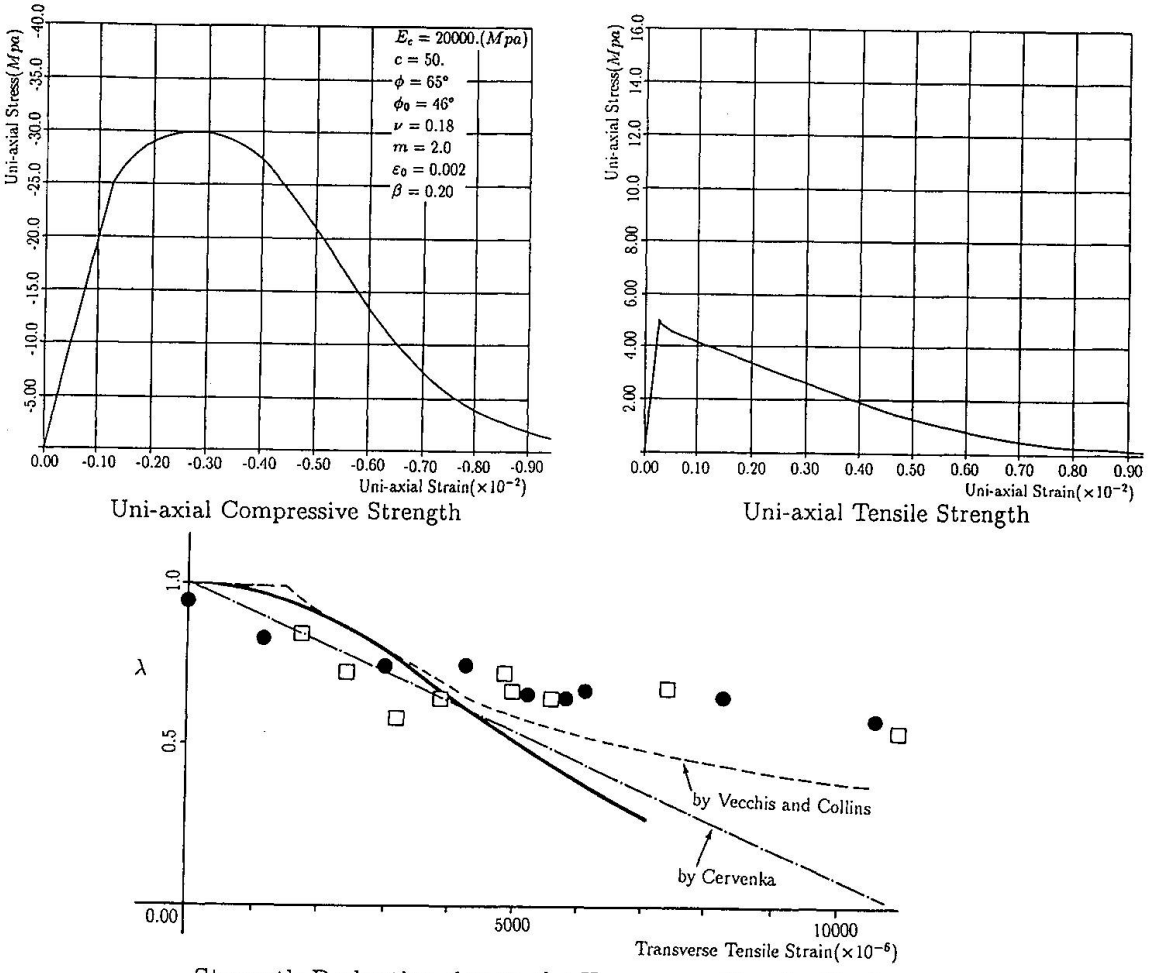

Fig.9 Strength Reduction Calculated

4. Conclusion

In the limit state design of reinforced concrete, it is paramount requisite to make a good estimate of the ultimate load carrying capacity of structures. For commonly met structures like beams, slabs and walls, the concrete behavior in bi-axial tension and compression stress field has a substantial effect for their load carrying capacity especially when shear effect is predominant. The compressive strength reduction in one of the principal direction when the orthogonal tension is occurring to the other principal direction has been the phenomena that draw concrete engineer's attention. As the tensile strain is mainly in the large strain range of softening, which is composed of elastic strain and localizing strain, the stress field is neither easily experimentally measurable nor analytically obtainable. However, we definitely need more comprehensive, consistent and reliable knowledge in that area. The consistent mathematical representation of the phenomena has been made in this study and some numerical examples were shown. However, it is much desired that the more experimental results be accumulated

not only in tension compression area but compression and compression area. Finally, thanks are due to the graduate student K. Taniyama and Ge Hanbin who has carried out the numerical calculation and especially to H. Nagashima for preparing the manuscript in this study.

References

[1] Vecchio,F., and Collins,M.P., The Response of Reinforced Concrete to In-plane Shear and Normal Stresses, University of Toronto, Publication No.82-03 March 1982.

[2] CEB-FIP Model Code 1990 First Draft, CEB Bulletin, No.195, March 1990.

[3] Pramono,E., and Willam,K., Fracture Energy-Based Plasticity Formulation of Plain Concrete, ASCE, EM 1988.

[4] Tanabe,T., and Yoshikawa,H., Constitutive Equation of a Cracked Reinforced Concrete Panel, IABSE Colloquim on Computational Mechanics of Concrete Structures, Delft, pp.17-34.

[5] Chen,W.F., Plasticity in Reinforced Concrete, Mc Grawttill, New York.

[6] Vermeer,P.A., and de Borst,R., Non-Associated Plasticity for Soils and Rock, Heron, 29, No.3, pp1-64.

[7] Okamura,H., and Maekawa,K., Nonlinear Analysis of Reinforced Concrete, Proc. of JSCE, No.360,Aug.1987,pp.1-10.

[8] Sumi,K.,and Kawamata,S., Properties of Cracked Concrete in the RC WallS subjected to In-Plane Shear, Concrete Journal, Vol.27, No.10, JCI, pp.97-107.

[9] Shirai,N..and Noguchi,H., Compressive Deterioration of Cracked Concrete, ASCE Structures Congress and Pacific Rim Engineering, San Francisco, May 1989.

[10] Hamada,S., and Noguchi,H., Basic Experiments the Degradation of Cracked Concrete under Bi-axial Compression and Tension, The Annual Report of the AIJ, Structures, Oct.1988, pp.397-398.

Systematic Fracture Mechanics Study of Shear Failure in Beams under Distributed Load

Rupture par cisaillement de poutres sous charge répartie

Bruchmechanische Studie des Schubbruches von Bauteilen unter Gleichlast

Johan BLAAUWENDRAAD
Professor
Delft Univ. of Technol.
Delft, The Netherlands

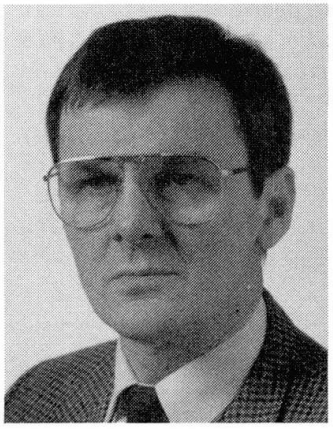

Johan Blaauwendraad, born 1940, obtained his civil engineering degree in 1962 at Delft University. He joined TNO for research, moved to Rijkswaterstaat, obtained his doctor's degree in 1973. Is now professor of Civil Engineering in Delft since 1979.

Q. B. WANG
Doctoral student
Delft Univ. of Technol.
Delft, The Netherlands

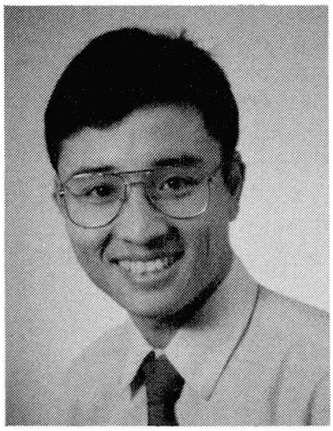

Qing Biao Wang, born 1962, received his civil engineering degree in 1988 at Delft University. He has been carrying out research investigating the shear strength of reinforced concrete beams using the finite element method.

SUMMARY

Shear failure is studied computationally in a systematic way for beams under distributed load with only longitudinal reinforcement. The shear capacity relies mainly on tensile tractions in the governing crack, aggregate interlock and dowel-action being neglectable. Scale effects are simulated correctly. Parameters are slenderness, brittleness, reinforcement ratio and the influence of a simultaneously acting normal compressive force.

RÉSUMÉ

A l'aide de l'ordinateur, la rupture par cisaillement est étudiée systématiquement pour des poutres sous charge répartie ne comprenant qu'une armature longitudinale. La résistance au cisaillement dépend essentiellement des contraintes de traction dans le système de fissuration principal, l'adhérence de la pâte de ciment aux aggrégats et l'effet de goujon des barres d'armature ne jouant qu'un rôle négligeable. Les effets d'échelle sont correctement pris en compte, tandis que les paramètres étudiés sont l'élancement, la fragilité, le pourcentage d'armature et l'action simultanée d'une force de compression axiale.

ZUSAMMENFASSUNG

Schubversagen wird auf numerische Weise systematisch für Träger ausschliesslich verteilter Belastung mit Biegebewehrung untersucht. Die Schubkapazität hängt vornehmlich ab von Zugspannungen in dem bestimmenden Riss. «Aggregate interlock» und «dowel» action können nicht nennenswert beitragen. Massstabeffekte werden gut simuliert. Die untersuchten Parameter sind die Schlankheit, Sprödigkeit, Bewehrungsmass und der Einfluss einer gleichzeitig aktiven Druckkraft.

1. PROBLEM STATEMENT

This study originates from the construction of tunnels of rectangular cross-section crossing rivers and canals.
Rijkswaterstaat (Dutch State Public Works) commissioned the research organisation TNO to execute a number of tests on beams under distributed loading. In these tests 2 parameters have been varied [1]. One is the ratio of the positive mid-span moment and the end-of-span negative moment. So this parameter controls the amount of 'clamping-in'. The other parameter is the ratio of length-of-span and depth. This parameter controls the slenderness of the beams.
In figure 1 five different ratios are shown for the mid-span moment and the end-of-span moment (for a fixed value of the slenderness parameter), together with the crack pattern which occurs. The fat-drawn crack is due to shear failure. In all 5 cases the maximum shear force occurs at the beam end, but the shear failure does not always occur at that place. In stead the failure crack sometimes moves inwards the beam-span. This phenomenon is rather confusing for a designer, who is used to analyzing his diagrams for moments and shear forces and after that considers his structure on a section-by-section basis. In fact he is accustomed to checking the sections in which maximum moments and shear forces occur and to specify reinforcement demand at those positions. This approach appears to be meaningless in the case of a beam under distributed loading, at least for the prediction of the shear capacity.
The aim of the present study is to complete the experimental findings by computational investigations. It is hoped to better understand the available experimental results, but also to find new results for load cases and structures which have not been included in the experiments. In fact, the paper refers strongly to Hillerborgs publication [2].

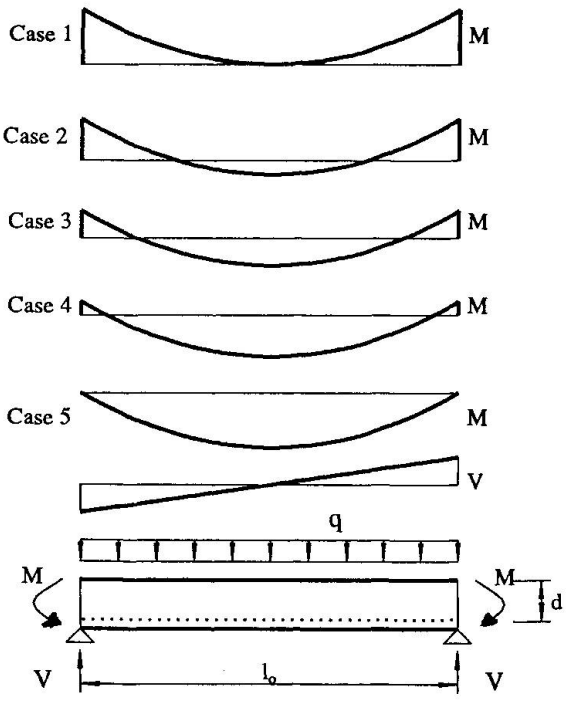

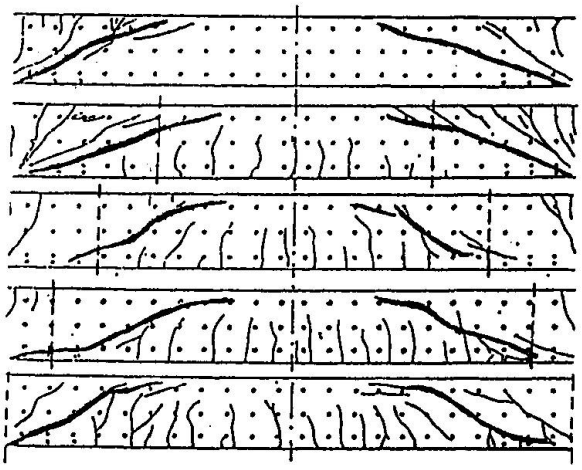

Fig.1
Five different moment lines (5 different moment parameters) and the respective crack patterns of the beams. All beams have the slenderness parameter $l_o/d = 4.5$ and d = 150 mm

2. ANALYSIS METHOD

The study has been started from the view-point of the predictor-corrector method, as proposed by Rots [3]. The program DIANA is used for all analyses.
In a discrete crack three different force transfer mechanisms can be taken into account:
- tensile traction (model Hillerborg)
- aggregate interlock (model Walraven)
- dowel action (results Fenwich)

For the tensile tractions normal to the crack faces a linear softening branch is adopted in the σ-w diagram for the stress σ and crack opening w. The tangent should be close to the value at tensile strength in the real curvilinear softening branch.
The aggregate interlock model of Walraven has been adopted, as reported in [4], which defines the tangential shear stress and the normal compression in a rough crack as nonlinear functions of the crack opening w, the crack-sliding Δ and the concrete compressive strength f_c.
For dowel-action a nonlinear spring has been programmed, whose stiffness is obtained from simulation of the dowel-experiments of Fenwich [5].
From a series of analyses it has been concluded that aggregate interlock and dowel-action do not contribute noticeable to the shear capacity. If the discrete crack is chosen properly (according to what is found in experiments), the crack faces are only loaded by tensile tractions (mode I). Only in the cover layer of concrete a crack-sliding Δ of some importance can occur, but not sufficient to mobilize an important contribution of aggregate interlock and dowel-action to the shear capacity. At peak load these contributions are negligible. They first start to grow after peak load has been reached, but at that time the contribution of the tensile tractions drops down rapidly. The conclusion is that the shear capacity must be fully provided by the tensile softening stresses.

3. PARAMETER STUDY FOR DISTRIBUTED LOAD

From preliminary calculations a number of lessons have been learned. To find a correct failure load the following applies:
- the smeared crack approach correctly simulates the beam stiffness, but is very time-consuming and does not converge properly for all analyses
- the analyses using one single discrete crack do not simulate the stiffness correctly, but predict the ultimate peak load well in short run time
- the crack tip does not reach the compressive zone for the cases studied, and the inclination of cracks is important.
- in a correct crack path no aggregate interlock can develop
- dowel action can only develop after passing of the peak load and can therefor be excluded
- scale effects are due to tensile softening in the crack and to the fact that bond does not follow scaling. Good performance of the model is found if a constant bond-interface is used equal to the beam width.

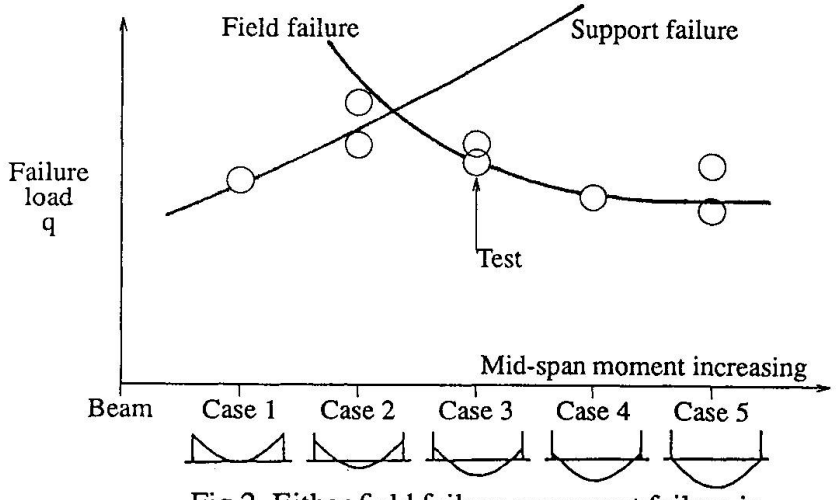

Fig.2. Either field failure or support failure is determining, depending on the moment parameter (the amount of clamping-in)

Starting from these findings a parameter study has been started for beams under distributed loading on basis of the predefined crack approach. When we closely inspect the crack patters in figure 1, it is noticed that two different failure mechanisms can occur, depending on the moment parameter (ratio of end-span moment and mid-span moment). In figure 2 is expressed the expectation that the two different failure types, field failure and support failure, can be studied separately and that for each moment parameter must be determined which one determines the lowest capacity and consequently failure. Test results support this expectation.
In this paper only the field failure is subject of examination. From here the length of the shear span is called *l (the distance between two counter-flexure points)*, the depth of the beam is d, the material property l_{ch} is a characteristic length defined by

$$l_{ch} = \frac{EG_f}{f^2_{ct}}$$

In this expression E is the elasticity modulus, G_f the fracture energy release and f_{ct} the concrete tensile strength. The reinforcement ratio for the longitudinal bottom reinforcement is ρ. The bond is determined by an elasto-plastic τ-Δ diagram. The stiffness in the diagram D and the maximum value of the bond stress τ_{max} are kept constant in all analyses. The width b of the beam is used for the total bond-interface. A normal force N can occur, which yields an additional constant compressive stress σ_N. The following parameters are studied:

(1) Slenderness
$$\frac{l}{d} = 6,9,12$$

(2) Brittleness number
$$\frac{d}{l_{ch}} = \frac{3}{4}, \frac{3}{2}, 3, 6$$

(3) Reinforcement ratio
$$\rho = \frac{1}{2}, 1, 2$$

(4) Axial compression
$$\frac{\sigma_n}{f_{ct}} = 0, 1, 2$$

The computations are all done using a constant reference depth d=1.0 m and width b=1.0 m.

A major decision is the choice of the shape and the position of the predefined crack. The inclination is chosen according to the elastic principle stresses in the centerline of the beam when no axial force is present. This appears to be in close agreement with experiments. A small vertical part is chosen near the longitudinal reinforcement. The length of this part is d/15.
From experiments the position of the cracks can be chosen very convincingly. There is no need to run many smeared crack analyses to produce the same results.
It is not necessary to draw the complete half beam into the computations. A beam part is chosen which roughly extends over a length d to the right and left from the beginning of the crack, and this part is loaded in accordance with the elastic cross-section stresses. A mesh of triangular 3-noded elements is applied in the surroundings of the crack path.
A series of results has been got. In figure 3 the influence of the slenderness l/d, the reinforcement ratio ρ and the brittleness number d/l_{ch} on the shear capacity q/q_{ref} is shown in one diagram. The reference load q_{ref} is the maximum load for the combination

$$\frac{l}{d} = 9, \qquad \frac{d}{l_{ch}} = 6 \qquad \text{and } \rho = 1\%$$

The influence of the reinforcement is moderate (about 5% between ρ = 1% and ρ = 2%). Doubling the slenderness from 6 to 12 increases the capacity by about a factor 3. Increase of the brittleness number by a factor 8 from 0.75 to 6 does drop down the shear capacity roughly by 30%. So the most important parameters are the slenderness and the brittleness number.
Figure 4 plots the shear strength against the slenderness l/d for ρ=1% and different d/l_{ch}. It appears that d/l_{ch} does not interfere much with the effect of l/d. Similar observation is obtained for ρ=2%.
Figure 5 has been made to investigate the influence of the reinforcement ratio ρ in a larger domain. The ratio ρ has been varied from 0 to 3 for a beam with

$\frac{l}{d} = 9$, $\frac{d}{l_{ch}} = 3$. Again q_{ref} refers to the combination $\frac{l}{d} = 9$, $\frac{d}{l_{ch}} = 3$ and, ρ = 1%.

Hereby ΣC is chosen to be equal to b for practical reason. For smaller ρ it is a reasonable assumption to reduce ΣC linearly with ρ and for larger ρ the limit value of b is used. In the same diagram is shown the curve according to Zutty and the rule of the Eurocode.
Figure 6 shows the influence of normal compressive stress. It is seen that the influence may modeled with a linear function.

Meanwhile continuing effort is made to conclude on an engineering model, such that designers can understand and use either the model or rules derived from it.

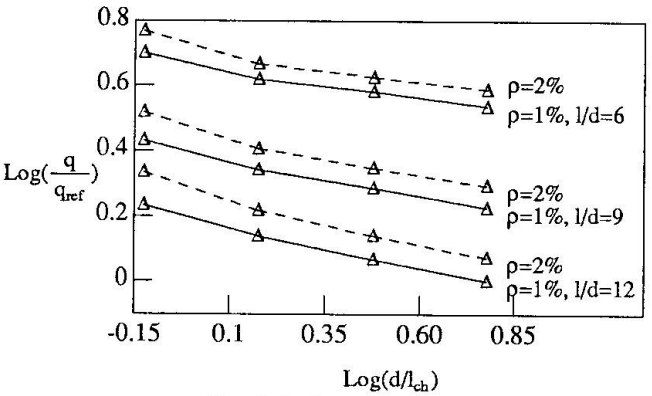

Fig.3. Influence of d/l_{ch}, ρ and l/d
(For q_{ref}: l/d = 12, d/l_{ch} = 6.0, ρ = 1%)

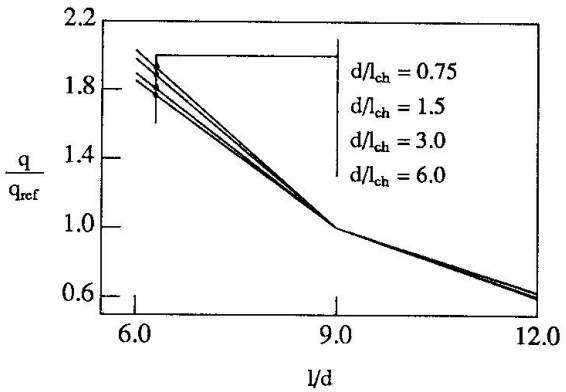

Fig.4. Influence of slenderness l/d
(ρ = 1%, for q_{ref}: l/d = 9)

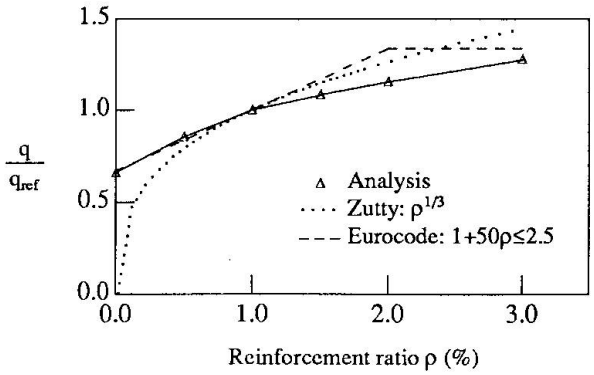

Fig.5. Influence of reinforcement ratio ρ
(l/d=9, d/l_{ch}=3.0, for q_{ref}: ρ = 1%)

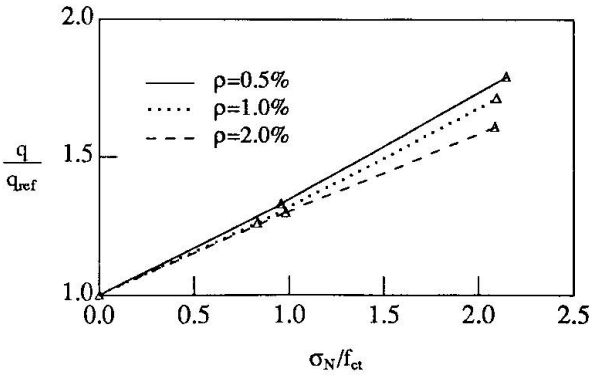

Fig.6. Influence of axial compressive stress
(l/d=9, d/l_{ch}=3.0, for q_{ref}: σ_N = 0)

4. CONCLUSIONS

1. Beams under distributed load and clamped-in conditions can fail in shear in two modes, here called support failure and field failure. The field failure can be modeled as a diagonal cracking failure. The field failures occur at positions which are supprizing to designers. Their convential section by section approach can not be applied in judging the shear capacity of beams.
2. The predictor-corrector method in which a smeared crack approach and a predefined discrete crack path are used sequentially, appears to be a necessary and successful way to predict the diagonal cracking shear failures.
3. The inclination of the predefined crack path must be chosen carefully. Shear failure occurs when the crack is so inclined that it cannot provide sufficient resistance.
4. The effect of dowel-action and aggregate interlock is negligible in the well-chosen crack path. Bond and tension-softening are important factors for shear capacity of diagonal cracking.
5. Size effect can be modelled correctly. The tension softening is most important. Bond has an additional effect.
6. The parameter study for field failure so far has revealed that the brittleness number and the slenderness have significant importance. Doubling the longitudinal reinforcement ratio does not have much effect. In the practical range the order of 10%
7. From continued research it is hoped to derive design rules or engineering models to be applied by designers.

5. ACKNOWLEDGEMENT

The support of prof. R. de Borst and dr. J.G. Rots in this project is highly appreciated.

6. REFERENCES

1. Gijsbers, F.B.J., Monnier, Th.: Analysis of the shear capacity of slabs and beams with a rectangular cross-section.
   Report TNO-IBBC nr. B-78-76/62.3.4003, 1978 (in Dutch).
2. Hillerborg, A.: "Reliance upon concrete tensile strength", Introductory report, proc. of IABSE colloquium on "structural concrete", Stuttgart, 1991.
3. Rots, J.G.: "Computational modeling of concrete fracture", Dissertation, Delft University of Technology, 1989
4. Walraven, J.C.: "Mechanisms of shear transfer in cracks in concrete", Report A26/79-02, Delft University of Technology, Nov. 1978.
5. Fenwich R.C. and Paulay, T.: "Mechanisms of shear resistance of concrete beams", J. of Structural Division, ASCE, Oct. 1968, pp. 2325-1339.
6. Blaauwendraad, J. and Wang, Q.B.: Overview of systematic study for shear failure in reinforced concrete beams and slabs without shear reinforcement under distributed load. Report Delft University of Technology, reportnr. 25.2-90-2-18

Model for Structural Concrete Members without Transverse Reinforcement

Modélisation d'un élément en béton dépourvu d'armatures transversales

Modell für Konstruktionsbauteile ohne Stegbewehrung

Karl-Heinz REINECK
Dr. Eng.
University of Stuttgart
Stuttgart, Germany

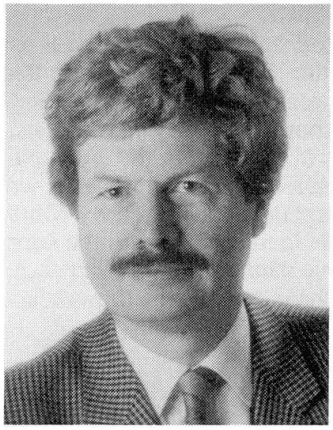

Karl-Heinz Reineck received his degrees at the University of Stuttgart. His research covers theoretical work and several experiment projects on the shear behaviour of structural members as well as large-scale tests on reinforced concrete-shells for offshore platforms. He is a member of the CEB-Commission «Member Design».

SUMMARY

The presented mechanical model for structural concrete members without transverse reinforcement explains the structural behaviour from cracking until failure. The loads are transferred by an inclined biaxial tension-compression field between the cracks and this can be visualized by a simple truss. For calculating the failure load the discrete cracks must be examined and the load is mainly transferred in the tension zone of the member by friction of the crack-faces and by the dowel force of the longitudinal reinforcement. An explicit equation for the ultimate shear force is derived following clear mechanical principles. The theory explains the size effect on «shear»-failures as well as the influence of axial compression or prestress and of axial tension or restraints, and it also yields satisfactory results for lightweight concrete members.

RÉSUMÉ

Ce modèle présente le comportement d'une telle structure de la fissuration à la rupture. L'effort tranchant se transmet entre les fissures par une traction et une compression que l'on modélise par un treillis. Le calcul de la résistance doit tenir compte des fissures elles-mêmes et des effets fondamentaux de l'effort tranchant par rapport à la friction des surfaces des fissures ainsi que l'effet de goujon des barres d'armature. L'équation explicitant la résistance ultime au cisaillement est dérivée suivant des principes de mécanique clairs. La théorie explique l'influence de la taille de l'élément en béton sur la rupture par cisaillement. L'influence négative on positive sur la charge ultime des forces de compression ou de traction axiales, ainsi que de la précontrainte peut donc être décrite. L'utilisation de relations constitutives appropriées montre que le modèle examiné donne des résultats satisfaisants dans le cas d'éléments légers en béton.

ZUSAMMENFASSUNG

Das vorgestellte mechanische Modell für Konstruktionsbetonbauteile ohne Stegbewehrung erfasst das Tragverhalten von der Rissbildung bis zum Bruch. Die Querkraft wird durch ein zweiachsiges Zug-Druck-Spannungsfeld zwischen den Rissen übertragen und kann vereinfachend durch ein Fachwerk veranschaulicht werden. Zur Berechnung der Traglast müssen die diskreten Risse und die wesentlichen Querkrafttragwirkungen betrachtet werden: die Rissreibung und die Dübelwirkung der Längsbewehrung. Es wird eine explizite Beziehung für die Bruchquerkraft nach klaren mechanischen Prinzipien abgeleitet. Die Theorie erklärt den Massstabeinfluss bei «Schub»-brüchen, den Einfluss von Längsdruckkräften, der Vorspannung und von Längszugkräften oder Zwangsbehinderungen und sie liefert auch befriedigende Ergebnisse für Leichtbetonbauteile.

1. INTRODUCTION

In present codes members without transverse reinforcement like slabs are still designed with respect to resist shear forces with purely empirically derived formulae. Since such formulae are limited to the past experimental evidence (which often is not clearly described) they do not cover all "shear problems" like that of fully cracked members in silos or foundations with large depths and very low reinforcement ratios. Therefore a clear theory based on a model for the structural behaviour is needed so that practising engineers can solve the future tasks. Such a model for members without transverse reinforcement is also a prerequisite for a consistent design concept for structural concrete since these members form the link between members with transverse reinforcement and unreinforced concrete members. Since the latter obviously require the concrete tensile strength, a consistency in modelling strutural concrete can only be reached if its use is clearly acknowledged.

The only load transfer of a point load on a member without using the concrete tensile strength (apart from the anchorage) are direct struts from the load to the supports tied together by the non-staggered tension chord. This model complies with the lower bound theorem of the theory of plasticity. It yields the full bending capacity at midspan, but this is contradicted by many tests, as e.g. Kani /1/, Leonhardt/ Walther /2/ and Bresler/Scordelis /3/. The reason is obvious from the crack pattern: the assumed compression strut is very flat and crosses the widely opening failure crack. The model is wrongly applied and the theory of plasticity is not valid for this case, as was again recently confirmed by Muttoni /4/. The direct transfer of the total load by inclined struts is only possible if the load is so near to the supports, that the struts are situated over the cracks. This also means, that the shear force cannot only be transferred in the compression zone as pretended e.g. by Kotsovos /5/, but that there is a shear transfer in the cracked tension zone of members without transverse reinforcement.

2. MODEL

2.1 Assumptions

The failure of members without transverse reinforcement is characterized by a single crack propagating into the compression zone and therefore the pattern of the discrete cracks is modelled as shown in Fig. 1 for the well-known test beam with a point load. The B-region with shear force then consists of the solid concrete "teeth" between the cracks as established by the works of Kani /1/, Fenwick /6/ and Taylor /7/. In each tooth the decrease ΔT of the force in the tension chord is equilibrated by an equivalent force in the compression chord and the following shear carrying actions:

- dowel force V_d of longitudinal reinforcement.
- friction along the cracks with the vertical component V_f; the term friction is used instead of "aggregate interlock" since it applies to all concrete types.

Both actions are combined with a shear force component in the compression zone, but this does not indicate an inclined compression chord. All assumptions are further explained in /9/, where the model is derived and justified and the results are compared with tests.

2.2 Equilibrium

The load is transferred by all the shear carrying actions (Fig.1a):

$$V = V_c + V_f + V_d \tag{1}$$

From the equilibrium of moments of a tooth (Fig.1b) as well as of the isolated compression zone alone, the following equation may be derived for the shear force component in the compression chord (notation see Fig.1):

$$V_c = \frac{2}{3}\,\frac{c}{z}\,V \tag{2}$$

From that follows that only a small proportion of the total shear force is transferred in the compression chord. Consequently the load is mainly carried in the cracked tension zone. With Eq.(2) the term V_c can be replaced in Eq.(1) and with $z = d - c/3$ the vertical equilibrium is given by:

$$V = \frac{z}{d-c}\left(V_f + V_d\right) \tag{3}$$

The moment equilibrium of the free-body diagram in Fig.1a yields an equation for the force in the longitudinal steel depending on the moment and the shear carrying actions. With Eq.(3) the force V_f may be replaced and the following equation for the strain in the longitudinal steel be derived:

$$\epsilon_s = \frac{1}{E_s A_s z}\left[V\,(x + \Delta x) + N\,z_c - V_d \frac{z}{ta}\right] \qquad \text{with : } \Delta x = \frac{d-c}{ta}\left(1 + \frac{2}{3}\frac{c}{z}\right) \quad ; \; ta = \tan\beta_r \tag{4}$$

Similarily the force and the strain in the compression chord may be determined.

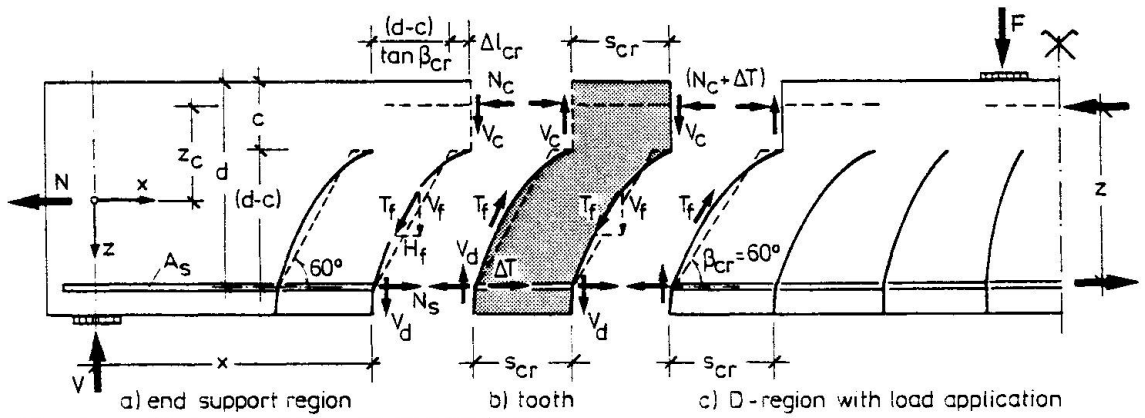

Fig.1: Member with tooth-elements and its forces

2.3 Stress Fields in the Tension Zone

The distribution of the friction stresses along the crack depends on the crack shape as well as on the proportion between the shear carrying actions, whereby both parameters are interrelated with each other. Instead of iteratively determining an "exact" distribution for a defined crack shape, a simple assumption is made for a statically admissable stress field in the tension zone.

The distribution of the friction stresses τ_f is made up by a constant part τ_{f1} (Fig.2a) and a parobolic distribution τ_{f2} (Fig.2b). The latter considers that the dowel action reduces the slip in the lower part of the crack and therefore its value is related to the dowel force. The equilibrium of the shear stresses along the neutral axis (Fig.2b) yields the condition:

$$\tau_{f2} = 2 \cdot v_{n,d} \qquad \text{with } v_{n,d} = V_d / b_w (d-c) \tag{5}$$

With the given τ_f-distribution the shear force V_f in Eq.(3) may be expressed by the representative shear stress τ_f at the mid-height of the crack:

$$V = b_w \cdot z \cdot \tau_f + \frac{3}{4} \frac{z}{d-c} V_d \tag{6}$$

The shear force may now be determined for any load stage after cracking if constitutive laws are formulated for the resistances τ_f and V_d as done in /9/.

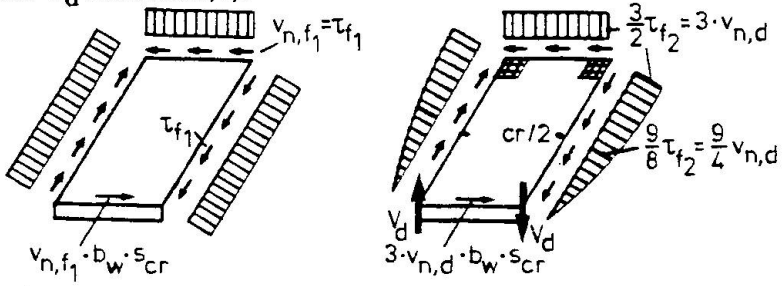

Fig.2: Distribution of friction and shear stresses in tension zone of tooth /9/

However, the model is not complete if not also the stress field in the tooth between the cracks is known so that "the structural action may be visualized" (Breen /8/). Since the stresses involved are small the linear elastic theory may be applied. The constant friction stresses τ_{f1} result in an inclined biaxial compression tension field (Fig.3a). The stress field for the dowel action with the combined friction stresses τ_{f2} is not elementary and therefore a strut-and-tie model is derived (Fig.3b). The concentrated tension tie for the dowel force spreads out and is equilibrated by the biaxial compression-tension field in the concrete resulting from the friction stresses.

2.4 Truss Model

The stress field between the cracks is mainly characterized by the inclined biaxial tension-compression field, which was first proposed in /10/. It is therefore obvious, that the simple truss shown in Fig.4 represents well the main feature of the structural action of members without transverse reinforcement. With that the concept of strut-and-tie models can also be extended to members or parts of members which are unreinforced. It must, however, be pointed out that the failure cannot be assumed by simply limiting the capacity of the tensile struts to the axial tensile strength of the concrete, but that the discrete crack and the shear carrying mechanisms must be looked at.

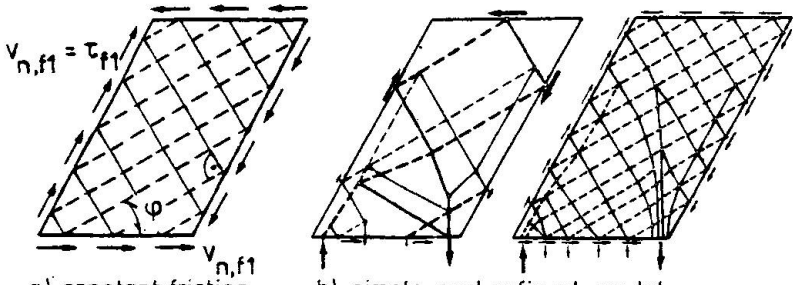

Fig.3: Stress fields between cracks

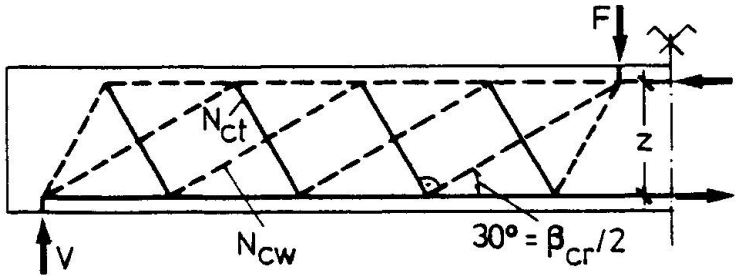

Fig.4: Truss model for members without transverse reinforcement

3. CONSTITUTIVE RELATIONS

For the steel and the concrete in compression bi-linear stress-strain relations can be assumed. The axial tensile strength of the concrete of

$$f_{ct} = 0,246 \cdot f_c^{2/3} \tag{7}$$

is an average value determined from the relative few tests where the tensile strength was actually determined with control specimens. With that the ultimate dowel force of the longitudinal reinforcement can be determined according to the proposal by Baumann /11/ or Vintzeleou and Tassios /12/.

The transfer of forces in cracks depends not only on the tensile strength of the concrete, but also on the roughness as well as on the crack widthΔn and the slipΔs increase as clearly described by Walraven /13/. It was assumed that the limiting friction stress is that transferrable without normal stress on the crack surface:

$$\tau_{fu} = 0,45 \cdot f_{ct} \left(1 - \frac{\Delta n}{\Delta n_u}\right) \quad \text{with} \quad \Delta n_u = 0,9 \text{ mm} \tag{8a}$$

With this value a critical slip of the crack faces is reached:

$$\Delta s_u = 0,336 \ \Delta n + 0,01 \ [\text{mm}] \tag{8b}$$

4. ULTIMATE CAPACITY

After the limiting friction stress τ_{fu} and the critical slip Δs_u acc. to Eq.(8) are reached, the tooth rotates and separates from the compression zone. The crack width at the mid-height of the crack can be derived from the horizontal crack opening Δu due to the elongation of the longitudinal steel and the slip (Fig. 5) giving the failure criterion:

$$\Delta n = 0,71 \cdot \varepsilon_s \cdot s_{cr} \tag{9}$$

With that the friction stress τ_{fu} acc. to Eq.(8a) is known and may be inserted in Eq.(6) for the total shear force. If then the Eq.(4) is used to replace the steel strain the following explicit equation for the ultimate load may be derived in the critical section with x_u=(a-1,5d):

$$V_u = \frac{b_w \ d \ 0,4 f_{ct} - 0,16 \frac{f_{ct}}{f_c} \lambda \frac{z_c}{d} N + V_{du}}{\left[1 + 0,16 \frac{f_{ct}}{f_c} \lambda \left(\frac{a}{d} - 1\right)\right]} \tag{10}$$

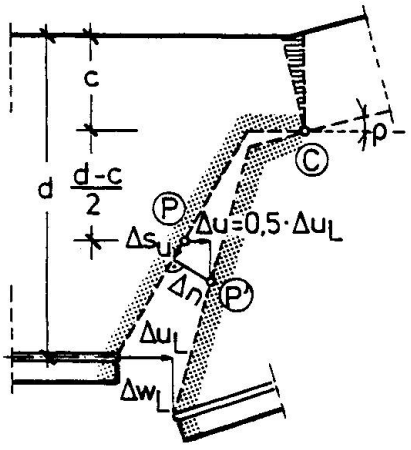

Fig.5: Kinematic consideration for crack width

Thereby the parameter λ is a dimension-free value for the crack width:

$$\lambda = \frac{\varepsilon_{sy} \cdot d}{\omega \cdot \Delta n_u} = \frac{f_c}{E_s \cdot \rho} \cdot \frac{d}{\Delta n_u} \quad \text{with} \quad \omega = \rho \frac{f_y}{f_c} \tag{11}$$

It comprises the well-known influence of the longitudinal reinforcement ratio as well as that of the depth of the member. With that a simple dimensioning diagram for the dimension-free ultimate shear force can be presented (Fig.6).

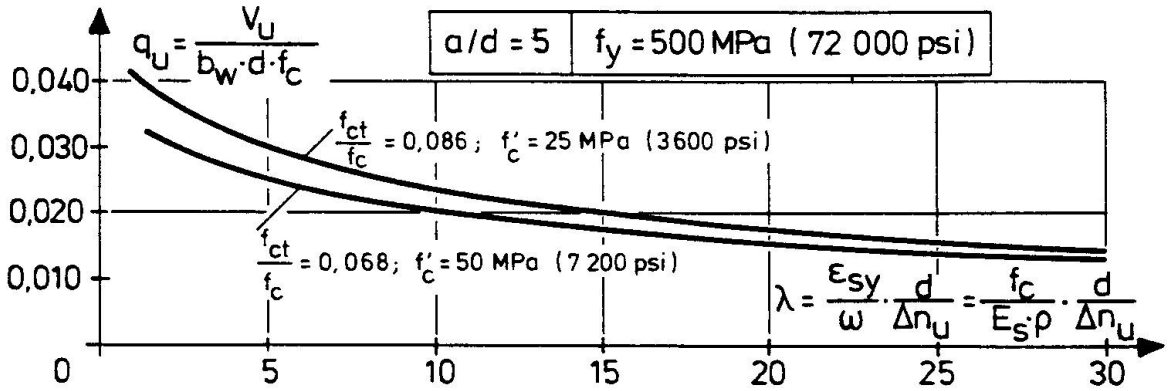

Fig.6: Dimensioning diagram for the ultimate shear force or load

5. DISCUSSION

5.1 Size Effect

The influence of the absolute depth of the member on the ultimate shear force is now obvious: the crack width increases proportionally with the crack height or the depth of the member (Fig.5), and consequently acc. to Eq.(8) the friction stress as the dominant shear carrying capacity is reduced. A further smaller size effect is also due to the dowel action /9/.

The proposed model is conservative if the crack width is very small as for thin members. Then the total length of the crack may be within the fracture zone near the crack-tip and small tensile stresses can be transferred up to a maximum crack width of about 0,15mm (Hillerborg and König /8/). This is shown in Fig.7 where the distributions of these tensile stresses along the crack are plotted for different test beams from Walraven /14/: the crack width increases with increasing depths and the extent of the fracture zone decreases. Since the model already relies on these tensile stresses within the curved part of the crack near its top (see Fig.3 and /9/), only the shaded area in Fig.7 remains for an additional contribution to the capacity of the member. For all members with larger depths the vertical component of the resultant T_{ct} is small and contributes only 5 to 7 % to the ultimate dimension-free shear force; only in case of the beam A1 it increases to 20 % since the crack widths remain very small. However, such members with small depths normally fail in "bending" (like this beam A1), unless they are extremely heavily reinforced.

A further size effect is on the cracking moment and thereby on the steel strain due to the tension stiffening effect of the concrete between cracks. However, this is only worth considering for members with extremely high values λ, like e.g. foundation slabs with 2m depth and very low reinforcing ratios /9/.

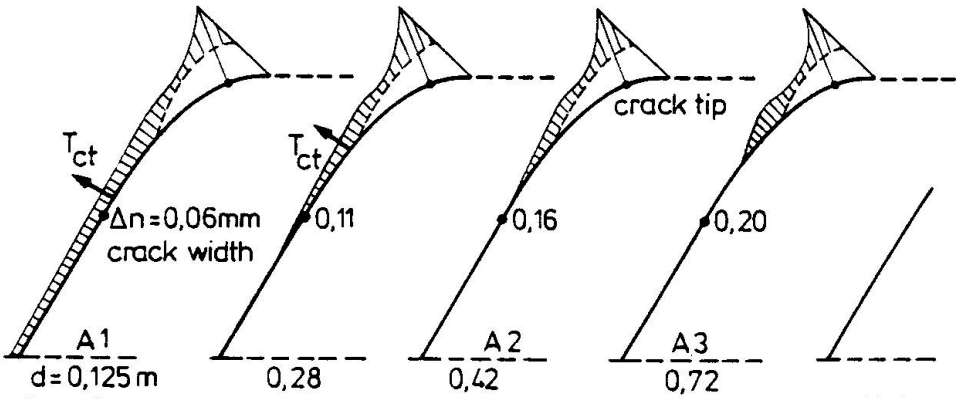

Fig.7: Distribution of tensile stresses in the fracture zone for some test beams with increasing depth

5.2 Axial Forces and Prestress

Axial forces were considered in the equilibrium equation for determining the force in the tension chord leading to Eq.(6), and Fig.8 gives an examples of its influence on the ultimate shear force. Axial compressive forces increase and tensile forces decrease the capacity as qualitatively already known. This is the more pronounced the higher the depth of the member is, since then the crack width is larger and more sensitive towards changes in the steel strain.

The proposed model and theory can also consistently be extended to fully cracked members due to high axial tension (Fig.8) or even restraints /9/. In such a case the shear force can only be transferred by friction along the crack and by the dowel forces of both reinforcement layers. Thereby the amount of the top-reinforcement, as expressed by the parameter η in Fig.8, is of course decisive for the crack width and consequently the possible frictional resistance.

The structural model for a prestressed member is the same as given in Fig.4, apart that the inclinations of the compression struts may be slightly flatter due to the flatter crack inclinations. The influence of prestress on the ultimate load is best explained by looking at the stiffness of the tension chord (which is a prestressed tie), since its strain governs the width of the failure crack. The tension chord of a p.c.-member with the same mechanical reinforcing ratio is different in comparison to a r.c.-member:

- the strain will normally be smaller, but can also be larger if almost the yield strength is reached;
- the dowel force is smaller, because less steel area is needed and smaller diameters are used.

This is reflected in the comparison of ultimate capacities in Fig.9. The p.c.-member exhibits larger failure loads for large depths than the corresponding r.c.-member, but for small depths there is almost no difference.

5.3 Lightweight Concrete

The proposed model is also valid for lightweight concrete (LC) and only the constitutive relations must be adapted. The concrete tensile strength is lower than for normal concrete and a reduction to 66 % can be assumed /9/. The friction capacity acc. to Eq.(8a) is also reduced due to the lower tensile strength, but furthermore higher values for the critical slip occur than given in Eq.(8b):

$$\Delta s_u = 0{,}38 \cdot \Delta n + 0{,}01 \quad [\text{mm}] \tag{12}$$

With these minor modifications the proposed theory gives quite satisfactory results in comparison with an empirical formulae by Walraven /14/ as shown in Fig. 10.

REFERENCES

1. Kani, G.N.J.: The riddle of shear failure and its solution. ACI-Jour.61 (1964), April, 441-467
2. Leonhardt, F.; Walther, R.: Schubversuche an einfeldrigen Stahlbetonbalken mit und ohne Schubbewehrung. DAfStb H.151, Berlin, 1962
3. Bresler, B.; Scordelis, A.C.: Shear strength of reinforced concrete beams. ACI-Jour. 60 (1963), 51-74
4. Muttoni, A.: Applicability of the theory of plasticity for dimensioning reinforcing concrete (in German). Dr.-thesis, ETH Zürich, 1989, 1-180
5. Kotsovos, M.D.: Compressive force path concept: basis for reinforced concrete ultimate limit state design. ACI Struct. Journal V.85, Jan.-Feb. 1988, 68-75
6. Fenwick, R.C.; Paulay, T.: Mechanisms of shear resistance of concrete beams. ASCE-Journal Struct. Div. V.94, 1968, ST 10, Oct., 2325-2350
7. Taylor, H.P.J.: The fundamental behaviour of reinforced concrete beams in bending and shear. In: ACI-SP 42, 43-77, Detroit, 1974
8. IABSE Colloquium "Structural Concrete". Introd. Reports. Stuttgart 1991
9. Reineck, K.-H.: A mechanical model for the behaviour of reinforced concrete members in shear (in German), Dr.-thesis., Univ. Stuttgart, 1990, 1-273
10. Reineck, K.-H.: Models for the design of reinforced and prestressed concre members. CEB-Bull.146, 43-96, Paris, 1982
11. Baumann, Th.: Tests on the dowel-action of the longitudinal reinforcement of r.c.-beam (in German). DAfStb 210, W. Ernst u. Sohn, Berlin, 1970, 42-83
12. Vintzeleou, E.N.; Tassios, T.P.. Mathematical models for dowel action under monotonic conditions. Mag. of Concrete Research 38 (1986), 13-22
13. Walraven, J.C.: Aggregate interlock: a theorectical and experimental analysis. Dr.-thesis, Delft Univ., 1980, 1-197
14. Walraven, J.C.: The influence of depth on the shear strength of lightweight concrete beams without shear reinforcement. Report S-78-4, Stevin Laboratory, Delft University, Dept. of Civil Eng.
15. Kirmair, M.: Das Schubtragverhalten schlanker Stahlbetonbalken - theoretische und experimentelle Untersuchungen für Leicht- und Normalbeton. DAfStb 385, Berlin, 1987

Full-Scale Shear Tests on two Bridges

Essais de cisaillement in situ sur deux ponts

Querkraftversuche in voller Skala auf zwei Brücken

Mario PLOS
Res. Assist.
Chalmers Univ. Technol.
Göteborg, Sweden

Kent GYLLTOFT
Prof. Dr.
Chalmers Univ. Technol.
Göteborg, Sweden

Krister CEDERWALL
Prof.
Chalmers Univ. Technol.
Göteborg, Sweden

SUMMARY

Full-scale shear tests were performed on two concrete highway bridges constructed in 1980. The test results reveal short-comings in the design models when a combination of shear and moment actions leads to failure. The results show the need for better design models based on a clear physical understanding of failure. Fracture mechanics can be used together with the finite element method to obtain a better understanding of the failure process.

RÉSUMÉ

Les tests de cisaillement concernent deux ouvrages construits en 1980, les essais ayant été menés sur les ponts eux-mêmes. Les résultats montrent des défauts dans les modèles d'étude existants lorsque la rupture est due à l'action combinée des moments et de l'effort tranchant. Il s'agit donc d'établir de meilleurs modèles basés sur une compréhension physique claire du phénomène de rupture. La mécanique de la rupture utilisée conjointenement à la méthode des éléments finis permet d'obtenir une meilleure compréhension dans ce domaine.

ZUSAMMENFASSUNG

Grossversuche zur Schubtragfähigkeit von zwei 1980 erbauten Betonstrassenbrücken wurden durchgeführt. Die Versuche zeigen Mängel am Berechnungsmodell auf, wenn eine Kombination von Querkraft und Biegemoment zum Bruch führt. Die Ergebnisse beweisen die Notwendigkeit von besseren Berechnungsmodellen basierend auf physikalischem Verständnis des wirklichen Bruches. Bruchmechanik wird zusammen mit der Finite Element Methode verwendet, um ein besseres Verständnis des Bruchverhaltens gewinnen.

1. INTRODUCTION

The design rules for shear capacity set out in the European concrete codes is mainly based on laboratory tests on a comparatively small scale. In two full-scale tests we had the possibility to investigate the shear capacity for considerably larger structures than is normal in laboratories. The full-scale tests were performed on two concrete highway bridges, constructed in 1980. Both bridges were loaded close to one of the supports in order to cause shear failure.

The purpose of the tests was to improve knowledge by examine the bearing capacity of the bridges, and to study how these big and complex structures act under shear load leading to failure. The test results were compared with the design model in the Swedish concrete code. The results indicate that the design models are able to predict the shear capacity in cases where typical shear failures are achieved. In more complex cases, however, when a combination of shear and moment actions leads to failure, clear shortcomings were found in the design models of the code.

The tests are also intended to be used to improve methods of analysis. Finite element models of the bridges intended for fracture mechanics analysis are now under evaluation.

2. FULL SCALE SHEAR TESTS

2.1 The bridges

Full scale shear tests were performed on two concrete portal frame bridges. One of the bridges was a non-prestressed slab frame bridge with a free span of 21 m (fig 1 and 2).

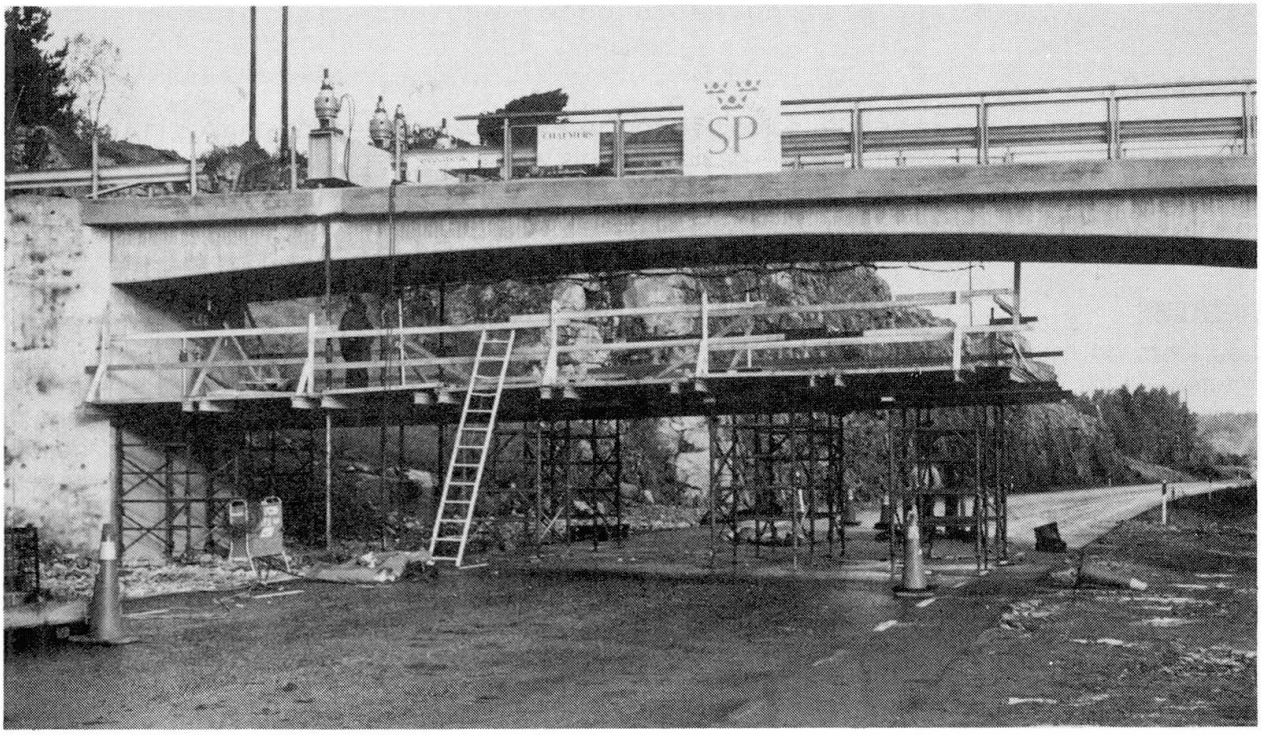

Fig. 1 Non-prestressed bridge during test preparation.

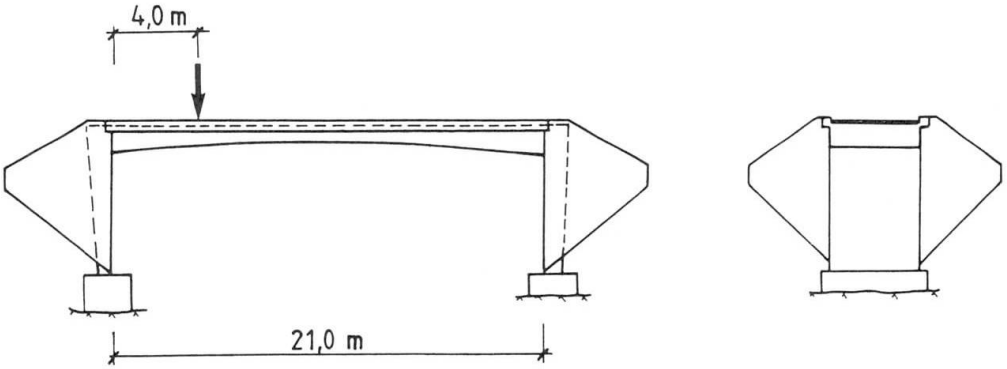

Fig. 2 Non-prestressed bridge

The other bridge was prestressed and had a free span of 31 m (fig 3 and 4). The span consisted of two post-tensioned beams connected by a bridge deck slab. The beams and the slab were connected with the front walls at the supports, forming a frame.

2.2 Test arrangements

The loads were applied through steel bars anchored to the rock under the bridges and transferred to the bridges by hydraulic jacks (fig 5). Loads, deflections and strains were measured during the tests, and crack growth was registered. The concrete strength was tested on cylinders drilled out of the bridges.

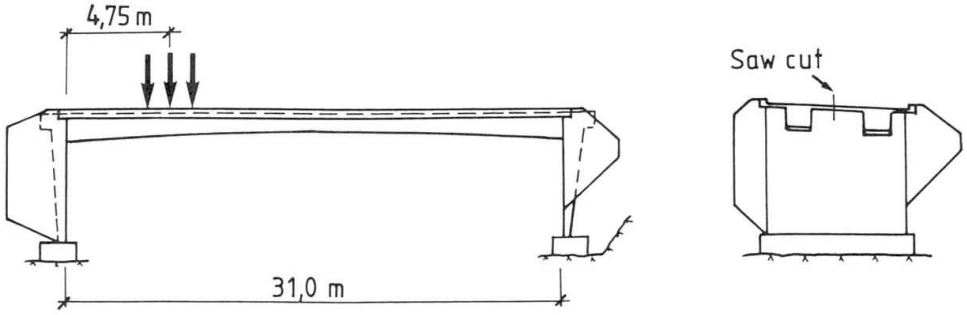

Fig. 3 Prestressed bridge

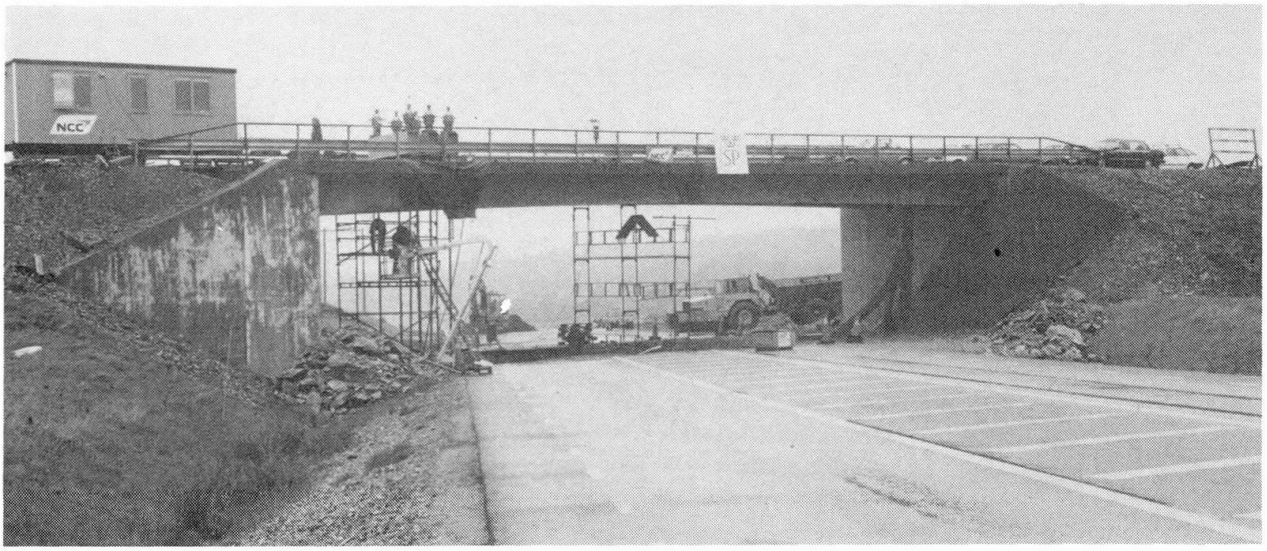

Fig. 4 View of the prestressed bridge

2.3 Test performance

The non-prestressed bridge was loaded 4,00 m from one of the supports and failed at a load of 4,5 MN due to a sudden diagonal shear crack (fig 6). The bridge was substantially cracked due to bending, and some shear-bending cracks were observed close to the loading section before the failure occurred.

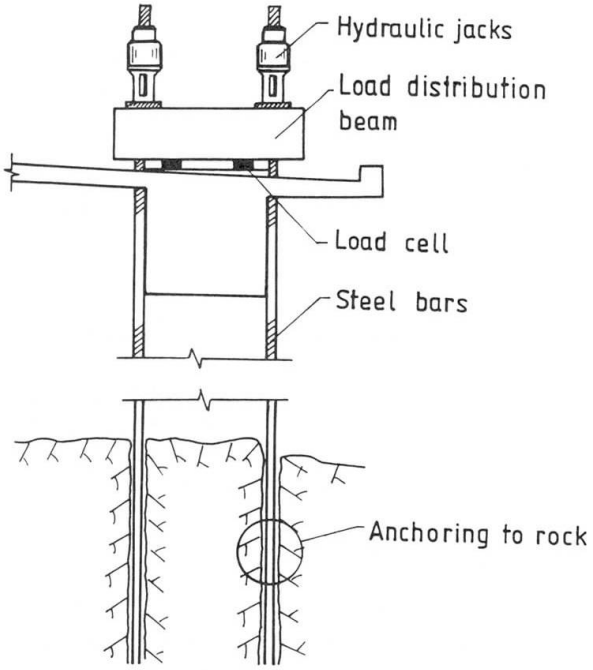

Fig. 5 Loading arrangement

The failure of the prestressed bridge was more complicated. Before the test this bridge was cut longitudinally between the two main beams and one of the beams was loaded about 4,75 m from one of the supports. After extensive cracking due to bending, together with a few shear-bending cracks, the support closest to the load unexpectedly failed at a load of 8,5 MN. The support failure lead to a redistribution of the moment, with increasing moment in the loading section.

When the support failed, the load decreased to 6,0 MN. Further loading with the jacks lead to large deformations and several inclined cracks in the shear span. The final failure occurred at a load of 6,3 MN, when the concrete at the upper edge of the loading section crushed due to compression (fig 7).

Fig. 6 Shear failure in the non-prestressed bridge

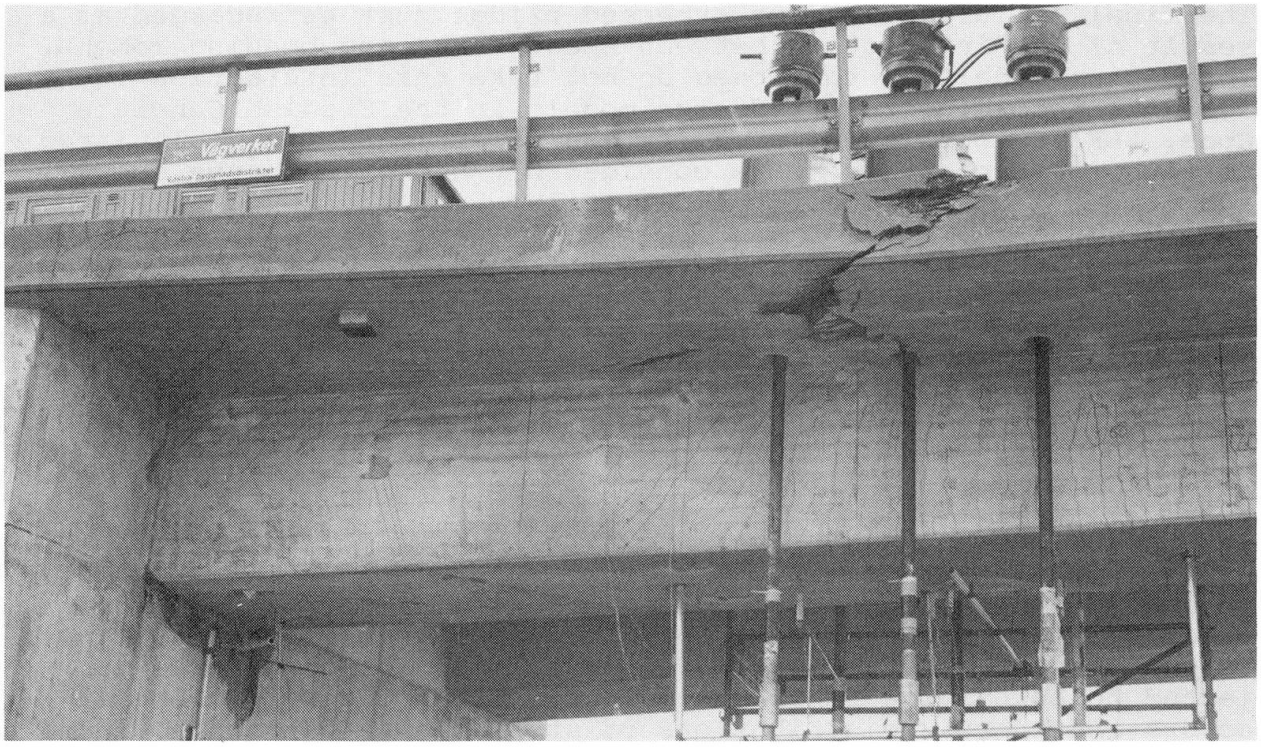

Fig. 7 Failure in the prestressed bridge. Cracking, support failure and concrete compression failure at the top of the loading section can be seen.

3. EVALUATION

The main purpose of the evaluation was to compare the bridges' real shear force at failure with their shear capacities according to the design model in the Swedish Concrete Code, BBK 79 /1/. Both the real shear force along the bridges and their shear capacities are dependent on the stiffness of the bridges and the degree of restraint at the supports. Due to cracking of the concrete and, for the prestressed bridge, failure in the support, stiffnesses and restraint conditions changed during loading.

To determine the stiffnesses and the degrees of restraint, computer programmes based on the finite element method were used. The stiffnesses were approximately calculated from the crack formation registered during the tests. By adjusting the calculated stiffnesses and varying the degree of restraints in the finite element model so that the calculated deflections were the same as the measured deflections of the bridges, proper models of the bridges were created. By analysing the obtained models the bridges moment and shear force distribution were determined. The shear capacities according to codes were then calculated and compared with these shear forces present in the bridges at failure.

4. RESULTS

In the non-prestressed bridge a typical shear failure occurred. The moment and shear distribution of this bridge are under evaluation, but preliminary results indicate good agreement between the capacity according to the model in the code and test results.

The final failure in the prestressed bridge must be regarded as a result of the interaction between shear force and bending moment. The design models in the codes do not take this interaction into account. According to the design models in the Swedish Concrete Code, BBK 79, both shear capacity and moment capacity, calculated as separate capacities, were considerably higher than the shear and moment in the bridge at final failure.

It should however be observed that the final failure was achieved at a load level lower than the maximal. The difference between calculated shear capacity and shear force in the bridge was much smaller at maximum load level than at the final failure. The moment in the loading section, however, increased considerably from maximum load level until final failure occurred. The effect of moment must therefore have a decisive influence on the failure.

5. CONCLUSIONS

To sum up, the design models used in the codes for calculation of shear capacity seems to work well for structures subjected mainly to pure shear action. In more complex cases, for structures subjected to both large shear and moment actions, where prestress occurs and where redistributions of stesses have taken place, the design models are unable to predict capacity. It is therefore not sufficient to modify the design models used today. Instead research should be intensified to find models that better describe what happens when structures are subjected to loading until failure, so that the design can be based on a clear physical understanding of the failure.

Fracture mechanics together with the finite element method will be used to analyse these bridges to obtain a better understanding of the failure process, but also to further develop fracture mechanics as a tool in the analysis.

6. ACKNOWLEGEMENT

The tests have been performed in cooperation with The Swedish National Testing and Research Institute (SP), the Swedish Road Administration and Luleå University of Technology.

REFERENCES

1. Statens betongkommitte', Bestämmelser för betongkonstruktioner, BBK 79, Utgåva 2 (Regulations for concrete structures, second edition), AB Svensk Byggtjänst, 1988 (in Swedish).

2. KJELLGREN L. and BERGSTRÖM G., Skjuvförsök på spännarmerad rambro (Shear test on prestressed concrete frame bridge), Div. of Concrete Structures, Chalmers University of Technology, Diploma thesis 90:1, Göteborg, February 1990 (in Swedish).

3. VO MINH H. and PLOS M., "Skarvning av armering i ramhörn (Splicing of reinforcement in frame corners)", Div. of Concrete Structures, Chalmers University of Technology, Diploma thesis 88:2, Göteborg, April 1988 (in Swedish).

Stirrups or Fibers

Etriers ou fibres

Bügeln oder Fasern

Fernand MORTELMANS
Professor
Cath. Univ. of Leuven
Leuven, Belgium

Fernand Mortelmans, born 1926, received his engineering degree and Ph.D. at the State University of Ghent. Currently he is carrying out research on reinforced concrete beams subjected to combined action of bending moment and shear force, cracks, steel fibers and detailing of reinforcement. He has designed several important structures in Belgium.

Lucie VANDEWALLE
Senior Assistant
Cath. Univ. of Leuven
Leuven, Belgium

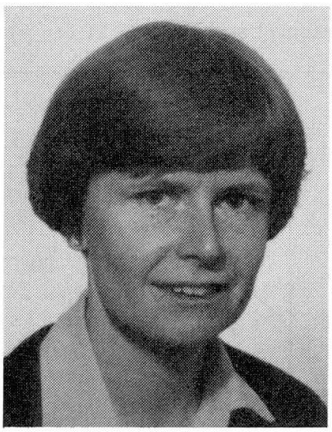

Lucie Vandewalle, born 1958, received her engineering degree and Ph.D. at the Catholic University of Leuven. Her field of research mainly concerns reinforced concrete and bond between steel and concrete.

SUMMARY

It is usual that the longitudinal reinforcement of a beam is calculated by means of the bending moment and the transverse reinforcement by means of the shear force. From extensive research carried out at the K.U. Leuven it was shown that in the compression zone of a beam a great part of the shear force is taken up. Consequently, more shear force can be taken up by the extension of the compression zone, i.e. by the provision of more longitudinal reinforcement. In this contribution an attempt is made to show that the global detailing of reinforcement may be determined by the interaction of bending moment, longitudinal and shear force.

RÉSUMÉ

Il est d'usage de déterminer l'armature longitudinale et transversale en considérant respectivement le moment fléchissant et l'effort tranchant dans une poutre. Une recherche étendue à la K.U. Leuven a démontré qu'une partie importante de l'effort tranchant est reprise dans la zone comprimée. Il est donc possible de reprendre un effort tranchant plus élevé en augmentant la zone comprimée, c.à.d. en renforçant l'armature de traction. Dans la présente communication on tente à démontrer que le dispositif complet et détaillé de l'armature peut être déterminé à partir de l'ensemble du moment fléchissant et de la force longitudinale et transversale.

ZUSAMMENFASSUNG

Es ist üblich, dass die Längsbewehrung eines Balkens aus dem Biegemoment, und die Querbewehrung aus der Querkraft berechnet wird. Aus einer umfassenden, an der K.U. Leuven durchgeführten Untersuchung hat sich ergeben, dass in der Druckzone eines Balkens ein grosser Teil der Querkraft aufgenommen wird. Es kann folglich mehr Querkraft durch Ausdehnung der Druckzone, d.h. durch Zulegen von Längsbewehrung aufgenommen werden. In diesem Beitrag wird versucht nachzuweisen, dass die gesamte Bewehrungsdetaillierung durch die Zusammenwirkung von Biegemoment, Längs- und Querkraft bestimmt werden kann.

1. INTRODUCTION

During the design of concrete structures, the determination of concrete dimensions and the detailing of reinforcement are of major concern. It is usual to calculate the longitudinal reinforcement and the transverse reinforcement independently of each other. The longitudinal reinforcement results from the bending moment and the normal force, the other reinforcement is necessary for the shear force.
This of course is a rough approach : internal forces are invented by engineers but fysically they do not exist.

2. INTERACTION BENDING MOMENT/SHEAR FORCE FOR A GIVEN CROSS SECTION

About twelve years ago, the so-called M-N-V- (bending moment (M), normal force (N) and shear force (V)) research program was started at the K.U.Leuven. From this investigation a **mathematical model** for the ultimate limit design has been developed, which permits taking into account :

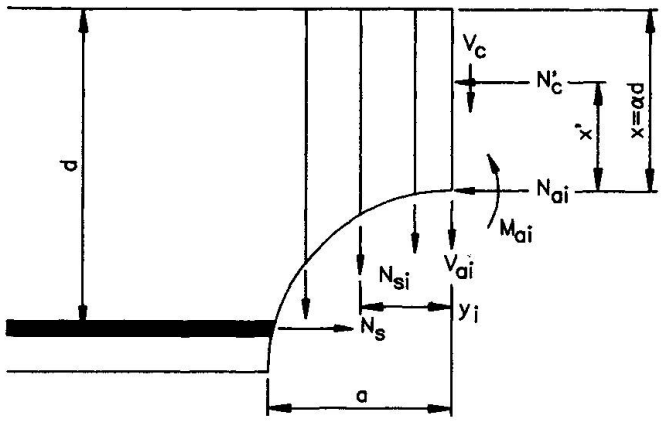

Fig. 1

- the normal force in the compression zone (N'_c)
- the absorbable shear force in the compression zone (V_c)
- the forces in the stirrups (N_{si})
- the force in the tension reinforcement (N_s)
- the aggregate interlock (M_a,V_a,N_a)
- the shape of the crack.

The section is subjected to combined bending, compression and shear (M, N, V).
The normal force (N_c) and its situation (x') in the compressed zone can be calculated from the stress-strain diagram, proposed by CEB : [1]

$$\sigma_c = f_c \frac{\varepsilon_c}{2} \left(2 - \frac{\varepsilon_c}{2}\right) \qquad \text{for } 0 < \varepsilon_c \leq 2\ ‰ \qquad (1)$$

$$= f_c \qquad \text{for } 2 < \varepsilon_c \leq 3.5\ ‰$$

If also shear stresses act in addition to longitudinal stresses, several failure criteria can be used.
In our case (normal stress + shear stress) the simplest relation σ_I/σ_{II} is a lineair function. It seems to be also a safe one.
From this relation the absorbable shear stress can be calculated

$$\tau_c = \sqrt{\frac{1}{4}\left[\left(\frac{1-K}{1+K}\right)^2 - 1\right]\sigma_c^2 + \frac{(1-K)K}{(1+K)^2}\sigma_c + \left(\frac{K}{1+K}\right)^2} \quad \text{with } K = \frac{f_{ct}}{f_c} \qquad (2),(3)$$

This elliptic criterion is shown in figure 2.

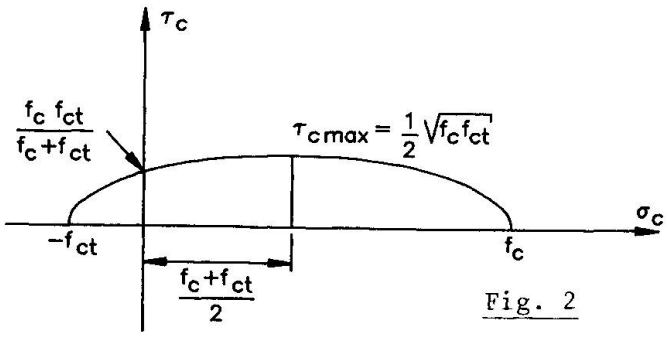

Fig. 2

From the shear stress-diagram the shear force V_c can be calculated [2][3]. V_c as well as N_c are parameter functions of the deformation ε_{cu} of the concrete on the upper side.
It is then possible to draw a diagram n_c/v_c with

$$n_c = \frac{N_c}{\alpha\ b\ h\ f_c}$$

$$v_c = \frac{V_c}{\alpha\ b\ h\ f_c},$$

valid for a rectangular cross section (see Fig.3).

This relation n_c/v_c has been confirmed by test results (see x in Fig. 3)[2,3,4]

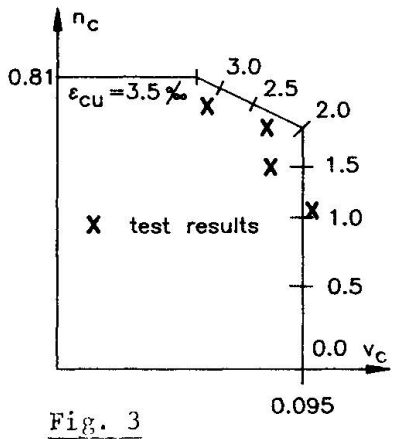

Fig. 3

Finally the horizontal projection of the crack has also been formulated by experiment for rectangular as well as for T shaped sections [6,7].
The influence of the aggregate interlock has been translated by the formulas, proposed by Prof. Walraven [5]. The shape of the crack has been determined in an experimental way [6].
The force in the reinforcement depends of course on the σ_s/ε_s-diagram of the steel.
The relation crack width/steel stress is based on the τ/δ relation mentioned in [8].
Expressing the equilibrium of the section, we find an interaction diagram N/V for a given longitudinal force and given dimensions of the cross-section :

$$\begin{cases} N_c + N_{ai} - N_s = N & (4) \\ V_c + V_{ai} + \Sigma N_{si} = V & (5) \\ N_c x' + M_{ai} + \Sigma N_{si}\ y_i + N_s(d-v) = M & (6) \end{cases}$$

Since the interaction between the different forces does not follow a lineair course, the calculation can only be carried out step by step by means of a computer.
Given for example

$b = 300$ mm
$d = 650$ mm
$f_{ck} = 27$ N/mm^2
$A_s = 4$ ⌀ 20 BE 400
3 ⌀ 20 BE 400
2 ⌀ 20 BE 400
$N_c = 0$

the interaction bending moment/shear force can be computed.
In Fig. 4 the interaction

$$m = \frac{M}{\alpha\ b\ h^2\ f_{cd}} \quad (7)$$

$$v = \frac{V}{\alpha\ b\ h\ f_{cd}} \quad (8)$$

is plotted for several values of A_s (4 ⌀ 20, 3 ⌀ 20 and 2 ⌀ 20) and several values of stirrup percentages ($\bar{\omega}_b$ = 0 - 0,1 - 0,2).

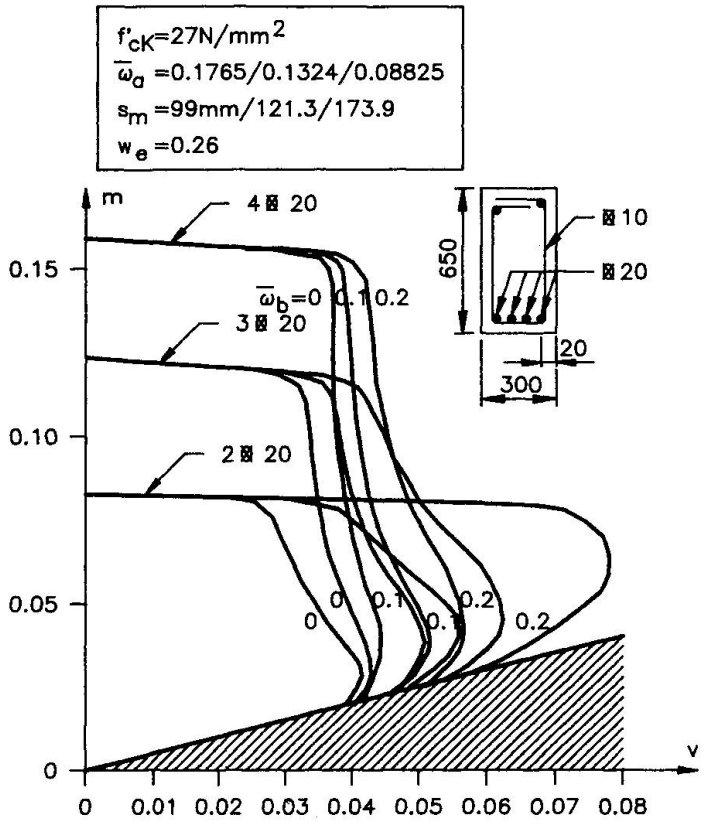

Fig. 4

3. INFLUENCE OF STIRRUPS

From the investigation as explained in 2 some important conclusions can be drawn.

1. The compression zone takes up a considerable part of the shear force.
2. The contribution of the stirrups is rather restricted.
3. The influence of the stirrups diminishes when the tension reinforcement increases.
4. The aggregate interlock decreases when the tension reinforcement is reduced.

It may be stated that when the area of the tension reinforcement increases - as a result of which the size of the compression zone expands - more shear force can be taken up by the concrete. The stirrups may then become unnecessary. So, more shear force can be taken up by increasing the tension reinforcement or by applying a (limited) prestressing.

The mathematical model is applicable both for reinforced concrete, for prestressed concrete and for partially prestressed concrete.

At the moment, an attempt is being made to incorporate the mathematical model in a calculation method, which is easy to handle in practice.

When the aggregate interlock is not taken into account - which means an additional safety - the calculation already becomes a good deal more simple.

4. RELATION BENDING MOMENT/SHEAR FORCE FOR A GIVEN LOAD

Let us consider a beam on two supports (length ℓ) with a uniformally distributed load (p). The longitudinal force is zero. The bending moment M and the shear force V at a distance x from the left support can be formulated as ($t = x/\ell$) :

$$M = \frac{p\ell^2}{2}(1 - t)t$$

$$V = \frac{p\ell}{2}(1 - 2t) \qquad (9)$$

Eliminating t between M and V and introducing the notations m_p, v_p and λ

$$m_p = \frac{M}{b\ h^2\ f_{cd}} \qquad (10)$$

$$v_p = \frac{V}{b\ h\ f_{cd}} \qquad (11)$$

$$\lambda = \frac{p\ell^2}{8\ b\ h^2\ f_{cd}} \qquad (12)$$

we find an interaction m_p/v_p

$$m_p = \lambda\ [1 - (\frac{v_p}{\lambda})^2\ (\frac{\ell}{h})^2] \ . \qquad (13)$$

This interaction m_p/v_p due to the load p is to be secured by the interaction diagram m_o/v_o that the section is capable to bear ($m_o = \alpha$ m, $\alpha_o = \alpha$ v).
In the figure 5 both interactions are drawn schematically.
Full lines represent the load relation, dotted lines concern the "bearing capacity" of the chosen section for stirrup percentages $\bar{\omega}$ = 0 - 0,1 and 0,2.
For the case drawn in figure 5 it is clear that for a slender beam (h/ℓ = 0,05 and even h/ℓ = 0,10) no stirrups are required.
When h/ℓ increases - for example h/ℓ = 0,15 - stirrups become necessary from the point A to the point B.
So it is clear that a lot of beams can be designed without stirrups. On the other hand less slender beams may need some stirrups near to the support. At the addition of steel fibers in the concrete mix the interaction lines m_o/v_o move to the right. This has been proved by dr.ir. L. Van de Loock [9] in his doctor's thesis.

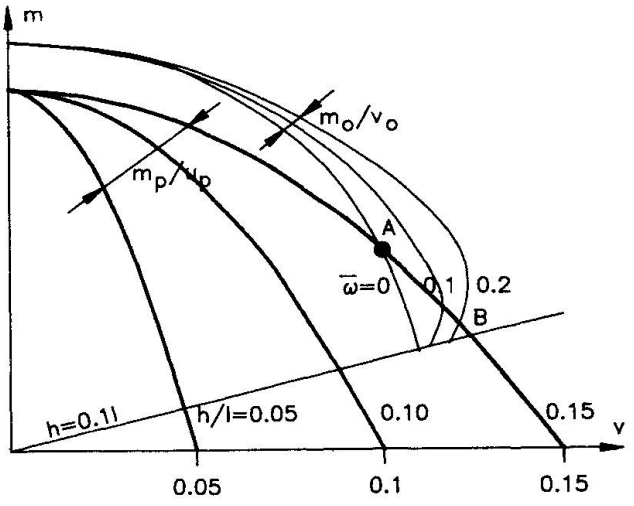

Fig. 5

5. DETAILING OF THE REINFORCEMENT

Even if no stirrups are necessary, it seems to us that it is advisable to add a limited quantity of fibers in the concrete in order to secure a minimum tensile strength and an adequate post cracking behaviour.
Of course, not all the beams can be considered for reinforcing without stirrups. We think that a scientific dosage of longitudinal reinforcement, steel fibers (15 to 20 kg/m^3) and stirrups makes it possible to design more economically most of the common beams. Besides, it is known that cracks often start at the location of the stirrups.

REFERENCES

1. CEB. Modelcode 1978

2. MORTELMANS F., "Interaction diagram bending moment/shear force considering the absorbable forces in the cracked and the non cracked concrete", internal paper 20-ST-13 of 18-10-1984, Leuven.

3. MORTELMANS F., "Relatie tussen buiging en dwarskracht" (relation between bending moment and shear force), Cement nr. 10, 1985.

4. MORTELMANS F., VANDEWALLE L., "A new criterion for concrete in compression", Rilem Workshop on applications of fracture mechanics to concrete structures, Abisko (Zweden), 28-30 June 1989, (will be published by Chapman and Hall).

5. WALRAVEN J.C., "Aggregate Interlock : A theoretical and experimental analysis", University Press, Delft 1980.

6. VANDEWALLE L., CARNOY D., "Scheurpatroon van balken in gewapend beton", Afstudeerwerk K.U.Leuven, 1981.

7. HEMMATY Y., "Crack Pattern of T-section. Beams in reinforced concrete", Masters Degree 1986.

8. VOS E., REINHARDT L., "Bond resistance of deformed bars, plain bars and strands under impact loading", report 5-80-6, Delft.

9. VAN DE LOOCK L., "M-D model voor betonnen balken met rechthoekige sectie voorzien van langswapening en staalvezels" (M-V model for concrete beams with rectangular cross section with longitudinal reinforcement and steel fibers), Ph. D., K.U.Leuven 1989.

Detailing for Shear with the Compressive Force Path Concept

Cisaillement et concept de champ de forces de compression

Atallah S. KUTTAB
Assistant Professor
Birzeit University
Birzeit

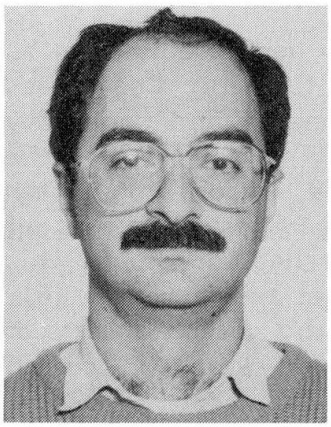

Atallah Kuttab is a member of CEB Task Force Group GTG 24 «Practical Design Utilising Multiaxial States of Stress», and member of CEB Permanent Commission PC 4 «Members Design».

David HALDANE
Senior Lecturer
Heriot-Watt Univ.
Edinburgh, Scotland

David Haldane is actively involved in the numerical modelling and the experimental validation of the behaviour of structural concrete members particularly in the fields of deep beams and impact loading.

SUMMARY

The paper presents the results from tests on simple beams which were reinforced in compliance with the compressive force path concept using stirrups that did not extend the full depth of the beam. The test specimens when compared with conventionally reinforced ones showed higher strength and ductility. Furthermore, it is shown that the classification of beams according to their shear span to effective depth ratio is not only confusing but unnecessary.

RÉSUMÉ

Ce rapport présente les résultats de tests effectués sur des poutres simples en béton, armées sur la base du concept de champ de forces de compression et possédant des étriers courts ne s'étendant pas sur toute le hauteur de la poutre. Les échantillons expérimentaux se sont montrés plus résistants et ductiles que les échantillons armés de façon conventionnelle. De plus, il est démontrée que la classification des poutres en function du rapport «a/d» dans ce cas porte non seulement à confusion mais n'est pas nécessaire.

ZUSAMMENFASSUNG

Im vorliegenden Artikel werden die Versuchsergebnisse von einfachen Stahlbetonträgern, die nach dem «compressive force path concept» mit nicht über die ganze Höhe des Trägers reichenden Bügeln bewehrt wurden. Die Versuche zeigten im Vergleich zu konventionell verstärkten Trägern erhöhte Festigkeit und Duktilität. Darüber hinaus wurde deutlich, dass die Klassifikation von Trägern in Bezug auf das «a/d» Verhältnis nicht nur verwirrend, sondern unnötig ist.

1. INTRODUCTION

The practice of detailing reinforced concrete members is somewhat irrationally dependent to a large extent on its structural function. As an example, the provision of transverse reinforcement in a column implies that compressive zones in general require the presence of such reinforcement; while on the other hand, the introduction of transverse reinforcement to a simple beam is largely dependent on whether or not shear stresses are present. This apparent inconsistency in present day practice appears to have originated from the adoption of design principles based on an uniaxial state of stress. In addition, the design of structural concrete for some cases, for example shear design, follows physical models which do not represent the true behaviour.

In this context, MacGregor (1) described the ACI(2) shear design equations as "empirical mubo-jumbo". The tendency in present Code Drafting Committees (2,3,4,5) is to move towards procedures comparable in rationality and generality to the plane sections approach for flexure and axial load. The objective of the design procedures for shear is to try to assess the amount of shear reinforcement required to carry that portion of the shear forces in excess of that which can be sustained by the concrete alone. In order to achieve this aim various approaches based on concepts such as the latest truss models (6), the compression field theory (7), the lower and upper-bound of the theory of plasticity (8), etc are being adopted. Essentially, the element which is common to these models is the assumption that the diagonally cracked concrete forms the strut through which the load is transferred from the point of application to the support. This has necessitated extensive research in order to determine the characteristics of diagonally cracked concrete (7) and the impact of size effects related to concrete in tension (9). This approach has resulted in semi-empirical relationships which have required continuous modification to "fit" the results which were available from experimental investigations. The complexity of the approach lies in the modelling of physically unstable media, due to the continuous cracking of concrete, in the analysis which poses problems in satisfying both equilibrium and compatibility of strains in the idealised structure.

In fact, research over the past three decades which was aimed at resolving the riddle of shear, most notably the work by Kani (10), has resulted in models based either on the behavioural characteristics of the concrete cantilevers which form between adjacent flexural cracks, or the development of arch action in the beams as the ultimate loads were approached. Kotsovos (11) has more recently used the compressive force path concept to explain the behaviour of simple beams in shear. It was concluded that the concrete below the neutral axis did not contribute significantly to the shear capacity of the beam. This was in direct agreement with the findings of the investigations carried out by Kani (10) in which the approach based on the strength of the concrete cantilevers and the one based on the presence of arch action were totally dependent on the strength of the concrete in the compression zone. The indications from published research work are that for concrete beams unreinforced for shear, the concrete in the compression zone is almost entirely responsible for the ability of the section to resist the applied shear loadings.

It is advocated here, based on the behaviour of unreinforced concrete in shear, that the shear capacity of a beam could be enhanced and thus increasing its

overall strength by confining the concrete in the compression zone. This is normal practice in the case of either disturbed regions or axial members (12). The adoption of such an approach would therefore transform the complexity of the flexure-shear interaction to one of designing a compression member. A series of tests has been undertaken on simple beams reinforced with stirrups which did not extend down over the full depth of the beam thus locally confining the concrete in the enclosed compression zone. In addition to observing the strength variations between the individual beams comparisons have been made with the behaviour of beams which were conventionally reinforced.

2. RESEARCH SIGNIFICANCE

This investigation forms part of a research programme whose principal objective is the development of a set of design procedures for structural concrete members which are compatible with their true behaviour. It is believed that the adoption of concepts based on observed failure modes will result in simpler and more realistic approaches to the analysis and design of such structural concrete members.

3. TEST SPECIMENS AND EXPERIMENTAL RESULTS

The test beam specimens, which were all under-reinforced, are described in Figure 1. Typical failure modes and load-deflection relationships for the various specimens are illustrated in Figures 2 and 3 respectively.

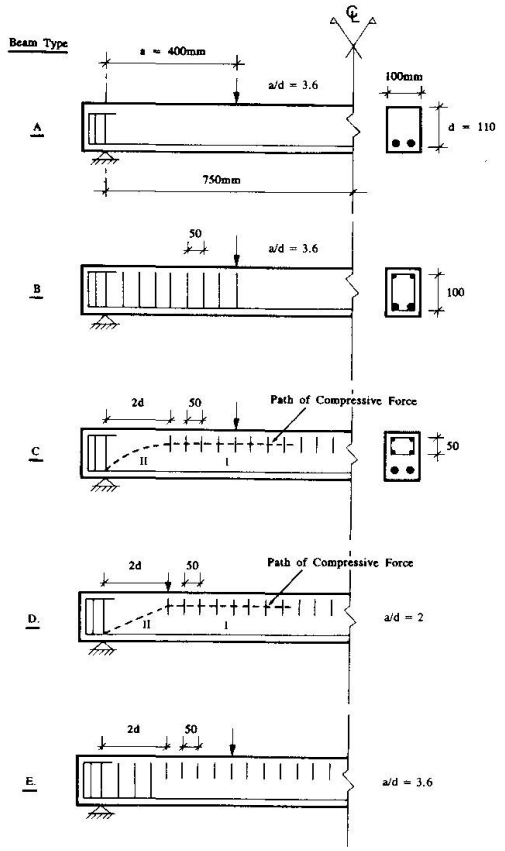

FIGURE 1. TEST SPECIMENS.

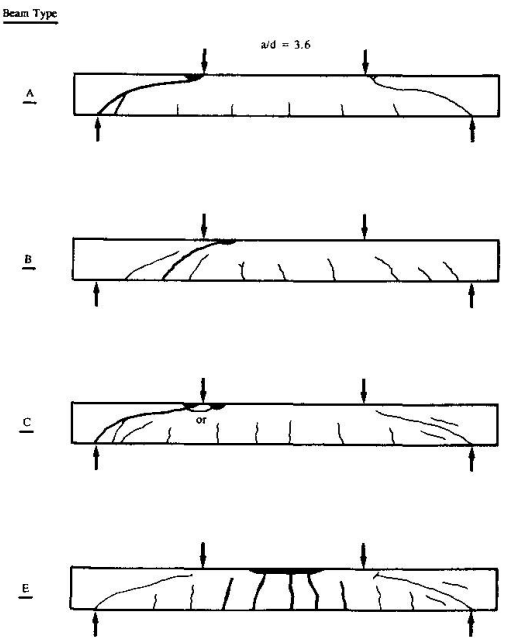

FIGURE 2. MODES OF FAILURE.

Notes:

1. Concrete strength is 28MPa (28 days).
2. Diameter and strength of main steel reinforcement is 12mm and 410MPa respectively.
3. Diameter and strength of transverse steel reinforcement is 6mm and 280MPa respectively.

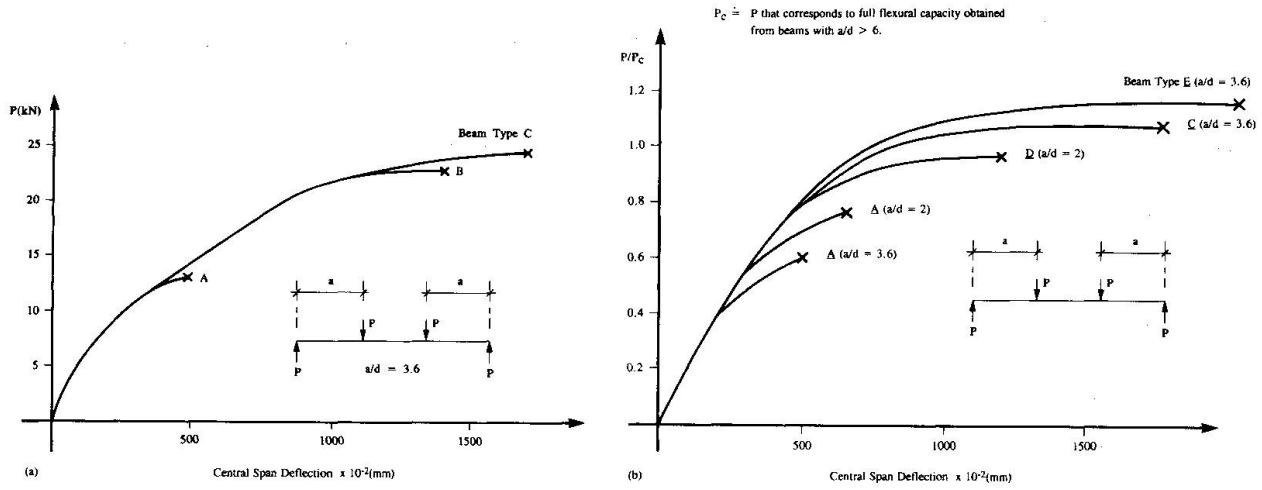

FIGURE 3 (a & b). LOAD DEFLECTION RESULTS.

4. DISCUSSION OF RESULTS

4.1 Modes of Failure

The resulting modes of failure of the beams without stirrups (type A beam in Figure 2) and those reinforced in compliance with Code provisions (type B beam in Figure 2) were as expected. In the case of the type C beams shown in Figure 2, the failure mode cannot be explained in terms of current theories. It was expected, and in accordance with the current theories of beam behaviour, that the failures of the type A and the type C beams would be similarly controlled by their shear capacity since both were unreinforced for shear. However, the type C beams were able to attain their full flexural capacity. The crack patterns present in the type C beams were comparable to those obtained in the type B beams in terms of extensiveness, but characteristically similar to those present in the type A beams. The type C beams contained a major diagonal crack, similar to the one found in the type A beams, which was prevented from splitting the compression zone by the presence of the transverse reinforcement. This allowed the type C beams to develop their full flexural capacity and thus behave in a characteristically ductile manner.

4.2 Load Capacity and Ductility

The type C beams, in which only the compression zone was reinforced with stirrups, and in accordance with the latest truss models or compression field theory, were expected to have the same load carrying capacity as those without stirrups i.e. type A beams. From Figure 3(a) it was found that their load carrying capacity exceeded that of the type A beams by about 90%. In the case of the type C beams, the shear load could not have been carried by a truss structure as generally assumed in present Codes of Practice. The type C beams were found to have a 7% higher load carrying capacity and an approximately 20% higher ductility than the type B beams despite the fact that the type of stirrups normally forming the ties in the truss structure were not present in this case. The increased ductility exhibited by the type C beams could be explained by considering the forces to which the compression zone is

subjected to when the concrete becomes an unstable media due to continuous cracking. In the type B beams, the forces carried by the concrete after cracking are transferred to the stirrups which are anchored in the compression zone. It can be argued that this sudden transfer of stresses will produce impact loading on the compression zone which in turn would initiate a premature failure due to local crushing of the compression zone. This will therefore result in a reduction in the ductility of the beam. Alternatively, for the case of the type C beams the equilibrium of stresses at a section is solely controlled by the characteristics of the concrete in the beam. The provision of passive confinement by the introduction of stirrups in the compression zone creates a multiaxial state of stress in that region which would be able to satisfy equilibrium and compatibility conditions. The degree of ductility exhibited by the beams will depend to a large extent on the level of confinement provided in the compression zone.

4.3 Dependence on "a/d" value

Based on the compressive force path concept, the provision of the necessary transverse reinforcement in the beams, such that they will attain their full flexural capacity, would follow the same procedure regardless of the value of their shear span to effective depth ratio, a/d (13). For example, the compressive zone denoted by I in Figure 2 (type C and type D beams), requires confinement (by the provision of stirrups) regardless of the value of a/d and irrespective of whether or not it is subjected to shear forces. The region denoted by II in Figure 2 (type C and type D beams) follows traditional deep beam behaviour and therefore does not prevent the beam attaining its full flexural capacity. In fact, the type C and D beams were reinforced accordingly. The normalised results together with those of type A beams are shown in Figure 3(b) for comparative purposes. Both types of beams attained the full flexural capacity with higher ductilities than the type A beams. However, the provision of conventional stirrups in the deep beam region as in type E beams (refer to Figure 1) improved both ductility and strength as shown in Figure 3(b).

5. SUMMARY AND CONCLUSIONS

a) The load carrying capacities and ductilities of beams (Figure 3) were enhanced when the compression zone was passively confined with stirrups which did not extend down the full depth of the beam (Figure 1).

b) The special detailing approach adopted in the case of the type C beams (Figure 1) has recognised and attempted to conform to the true flow of stresses in the beam. The approach was essentially based on the compressive force path concept which accepts that the concrete below the neutral axis does not make a significant contribution to the load capacity of the beam. The acceptance and subsequent validation of such an approach will, for example, lead to the removal of the requirement for further investigations into the constitutive relationships for cracked concrete and the significance of the associated size effects in this context.

c) The complex problem of flexure-shear interaction could potentially be reduced to one of the design of axial members. Therefore, the work done on axial loaded concrete members (12) is expected to be directly applicable to this subject area.

d) When the analysis and design of structural concrete members is based on observed modes of behaviour it is anticipated that more rational procedures will be evolved. For example the existing classification of procedures for beam design which are normally dependent on the a/d ratio will become redundant and will lead to the removal of the lack of rationality which presently exists.

ACKNOWLEDGEMENT

The specimens were tested by the students Ziyad Abu Hassanein and Hasheim Skeik from Birzeit University in partial fulfillment of their graduation requirements. Their assistance is gratefully acknowledged.

REFERENCES

1. MACGREGOR, J.G., Challenges and Changes in the Design of Concrete Structures, Concrete International: Design and Construction, Vol. 6, No. 2, February 1984, pp. 48-52.
2. ACI COMMITTEE 318, Building Code Requirements for Reinforced Concrete, ACI 318-89) American Concrete Institute, Detroit, 1989.
3. Design of Concrete Structures for Buildings, (CAN3-A23.3-M84) Canadian Standards Association, Rexdale, 1984, 281pp.
4. Code of Practice for Design and Construction, (BS8110) British Standards Institution, London, 1985, Part 1, 154pp.
5. CEB-FIP Model Code for Concrete Structures, Comite Euro-Internationale du Beton and Federation Internationale de la Preconstrainte, English Edition, Paris, 1978, 156pp.
6. SCHLAICH, J., SCHAFER, K., and JENNEWEIN, M., Toward a Consistent Design of Structural Concrete, PCI Journal, May/June 1987.
7. COLLINS, P.C., and MITCHELL, D., A Rational Approach to Shear Design - The 1984 Canadian Code Provisions, ACI Journal, Vol. 83, November/ December 1986, pp. 925-933.
8. NIELSON, M.P., BRAESTRUP, M.W., JENSEN, B.C., and BACH, F., Concrete Plasticity, Special Publication, Danish Society for Structural Science and Engineering. Lyngby/Copenhagen, October 1978, 129pp.
9. BAZANT, Z.P., and OH, B.H., Crack Band Theory for Fracture of Concrete, Materials and Structures, Vol. 16, No. 93, May/June 1983, pp. 155-177.
10. KANI, G.N.J., The Riddle of Shear Failure and Its Solution, ACI Journal, Vol. 61, No. 4, April 1964, pp. 441-467.
11. KOTSOVOS, M.D., Compressive Force Path Concept: Basis for Reinforced Concrete Ultimate State Design, ACI Structural Journal, Vol. 85, No. 1, January/February 1988, pp. 68-75.
12. KUTTAB, A.S. and DOUGILL, J.W., Grouted and Dowelled Jointed Precast Concrete Columns: Behavior in Combined Bending and Compression, Magazine of Concrete Research (London), Vol. 40, No. 144, September 1988, pp. 131-142.
13. KUTTAB, A.S., Assessment of Concrete Structures Utilising Multiaxial Properties, Proceedings of the International Symposium on "Re-Evaluation of Concrete Structures" organised by the Danish Concrete Institute (DABI), Copenhagen/Lyngby, June 1988.

Shear in Structural Concrete: a Reappraisal of Current Concepts

Cisaillement du béton armé: nécessité de reconsidérer les concepts courants

Schubtragfähigkeit: Fragwürdige Bemessungsgrundlagen

Michael D. KOTSOVOS
Dr. Eng.
Imperial College
London, UK

Michael D. Kotsovos obtained his Ph.D. in 1974 and his D.Sc. in 1981. Twice he has been awarded Henry Adams diplomas by the Institution of Structural Engineers, London. His research interests cover most aspects of structural concrete behaviour under static and dynamic loading conditions.

SUMMARY

Evidence is presented which demonstrates that current design concepts are incompatible with the ultimate limit state of reinforced concrete beams. It is found that shear capacity is associated with the strength of the compressive zone and not, as widely considered, the portion of the beam below the neutral axis. The mechanism of shear resistance and the causes of failure are identified and it is shown that modelling a reinforced concrete beam as a frame with inclined legs tied by the tension reinforcement can lead to reliable design solutions which are both more economical and safer than those resulting from current design models. It is suggested that any skeletal structural form can be considered as an assemblage of elements formed between consecutive points of inflection with the elements being described by the proposed model.

RÉSUMÉ

La preuve est établie que les concepts courants de dimensionnement sont incompatibles avec l'état de limite ultime des poutres en béton armé. La résistance au cisaillement est en réalité associée à la résistance de la zone comprimée et non pas à la zone située au-dessous de l'axe neutre, comme couramment considéré. On décrit ainsi le mode de résistance au cisaillement, de même que les causes de rupture; une poutre en béton armé modélisée par un cadre aux bords inclinés et reliés par l'armature de traction peut mener à des solutions de dimensionnement fiables qui sont bien plus sûres et économiques que celles résultant des modèles de conception courants. On suggère donc de considérer toute forme d'ossature comme un assemblage d'éléments décrits précédemment se formant entre deux points d'inflexion consécutifs.

ZUSAMMENFASSUNG

Versuchsergebnisse über die mangelhafte Beschreibung des Stahlbetonverhaltens mittels derzeitiger Bemessungsgrundlagen werden vorgetragen. Es wird gezeigt, dass die Schubtragfähigkeit nicht, wie üblich angenommen, dem unterhalb der Nullinie liegenden Balkenanteil zugeordnet ist, sondern der Tragfähigkeit der Betondruckzone. Der Mechanismus des Querkraftwiderstands und die Fehlerursache werden ermittelt. Es wird anschaulich vorgeführt, dass die Abbildung des Stahlbetonbalkens durch einen Rahmen mit schrägliegenden Beinen und Zugband zu zuverlässigen Bemessungslösungen führen, die nicht nur wirtschaftlicher, sondern auch sicherer als die Lösungen mittels derzeitiger Bemessungsgrundlagen wie Fachwerkträger und Druckstab mit Zugband sind. Es wird vorgeschlagen, das Stahlbetonskelett als Zusammenstellung solcher Elemente zwischen den aufeinanderfolgenden Momentennullpunkten zu betrachten.

1. INTRODUCTION

Current methods used for shear design often yield poor predictions of shear capacity. Fig. 1 provides an indication of such predictions and demonstrates the possibility for current Code provisions [1-5] to yield predictions which can be over-conservative in certain cases and unsafe in others. Clearly, the cause for such predictions should be attributed to the underlying concepts, common to all current shear design methods, rather than the various formulations used by particular methods for the implementation of the concepts in design.

In view of the above, it is considered that a reappraisal of the current design concepts should be a prerequisite for any future Code revision. Such a reappraisal, which is essential not only for improving existing design models but also, if necessary, for developing new ones, has formed the subject of recent work which has been aimed at identifying the fundamental causes of the observed behaviour of structural concrete members. The paper summarizes the main results of the work and describes a first attempt to implement them in design.

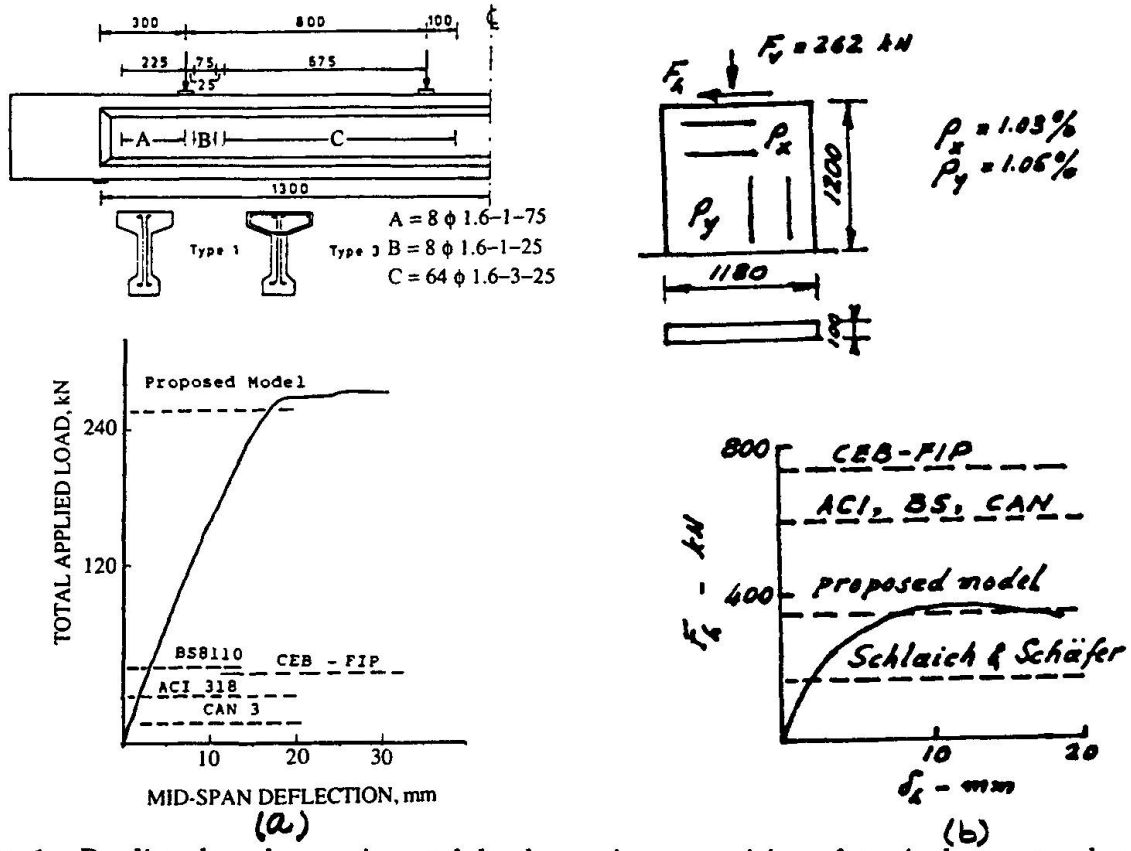

Fig. 1 Predicted and experimental load-carrying capacities of typical structural concrete members tested by (a) Kotsovos & Lefas [11] and (b) Maier & Thurlimann [12].

2. CONCEPTS UNDERLYING SHEAR DESIGN

Current methods for the design of structural concrete members are invariably based on the view that shear resistance is mainly provided by the portion of the member outside the compressive zone. In the absence of transverse reinforcement, such resistance is provided by concrete with main contributor the aggregate interlock which is effected by the shearing movement of the surfaces of inclined cracks. Shear failure is considered to occur when the shear capacity of a critical section is attained and, in order to prevent it, transverse reinforcement is provided to carry the portion of the shear force that cannot be sustained by concrete alone. Such reinforcement is designed on the basis of the assumption that the interaction between concrete and reinforcement can be described by a suitable strut and tie or truss model the strength of which may or may not rely on the contribution of aggregate interlock. In the former case, the model struts are considered to intersect the inclined cracks - and, hence, aggregate interlock is essential for the load-carrying capacity of the struts -

whereas in the latter, a strut is considered to be formed by concrete between consecutive inclined cracks.

3. TEST OF VALIDITY OF CONCEPTS

A test of the validity of the above concepts has been based on an investigation of the behaviour of RC beams, with various arrangements of transverse reinforcement (see Fig. 2a), subjected to two-point loading with various shear span to depth ratios (a_v/d) [6]. The main results of this programme are also given in Fig. 2a in the form of load-deflection curves for the beams tested.

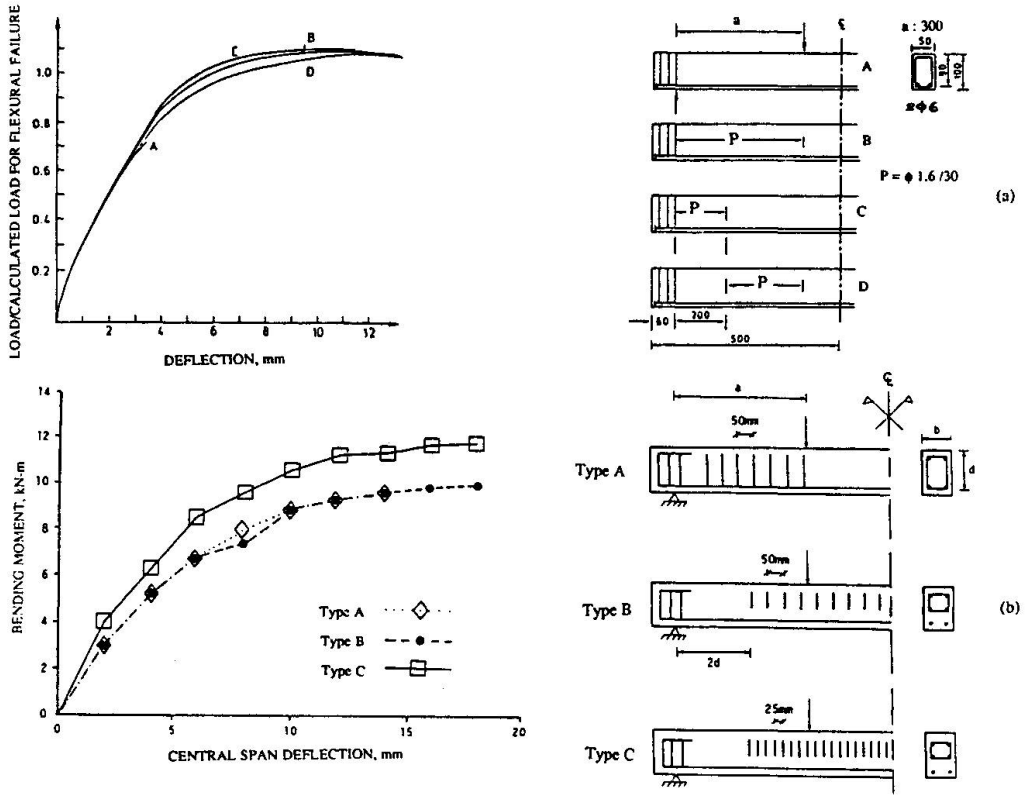

Fig. 2 Typical load-deflection relationships for beams with various stirrup arrangements tested by (a) Kotsovos [6] and (b) Kuttab [8].

On the basis of the concept of shear capacity of critical sections all beams with their shear span without transverse reinforcement, either throughout or over a large portion of its length, should have a similar load-carrying capacity. And yet, beams C and D were found to have a load-carrying capacity significantly higher than that of beams A. In fact, beams C and D exhibited ductile behaviour - a characteristic of under-reinforced concrete beams exhibiting a flexural mode of failure - and their load-carrying capacity was double that of beams A. These results clearly indicate that such behaviour cannot be explained in terms of the concept of shear capacity of critical sections.

The evidence presented in Fig. 2a also contrasts the view that aggregate interlock makes a significant contribution to shear resistance. This is because the large deflections exhibited by beams C and D led to a large increase of the inclined crack width and thus considerably reduced, if not eliminated, aggregate interlock. In fact, near the peak load, the inclined crack had a width in excess of 2 mm which is by an order of magnitude larger than that found by Fenwick and Paulay [7] to reduce aggregate interlock by more than half. It can only be concluded, therefore, that, in the absence of transverse reinforcement, the main contributor to the shear resistance of an RC beam at its ultimate limit state is the compressive zone, with the region of the beam below the neutral axis making an insignificant, if any,

contribution.

As for the concepts discussed so far, the test results are also in conflict with the truss or strut and tie concepts. A large portion of the shear span of beams C and D cannot behave as the models imply, since neither the absence of transverse reinforcement allows the formation of ties nor the presence of a wide inclined crack permits the formation of a strut. And yet, the beams sustained loads significantly larger than those widely expected. Such behaviour indicates that, in contrast with widely held views, truss or strut and tie behaviour is not a necessary condition for the beams to attain their flexural capacity once their "shear capacity" is exceeded.

The validity of the conclusions drawn from the results discussed above is supported by the results (see Fig. 2b) obtained in a more recent experimental work [8] which involved the testing of the RC beams also shown in Fig. 2b. The figures indicate not only that restricting the transverse reinforcement within the compressive zone does not reduce the load-carrying capacity of the beams, but also that designing such reinforcement so as to provide a more effective confinement to the compressive zone improves significantly both strength and ductility. It would appear, therefore, that, in contrast with current views, it is the compressive zone, and not the portion of a structural concrete member outside this zone, that provides shear resistance to the member.

4. MECHANISMS OF SHEAR RESISTANCE AND FAILURE

The underlying causes of shear resistance of the compressive zone have been investigated by testing RC T-beams with a web width significantly smaller than that considered, in compliance with current thinking, to provide adequate shear resistance [9]. Design details of a typical beam with a 2.6 m span tested under six-point loading are shown in Fig. 3 which also shows a typical mode of failure. The tests indicated that the load-carrying capacity of the beams was up to three times higher than that predicted on the basis of the currently accepted concepts. It was also found that failure usually occurred in regions not regarded by current Code provisions as the most critical. As the web width of these beams was inadequate to provide shear resistance, the above results support the view that the region of the beam above the neutral axis - the flange in the present case - is the main, if not the sole, contributor to shear resistance.

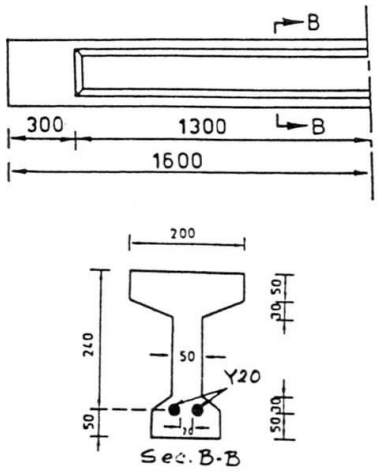

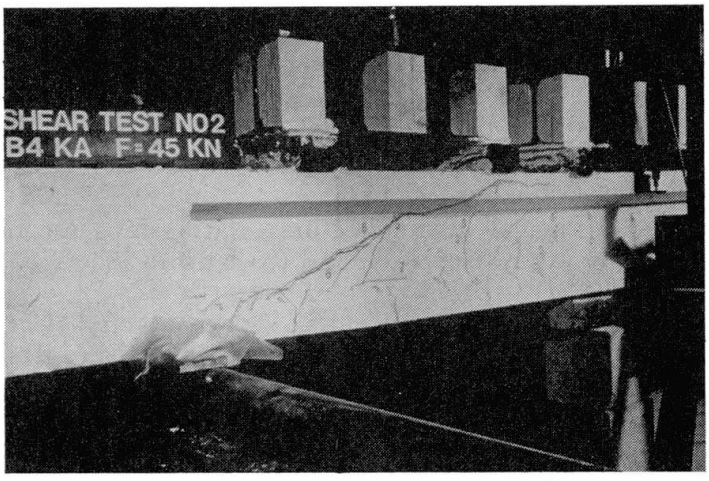

Fig. 3 RC T-beams under six-point loading. Design details and mode of failure [6].

It is also interesting to note in Fig. 3 that the inclined crack, which eventually caused failure, penetrated very deeply into the compressive zone. In fact, it locally reduced the depth of the neutral axis to less than 5% of the beam depth. In view of such a small depth of the compressive zone, it may be argued that concrete is unlikely to be able to sustain the high tensile stresses caused by the presence of the shear force. Such an argument is usually based on the erroneous assumption that concrete behaviour within the compressive zone of a beam at its ultimate limit state is realistically described by using uniaxial stress-strain characteristics. This assumption is in conflict with recent experimental information which has demonstrated quite conclusively that the stress conditions within the compressive zone

of an RC beam at its ultimate limit state are triaxial [6,10]; in fact, concrete in the region of a section through the tip of a deep flexural or inclined crack is subjected to a wholly compressive state of stress which represents the restraining effect of the adjacent concrete [10]. It is considered that a part of the vertical and horizontal components of this compressive state of stress counteracts the tensile stresses developing in the presence of the shear force. Hence, in spite of the presence of such a force, the state of stress remains compressive and this causes a significant enhancement of the local strength; a schematic representation of the mechanism providing shear resistance is shown in Fig. 4. However, eventually the shear force increases beyond a critical level and results in the development of tensile stresses sufficiently large to eliminate the restraining effect of the adjacent concrete thus creating a compression/tension stress field which reduces abruptly the local strength and causes failure.

5. IMPLEMENTATION IN DESIGN

A recent attempt to summarize the experimental information discussed in the preceding sections and present it in a unified and rational form has led to the formulation of the concept of the compressive force path [6]. On the basis of this concept, the load-carrying capacity of a structural concrete member is associated with the strength of concrete in the region of paths along which compressive forces are transmitted to the supports. The path of the compressive force may be visualized as a "flow" of compressive stresses with varying section perpendicular to the path direction and with the compressive force representing the stress resultant at each section (see Fig. 5). Failure has been shown to relate with the presence of tensile stresses in the region of the path and such stresses may develop due to a number of causes, the main ones being associated with changes in the path direction, the varying intensity of the compressive stress field along the path, bond failure at the level of the tension reinforcement between two consecutive flexural or inclined cracks, etc.

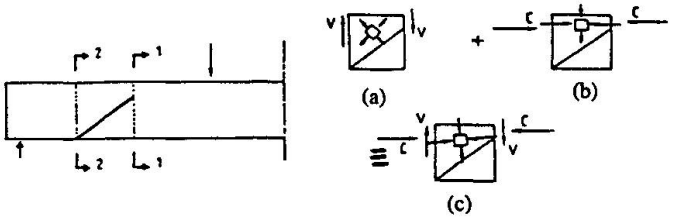

Fig. 4 Mechanism providing shear resistance.

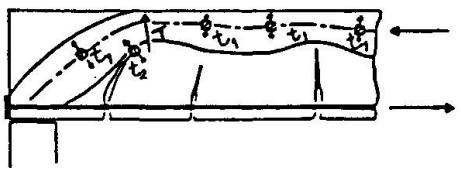

Fig. 5 Compressive force path.

The above concept has been implemented in design by modelling an RC beam as a frame with inclined legs tied by the tension reinforcement (see Fig. 6) with the frame providing a simplified representation of the compressive force path. In compliance with the proposed concept, failure of the model should occur due to failure of either the horizontal or inclined members of the frame or the joint of these members. A full description of the model together with design examples and experimental verification forms the subject of other publications [eg. 11] where it is shown that the resulting design solutions are not only more economical but also safer than those obtained by using the methods recommended by current Codes of practice. A typical example of the application of the above model in design is given in Fig. 1a which shows the design details of a simply supported beam subjected to four-point loading together with the load-deflection curve established by experiment. The Figure also includes the values predicted for load-carrying capacity by current Codes as well as that predicted by the proposed model and it is interesting to note that while the beam strength is closely predicted by the proposed model, it is between approximately 5 and 20 times larger than the Code predicted values. It is also important to note that the above model can form the basis for the design of more complex skeletal structural forms such as, for example, continuous beams, frames, etc. In such cases, the model shown in Fig. 6 represents an element of a skeletal structural form between two consecutive points of zero bending moment, as indicated in Fig. 7, with the transverse reinforcement at the point of zero moment being designed so as to represent an internal support forming between two

consecutive beam elements.

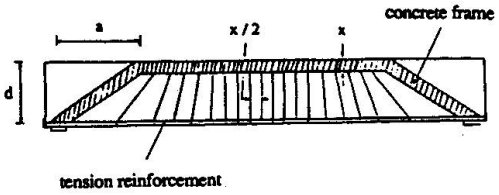

Fig. 6 Model for simply-supported beams.

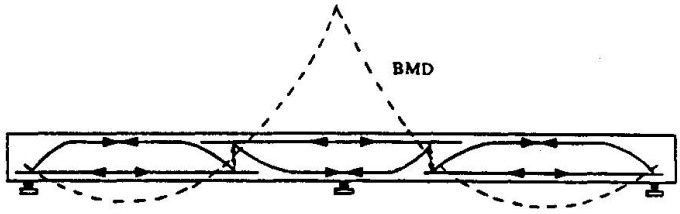

Fig. 7 Model for a continuous beam.

6. CONCLUSIONS

1. The concepts underlying shear design methods are found to be incompatible with the observed behaviour of RC beams. Shear capacity is shown to be provided by the compressive zone and not, as widely believed, the portion of the beam below the neutral axis.

2. Shear resistance is associated with the development of a triaxial compressive state of stress in the region of the tip of deep inclined cracks and failure eventually occurs due to the development of transverse tensile tensile stresses within the compressive zone.

3. Modelling an RC beam as a frame with inclined legs tied by the tension reinforcement is shown to lead to design solutions which are both safer and significantly more economical that those currently obtained. Such a model may be considered to represent the portion forming between consecutive points of inflection of any skeletal structural concrete configuration.

7. REFERENCES

1. American Concrete Institute. Building Code Requirements for Reinforced Concrete, ACI 318-83 (1983).

2. British Standards Institution. Code of Practice for Design and Construction, BS8110, 1 (1985).

3. Canadian Standards Association. Design of Concrete Structures for Buildings, CAN3-A23.3-M84 (1984).

4. CEB-FIP Model Code for Concrete Structures. Bulletin d' Information 124-125 (1978).

5. Schlaich J. and Schafer K. Konstruieren im Stahlbeton, Beton-Kalender 1984, Wilhem Ernst und Sohn, Berlin, 87-1004.

6. Kotsovos, M. D. Compressive force path: Basis for ultimate limit state reinforced concrete design. ACI Journal, 85 (1988), 68-75.

7. Fenwick, R. C. and Paulay, T. Mechanisms of shear resistance of concrete beams. Journal of the Structural Division, ASCE, 94 (1968), 2325-2350.

8. Kuttab A. Beam Tests. Presented at meeting of CEB Task Group 24 held in Dubrovnik (1988).

9. Kotsovos, M. D. , Bobrowski, J., and Eibl, J. Behaviour of RC T-beams in shear. The Structural Engineer, 65B (1987), 1-10.

10. Kotsovos, M. D. Consideration of Triaxial Stress Conditions in Design: A Necessity. ACI Journal, 84 (1987), 266-273.

11. Kotsovos, M. D. and Lefas, I. D. Behaviour of reinforced concrete beams designed in compliance with the compressive force path. ACI Structural Journal, 87 (1990), 127-139.

12. Maier J. and Thurlimann B. (1985) Bruchversuche an Stahlbetonscheiben. Bericht No. 8003-1, Institut für Baustatik und Konstruktion, ETH Zurich.

Shear Strength of Beams at Very Low Temperatures

Résistance à l'effort tranchant de poutres à très basses températures

Schubtragfähigkeit von Stahlbetonbalken im Tieftemperaturbereich

Luc TAERWE
Lecturer
Univ. of Ghent
Ghent, Belgium

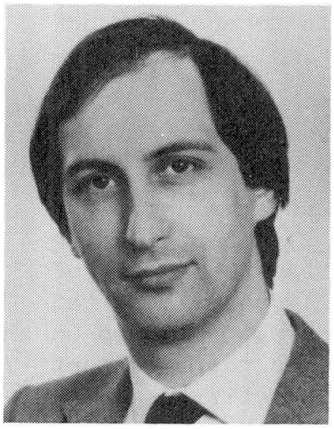

Luc Taerwe graduated as Civil Engineer at the University of Ghent in 1975 where he also obtained his Doctor's degree. At the Magnel Laboratory he is involved in research on nonlinear behaviour of concrete structures, high strength concrete, quality assurance and stochastic modelling. He is the recipient of several scientific awards.

Hendrik LAMBOTTE
Prof. Emeritus
Univ. of Ghent
Ghent, Belgium

Hendrik Lambotte was Director of the Magnel Laboratory for Reinforced Concrete from 1983 to 1990 and Full Professor involved in teaching and research on reinforced and prestressed concrete. He is chairman of the Belgian Standardization Committee on Concrete, member of the Advisory Committee of CEB and of the Editorial Group of EC 2.

SUMMARY

Loading tests on 14 reinforced concrete beams were performed both at ambient temperature and at −165°C. Most beams failed in shear. From the results, it follows that under cryogenic conditions shear strength increases considerably. This effect is mainly due to the increase of concrete tensile strength at low temperatures. Also restrained thermal shortening of the reinforcing steel has a beneficial effect.

RÉSUMÉ

Une série de 14 poutres en béton armé a été soumise à un essai de mise en charge et ceci à températures ambiantes et à −165°C. La plupart des poutres présentent une rupture à l'effort tranchant. Les résultats des essais montrent que la résistance à l'effort tranchant augmente considérablement en environnement cryogénique. Ce phénomène peut être attribué principalement à l'augmentation de la résistance à la traction du béton à basses températures. La contraction thermique empêchée de l'acier à également un effet favorable.

ZUSAMMENFASSUNG

An einer Reihe von insgesamt 14 Stahlbetonbalken wurden Schubversuche durchgeführt, sowohl bei Umgebungstemperatur als auch bei −165°C. Die meisten Balken erwiesen einen Schubbruch. Aus den Versuchsergebnissen folgt, dass die Schubtragfähigkeit erheblich zunimmt im Tieftemperaturbereich, was hauptsächlich am günstigen Einfluss der niedrigen Temperaturen auf die Betonzugfestigkeit zugeschrieben werden kann. Auch die verhinderte thermische Dehnung des Betonstahls hat einen günstigen Einfluss.

1. INTRODUCTION

Knowledge of the structural behaviour of concrete members at very low temperatures is particularly important for the design of storage tanks for liquefied natural gas (LNG). In the case of LNG tanks with elevated base slab (e.g. at Zeebrugge, Belgium) the area around the supporting columns has to be checked for punching shear not only under regular but also under accidental loading conditions involving cooling of the slab from above due to spill from the inner steel container. Also the wall to base connection is an area subjected to important shear forces. Hence the need to investigate the influence of very low temperatures on shear resistance of reinforced concrete beams and slabs. In this paper, the results of loading tests on beams are discussed by addressing the influence of low temperatures on material properties and by considering the action effects caused by internal restraints. As pointed out by Breen [1], particular types of loading and restraints are among the technical challenges that remain to be explored. Moreover, shear strength is one of the typical fields where reliance on concrete tensile strength is taken into account, as indicated by Hillerborg in [2].

2. TEST PROGRAM

Loading tests were performed on 14 reinforced concrete beams with a span of 1.5 m, a width b = 400 mm and a total depth h = 200 mm (fig. 1). The effective depth d equals 165 mm and the tensile reinforcement of the beams consists of deformed TEMPCORE bars Ø 14 mm. The beam designation (table 1) consists of the capitals P (preliminary), R (reference) and L (low temperature) followed by the longitudinal reinforcement ratio $\rho_s = A_s/bd$ in % and the web reinforcement ratio $\rho_{sw} = A_{sw}/bs$ also in % (s denoting stirrup spacing). The stirrups consist of 4 legged closed stirrups, 6 or 8 mm in diameter. By way of example, the dimensions and the reinforcement of beams R/1.86/0.20 and L/1.86/0.20 are shown in fig. 1.

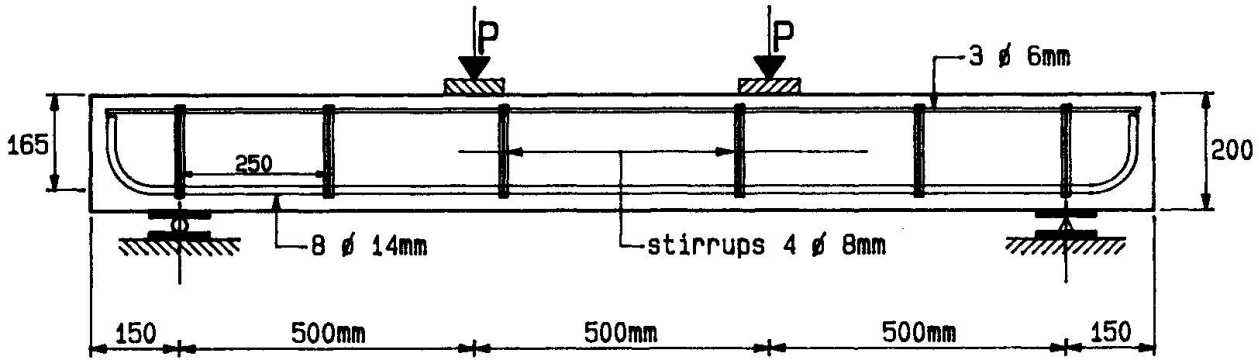

Fig. 1 Dimensions and reinforcement of beams R/1.86/0.20 and L/1.86/0.20

The beams designated P and R were tested at room temperature (20°C) at an age of respectively 28 days and 3 months. The upper face of the beams designated L, was cooled with liquid nitrogen (-196°C) until, at the level of the tensile reinforcement, a temperature of about -165°C was reached. This latter value corresponds to the temperature of liquefied natural gas. Cooling took about 6 hours. Subsequently the loads were gradually increased up to failure. Vertical copper strips, partially embedded in the beams' upper surface, served to retain the liquid nitrogen. Insulating pannels were glued at the side faces, in order to obtain a uniform temperature distribution over the width of the beams.

Beam designation	ρ_s (%)	ρ_{sw} (%)	s (mm)	P_u (kN)	τ_u (N/mm^2)	Type of failure
P/0.93/0.00	0.93	0	-	105	1.59	shear
P/1.86/0.00	1.86	0	-	122	1.85	shear
R/0.93/0.00	0.93	0	-	107	1.62	bending
R/0.93/0.19	0.93	0.19	150	108	1.64	bending
R/1.40/0.00	1.40	0	-	120	1.82	shear
R/1.86/0.00	1.86	0	-	136	2.06	shear
R/1.86/0.20	1.86	0.20	250	201	3.05	shear
R/1.86/0.34	1.86	0.34	150	195	2.95	bending
L/0.93/0.00	0.93	0	-	150	2.27	shear
L/0.93/0.19	0.93	0.19	150	189	2.86	bending
L/1.40/0.00	1.40	0	-	194	2.94	shear
L/1.86/0.00	1.86	0	-	278	4.21	shear
L/1.86/0.20	1.86	0.20	250	315	4.77	shear
L/1.86/0.34	1.86	0.34	150	275	4.17	shear

Table 1 Survey of beam characteristics

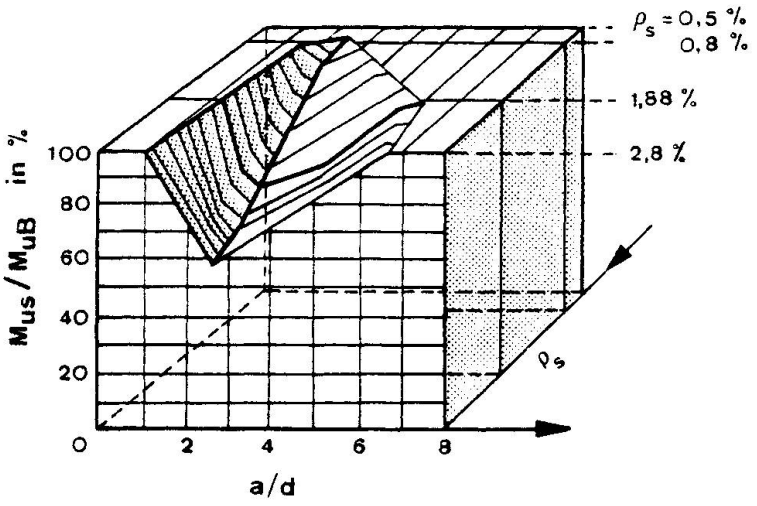

The beams were submitted to two point loads at a third of the span. Hence the shear span "a" equals 500 mm and a/d = 3. This latter value is known to be the most critical for shear strength [3]. In fig. 2 Kani's "shear failure valley" for beams without shear reinforcement is shown [3]. The diagram depicts the influence of a/d and ρ_s on the ratio of the ultimate moment corresponding to shear failure (M_{uS}) to the ultimate moment for bending failure (M_{uB}).

Fig. 2 Kani's shear failure valley [3]

Stirrup spacing s = 150 mm corresponds to z/s = 1, where z = 0.9 d equals the depth in the equivalent truss model. In the case of s = 250 mm, the ratio z/s equals 150/250 = 3/5 which is the lower value of the crack inclination θ allowed in the "accurate" shear design method according to the CEB-FIP Model Code for Concrete Structures (1978 Edition).

3. MATERIAL PROPERTIES

The beams and the accompanying test specimens were cured in a moist room at 20°C until 24 hr before testing. Mean concrete strength characteristics are given in table 2. Due to the low temperature effect, compressive strength $f_{c,cub}$ increased by a factor 1.78 and flexural tensile strength f_{ctb} by a factor 1.49.

Beam type	28 days	3 months					
	$f_{c,cub}$	$f_{c,cub}$		f_c	f_{ct}	f_{ctb}	
	20°C	20°C	-165°C	20°C	20°C	20°C	-165°C
P	63.4	70.7	-	-	-	-	-
R	62.2	70.8	-	62.8	3.53	8.53	-
L	-	72.0	128.0	61.9	4.50	8.75	13.08

Table 2 Concrete strength characteristics in N/mm^2

For the longitudinal tensile reinforcement f_y = 504 N/mm^2 and f_{st} = 588 N/mm^2 were obtained as mean values at 20°C. For the type of reinforcing steel used it was found in previous research programs that the yield stress at -165°C increased by about 50 % compared to the value at 20°C [4]. However, calculated ultimate moments for the beams considered indicate that in this case the increase might be about 70 %. The ratio f_{st}/f_y approaches 1 under cryogenic conditions.

4. TEST RESULTS

The ultimate loads P_u and the type of failure are mentioned in table 1. Shear failures occured due to flexure shear cracking in the shear spans. For all beams, included those failing in bending, the nominal shear stress $\tau_u = V_u/bd$ is indicated in table 1.

5. DISCUSSION OF TEST RESULTS

5.1. General analysis

Comparison of the τ_u-values for similar beams failing in shear both at 20°C and -165°C, yields ratios varying between 1.43 and 2.04. This increase in shear resistance must mainly be attributed to the increase in tensile strength of the concrete due to the low temperatures (see also section 5.2).

The observation that for two identical beams, P/0.93/0.00 and R/0.93/0.00, the first fails in shear and the latter in bending can be explained by the fact that the value of ρ_s corresponds to the onset of Kani's shear failure valley (fig. 2). Hence, due to the scatter inherent to this type of test, either failure mode is equally likely to occur. However, at low temperatures, the shear failure mode is clearly predominant. The presence of stirrups in beam L/0.93/0.19 is not apparent form the failure load since beam L/0.93/0.00 failed already in bending.

Beam R/1.86/0.20, failing in shear, was probably already very near to the transition from shear to bending failure as beam R/1.86/0.34 fails at a slightly lower load in bending. At low temperatures shear failure is predominant for ρ_s = 1.86 %. The difference in web reinforcement ratio for the three beams L/1.86 is not reflected in the failure loads. Probably the onset of yielding of the tensile reinforcement initiated shear failure.

According to [3], the stirrups become active from a value $\tau_{oD} = 0.24\sqrt{f_{c,cub}}$ on. For beam R/1.86/0.20 this corresponds to a shear force $0.24\sqrt{70.9} \times 0.9 \times 165 \times 400$ = 120 kN. This value is in very good agreement with the experimental

strain measurements. These also indicate yielding of the stirrups at ultimate and hence the corresponding force equals $F_{sw} = f_y \times A_{sw} = 472 \times 201 = 95$ kN. Summation of both contributions yields 215 kN as estimate of the experimental value of 201 kN.

5.2. Influence of tensile strength on shear resistance

The influence of tensile strength on shear resistance is accounted for by a factor $\sqrt{f_c}$ in the formulas for the ultimate nominal shear stress. According to [3] the nominal shear stress for beams without stirrups is given by

$$\tau_{u,1} = 0.18 \sqrt{f_{c,cub}} \sqrt[3]{100\ \rho_s} \qquad (1)$$

for the particular values of the scale factor and a/d applicable to the beams considered. In [5], the following modification of the ACI 318 Building Code formula (11-6) was proposed

$$\tau_{u,2} = 0.15 \sqrt{f_c} + 62.6\ \rho_s \frac{d}{a} \qquad (2)$$

The calculated values are mentioned in table 3 and compared with the experimental values τ_u. For the cooled beams, the material properties at -165°C have been considered. Formulas (1) and (2) underestimate the experimental values by about 10 % and 25 % respectively, at least for the beams tested at 20°C and beam L/0.93/0.00. A better fit can be obtained for (1) by increasing the first factor up to 0.20 and for (2) by doubling the second term.

Beam	τ_u (N/mm^2)	$\tau_{u,1}$ (N/mm^2)	$\frac{\tau_u}{\tau_{u,1}}$	$\tau_{u,2}$ (N/mm^2)	$\frac{\tau_u}{\tau_{u,2}}$
P/0.93/0.00	1.59	1.41	1.13	1.33	1.20
P/1.86/0.00	1.85	1.75	1.06	1.51	1.23
R/1.40/0.00	1.82	1.67	1.09	1.49	1.22
R/1.86/0.00	2.06	1.79	1.15	1.56	1.32
L/0.93/0.00	2.27	1.99	1.14	1.78	1.27
L/1.40/0.00	2.94	2.28	1.29	1.88	1.56
L/1.86/0.00	4.21	2.55	1.65	1.97	2.14

Table 3 Experimental and calculated nominal shear stresses.

From table 3 it follows that for the lower temperatures and the higher ρ_s values the underestimation becomes very important which indicates that phenomena other than those accounted for by (1) and (2) must have a beneficial contribution to shear resistance.

5.3. Other phenomena affecting shear resistance at low temperatures

Under cryogenic conditions, the coefficient of thermal expansion of steel is only slightly reduced whereas that of concrete significantly decreases, depending on the moisture content. As pointed out in [4], the restrained differential shortening in a reinforced concrete section causes a kind of artificial prestressing. Considering a symmetrical section subjected to a uniform temperature drop ΔT, the compressive stress in the concrete can be calculated by the following formula

$$\sigma_c = \frac{E_s.\rho.(\alpha_{ts} - \alpha_{tc}).\Delta T}{1 + (\alpha - 1)\ \rho} \qquad (3)$$

where α_{ts} and α_{tc} are the coefficients of thermal epansion of steel and concrete and ρ is calculated as $(A_s + A_{sc})/bh$. In the case of a non-symmetric reinforcement arrangement, this formula still holds for the stress at the centroid of the equivalent section $A_c + \alpha A_s$. Introducing $\Delta T = 190°C$, $E_c = 35000$ N/mm^2, $\alpha_{ts} - \alpha_{tc} = 3.10^{-6}/°C$ and the appropriate values of ρ, one finds $\sigma_c = 0.96$ N/mm^2 ($\rho_s = 0.93$ %), $\sigma_c = 1.36$ N/mm^2 ($\rho_s = 1.40$ %) and $\sigma_c = 1.74$ N/mm^2 ($\rho_s = 1.86$ %). The induced compressive stress σ_c has a beneficial influence on the principal tensile stress $\sigma_I = \sqrt{\sigma_c^2/4 + \tau_c^2} - \sigma_c/2$.

This effect is merely related to the first contributing term in (2) and does not fully account for the observed higher τ_u values at low temperatures and highest ρ_s values. The second term in (2), which reflects the influence of A_s, must also increase because of higher bond strength, and smaller crack widths and deflections at the same load level. These phenomena, confirmed by experimental observations, hamper propagation and opening of the inclined cracks.

6. CONCLUSIONS

From loading tests on reinforced concrete beams both at reference temperature (+20°C) and under cryogenic conditions (-165°C), it can be concluded that the beneficial effect of very low temperatures on shear strength has to be attributed to the following phenomena (in descending order of importance)

- increased tensile strength of concrete
- restrained thermal shortening of the steel, creating a kind of prestressing
- higher bond strength and smaller crack widths, causing a higher contribution of the shear strength term proportional to ρ_s.

ACKNOWLEDGMENT

The authors gratefully acknowledge research grant no. 2.9002.85 from the Belgian Fund for Joint Basic Research.

REFERENCES

1. BREEN J., Why structural concrete. Introductory Report, IABSE Colloquium "Structural Concrete", 1991, Stuttgart.

2. HILLERBORG A., Reliance upon concrete tensile strength. Introductory Report for Theme 2.5, IABSE Colloquium "Structural Concrete", 1991, Stuttgart.

3. LEONHARDT F., Schub bei Stahlbeton und Spannbeton - Grundlagen der neueren Schubbemessung. Beton- und Stahlbetonbau 11/1977, pp. 270-277, 12/1977, pp. 295-302.

4. LAMBOTTE H., TAERWE L., DE SAINT MOULIN I., Shear resistance at low temperatures of deep hyperstatic reinforced concrete beams. Proceedings "Symposium on Transport and Storage of LPG & LNG", Brugge, 1984, Royal Flemish Society of Civil Engineers (K.VIV), pp. 357-364.

5. SMITH K., VANTSIOTIS A., Deep Beam Test Results Compared with Present Building Code Models. ACI Journal, July-August, 1982, pp. 280-287.

Shear Strength of Beams without Shear Reinforcement

Cisaillement des poutres en béton précontraint dépourvues d'étriers

Schubtragfähigkeit von Spannbetonbalken ohne Schubbewehrung

Tamon UEDA
Assoc. Prof.
Univ. of Tokyo
Tokyo, Japan

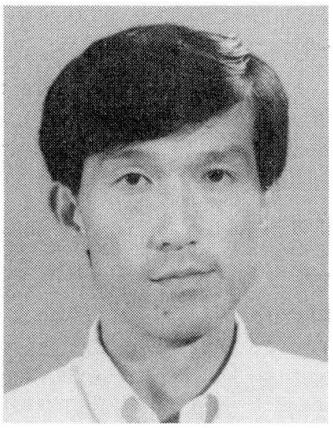

Tamon Ueda, born in 1954, obtained his Doctor of Engineering degree from University of Tokyo in 1982. He served as Assistant and Associate Professor at Asian Institute of Technology. His research interests relate to the deformation mechanism of concrete.

Heru Darjudi Eko PUTRO
Civil Eng.
Asian Inst. of Technol.
Bangkok, Thailand

Heru Darjudi Eko Putro obtained his Master of Engineering degree from Asian Institute of Technology in 1990. Currently he is in a consulting firm in Jakarta.

SUMMARY

Strengths of shear compression failure in prestressed concrete beams can be predicted by the finite elements method analysis, in which a main shear crack is modelled as a discrete crack. Compression failure of concrete in the maximum moment region causes shear failure of the beams. A narrower compression zone is considered to make the shear strength less than the flexural strength. Force transferred along the main shear crack does not affect the shear strength of the beam too much.

RÉSUMÉ

La résistance ultime au cisaillement des poutres en béton précontraint peut être prévue à l'aide d'une analyse non-linéaire par la méthode des éléments finis, où chaque fissure de cisaillement est modélisée comme une fissure discrète. La rupture en compression du béton dans la zone de moment maximum est responsable dans les poutres de la ruine par cisaillement. Une zone comprimée plus étroite rend la résistance au cisaillement plus faible que la résistance flexionnelle. La force transmise le long de la fissure principale d'effort tranchant n'a qu'un faible effet sur la résistance au cisaillement de la poutre.

ZUSAMMENFASSUNG

Die Tragfähigkeit von Spannbetonbalken mit Schubdruckbrüchen kann mit einer Finite Element Berechnung ermittelt werden, bei der ein Hauptschubriss diskret modelliert wird. Betondruckversagen im Bereich des grössten Biegemoments verursacht den Schubbruch. Kleinere Druckzonenhöhen vermindern die Schubtragfähigkeit stärker als die Biegetragfähigkeit. Die Kraftübertragung längs des Hauptschubrisses beeinflusst die Schubtragfähigkeit nur gering.

1. INTRODUCTION

Shear strength of reinforced concrete beams has been clarified by many studies, most of which were of experimental approach. Studies on shear strength of beams subjected to axial force, such as prestressed concrete, however, have not been conducted sufficiently yet. Since the accuracy in the shear strength prediction is poor in the case with axial force, a rational prediction method is urgently required. In this study, therefore, prediction of shear strength of prestressed concrete beams without shear reinforcement was done by a nonlinear finite element method (FEM). In the FEM constitutive laws, which have been greatly developed in recent years, were implemented. As results of the FEM analysis, several intersting and useful points were newly found on the shear strength prediction.

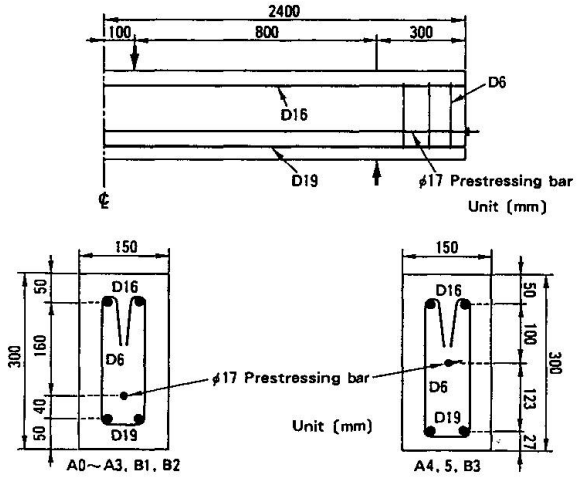

Fig.1 Specimen

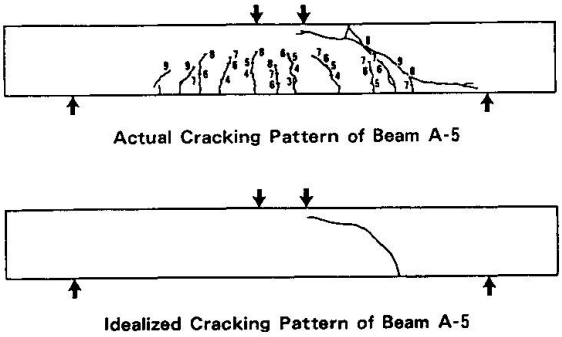

(a) Observed and analyzed cracks

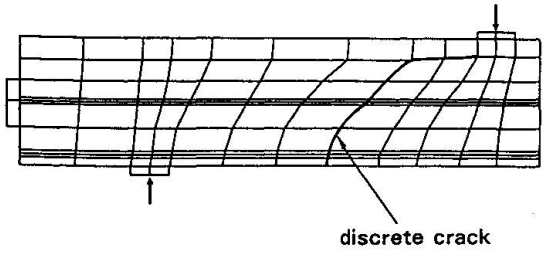

(b) Meshing and discrete crack

Fig.2 Observed and modeled cracks

2. OUTLINE OF FEM ANALYSIS

The program used for the FEM analysis was "COMM2"[1] in which Maekawa model is applied for concrete element. The bond link elements which are available in COMM2 were used for force transfer along shear crack and for bond force between concrete and steel. The force transferred along shear crack was calculated by Li & Maekawa model[2] for the case that slip occurred (δ>0.001mm), and Reinhardt et al's model[3] was used for the case of no slip (δ<0.001mm). The model for the bond force was Shima et al's model[4]. The main shear crack was modeled as a discrete crack whose location and configuration were determined according to the observed shear crack in the previous study[5]. The details of nine specimens[5] which were analysed are shown in Fig.1 and Table 1. An example of observed cracking pattern and the corresponding meshing pattern were given in Fig.2. All the concrete elements adjacent to the discrete crack were assumed not to crack, while the other concrete elements were ordinary one in which crack was modeled as smeared crack. The prestressing force was applied by imposing the force at a node of a steel element for the anchor plate in the actual beam[5]. The magnitude of the imposed force was equal to the observed effective prestressing force[5].

3. ANALYTICAL RESULTS

3.1 Effect of Prestressing Force on Shear Strength

Specimen	f_c'	P_{eff}	x_1	x_2	x_3	$V_{su,exp}$	$V_{su,FEM}$	$V_{su,cal}$	(7)	(7)	$V_{fu,cal}$	$V_{su,cal2}$	$V_{su,cal3}$
	MPa	kN	mm	mm	mm	kN	kN	kN	—	—	kN	kN	kN
(1)	(2)	(3)	(4)	(5)	(6)	(7)	(8)	(9)	(8)	(9)	(10)	(11)	(12)
A-0	26.6	0	28	55	119	44.1	40.5	40.4	1.08	1.09	75.8	42.7	28.1
A-1	24.6	48	43	85	136	51.5	53.9	54.7	0.96	0.94	76.5	59.1	42.5
A-2	26.6	112	57	90	145	59.3	54.1	61.9	1.10	0.96	84.8	62.8	52.3
A-3	24.6	152	66	115	162	72.6	62.6	69.6	1.14	1.04	83.7	76.8	65.1
A-4	36.5	99	62	65	102	63.3	63.2	64.4	1.00	0.98	83.3	75.6	57.8
A-5	36.5	0	34	55	86	46.6	63.5	55.5	0.73	0.84	77.7	64.3	38.5
B-1	57.5	148	38	55	84	89.2	101.4	87.5	0.88	1.02	118.6	110.1	77.9
B-2	57.5	41	-	40	83	67.7	70.9	65.4	0.96	1.03	117.7	73.9	42.2
B-3	57.5	152	37	60	83	78.5	79.3	94.6	0.99	0.83	102.5	96.3	70.1

Note (2) Cylinder strength at test
(3) Effective prestressing force
(4) Observed depth to shear crack at loading point
(5) Calculated depth to neutral axis at maximum moment region when flexural failure
(6) Depth to neutral axis obtained by FEM at maximum moment region when shear failure
(7) Measured ultimate shear strength
(8) Ultimate shear strength obtained by FEM
(9) Calculated ultimate shear strength using x_2
(10) Calculated ultimate flexural strength
(11) Shear strength calculated by the method in the previous study[6]
(12) Shear strength calculated by the method in the previous study[7]

Table 1 Shear strengths

Comparing the analytical strengths, $V_{su,FEM}$ with the experimental strengths, $V_{su,exp}$, shown in Table 1 and Fig.3, it can be said that the shear strengths of all the specimens are predicted well by the FEM except specimen A-5. It was found in the FEM analysis that the ultimate shear strengths were controlled by compression failure (strain softening) of concrete element in compression zone of the maximum moment region. Although the concrete compression failure looked the same as in flexural failure of the beams, the ultimate strengths are much less than the calculated flexural strengths as shown in Table 1. The reason for this fact can be found in concrete strain distribution at a cross-section in the maximum moment region. As shown in Table 1 and Fig.4, depths to the neutral axis, x_2, obtained from the concrete strain distribution calculated by the FEM, are much less than depths, x_3, calculated by a conventional method for ultimate flexural strength using an equivalent stress block. This narrow compression zone leads

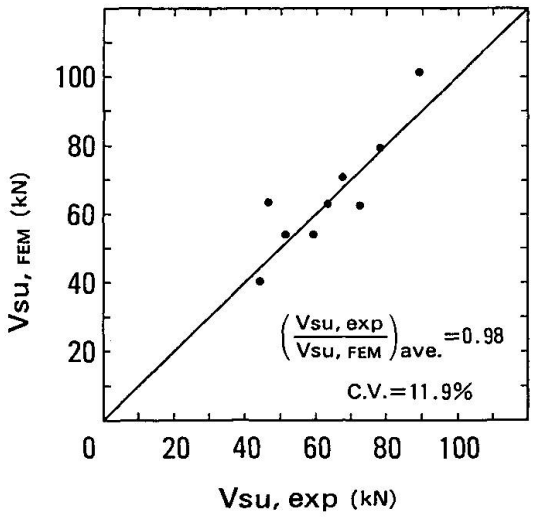

Fig.3 Test and FEM predictions

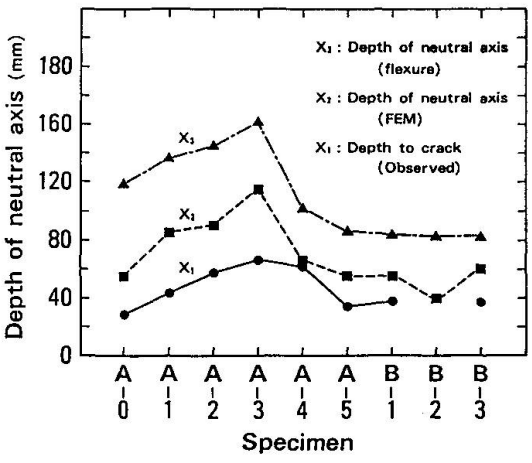

Fig.4 Depths of compression zone

earlier concrete failure in compression zone, which means that the shear strength is less than the flexural strength. It is also seen in Fig.4 and Table 1 the depth to the neutral axis at shear compression failure is significantly greater than the depth to shear crack, x_1. Shear cracks penetrated in the compression zone.

The FEM analysis predicts adequately increase in the shear strength with increase of prestressing force as observed in the experiment[5]. Table 1 and Fig.4 indicate that among specimens A-0 to A-3 the computed depth of compression zone, x_2, increases with increase of prestressing force. This increase of compression zone depth causes increase of the shear strength.

An observed depth to shear crack tip, x_1, was greater in a beam with a greater prestressing force. Location of shear cracking in compression zone varies as prestressing force varies. In order to see the effect of depth to shear crack tip on the shear strength, the shear strengths were calculated by the FEM for two cases of the depths, 20mm and 70mm. The calculated strengths, however, were not so different. It seems that the difference in the depth to shear crack tip hardly causes the difference in the shear strength.

The FEM analysis indicates that the depth of compression zone just outside the maximum moment region is greater than that in the maximum moment region. Therefore, despite combination of flexural moment and shear force, the principal compressive stress is much less than that in the maximum moment region. This is considered to be the reason why the failure of concrete did not occur outside the maximum moment region. The concrete compression failure in compression zone of the maximum moment region is failure criterion for the case of shear compression failure of a beam. To calculate the shear strength, therefore, the depth to the neutral axis should be evaluated by some means. The shear strengths, $V_{su,cal}$, in Table 1 and Fig.5 were calculated by a conventional method for ultimate flexural strength with an equivalent stress block and neutral axis depth given by the FEM analysis. Similar ways for calculation of the shear strength were proposed by the previous studies[6][7]. Although simplified assumptions were adopted, the predicted shear strengths, $V_{su,cal}$, have a good agreement with the experimental ons, $V_{su,exp}$, as shown in Fig.5 and Table 1, while the values predicted by the previous studies[6][7] have less agreements. Figure 5 implies that the ultimate strength for shear compression failure may be estimated easily if estimation of the neutral axis depth is possible.

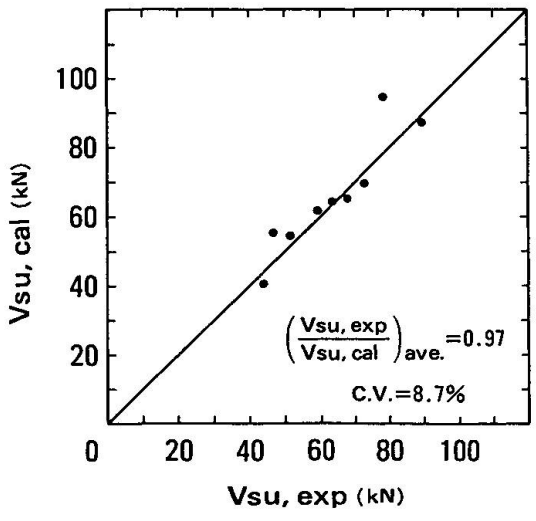

Fig.5 Test and simplified predictions

3.2 Effect of Force Transferred along Shear Crack

The force transfer model along a discrete shear crack was varied to see its effect on the shear strength. There were four cases in which the stiffness of the model was varied in such a way that it was 100%, 10%, 1% or 0% of the original model's stiffness. The shear strengths for the four cases were 100%, 91%, 89% and 23% of that with the original model. With 0% of the stiffness the shear strength was greatly

reduced, but with 1% of the stiffness reduction in the strength was only 11%. Length of the shear crack in the analysis was shorter than the observed one for every case. For another case, 0% of the stiffness was implemented only along the shear cracked part in the case of 100% stiffness, while in the vicinity of tip of the discrete shear crack 100% of the stiffness was implemented. In this case the shear strength was 95% of that with 100% of the stiffness at all the part of the discrete shear crack.

From the FEM analysis it was observed that slip (δ>0.001mm) takes place at most of the part along the shear crack. In the analysis, therefore, Li & Maekawa's model was used for most of the part along the shear crack. Considering this fact, Reinhardt's model was assumed under any amount of slip to see the effect of type of force transfer model on the shear strength. The predicted shear strength in this case was 97% of that of the original case.

From comparison of the predicted shear strengths of the beams with a various force transfer model along the discrete shear crack, it can be said that effect of the force transferred along a main shear crack on the shear strength is negligibly small. Only the force transferred near the tip of the shear crack which is close to the loading point and in the compression zone affects the shear strength. Estimated transferred stresses along the shear crack were considerably smaller than the stresses in concrete near the shear crack. This fact seems to support the little effect of the force transfer model on the shear strength.

3.3 Effect of Crack Model Type

In this study type of shear failure is "shear compression failure", for which shear cracking does not mean ultimate state. In this sense tensile strength of concrete has less significant than in shear tension failure. Furthermore, model for post-cracking is rather little significant for the ultimate shear strength as discussed in the previous subsection It was found, however, that whether discrete crack or smeared crack was assumed for a main shear crack did affect the shear strength of the beam. In the original FEM analysis a discrete crack was assumed, and concrete elements next the discrete crack were assumed to be non-cracking elements. In another case smeared cracking was assumed for all the concrete elements. The predicted strength in this case was 78% of the original case. It seemed that more cracking elements in compression zone at the maximum moment region caused early failure.

4. CONCLUSIONS

(1) The FEM analysis, in which concrete is modeled as nonlinear material subjected to bi-axial stress state and a main shear crack is modeled as a discrete crack, can predict the strengths for shear compression failure in reinforced concrete beams subjected to axial force.
(2) Shear compression failure is caused by compression failure of concrete in compression zone at the maximum moment region. The depth of the compression zone is less than that in flexural failure, so that the shear strength is less than the flexural strength.
(3) Using the depth of compression zone obtained by the FEM analysis, the strength for shear compression failure can be estimated by the conventional method of flexural strength.
(4) Cracking and post-cracking models, which is force transfer model along the

discrete shear crack, affect little the predicted shear strength. Whether discrete crack or smeared crack is assumed for the main shear crack, however, influences the prediction of the shear strength.

ACKNOWLEDGEMENT

This study was supported in part by Saito Memorial Research Foundation of Prestressed Concrete Technology.

REFERENCES

1. MAEKAWA K., NIWA J. and OKAMURA H., Computer Program "COMM2" for Analysing Reinforced Concrete. Proceedings of JCI 2nd Colloquium on Shear Analysis of RC Structures, October 1982, pp.79-86 (in Japanese).
2. LI B., MAEKAWA K. and OKAMURA H., Contact Density Model for Stress Transfer across Cracks in Concrete. Journal of the Faculty of Engineering, the University of Tokyo(B), Vol.XL, No.1, March 1989, pp.9-52.
3. REINHARDT H., CORNELISSEN H. A. W. and HORDIJK D. A., Tensile Tests and Failure Analysis of Concrete, Journal of Structural Engineering, ASCE, Vol.112, 1986, pp.2462-2477.
4. SHIMA H., CHOU L. L. and OKAMURA H., Micro and Macro Models for Bond in Reinforced Concrete. Journal of the Faculty of Engineering, the University of Tokyo(B), Vol.XXXIX, No.2, September 1987, pp.133-194.
5. HORIBE K. and UEDA T., Influence of Axial Force on Shear Behavior of Reinforced Concrete Beams. Proceedings of 40th Annual Convention of JSCE, Div.5, September 1985, pp.319-320 (in Japanese).
6. ZOWYER E. M., Shear Strength of Simply-Supported Prestressed Concrete Beams. Structural Research Series No.53, Civil Engineering Studies, University of Illinois, Urbana, Illinois, June 1953.
7. EVANS R. H. and SCHMACHER E. G., Shear Strength of Prestressed Beams Without Web Reinforcement. Journal of ACI, Vol.60, November 1963, pp.1621-1643.

Precast Reinforced Concrete Planks as Structural Members

Plaques en béton armé préfabriquées utilisées comme éléments de construction d'une structure

Vorgefertigte Stahlbetonplatten als tragende Bauteile

John T. BLADES
Structural Engineer
Rankine & Hill Pty Ltd
Sydney, Australia

John Blades, born in Sydney, 1959, received an Honours degree in Civil Engineering from the University of Sydney and a Master of Engineering Science degree from the University of New South Wales. He has been involved in the structural design of reinforced concrete and structural steelwork for industrial and commercial structures and prestressed concrete bridges.

Leon A. GRILL
Civil Engineer
Private Consultant
Sydney, Australia

Born in Vienna, Austria. Graduated «Cum Laude» from 1948 Politechnicum School of Bucharest. Twenty-two years of experience in the design of civil and structural projects in Uruguay, Argentina and Brazil. From 1971 to 1986, Head of the structural checking section of Rankine & Hill in Australia. Presently contracted as a Private Consultant to the same company.

Neil C. MICKLEBOROUGH
Sen. Lecturer
Univ. of New South Wales
Sydney, Australia

Neil Mickleborough studied at both Carleton University, Ottawa, Canada and the University of Tasmania, Australia, where he received his Ph.D. in Structural Engineering in 1979. He worked as a structural design engineer until 1983 when he took up his present appointment. Dr. Mickleborough has published in the areas of reinforced and prestressed concrete, as well as structural dynamics. Recently he has had a book published on prestressed concrete design.

SUMMARY
This paper investigates the differences in behaviour of «thin» precast reinforced simply supported concrete when subjected to static and impact loads. Many such planks have failed dramatically in practice. The causes and modes of failure are presented. The importance of detailing and the tensile strength of the concrete are discussed and practical guidelines are given for the design and detailing of such elements.

RÉSUMÉ
Cet article examine les différences de comportement des plaques minces en béton armé simplement appuyées, soumises à des charges statiques et à des chocs. Dans la pratique, nombreuses ont été les plaques qui se sont dramatiquement effondrées; ainsi, causes et modes de ruine sont présentés. Les détails constructifs, ainsi que la prise en compte de la résistance en traction du béton sont discutés; des directives pratiques sont données pour la conception et le détail de tels éléments.

ZUSAMMENFASSUNG
Dieser Artikel untersucht das unterschiedliche Verhalten von dünnen vorgefertigten Einfachplatten statischer und dynamischer Belastung. Viele von diesen Platten haben in der Praxis dramatisch versagt und die Ursachen des Versagens werden erläutert. Es wird die Bedeutung der Berechnungsführung und der Betonzugfestigkeit diskutiert und praktische Richtlinien für Entwurf und Detaillierung von solchen Bauteilen werden gegeben.

1. INTRODUCTION

This paper is based on work carried out for a thesis at the University of New South Wales in 1988 [1].

Precast reinforced concrete planks are used, in Australia, as structural members in three main areas:

a) Treads in steel stringer stairs. This is particularly common in stairs where the use of steel sections to frame the stair and "thin" concrete planks as treads reduces the imposed dead load on the whole structure and makes for ease of construction. Fig. 1 shows such a stair in a major hotel in Sydney, planks being of dimensions 2,200 x 280 x 70mm thick, spanning 1,350mm.

b) Planks in steel framed pedestrian footbridges.

c) Footway slabs which span over electrical services on roadbridges.

In each of these applications, the loading can be applied statically or dynamically as an impact load.

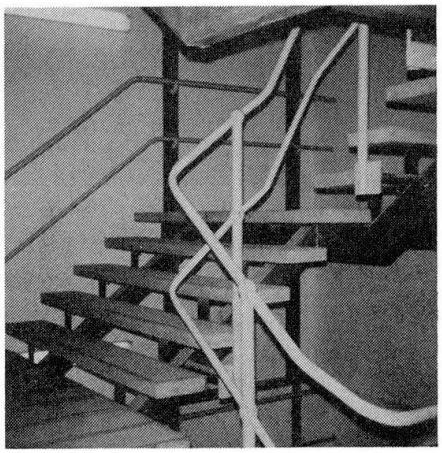

Fig. 1 Treads in a Hotel Fire Stair

Such planks are in common use and over the years many have failed dramatically in flexure due to incorrect analysis, design and/or detailing. With respect to analysis, much of the problem seems to have been, as stated by Breen [3], that designers have focused on "local section behaviour rather than the overall action."

The aim of the project was to study the behaviour in detail and produce practical recommendations for the design and detailing of such planks.

2. THE MODEL

2.1 General

The planks tested in the laboratory are shown in Fig. 2. These test planks were designed using ultimate strength theory to the Australian Standard AS 3600 (Concrete Structures Code) [5]. The live load of 1.4 kN is for stair treads and is from AS 1170, Part 1 [5]. The dimensions and span are typical for such planks in practice.

The test plank thickness was varied to establish the importance of this dimension.

The position of the reinforcement in the cross-section was varied because it was considered that these planks fail in practice primarily due to the fact that "the dimensions of the precast treads are such that the reinforcement provided is near or at the neutral axis of the section and is therefore unutilised when the first loading occurs" [2].

The steel reinforcement used was welded wire fabric, which is common practice within Australia, and has a yield strength of 450 MPa. The concrete was of approximately 20 MPa compressive strength with 10mm aggregate and 80mm slump. No admixtures were used. The curing procedure adopted was typical of that used in practice by precast concrete manufacturers in Sydney.

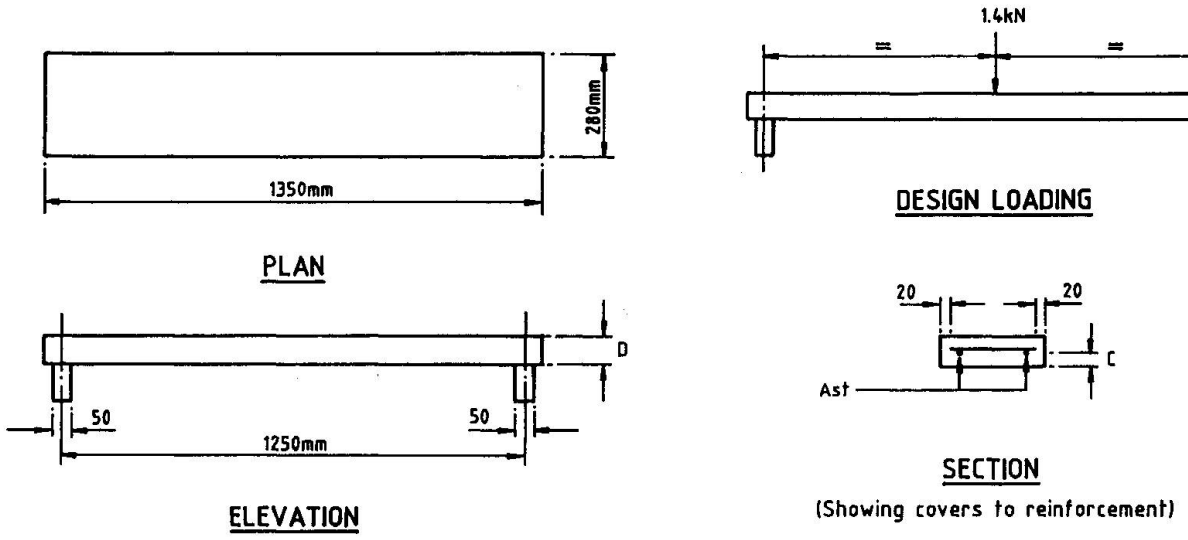

Depth D (mm)	Cover c (mm)	Area of Tensile Reinforcement Ast (mm^2)
70	15	62.3
	25	62.3
60	15	62.3
	25	79.2
50	15	79.2
	20	100.5

Fig. 2 Plank Design Details

Two sets of planks were made, one for testing under static loads, the other under impact loads.

2.2 Static Loading

The main aim of the static loading was to study, under controlled laboratory conditions, the pre-cracking, cracking and post-cracking behaviour of the precast reinforced concrete planks. The applied load and the displacement under the load were measured and the resultant cracking patterns were observed and recorded (photographically) at various load stages throughout the testing procedure.

2.3 Impact Loading

For impact loading the same aim applied as for the static loading. The applied impact load, the maximum impact force absorbed by the plank and the displacement under the impact load were measured. The resultant cracking patterns were observed and recorded (photographically) at various loading stages throughout the testing procedure.

The type of loading used was repeated impact with increments of increasing mass. A load was 'dropped' onto the plank then raised to the required drop height with a further mass increment then being added before dropping the load again on to the plank. This modelled very realistically the type of repeated impact load such elements would undergo in practice (see Section 1).

The drop mass was increased in approximately 12.5kg increments with the masses being clamped together. The load was applied to the planks through a steel ring (120mm OD x 25mm) welded to the underside of the load carrier. This, it was believed, would model the load application through the sole or heel of a foot on a plank in service. The drop height was set at 300mm based on the real in service drop height when a person runs down a flight of stairs.

The two parameters of greatest importance in studying the impact behaviour of the planks were found to be:

Mass ratio: $\alpha = \frac{\text{mass of plank}}{\text{mass of striker}} = \frac{m_p}{m_s}$

and

Dynamic Load Factor (DLF) $= \frac{y_i}{y_s}$

Where y_i = impact displacement due to load P
Where y_s = static displacement due to load P

3. EXPERIMENTAL RESULTS

3.1 Static Loading

The Load/Displacement plots for the 60mm thick planks are shown in Fig. 3. In the case of the plank with 15mm cover the plot resembled that of the stress/strain curve for the steel wire fabric, as expected for under-reinforced sections such as these where the behaviour of the tensile steel dominates behaviour of the cross-section. The behaviour of the plank with 25mm cover was entirely different. Here the reinforcement was near the centroid of the gross cross-section and due to the steel having very low stress, its behaviour did not dominate the behaviour of the cross section. The plot shows less ductility (than for 15mm cover) with a shorter linear relationship followed by sudden failure.

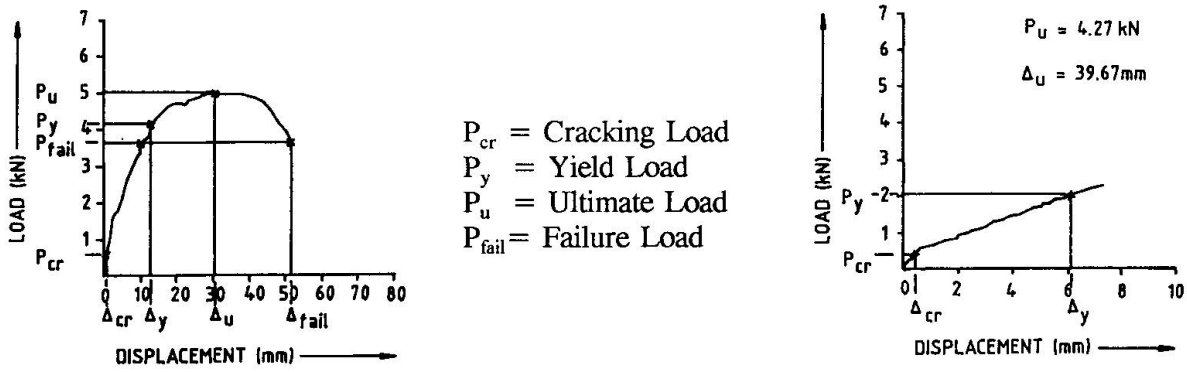

Cover = 15mm Cover = 25mm

f_c = 18 MPa, Thickness = 60mm

Fig. 3 Load/Displacement Plots - Static Loading

The cracking patterns for the 60mm thick planks are shown in Fig. 4. In the case of the plank with 15mm cover, the cracking was finer and more uniform, the cracks coincided with the positions of cross wires in the reinforcing fabric which caused crack initiation. In the case of the plank with 25mm cover, cracks occurred at mid-span with one or two major cracks which opened to as much as 6mm wide, causing the mid-span displacement and rotation of the plank.

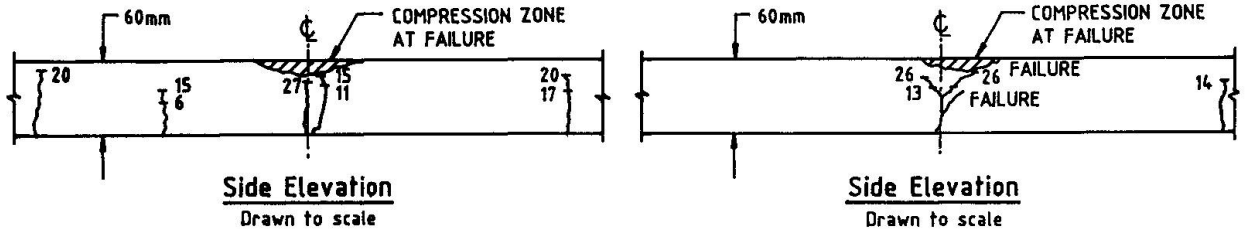

15mm Cover 25mm Cover

(numbers indicate loading stages)

Fig. 4 Cracking Patterns - Static Loading 60mm Thick Planks

3.2 Impact Loading

Generally, the behaviour of the planks with 15mm cover was similar to that for the planks with 25mm cover. The planks failed under the impact loading in a brittle manner. The failure was generally due to crushing of the concrete in the compression zone, which occurred more suddenly in the case of the more brittle planks with the reinforcement at mid-depth.

The cracking patterns for the 60mm thick planks are shown in Fig 5. The maximum crack widths which developed for the planks with reinforcement at mid-depth (25mm cover) were generally greater than for those with 15mm cover, the maximum being approximately 6mm as for the static loading. The planks with 25mm cover exhibited faster crack propagation and deeper crack penetration at an earlier load stage than did those with 15mm cover. This is because in the latter the tensile reinforcement had high stresses and was effective in controlling the formation and propagation of flexural cracks, being closer to the extreme tensile fibre of the concrete.

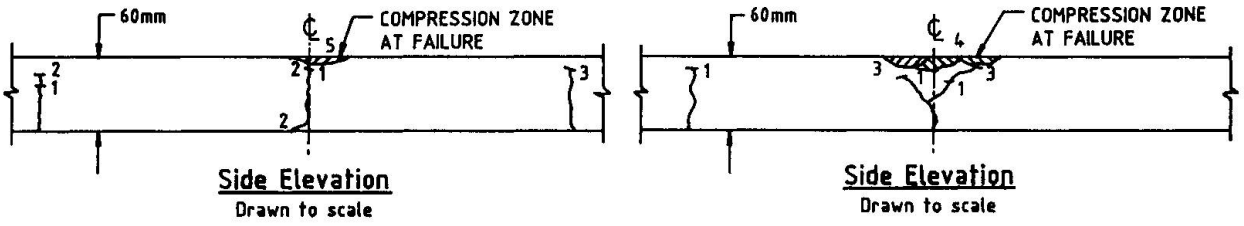

15mm Cover 25mm Cover

(numbers indicate loading stages)

Fig. 5 Cracking Patterns - Impact Loading 60mm Thick Planks

The Dynamic Load Factors (DLF) for the planks varied between 2.94 (50mm thick) and 8.40 (70mm thick). For each plank thickness, the value was higher for that with 25mm cover than 15mm cover.

4. CONCLUSION

4.1 Comparison Between Static and Impact Loadings

The loads required to cause cracking and failure under static loading were up to eight times higher than the cracking and failure loads observed under impact loading where the planks behaved in a very brittle manner. Generally, the planks with reinforcement at mid-depth exhibited more extensive cracking at the first load stage of the impact testing than did those with 15mm cover. This is due to the former being similar to a mass concrete element and therefore more brittle, with a faster rate of crack propagation.

For both the static and impact loadings, the ultimate load for the planks with reinforcement near mid-depth was approximately 85% of that for the planks with only 15mm cover.

In both types of loading, the displacements were generally reduced by placing the reinforcement at 15mm cover rather than at mid-depth.

As the mass ratio of the planks (α) decreases, the deformation or "lost" energy increases leading to more permanent deformation of the plank, less recovery (or restitution) and larger displacements. Thus, to reduce the energy loss and permanent deformation during impact, the plank mass should be kept as high as possible, as suggested by Grill [2]. The 50mm thick planks (the lowest mass ratio), generally behaved in an unstable manner and should be avoided in practice.

In relation to cracking, the cracks formed later and were better controlled by placing the reinforcement at only 15mm cover rather than at mid-depth, where the behaviour is similar to that

for mass concrete where the tensile strength of the concrete is very important. As Hillerborg says, "...a crack may form which has a tendency to propagate, as cracks in their turn give rise to stress concentrations. If the crack propagation is not prevented the structure (or plank) will crack" [5].

4.2 Review of Current Design Loading Requirements

The precast reinforced concrete planks for this project were designed using the recommended loadings of the current Australian Standard for Dead and Live Loads (AS 1170, Part 1, 1989) [5]. However, under impact loading they failed at less than half of the service design load of 1.4kN.

Such planks undergo impact loads in practice (e.g., persons running down a flight of stairs or across a footbridge). The Authors recommend that loading codes recognise this by giving a range of impact factors (say 1.5 to 4.0) by which one would multiply the static load depending on whether the structure were a major or minor pedestrian facility (e.g., major entrance/escape stair in a large hotel or maintenance stair/footway).

4.3 Design Recommendations

1. Plank Thickness $\geq$ 60mm (irrespective of span).
2. Design Live Load at least twice the current value of 1.4kN concentrated (or 2.2kN/m) to take account of impact.
3. Reinforcement - diameter $\leq$ 0.1 x plank thickness.
   - pitch of main longitudinal wires and cross wires = 100mm.
4. Cover to Main Longitudinal Tensile Reinforcement $\leq$15mm; $\neq$ 10mm.
5. For planks in locations exposed to the weather; specify hot-dipped galvanised reinforcement.
6. Minimum 28 day Compressive Strength of Concrete = 25MPa - all locations.

REFERENCES

1. BLADES J.T., Precast Reinforced Concrete Planks as Structural Members. Master of Engineering Science Thesis, School of Civil Engineering, The University of New South Wales, Australia, February 1988.

2. GRILL L.A., Building Failures: The Use of Experience for Diagnosis and Repair. Proceedings of the 12th Biennial Conference of the Concrete Institute of Australia, 1985.

3. BREEN J.E., Why Structural Concrete? Introductory Report: IABSE Colloquium on Structural Concrete, Stuttgart, April 1991.

4. HILLERBORG A., Reliance Upon Concrete Tensile Strength. IABSE Colloquium on Structural Concrete, Stuttgart, April 1991.

5. Standards Association of Australia, Concrete Structures Code, AS 3600-1988, Loading Code, Part 1 - Dead and Live Loads, AS1170, Part 1 - 1989.

Design and Detailing of Cellular Concrete Structures

Conception et détails des structures cellulaires en béton

Entwurf und Ausführung von Beton-Zellenkonstruktionen

Mohamed I. SOLIMAN
Professor
Ain Shams Univ.
Cairo, Egypt

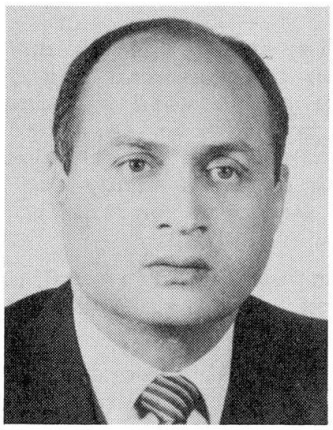

M.I. Soliman, born in 1946, obtained his B.Sc. degree in civil engineering from Ain Shams Univ., Cairo in 1969, his M.Sc. degree from the same Univ. in 1972, and an M.Eng. degree from McGill Univ., Canada in 1975 and his Ph.D. in 1979 from the same University. Dr. Soliman is the Liaison officer for Canada, CSCE.

SUMMARY

An experimental-theoretical study was conducted to investigate the general deformational behaviour of reinforced concrete cellular structures. Six reinforced concrete voided slabs, and six reinforced concrete box section girders were tested. The varying parameters of the voided slabs were the void's diameters and the percentage of reinforcement, while for the box section girders, the varying parameters were the percentage of reinforcement and the end conditions, (warping restrained or unrestrained). The finite element method was used in the analysis of these cellular structures. General conclusions are summarized.

RÉSUMÉ

Une étude expérimentale ainsi que théorique a été conduite afin d'examiner le processus de déformation des structures cellulaires en béton armé. Six dalles et six caissons ont été testés, en tenant compte des paramètres suivants: diamètre des vides et pourcentage d'armature pour les dalles, pourcentage d'armature et conditions aux limites (torsion libre ou empêchée) pour les caissons. La méthode des éléments finis a été utilisée dans l'analyse de ces structures cellulaires. Les conclusions sont résumées.

ZUSAMMENFASSUNG

Eine experimentelle und theoretische Studie wurde durchgeführt, um die allgemeine Verhaltensweise von Stahlbeton-Zellenkonstruktionen zu ermitteln. Sechs Stahlbeton-Hohlplatten mit verschiedenen kreisförmigen Aussparungen oder unterschiedlicher Bewehrung und sechs Stahlbeton-Kastenträger mit unterschiedlicher Bewehrung und verschiedenem Endzustand (Krümmung, eingespannt oder nicht eingespannt) wurden getestet. Die Methode der Finite Elemente wurde benutzt, um diese Strukturen zu analysieren. Die allgemeinen Schlussfolgerungen sind zusammengefasst.

1. INTRODUCTION

Reinforced concrete is particularly well suited for use in bridges, because of its durability , rigidity and economy, as well as the comparative ease, with which a pleasing appearance can be achieved. In the recent years, there has been a general tendency to adopt cellular construction for reiforced concrete small & medium-span bridges. This has been a result of functional structural and aesthetic requirements coupled with economic considerations.

In the present work an experimental and theoretical study was conducted to define and explain the general deformational behaviour of reinforced concrete cellular structures under symmetrical and unsymmetrical cases of loading within the serviceability and uultimate states and up to the failure of this type of structures.

The specified aims of this study was to define a simplified method for the design of R.C. voided slab bridges and box girders. Also, this study aims to study the effect of changing the void's diameter, the location and percentage of the longitudinal and transverse reinforcement on the characteristics of load distribution betweenthe webs of the voided slsbs from zero up to the failure load. Also the aim of this study was to investigate the effect of the warping restraint at the supports on the torsional and warping behaviour of R.C. box girder bridges.

The finite element method was used in this study for the analysis of the voided slabs, and the box girders. The adaptability and validity of this method is discussed.

The results of this experimental-theoretical study were combined with other available information and the code provisions to formulate some recommendations to simplify the analysis, design and detailing of this type of structures.

2. ANALYSIS

In the analysis and design of voided slabs or box girders, the commonly used approach is to assume the concrete to be uncracked and linearly elastic, and thus ignoring the reinforcement. This approach has the advantage of simplicity and closely modeling the bahaviour of the structure within the service load level. However, this approach lags accuracy, and may lead to unnecessary overestimating the dimensions of these structures. In addition, it cannot predict the nonlinear behaviour of the reinforced concrete cellular structure up to failure.

2.1 Finite Element Analysis

2.1.1 Element used

In this study a layered rectangular element was used with 7 degrees of freedom per node for the voided slabs, and 6 degrees of freedom per node for the box girder.

The rigidity matrix of the rectangular element was developed using the concept of layered plates, (i.e. the integration involving the material properties is being done layer by layer [7,12]). The structures were divided into a number of layers of different elastic properties as follows;

i- The voids were replaced with an orthotropic solid core layer of equivalent properties as the actual voids.

ii- The steel reinforcement was replaced with a smeared orthotropic layer which resists only normal stresses, and Poisson's ratio is considered to be equal to zero.

iii- The solid concrete layers were considered as isotropic solid layers in the elastic stage, and orthotropic in the inelastic stages.

2.1.2 Material Nonlinearity

The analytical model for concrete which was used in the present analysis was originally developed by Darwin and Pecknold [4]. In Darwin's model, concrete was assumed to be an orthotropic material in the two principal stress directions. In this model the concrete was treated as an incrementally linear elastic material. At the end of each increment, (or iteration), material stiffness were crrected to reflect the latest changes in deflection and strain. Also in this study the smeared cracking model was adopted in the solution(1,7). The advantages of this model was that it offers an automatic generation of cracks without the redefinition of the finite element topology,and second, it offers a complete generality in possible crack direction. The failure criteria used in this model was that proposed by Kupfer and Gerstle (8).

The steel is considred as an approximately elastic plastic material with yield stresses fy and elastic modulus Es. After the yielding of the steel its tangent modulus of elasticity was reduced. It was further assumed that the reinforcement carry only axial stresses in its direction, hence, the principal stress directions was always taken in the global x-y directions, the same as the reinforcement arrangement. Perfect bond was assumed between the steel and concrete layers.

Finally the nonlinear finite element analysis was performed in an incremental manner using an iterative scheme within each load increment. The Newton-Raphson, or the modified Newton-Raphson scheme were used for stiffness updating.

3. EXPERIMENTAL WORK

3.1 The voided slabs

Six reinforced concrete voided slabs with 10 voids were tested. The dimensions of these slabs are 1.04 x 1.80 m. and thickness 12 cm. These slabs were tested, as simply supported on spsn of 1..60 m., twice. Once with a single concentrated load acting at center of gravity of the slab within the elastic range, and the second time, with an eccentric concentrated load, of eccentricity 0.3 m. from the center of the mid section. The six slabs were divided into two groups, each group consisted of three slabs as follows;

Group (1) : The three slabs had a bottom reinforcement of 10 ϕ 6 mm/m' in the longitudinal direction and 10 ϕ 6 mm/1.5 m' in the transverse direction. The varying parameter was the void's size (For slab S1/6 the void diameter was 63 mm., slab S2/6 the void diameter was 50 mm. and for slab S3/6 the void diameter was 40 mm). The spacing of center line of voids was 0.1 m.

Group (2) : The three slabs had the same void sizes as used in group (1) but the reinforcement used was ϕ 8 mm instead of ϕ 6 mm. The slabs were named S1/8, S2/8 and S3/8, respectively.

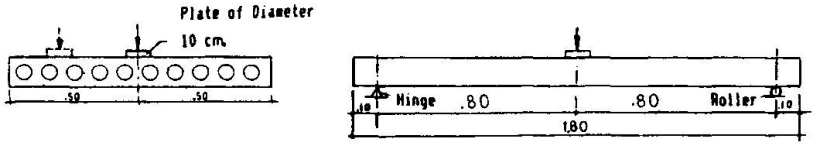

Fig. 1 Test setup for the voided slabs

3.2 The box girders

Six Medium size direct model of R.C.box section girders were tested. The six models had the same length, (2.30 m), and cross-sectional dimensions, (the outer and inner dimensions were 400x260 mm and 260x120 mm. respectively), but they had a different end conditions, (warping restrained or unrestrained).

Also, they had a different percent of reinforcement in both the longitudinal and the transverse directions. These girders were divided into the following two groups;

Group (3) : [G1,G2,G3], consisted of three models which had no transverse diaphragms at the supports, (warping unrestrained condition). Within this group, three girders had a different percent of reinforcement in both the longitudinal and transverse directions.

Group (4) : [G4,G5,G6], consisted of three models which had two end diaphragms of length 400 mm. at both ends to simulate the warping restraint condition at the supports. Also within this group, these girders had a different percent of reinforcement in both directions similar to those of group (3).

All these girders were tested on a fixed end condition of clear span 1.50 m. and were loaded with an eccentric cocentrated load at the midspan section to provide a combined torsion, bending and shear condition.

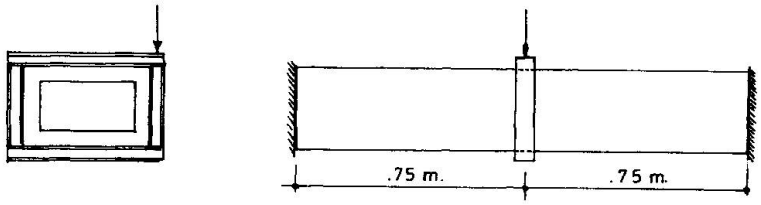

Fig. 2 Test setup for the box girders

4.BEHAVIOUR OF THE TESTED SPECIMENS

4.1 The voided slabs

The behaviour of the tested slabs can be summarized in the following points;

i) The first crack appeared at a load level of about one quarter of the ultimate load for all slabs.

ii) Increasing the transverse reinforcement, or decreasing the void depth ratio, leads to a more uniform load distribution between the webs of the voided slabs. This was observed by;
   a) Increase in the cracking load.
   b) Decrease in deflections and longitudinal strains of the loaded web and an increase in the transverse strains.

iii) Cracking due to longitudinal moments leads to a more uniform load distribution between the webs. This is due to the decrease in the longitudinal flexural stiffness of the slabs while the transverse flexural and torsional were approximately constant.

iv) As the void depth ratio increases, the ratio between the transverse and the longitudinal increases, while the ratio between the transverse and the longitudinal moment decrease. This was explained by the existence of shear deformations due to the cell distortions.

v) The effect of the torsional moment was obvious on the crack pattern of the slabs. This can be observed from the direction of cracking on the opposite sides of the slabs.

4.2 The box girders

The behaviour of the tested box girders can be summarized in the following points;

i) The end diaphragms had a slight effect on the cracking load but it increases the failure load.

ii) The end diaphragms reduce the vertical and lateral deformations of the loaded and unloaded webs.

iii) The longitudinal and transverse steel stresses at both the midspan and

support sections of the unrestrained condition were higher than those of the warping restraint condition at the supports. however, the box girders of group (3) reached the yield earlier than those of group (4).

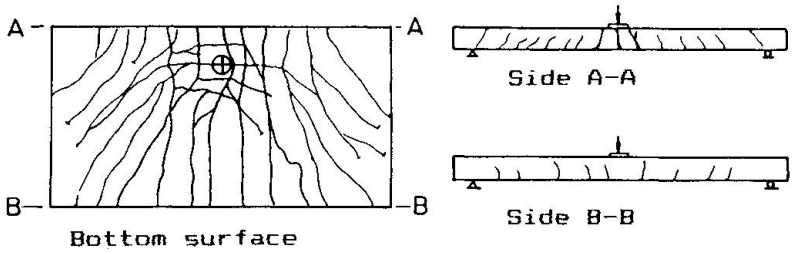

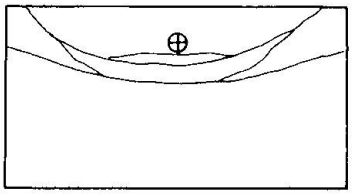

Fig. 3 Crack pattern of the tested voided slabs.

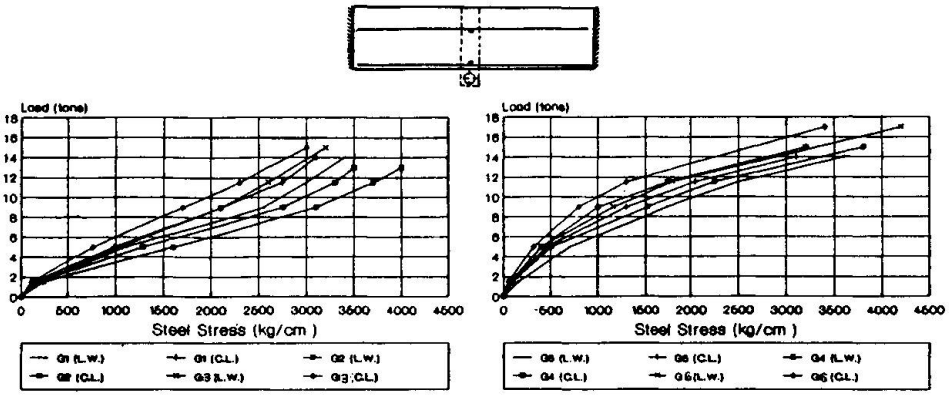

(Warping Unrestrained Group) (Warping Restrained Group)

Fig. 4 Load-Longitudinal steel stress in bottom slab of midspan section for all box girders.

5. CONCLUSIONS

1) The proposed finite element model, which considers the nonlinear behaviour of concrete and steel, is a powerful tool in the analysis of reinforced concrete cellular structures, especially after cracking of concrete.
2) The transverse stresses should be taken into consideration, and hence care should be given for the detailing of the transverse reinforcement of this type of structures.
3) Shear deformations have a significant effect on the behaviour of cellular structures and its effect should not be neglected, and hence, special web reinforcement, and detailing should be considered.
4) The values of the transverse moments should be calculated individually taking into cosideration the ratio between the longitudinal and transverse reinforcement, and shoud not be related to the longitudinal moment by Poisson's Ratio.
5) The effect of torsional and the effect of warping restraint should be considered in the analysis and design of box girders structures and accordingly the detailing of the longitudinal and trasverse reinforcement at the support region is very important.

6. REFERENCES

1. ASCE Committee on Concrete and Masonary structures, Finite Element Analysis of reinforced Concrete, State-of-the-Art Report, ASCE, USA, 1982.
2. Bakht, B.; Jaeger, L.G. and cheung, M.S., Cellular and Voided Slab bridges, Journal of the Structural Division, Proceedings of the American Society of Civil Engineers. ASCE, Vol. 107. No. ST9, Sept. 1981. pp.1797-1813.
3. Clark, L.A., Comparisons of Various Methods of Calculation the Torsional Inertia of Right Voided Slab Bridges. Technical Report 42.508,Cement and Concrete Association, London, June 1975. pp 34.
4. Darwin, D. and Pecknold, D.A., Nonlinear Biaxial Stress-Strain Law For concrete, Journal of the Engineering Mechanics Division, ASCE, Vol. 103, No. EM4, Aug. 1977. PP. 229-241.
5. Elliot, G. and CLARK, L.A., Circular Voided Concrete Slab Stiffnesses, Jounal of the Structural Division, Proceedings of the American Society of Civil Engineers.ASCE, Vol. 108. ST11, Nov.1982. pp. 2379-2393.
6. Rehiem, F.A. Analysis and Behaviour of Box Girder Bridges, M.Sc. Thesis, Civil Eng. Dept., Ain Shams University, Cairo, Egypt, Oct. 1990.
7. Fouad, N.A. Analysis of Reinforced concrete Voided Slabs, M.Sc. Thesis Civil Eng. Dept., Ain Shams University Cairo, Egypt, Sept. 1989.
8. Kupfer, H.B. and Gerstle, K.H., Behaviour of Concrete Under Biaxial stresses, Journal of the Engineering Mechanics Division, ASCE, V01. 99, No EM4, Aug. 1973, PP. 853-866.
9. ROWE, R.E.,Concrete Bridge Design, London, OR Books Ltd, 1962. pp. 336.
10. El Behairy, S.A, Soliman, M.I., and Fouad , N.A., Behaviour of Voided Reinforced concrete slabs, 3rd Arab Conference for structural Enginnering, Al-Ain, Emirates, March 1989.
11. El Behairy, S.A., Soliman, M.I., and Fouad, N.A., Beraviour and Analysis of Voided Concrete Slabs, IABSE Symposium Lisbon, September 1989.
12 El Behairy, S.A., Soliman, M.I., and Fouad, N.A., Nonlinear Finite Element Analysis of Voided Reinforced Concrete Slabs, 1990 Annual Conference of the Canadian Society for Civil Eng., Hamilton, Ontario, Canada, May 1990.
13 El Behairy, S.A., Soliman, M.I., and Fouad, N.A., Nonlinear Behaviour of Reinforced Concrete Voided Slab Bridges. Third International Conference on Short and Medium Span Bridges, Toronto, Canada, August1990.
14. Soliman, M.I., Behaviour and Analysis of a Reinforced Concrete Box Girder Bridge, Ph. D. Thesis, Department of Civil Engineering and applied Mechanics, McGill University, Montereal, March 1979.

Cracking and Shear Capacity of Prestressed Hollow Core Slabs

Résistance à la fissuration et à l'effort tranchant des dalles alvéolées précontraintes

Kapazität der vorgespannten Hohlplatten

Matti PAJARI
Senior Research Scientist
Techn. Res. Centre of Finland
Espoo, Finland

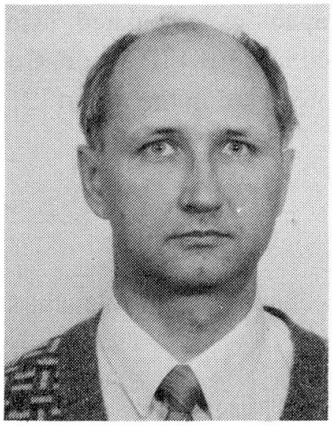

Matti Pajari, born 1948, received his Lic Tech at Helsinki University of Technology and has, since 1979, been involved in research and development projects concerning concrete structures.

SUMMARY

Predicted and observed cracking and shear capacities of prestressed hollow core slabs are compared. The flexural tensile strength of the concrete seems to be independent of the thickness of the slab. The shear compression failure is not needed to predict the observed shear capacities. A reliable criterion for the shear tension failure is obtained by setting the maximum principal stress in the web equal to the direct tensile strength of the concrete.

RÉSUMÉ

On compare ici les valeurs prévues et observées de la résistance à la fissuration et à l'effort tranchant de dalles alvéolées précontraintes. La résistance à la traction du béton fléchi semble être indépendante de l'épaisseur de la dalle. La connaissance de la rupture par cisaillement de la dalle comprimée n'est pas nécessaire pour prévoir la capacité de résistance à l'effort tranchant observées. Un critère fiable pour évaluer la ruine par effort tranchant de la dalle en traction peut être obtenu en introduisant dans la section une contrainte principale maximale égale à la résistance à la traction du béton.

ZUSAMMENFASSUNG

Berechnete und gemessene Rissmomente- und Schubtragfähigkeiten von vorgespannten Hohlplatten werden verglichen. Die Biegezugfestigkeit des Betons scheint unabhängig von der Dicke der Hohlplatte zu sein. Es ist nicht nötig, den Schubdruckbruch bei der Berechnung der Schubtragfähigkeit zu berücksichtigen. Ein zuverlässiges Kriterium für den Schubzugbruch ist es, die grösste Hauptspannung im Steg gleich der Zugfestigkeit des Betons zu setzen.

1. INTRODUCTION

The production method of extruded prestressed hollow core slabs does not allow the use of crosswise reinforcement. For this reason, the shear stresses and the local tensile stresses due to the transfer of the prestressing force must be carried by the concrete itself. The same is true also for the positive bending stresses due to the prestressing moment. In the following, discussion is limited to slabs that can be modelled by a simply supported beam without torsion. Possible failure or cracking at the release of the prestressing force or during transportation or installation are also excluded. The purpose is to show the correspondence between results of full scale tests and theoretical load-bearing capacities calculated using basic structural mechanics and the material properties closely related to CEB-FIP Model Code [1]. The theory and the results of the loading tests are discussed in more detail in the report [2].

2. CRITICAL LIMIT STATES

Fig. 1 shows possible failure mechanisms and relevant serviceability limit states for prestressed hollow core slabs.

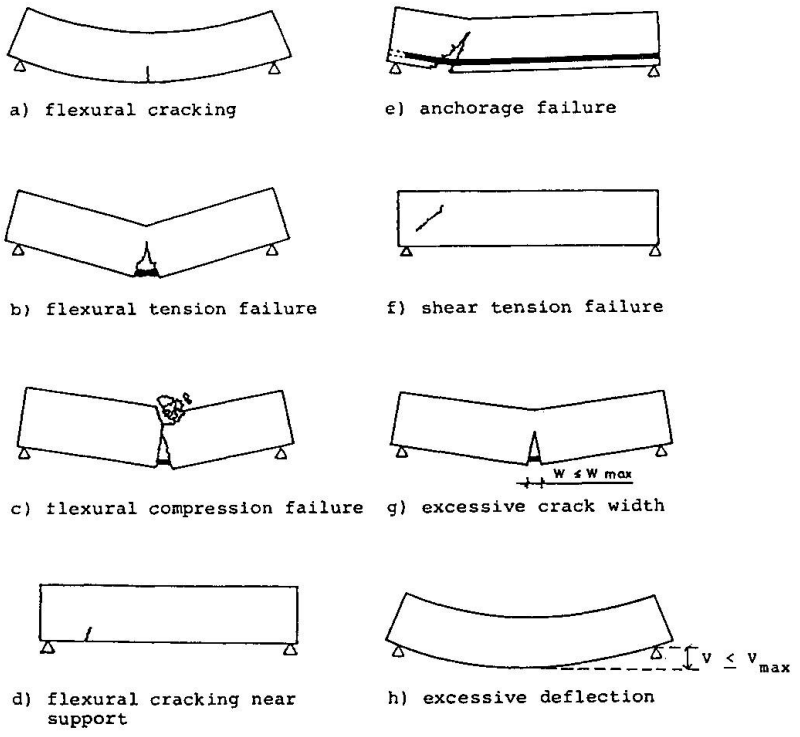

Fig. 1 Relevant limit states.

The limit states where the tensile strength of concrete is of minor importance are not discussed here. To these belong flexural tension failure, flexural compression failure, excessive crack width and excessive deflection.

2.1 Flexural cracking

The horizontal bending stress σ is obtained from

$$\sigma = \frac{-P}{A_r} + \frac{-Pe + M_g + M_q}{I_r / y} \qquad (1)$$

where P is the prestressing force of strands with due regard to the losses of prestressing, A_r the reduced area of cross-section (steel reduced to concrete), y the vertical coordinate with origin at the centroid of the reduced cross-section and positive direction downwards, I_r the reduced second moment of area of the cross-section, e is y coordinate of the strands, M_g the bending moment due to the self-weight of the slab and M_p bending moment due to the imposed load. By setting σ equal to the flexural tensile strength of concrete f_{ctf} and y equal to the y coordinate of the bottom fibre of the slab, cracking moment capacity can be solved from Eq. 1.

2.2 Anchorage failure and shear compression failure

If the strands are anchored firmly enough, the presence of an inclined crack does not cause the structure to fail. Instead, the crack width increases with increasing load until the strands yield or break (flexural tension failure, Fig. 1b), slip (anchorage failure, Fig. 1e) or the concrete is crushed at the top of the slab (shear compression failure). For concrete to be crushed at the top surface, the crack width and strand slip at the bottom surface must be so great that a test which seems to end in compression failure, might equally well be regarded as having ended in anchorage failure. It was assumed that shear compression failure need not be examined separately. The anchorage capacity was checked according to the free body diagram shown in Fig. 2. Only cross-sections cracked in flexure were considered.

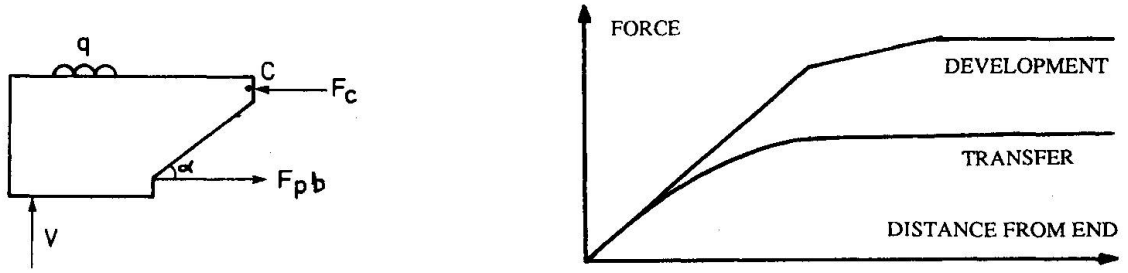

Fig. 2 (a) Free body diagram for anchorage failure.
(b) Development of anchorage force and transfer of prestress.

2.3 Shear tension failure

Shear tension failure refers to cracking that starts in the web and leads to a brittle failure (Fig. 1f). If diagonal cracking takes place near the support, the development length of the

strands is too short to prevent collapse. The simplest way of assessing such a failure is to compare the greatest principal stress in the web with the tensile strength of concrete. Finite element calculations have shown that in hollow core slabs with circular voids the most critical cross-section for shear tension failure is about at distance H/2 from the support where H is the thickness of the slab [3]. The most critical point at this cross-section is close to the point where the cross-section is narrowest. As a first approximation, it was supposed that this point is critical for all slabs irrespective of the shape of the hollow cores. The greatest principal stress σ_{p1} was calculated by combining the horizontal stress σ obtained from Eq. 1 with the shear stress τ. τ was obtained from $\tau = VS/(I_r b)$ where V is the shear force, S the first moment of area and b the width of the concrete cross-section, width of the voids excluded. I_r is the same as in Eq. 1.

3. MATERIAL PROPERTIES USED WHEN SIMULATING LOADING TESTS

The modulus of elasticity E_c and the characteristic tensile strength of concrete f_{ctk} were obtained from

$$E_c = 4800\, f_{ck}^{1/2} \tag{2}$$

$$f_{ctk} = 0.20\, f_{ck}^{2/3} \tag{3}$$

where f_{ck} is the characteristic cube strength of concrete (150 mm cubes). The strength of steel used in calculations was 1600 MPa and the modulus of elasticity 195 000 MPa. The parabolic curve used for the transfer of the prestressing force and the trilinear curve used for the development of anchorage force are shown schematically in Fig. 2b.

4. LOADING TESTS

Finnish quality control tests and shear tests carried out by Jonsson [2,3], cf. Fig. 3., were used to verify the proposed calculation method. In both test series, both the geometry of the slab and the strength of the concrete were measured. These were used in the calculations. The prestress was not measured but taken from the documents of the slab producers.

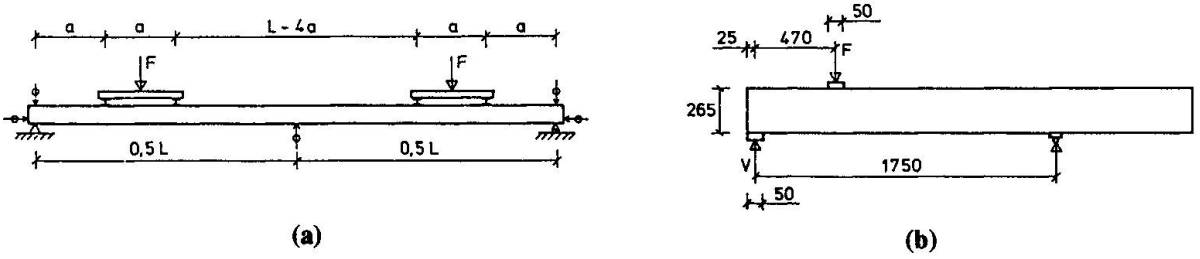

Fig. 3 Test layout. (a) quality control tests, (b) Jonsson's tests.

4.1 Cracking capacity

The ratio $\alpha_{cr} = M_{pre}/M_{obs}$, i.e. ratio predicted/observed cracking moment was calculated for each slab by using two different values for the flexural tensile strength f_{ctf}. The results are shown in Table 1. When f_{ctf} was chosen according to Mayer [4], the share of slabs for which α_{cr} was greater than 1.0 was far too big. Furthermore, this share increased with increasing flexural tensile strength. When f_{ctf} was chosen equal to $1.1*f_{ctk}$, the probability for $M_{pre} > M_{obs}$ was of the order 20% for all slab thicknesses. This is still greater that one should expect if $1.1*f_{ctk}$ is regarded as the 5% fractile of the flexural tensile strength. Obviously f_{ctf} should still have been reduced.

Thickness of slab mm	Number of slabs	f_{ctf}/f_{ct} (Mayer)	Share of slabs with $M_{pre} > M_{obs}$	f_{ctf}/f_{ct}	m	s	Probability for $\alpha_{cr} > 1$ %
150	46	1.5	43	1.1	0.875	0.130	17
200	92	1.4	35	1.1	0.893	0.119	18
265	90	1.3	31	1.1	0.905	0.125	22
400	25	1.2	28	1.1	0.947	0.057	18

Table 1 Comparison of predicted and observed cracking capacities for two choices of f_{ctf}. m is the mean and s the standard deviation for the ratio $\alpha_{cr} = M_{pre}/M_{obs}$.

4.2 Shear capacity

The ratio $\alpha_v = V_{pre}/V_{obs}$, i.e. ratio of predicted/observed shear capacity, was calculated for each slab. Here are discussed only slabs that were subject to an experimental or predicted shear failure. When compared to the observed capacities, the predicted capacities were acceptable for others but for the 400 mm slabs far too high. In fact, the assumption of the most critical point

Thickness of slab mm	Number of slabs	f_{ctf}/f_{ct}	m	s	Probability for $\alpha_v > 1$ %
150(F)	3	1.1	0.898	0.045	1.2
200(F)	24	1.1	0.881	0.140	19.0
265(F)	25	1.1	0.817	0.118	6.2
265(J)	42	1.1	0.767	0.130	3.6
400(F)	27	1.1	0.848	0.112	8.6

Table 2 Comparison of predicted and observed shear capacities for Finnish (F) and Jonsson's tests. m is the mean and s the standard deviation for the ratio $\alpha_v = V_{pre}/V_{obs}$.

stated in paragraph 2.3 is not correct. Finite element calculations show that the assumed stress distribution for the end of the 400 mm slabs with non-circular voids is not correct. The greatest principal stress may be even 40 - 50% higher than that obtained according to 2.3, and it is found lower and closer to the support. Based on this, the greatest principal stress calculated according to 2.3 for 400 mm slabs was multiplied by 1.4. The great value of p for the 200 mm slabs is mainly due to one questionable test result. The results are shown in Table 2.

5. CONCLUSIONS

In prestressed hollow core slabs, the flexural tensile strength of the concrete seems to be independent of the thickness of the slab. This is not in accordance with Hillerborg [5] and König & Duda [6]. The reason for the discrepancy may be due to the large hollow cores, which do not allow exploitation of the strain-softening behaviour of the concrete. It is recommended that the same value is used both for the flexural tensile strength and for the direct tensile strength.

The shear capacity can be predicted accurately enough using the characteristic tensile strength of the concrete and realistic methods to calculate the tensile stresses. A reliable criterion for the shear tension failure is obtained by setting the greatest principal stress in the web equal to the direct tensile strength of the concrete. For slabs with non-circular cross-section, the greatest principal stress in the web cannot be predicted adequately by using the elementary beam theory. The shear compression failure need not be considered.

REFERENCES

[1] CEB-FIP Model Code for concrete structures. Bulletin d'information CEB No. 124-125/ 1978.

[2] PAJARI, M., Design of prestressed hollow core slabs. Technical Research Centre of Finland, Research Reports 657 / 1978. 88 pp. + App.

[3] WALRAVEN, J. C. & MERCX, W.P.M., The bearing capacity of prestressed hollow core slabs. Heron 28(1983) 3, 46 pp.

[4] MAYER, H., Die Berechnung der Durchbiegung von Stahlbetonbauteilen. Deutscher Ausschuss für Stahlbeton, Heft 194 / 1967. 73 pp.

[5] HILLERBORG, A., Reliance upon concrete tensile strength. IABSE Colloqium "Structural Concrete, Stuttgart 1991.

[6] KÖNIG, G. & DUDA, H., Basic concept for using concrete tensile strength. IABSE Colloqium "Structural Concrete", Stuttgart 1991.

Behaviour of Beams and Punching in Slabs without Shear Reinforcement

Comportement des poutres et poinçonnement des dalles sans armatures d'effort tranchant

Tragverhalten von Balken und Durchstanzen von Platten ohne Schubbewehrung

Aurelio MUTTONI
Dr. sc. techn.
Grignoli, Martinola, Muttoni
Lugano, Switzerland

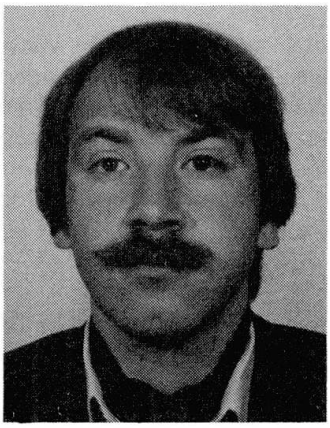

Aurelio Muttoni graduated in Civil Engineering at the Swiss Federal Institute of Technology in 1982 and subsequently undertook research on the applicability of the theory of plasticity to the design of reinforced concrete structures, obtaining his Ph.D. degree in 1989.

Joseph SCHWARTZ
Dr. sc. techn.
Frey, Consult. Eng.
Zug, Switzerland

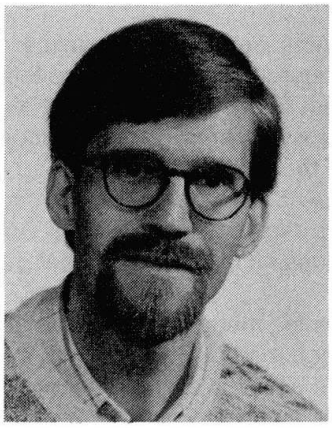

Joseph Schwartz graduated in Civil Engineering at the Swiss Federal Institute of Technology in 1981 and subsequently undertook research on the stability of masonry and reinforced concrete members, obtaining his Ph.D. degree in 1989.

SUMMARY
The cause of shear failure is investigated in beams and slabs without shear reinforcement. The main parameters influencing the structural behaviour are discussed. A theoretical model for the determination of the punching strength as a function of different parameters including size effect is proposed.

RÉSUMÉ
On analyse ici la cause de la rupture par cisaillement des poutres et des dalles sans armature d'effort tranchant. Un modèle théorique visant la détermination de la résistance au poinçonnement est proposé en traction de différents paramètres dont l'effet de taille.

ZUSAMMENFASSUNG
Die Ursache des Schubbruches von Balken und Platten ohne Schubbewehrung wird untersucht. Die Hauptparameter, welche das Tragverhalten beeinflussen, werden diskutiert. Ein theoretisches Modell zur Berechnung des Durchstanzwiderstandes in Funktion verschiedener Parameter einschliesslich «size effect» wird vorgeschlagen.

1. SHEAR ACTION IN BEAMS WITHOUT SHEAR REINFORCEMENT

The investigation begins with the consideration of the simple beam shown in Fig. 1. The reinforcement consists of longitudinal bars, which are completely anchored behind the supports. Not taking into account the tensile strength of the concrete and without shear reinforcement (stirrups) the only possible structural model is the so-called direct support, i.e. between the load and the reaction force a compression zone resembling a concrete strut is formed. The stress field proposed by Drucker [1] to describe this load bearing action is shown in Fig. 2. It is the solution according to plasticity theory.

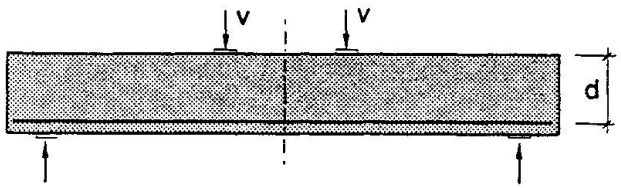

Fig. 1 Beam and loading

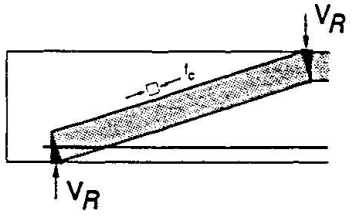

Fig. 2 Stress field

This stress field can under some circumstances deviate greatly from the actual structural action. While increasing the load V monotonically from zero to the level of the failure load V_R several phases of load bearing action may be recognized. After cracks due to bending develop, the load bearing action begins to deviate from that of the elastic model which presupposes homogeneous behaviour. If one assumes that there is no load transfer over the cracks then the new internal load bearing action can be described by the stress resultants shown in Fig. 3b. This load bearing model was already recognized by Kani [2] and described as follows: *"Due to the transverse cracks the tension zone is divided up into seperate concrete elements, which can be visualized as cantilever beams fixed in the upper compression zone".*

Further possible load bearing models are sketched together with the stress resultants in Figs. 3c and 3d. In the case of the structural model shown in Fig. 3c concrete compressive forces are assumed to be transferred across the cracks. This is possible as the roughness of the cracked surface causes an interlocking behaviour. Fig. 3d shows a structural model in which the longitudinal reinforcement also transmits forces in the transverse direction (so-called dowelling action). The effective stress field results from the combination of the three load bearing models mentioned, as also Hamadi and Regan [3], Reineck [4] and others have shown.

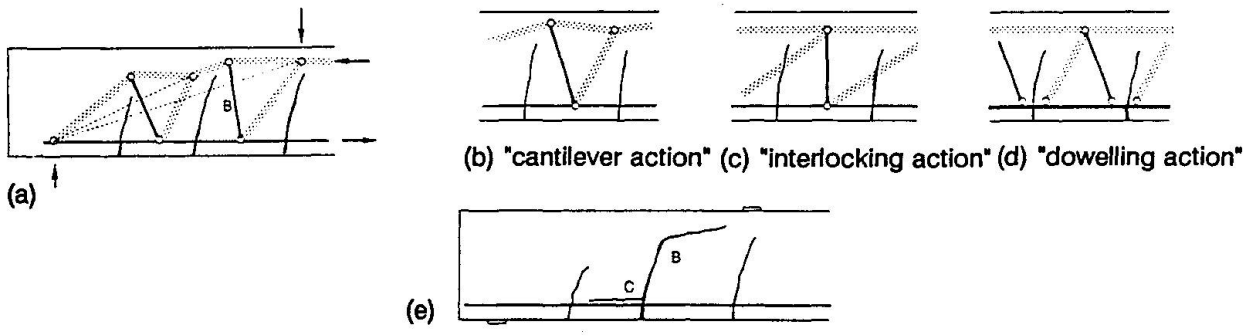

Fig. 3 Structural models after bending cracks develop with subsequent crack propagation

If the load is increased further the tensile strength is reached in region B (Fig. 3a). The original bending crack running almost vertical then propagates in a more or less horizontal direction. A typical crack pattern is shown in Fig. 3e. The propagation of this crack is accompanied by a collapse of the three abovementioned structural models. The cantilever and interlocking models lose their load bearing capacity because the concrete ties at B are broken. The dowelling action also becomes ineffective because a crack forms at C (Fig. 3e).

The new structural model, which could now become effective, is the plasticity solution already mentioned, i.e. the direct support model. Fig. 4a shows the crack pattern just prior to failure in a beam tested at the Institute of Structural Engineering at the Swiss Federal Institute of Technology, Zurich [5]. In this figure the stress field describing the direct support model has been introduced. The dimension of the strut has been determined

from considerations of equilibrium and full exploitation of the concrete strength f_c. It is clear that the main crack passes through the theoretical strut. The possibility of force transfer across the crack depends on the relative displacements of the crack boundaries and the roughness of the crack surface. The relative displacement vectors measured during the test are shown in Fig. 4b for two load steps $V = 0.87 \cdot V_R$ and $V = 0.95 \cdot V_R$. These displacements may be compared with the relationships between crack opening u and movement along crack v given in Fig. 4c. The curves represent the displacement vectors at which contact between the two crack boundaries is just no longer possible and thus force transfer ceases. They were measured on specimens, which were broken into two parts after being cut out of the test beam. A comparison of the two figures shows that practically no more force had been transferred over the crack in the test beam.

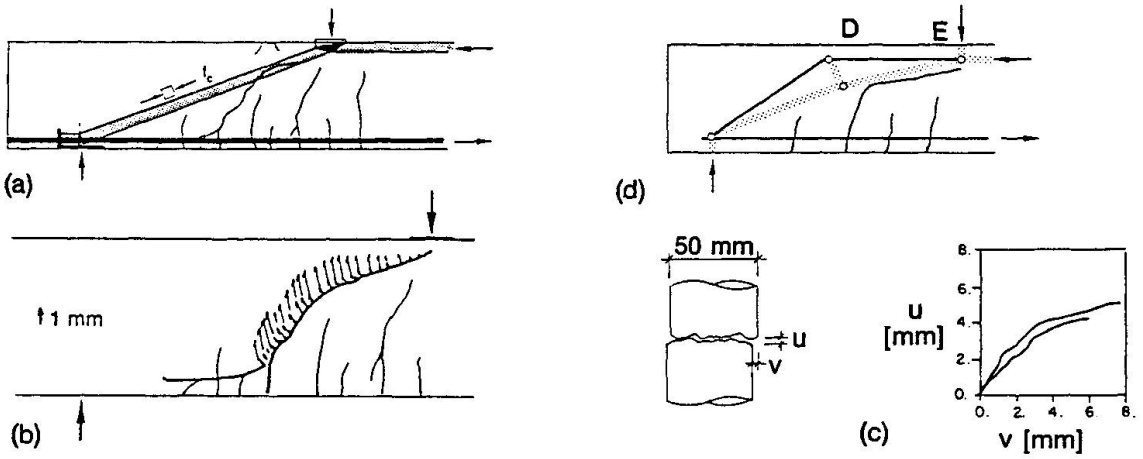

Fig. 4 Structural model; relative displacement of the critical crack

Therefore a stress field with a concrete strut running directly between the load and the support reaction is not possible. Such a strut is only admissible if it is deviated in the central region (Fig. 4d). The concrete strut acts together with a concrete tie, that also exhibits a deviation in the central part of the beam, so that the deviation forces can balance each other out. Failure occurs because the tensile strength in the region D is reached or because the strength in zone E, which is subjected to both tension and compression, is exceeded. Overstressing in this zone can be caused by the crack which propagates to the zone where the load is applied.

It may be easily seen that the load capacity of the stress field (with a bent strut) shown in Fig. 4d is smaller than that given by the plasticity theory (with a straight strut). Therefore the failure load is very dependent upon the crack pattern. Thus there results, especially for tests on small beams, a big scatter in the experimentally determined failure loads. Since the crack pattern depends on the initial state of stress and the load history, the failure load is also influenced by these factors. For this reason a theoretical estimate of the failure load is always encumbered by great difficulties and uncertainties. The position of the critical crack and thus the load capacity depends greatly on a number of parameters, for example slenderness of beam, geometry and axial force. These influences are described in [6].

The correlation between crack pattern and failure load indicates the possibility of improving the structural performance and increasing the failure load by favourably influencing the crack pattern by means of constructional measures. The zone where the strut corresponding to direct support should be formed can for example be kept free of cracks by prestressing the beam such that the load is supported directly from the beginning. This explains why prestressed beams exhibit a greater shear resistance than non-prestressed reinforced beams. A similar improvement in performance is evident when the reinforcment in the region subjected to shear action is not bonded to the concrete. Fig. 5 shows the crack patterns and the stress fields for two tests which differ only in the quality of the bonding. For beams having bond-free reinforcement or with a poor quality of bonding cracks form in the central part. As shown in Fig 5b the inclined strut is hardly affected by these cracks, so that the failure load can be as much as twice that of beams with good bonding quality (Fig. 5a). A further increase of the failure load can be achieved by placing reinforcement in the critical region. Fig. 6 shows the arrangement of reinforcement and the crack pattern at failure of a test reported by Muttoni and Thürlimann [6]. Wide cracks were only obtained in the unreinforced region, which allowed the direct support system to develop. As a result the load could be increased up to the point of yielding of the

longitudinal bars. The failure load was about double that of a similar beam which did not have reinforcement in the region of the concrete strut (Fig. 4a).

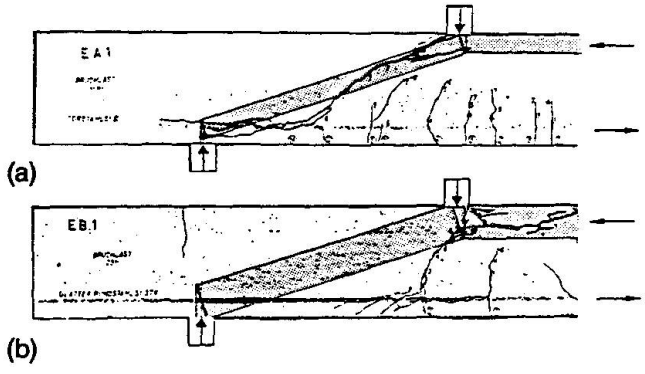

Fig. 5 Influence of bonding

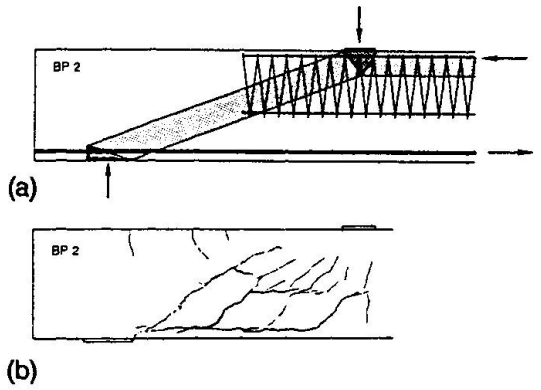

Fig. 6 Influence of reinforcement in the critical zone

2. PUNCHING SHEAR

With only small modifications the considerations concerning the internal structural behaviour of beams may be applied to the slab element shown in Fig. 7. Fig 8a shows the position of the stress resultants after tangential cracks have developed.

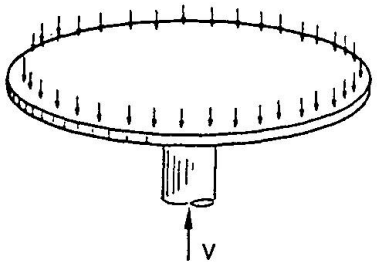

Fig. 7 Slab specimen

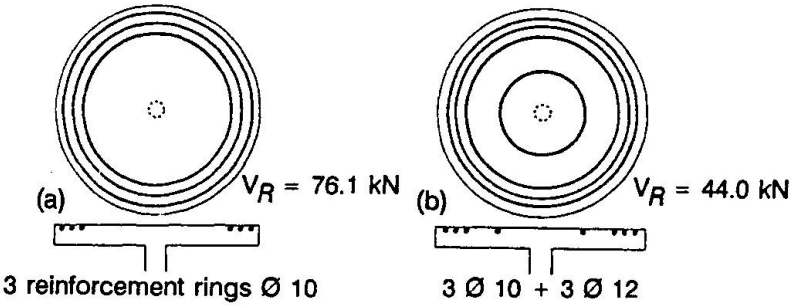

Fig. 9 Punching shear tests with ring reinforcement

As numerous punching shear tests have shown the curvatures in the radial direction are concentrated in the region of the columns, so that ring-shaped concentric bending cracks are only obtained in this region. In the other zones, however, only radial cracks are present. Since shear force is not transferred in the tangential direction, the stress state is not influenced by these cracks. In the region of tangential cracking a part of the shear force can be resisted by the interlocking action at the crack boundaries and by the dowelling action of the reinforcing bars (see Fig. 3). From Fig. 8a it is evident that the horizontal components of the compression and tension diagonals can be resisted by the reinforcement in the radial direction, by the radial compression zone and also by the deviation of the tangentially directed forces in the reinforcement and in the compression zone. On increasing the load the strength of the concrete tie is reached at A, so that the bending crack is propagated in the horizontal direction. The structural action that then results is similar to that obtained in the beam. As no force can be transferred across the crack a bent strut is formed with a tie that is also bent (Fig. 8b).

It has been shown experimentally that often the concrete compression in the radial direction in the compression zone near the column (point B) initially increases under monotonically increasing load and after reaching a certain load level begins to decrease until shortly before failure negative values may be exhibited. This observation is in agreement with the proposed model. The compression decreases once the main bending crack has propagated and its negative value (tensile strain) indicates that at B a tie has formed. Since the structural behaviour and the failure mechanisms are analogous to the those of the beam, for slabs also the same constructional solutions may in principle be employed. The crack pattern can be favourably influenced by omitting reinforcement in the region of the columns. As in the case of beams having reinforcement without

stirrups, whereby cracks can only develop in the vicinity of load application, for such a slab tangential cracks can only develop above the edge of the column. This kind of behaviour has been observed by Bollinger [7] in tests carried out on slab elements. The test shown in Fig 9a was reinforced with concentric rings placed at the boundary of the slab only. The punching shear force for this test was consistently higher than that for similar slabs which also had reinforcement in the region of the column. For the test shown in Fig. 9b the additional reinforcing ring in the critical region (greater amount of reinforcement) even caused a substantial reduction in the punching shear force.

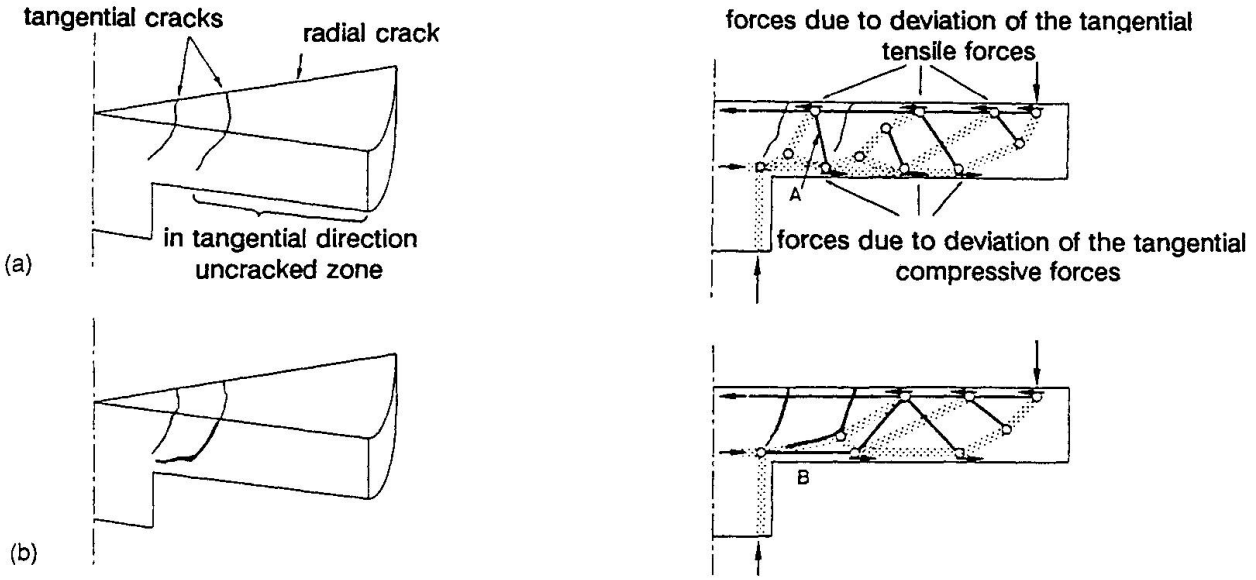

Fig. 8 Structural behaviour in the cracked state

Since in general the critical crack is responsible for the reduction in the failure load the punching shear force is inversely proportional to the width of crack. This is confirmed in Fig.10 in which the load is given as a function of the rotation φ in the region of the column for four slabs with different amounts of reinforcement.

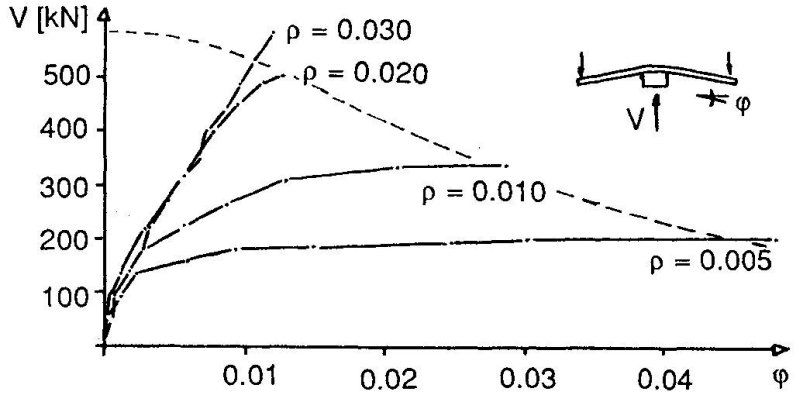

Fig. 10 Load-displacement diagrams of slabs

Since for the four slabs the thickness was kept constant the crack width is also proportional to the rotation φ. In Fig. 11a the punching shear forces and the corresponding deformations are shown for further test specimens. Since the crack width inside the slab is a direct function of the slab thickness, for this figure the product of rotation φ times statical depth d was chosen for the abscissa. The ordinate represents normalized nominal punching shear strength. The relationship between punching shear resistance and deformation is described satisfactorily by the curve given in Fig. 10. Good agreement with test results is also obtained when the slab thickness h alone is varied (Fig. 11b).

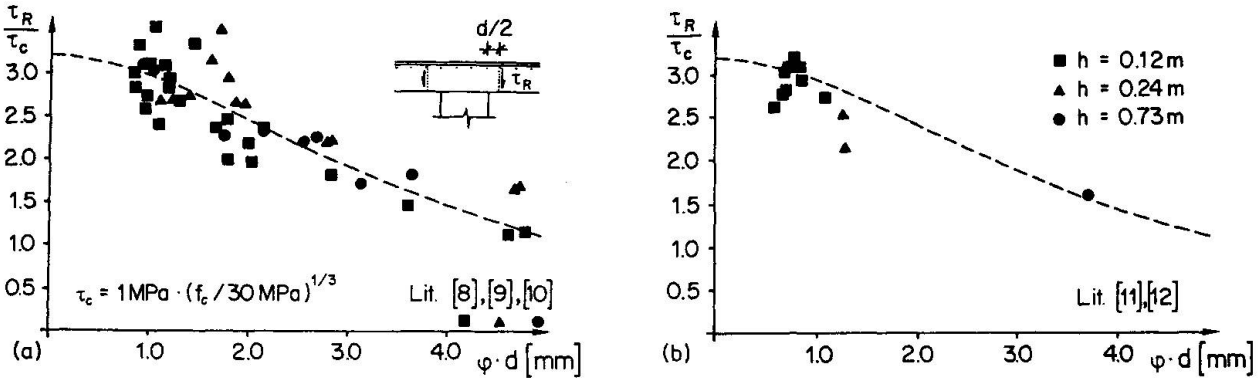

Fig. 11 Nominal punching shear strength in function of $\varphi \cdot d$

With the empirically determined curve for describing the ductility restrictions for axisymmetric slabs the punching shear force can be found analytically.

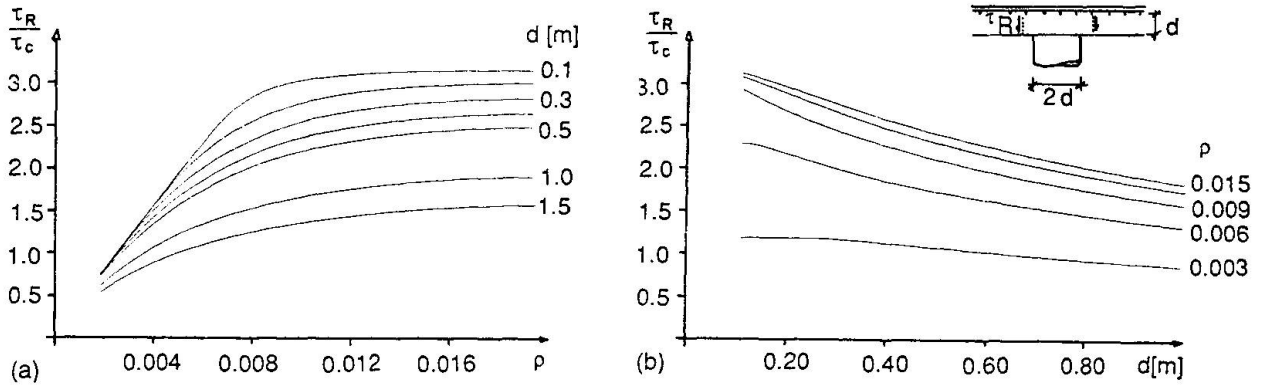

Fig. 12 Nominal punching shear strength in function of amount of reinforcement and slab thickness

From Fig. 12 it is evident that with increasing slab thickness a considerable reduction in punching shear resistance may result, i.e. the geometry or size-effect is important.

REFERENCES

1. DRUCKER D.C., On Structural Concrete and the Theorems of Limit Analysis. Internat. Association for Bridge and Structural Engineering, Zurich, IABSE-Reports 21, 1961.
2. KANI G., Spannbeton in Entwurf und Ausführung. Konrad Wittwer Publishers, Stuttgart, 1955.
3. HAMADI Y.D., REGAN P.E., Behaviour in Shear of Beams with Flexural Cracks. Magazine of Concrete Research, Vol. 32, No. 111, June, 1980.
4. REINECK K.-H., Models for Design of Reinforced and Prestressed Concrete Members. Comité Euro-International du Béton (CEB), Bulletin d'information No. 146/1982.
5. MUTTONI A., THüRLIMANN B., Schubversuche an Balken und Flachdecken ohne Schubbewehrung. Institute of Structural Engineering, ETH Zurich, 1986, unpublished report.
6. MUTTONI A., Die Anwendbarkeit der Plastizitätstheorie in der Bemessung von Stahlbeton. ETH Zurich, IBK, Report Nr. 176 (PH.D. Thesis), Birkhäuser Verlag, Basel, 1990.
7. BOLLINGER K., Zu Tragverhalten und Bewehrung von rotationssymmetrisch beanspruchten Stahlbetonplatten. University of Dortmund (Ph.D. Thesis), 1985.
8. ELSTNER R.C., HOGNESTAD E., Shearing Strength of R.C. Slabs. ACI Journal, July, 1956.
9. KINNUNEN S., NYLANDER H., Punching of Concrete Slabs without Shear Reinforcement. Kungl. Tekniska Hogskolans Handlingar, Stockholm, Report No. 158, 1960.
10. TOLF, P., Planiocklekens inverkan pa betongplattors hallfasthet vid genomstansning. Kungl. Tekniska Hogskolans, Stockholm, Meddelande No. 146, 1988.
11. NYLANDER H., SUNDQUIST H., Genomstansning av pelarunderstödd plattbro av betong med ospänd armering. Meddelande 104, Kungl. Tekniska Högskolan, Stockholm, 1972.
12. KINNUNEN S., NYLANDER H., TOLF P., Plattjocklekens inverkan pa betongplattors hallfasthet vid genomstansning. Försök med rektangulära plattor. M. 137, Kungl. Tekn. Högskolan, Stockholm, 1980.

Bond Model for Punching Strength of Slab-Column Connections

Modèle de liaison pour résistance au poinçonnement dans les têtes de colonnes en béton armé

Physikalisches Modell für das Durchstanzen von Flachdecken

Scott D.B. ALEXANDER
Univ. of Alberta
Edmonton, AB, Canada

Scott Alexander recently completed his Ph.D. in civil engineering at the University of Alberta. He is currently a research engineer with the Network of Centres of Excellence on High Performance Concrete.

Sidney H. SIMMONDS
Univ. of Alberta
Edmonton, AB, Canada

Sidney Simmonds received his Ph.D. in civil engineering at the University of Illinois in 1962. His research has been primarily in the area of design and behaviour of reinforced concrete structures and he is a member of a number of related technical committees.

SUMMARY
A physical model that explains the mechanism of punching failure in reinforced concrete column-flat plate connections is presented. Load is carried to the column face by arching action in the radial direction. The curvature of the arch is defined by the force gradient (bond) that can be developed in the reinforcement perpendicular to the arch. The validity of the model is demonstrated by comparing predicted capacities with results from tests of such connections.

RÉSUMÉ
Un modèle physique est présenté qui explique le mécanisme de rupture par poinçonnement dans les têtes de colonnes en béton armé, au droit de leur connexion avec une dalle. La charge est transmise au bord de la colonne de façon radiale, sous forme d'une action légèrement arquée. La courbure de cet arc est définie par le gradient de forces pouvant se développer dans l'armature qui se trouve perpendiculaire à l'arc. La validité de ce modèle est démontrée par la compression des capacités prévues de résistance, illustrée par les résultats d'essais effectués sur de tels systèmes de connexion.

ZUSAMMENFASSUNG
Es wird ein physikalisches Modell für das Durchstanzen von Flachdecken vorgestellt. Die Last wird über eine radiale Bogentragwirkung zum Stützenkopf übertragen. Die Bogenform wird durch den Abbau des Verbundes in der Ringbewehrung bestimmt. Die Gültigkeit des Modells wird durch den Vergleich mit Bruchversuchen bestätigt.

1 Introduction

The truss model[1] describes a slab-column connection as a space truss composed of steel tension ties and straight-line concrete compression struts. Although this model provides an excellent qualitative description for the behavior of slab-column connections, the location of the intersection between the effective centroid of the strut and the top mat reinforcing steel does not agree with the position of the strut as determined from measured bar force profiles at failure[2]. A model that retains the desirable characteristics of the truss model and is consistent with experimental measurements of strain is required.

A curved arch, as shown in Fig. 1, is consistent with measured bar force profiles. In plan, the arch is parallel to the reinforcement. As with the truss model, the horizontal component of the arch is equilibrated by tension in the reinforcement. By limiting the width of the arch to the width of the column support, the arch may be considered a purely radial component within the plate, thereby preserving the truss model concept of shear being carried radially by an inclined concrete compression strut. The geometry of the curved radial arch, however, cannot be determined from the bar force profile of the reinforcement tying the arch.

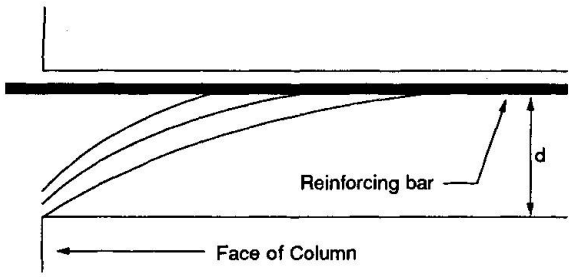

Fig. 1: Radial Arch

If the horizontal force component in the arch is assumed to be constant, then the shear carried by the arch varies from a maximum at the face of the column where the slope of the arch is large to a minimum, or perhaps zero, at the intersection of the arch and the reinforcing steel where the slope is small. The shear that was carried by the arch at the face of the column must be dissipated in a direction perpendicular to the arch at some distance away from the column. The rate at which shear can be dissipated determines the curvature of the arch.

In a reinforced concrete flexural member, moment is calculated as the product of the steel force, T, and an effective moment arm, jd. Moment gradient or shear results wherever the magnitude of the force or moment arm varies along the length of the member (x-axis).

$$V = \frac{d(Tjd)}{dx} = \frac{d(T)}{dx} jd + \frac{d(jd)}{dx} T \qquad [1]$$

Shear that is the result of a gradient in tensile force acting on a constant moment arm is carried by **beam action**. Shear resulting from a constant tensile force acting on a varying moment arm is carried by **arching action**. Whereas beam action at a particular cross-section requires bond forces at that cross-section, arching action requires only remote anchorage of the reinforcement.

Experimental observations suggest that beam action is the only possible mechanism of shear transfer in what amounts to a circumferential direction. For example, Kinnunen and Nylander[3], report that the deformed shape of test specimens under load is essentially conic, with little or no curvature in the radial direction. This requires a linear distribution of circumferential strain through the thickness of the plate, with maximum compressive strain at the slab soffit. This means that the flexural depth, jd, in the circumferential direction is relatively constant, and any shear carried in the circumferential direction must be carried by the two-way plate equivalent of beam action.

Beam action shear requires a force gradient in the reinforcement. Force gradient may be limited by either yielding of the reinforcement or by bond failure. For those connections that fail prior to widespread yielding, bond strength is the most important limitation on force gradient, hence, the term **bond model**.

2 Development of Bond Model

The orthogonally reinforced slab-column connection is modelled as a rectangular grillage, as shown in Fig. 2. Four strips, called radial strips, extend from the column parallel to the reinforcement. Any load reaching the column must pass through one of these four radial strips. The width of each strip is defined by the column width. The end of the strip farthest from the column support, called

the remote end, is placed at a position of zero shear. Thus, radial strips are loaded in shear on their side faces only. The total length of a strip is designated as L. The strength of the connection is determined by assessing both the flexural strength of each radial strip and the ability of the adjacent quadrants of two-way plate to load each radial strip.

Consider the free body diagram of one-half of a radial strip shown in Fig. 3. The half-strip must support the combined effect of any load applied directly to the strip (q), including the self-weight of the strip, and the internal shears and moments developed on the side faces of the strip by the adjacent quadrants of two-way plate. The near side face of the half-strip is loaded in shear (v), torsion (m_t) and bending (m_n) by the adjacent quadrant of two-way plate. The far side face lies on an axis of symmetry for the plate. Under concentric loading, both shear and torsion on this face are zero. The bending moment applied to the far side face of the half-strip is equal and opposite to the bending moment on the near side face.

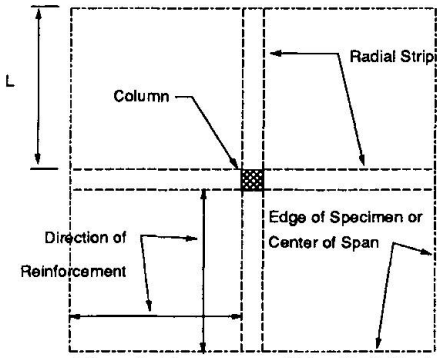

Fig. 2: Layout of Radial Strips

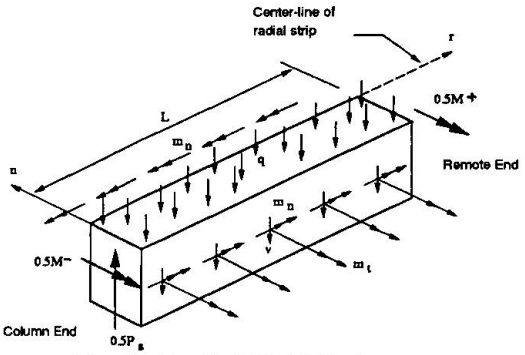

Fig. 3: Radial Half-Strip

The combination of shear and torsion on the side face of the radial half-strip is replaced by a statically equivalent line load, $\overline{v}$, acting on the strip. The term $\overline{v}$, referred to as the Kirchhoff shear, has its origins in elastic plate theory as a way of satisfying equilibrium at a free or simply supported edge of a plate.

$$\overline{v} = \frac{\partial m_n}{\partial n} + 2 \times \frac{\partial m_t}{\partial r} \qquad [2]$$

The Kirchhoff shear has two components. The first is a shear resulting from the gradient in bending moment perpendicular to the radial strip. This is referred to as **primary shear**. The second is a shear resulting from twisting moment gradient along the side face of the radial strip, called **torsional shear.**

Primary shear results from the gradient in bending moment perpendicular to the radial strip. If bending moment gradient perpendicular to the radial strip is the result of beam action alone, then:

$$\frac{\partial m_n}{\partial n} = \frac{jd}{s} \times F_b' = \tau \times jd \qquad [3]$$

where F_b' is the force gradient in the reinforcing bars perpendicular to the radial strip, s is the spacing and jd is the flexural moment arm. If F_b' is averaged over the bar spacing, the resulting term is the horizontal shear stress required for moment gradient, τ.

In a region dominated by beam action, a limiting value of force gradient in the reinforcement is the equivalent of a limiting shear stress. Any limit to the force gradient that can be sustained at the boundary between steel and concrete is a bond limitation on the quantity $\partial m_n/\partial n$. Alternatively, for very lightly reinforced plate-column connections, force gradient at the edge of the radial strip may be limited by the spread of yielding.

Torsional shear is the result of gradient in the torsional moment on the side face of the radial strip, in a direction parallel to the radial strip. The factors governing the magnitude of the torsional moment and the torsional moment gradient are not known, nor is it clear how these quantities might be measured. However, it is possible to outline some of the effects of torsional shear on the basis of equilibrium conditions.

For a concentrically loaded column, the torsional moment must approach zero at the column support as a result of symmetry. Because of the way the radial strip is defined, the magnitude of the torsional moment at the remote end must also be zero, either by symmetry or boundary condition. Since the torsional moment is zero at both ends of the radial strip, the total contribution to Kirchhoff shear made by torsional moment gradient must be zero. Hence, torsional shear affects only the distribution of Kirchhoff shear along the length of the radial strip, leaving primary shear as the root source of all shear load on the side face of a radial strip. The effective centroid of the shear load is moved closer to the column by the action of torsional shear.

Fig. 4 shows a radial half-strip of an interior slab-column connection, excluding the bending moments about the *n*-axis, with the torsions and shears on the side faces replaced by the Kirchhoff shear. The term $\overline{q}$ is a line load equivalent to the directly applied load, q. The radial strip supports all the loads by acting as a cantilever beam. The total flexural strength of the cantilever is the sum of M- and M+. Flexural equilibrium of the radial strip leads to Eq. 4 and vertical equilibrium produces Eq. 5. In each equation, the factor two accounts for the fact that both $\overline{v}$ and $\overline{q}$ are defined for a radial half-strip. The quantity P_s is the total load carried by one radial strip of an interior column-slab connection.

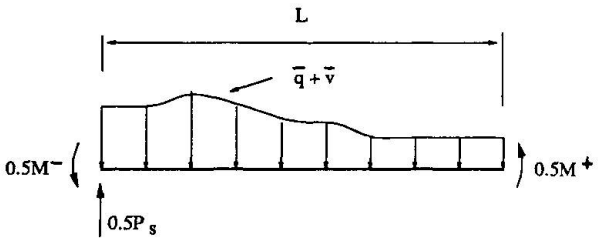

Fig. 4 Loading of Radial Half-Strip

$$M^+ + M^- = M_s = 2 \times \int_0^L (\overline{v} + \overline{q}) r\, dr \qquad [4]$$

$$P_s = 2 \times \int_0^L (\overline{v} + \overline{q})\, dr \qquad [5]$$

Expressions for the negative moment capacity, M-, at the column end of the strip and the positive moment capacity, M+, at the remote end of the strip, are given in Eq. 6.

$$M^- = \rho^- \times f_y jd^2 \times c_2 \qquad M^+ = k_r \times \rho^+ \times f_y jd^2 \times c_2 \qquad [6]$$

The factor, k_r, accounts for the proportion of bottom steel that can be developed by the rotational restraint provided at the remote end of the radial strip. It is reasonable to assume that any steel which passes through the column contributes to M_s. There is, however, a problem in dealing with reinforcing bars which are close to the column. Furthermore, for uniformly spaced reinforcement, the values of ρ- and ρ+ should not depend on whether the mat is bar centered or space centered. These problems are overcome by defining ρ- and ρ+ as:

$$\rho^- = \frac{A_{sT}}{b \times d} \qquad \rho^+ = \frac{A_{sB}}{b \times d} \qquad [7]$$

A_{sT} and A_{sB} are the total cross-sectional area of top and bottom steel, respectively, passing through the column plus one half the area of the first top or bottom bar on either side of the column. The term b is the column dimension plus the distance to the first reinforcing bar on either side of the column.

To evaluate the integrals of Eqs. 4 and 5, assumptions are made regarding the distribution of line load along the length of the radial strip. These assumptions both simplify and optimize the loading of the radial strip in a manner generally consistent with a lower bound approach.

- All Kirchhoff shear is assumed to be the result of primary shear. The torsional shear contribution is considered negligible because the deformations of a plate-column connection that fails in brittle punching are not consistent with the development of large torsional moments.
- At a distance l from the column end of the radial strip, the Kirchhoff shear decreases from the maximum value permitted by primary shear ($(\partial m_n/\partial n)_{max}$) to a value of zero. The length l is referred to as the loaded length of the radial strip.
- The direct load on the radial strip is assumed small compared to $\overline{v}$ and is neglected ($\overline{q} = 0$).

Based on these assumptions, the optimized loading of a radial half-strip is shown in Fig. 5. The loading term w is defined as:

$$w = \left(\frac{\partial m_n}{\partial n}\right)_{max} = F_b{}'_{max} \times \frac{jd}{s} = \tau_{max} \times jd \qquad [8]$$

It is convenient to consider w as the simplified, optimized Kirchhoff shear load acting on one side of a radial strip by an adjacent quadrant of two-way plate. Because a radial strip of an interior column-slab connection has two adjacent quadrants of two-way plate, the total line load on a radial strip of an interior column-slab connection is $2w$. For an edge or corner column, however, there will be radial strips that are parallel to the free edge of the plate and have only one adjacent quadrant of two-way plate. For these strips, the total line load is w.

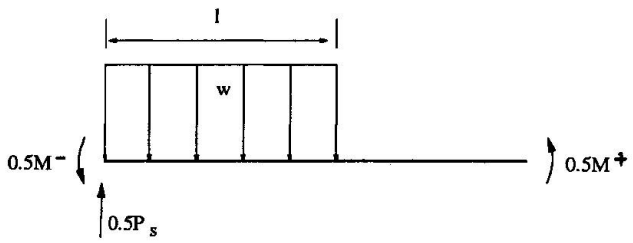

Fig. 5 Simplified Loading of Radial Half-Strip

Eq. 8 suggests that w may be based on either the maximum force gradient, $F_b{}'_{max}$, in the reinforcement perpendicular to the radial strip or a maximum critical shear stress, τ_{max}, applied on the side faces of the radial strips. $F_b{}'_{max}$ may be obtained from an estimate of the bond strength as governed by splitting failure. τ_{max} may be obtained from the critical value of shear stress as defined by building codes for one-way flexural members. Since most treatments of splitting bond failure focus on either lap splices or anchorage zones rather than locations at some distance from the ends of the bars, τ_{max} provides a more attractive basis for a predictive model for punching shear.

For simplicity, building codes usually replace $\tau_{max} \times j$ with v_c. The critical value of v_c according to the ACI Standard[4] and the corresponding value of w are:

$$v_c = 0.166 \times \sqrt{f'_c} \qquad w_{ACI} = d \times 0.166 \times \sqrt{f'_c} \qquad [9]$$

The assumptions made regarding the distribution of line load along the length of a radial strip and the method chosen for estimating w result in the simplified free body diagram shown in Fig. 5. Using this figure, Eq. 4 may be rewritten and solved for l as follows:

$$M_s = 2 \times \int_0^L (w) r\,dr = 2 \times \int_0^l (w) r\,dr = 2 \times \frac{wl^2}{2} \quad ; \quad l = \sqrt{M_s/w} \qquad [10]$$

Substituting l into Eq. 5 yields:

$$P_s = 2 \times \int_0^L (w)\,dr = 2 \times \int_0^l (w)\,dr = 2 \times wl = 2 \times \sqrt{M_s \times w} \qquad [11]$$

The punching capacity of a slab-column connection is obtained by summing the contribution of each radial strip.

3 Discussion

The bond model, using w_{ACI}, was applied to 115 tests reported in the literature. The ratios of test load to predicted load are shown in Fig. 5. The average ratio of test to predicted punching load is 1.29 with a coefficient of variation of 12.3 per cent. Using the ACI[4] and BS 8110[5] code procedures on the same body of data, the average test to predicted values are 1.59 and 1.06 and the coefficients of variation are 26.5 and 15.1 per cent, respectively.

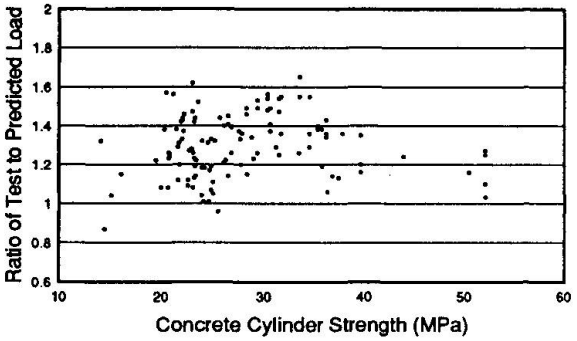

Fig. 6 Comparison of Test Results with Bond Model Predictions

The difference between the average test to predicted ratio for the ACI and BS 8110 codes can be attributed to differing design philosophies. The quality of these models should be judged on the consistency of their predictions rather than the magnitude of the average test to predicted ratio, since this can be adjusted simply by multiplying by a constant.

It is considered that the principal reason for the bond model consistently underestimating punching strengths is that the contribution of torsional shear is neglected. Despite this approximation, the bond model produces results that are more reliable than most building codes currently in use. Furthermore, the model is simple to apply and does not resort to the definition of artificial critical sections for shear.

The curved arch of the bond model is a natural progression from the straight-line compression strut of the truss model. In this way, the bond model is consistent with the truss model. The curvature of the arch requires a tension field within the concrete. The magnitude of this tension field is governed indirectly by the beam action shear perpendicular to the arch. As shown above, beam action shear as limited by bond can be represented as a critical shear stress. Thus, the bond model shows why the code approaches for estimating punching strength based on a critical shear stress acting on a critical shear section give satisfactory results.

The bond model links shear strength and bond strength at locations other than anchorage or splice locations. The importance of bond in the vicinity of the column has not been fully appreciated. The link between force gradient in the reinforcement and punching strength also explains why excessive yielding of the reinforcement in the vicinity of the column produces lower punching strengths.

4 References

1 ALEXANDER, S.D.B., and SIMMONDS, S.H. 1987. Ultimate strength of slab-column connections. American Concrete Institute Structural Journal, Vol.84, No.3, pp. 255-261.

2 ALEXANDER, S.D.B. 1990. Bond model for strength of slab-column joints. Ph.D. thesis. Department of Civil Engineering, University of Alberta.

3 KINNUNEN, S., and NYLANDER, H. 1960. Punching of concrete slabs without shear reinforcement. Transactions of the Royal Institute of Technology (Sweden), No.158, Stockholm, pp. 1-110.

4 ACI COMMITTEE 318-89: 1989 Building code requirements for reinforced concrete. American Concrete Institute, Detroit, MI.

5 BRITISH STANDARDS INSTITUTION, 1985. The structural use of concrete: Part 1, Code of practice for design and construction (BS 8110:Part 1). British Standards Institution, London.

Design of Slab-Column Frames

Conception de cadres dalles-colonnes

Entwurf von Stahlbeton-Plattenträger-Strukturen

James R. CAGLEY
President
Cagley & Associates
Rockville, MD, USA

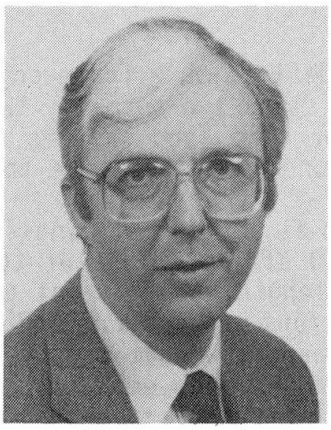

James R. Cagley is a fellow of the ACI and has served on the ACI 318 Standard Building Code Committee since 1973. He is registered in 32 states in the USA and has practiced in many other countries.

SUMMARY

In the last 10 years a significant number of slab-column frame structures have been designed and constructed in the Washington D.C. area. Flat plate construction has been very popular for many years in Washington because of the stringent building height limitations caused by a desire not to overshadow the nation's Capitol building. The use of slab-column frames allows a 10-story office building with a total height limitation of approximately 32 m. Elimination of exterior masonry walls and interior masonry partitions led designers to look for other methods of resisting wind loads. Hence, the development of the slab-column frame.

RÉSUMÉ

Dans les 10 dernières années, un nombre important de structures en cadres dalles colonnes ont été dimensionnées puis réalisées dans les environs de Washington DC, USA. La construction de bâtiments relativement plats a été très répandue depuis de nombreuses années du fait des restrictions impératives sur la hauteur des édifices en vue d'éviter qu'ils ne dominent le Capitole lui-même. C'est ainsi que l'utilisation des structures en cadre dalles-colonnes permet de construire des immeubles de bureaux de 10 étages, dont la hauteur n'excéde pas 32.00 m. L'élimination des parois extérieures et des galandages en maçonnerie a nécessité la recherche d'autres méthodes pour contreventer les bâtiments, d'où le développement de l'étude des cadres dalles-colonnes.

ZUSAMMENFASSUNG

In den letzten 10 Jahren wurden in Washington, DC viele Flachdecken entworfen und gebaut. Flachdecken waren in Washington auf Grund der Höhenbeschränkung für Gebäude, um das Kapitol nicht zu beschatten, für viele Jahre weit verbreitet. Die Verwendung dieser Bauweise machte es möglich, ein zehngeschossiges Bürogebäude mit einer Gesamthöhe von etwa 32 Metern zu errichten. Durch das Weglassen von Aussen- und Innentragwänden waren die Entwerfer gezwungen, die Rahmenwirkung mit den Stützen heranzuziehen.

1. INTRODUCTION

In the last 10 years a significant number of slab-column frame structures have been designed and constructed in the Washington, D.C. area. Flat plate construction has been very popular for many years in Washington because of the stringent building height limitations caused by a desire to not overshadow the nation's capitol building. The use of slab column frames allows for the construction of a 10 story office building with a total height limitation of approximately 105'. Elimination of substantial exterior masonry walls and interior masonry partitions caused designers to look for other methods of resisting wind loads. Hence, the development of the slab-column frame.

A slab-column frame is by definition a frame composed of slabs and columns in lieu of beams and columns. The slabs are normally two-way systems such as flat plates, flat slabs, waffle slabs or slab band systems. The purpose of using these types of systems is basically economy and a desire to avoid the use of shear walls.

In many building types such as office buildings, the use of shear walls causes many impediments to planning and efficient use of the floor space. If the core areas provide enough shear wall length, this is not a problem but often that is not the case and supplemental locations must be used. The economy of cast in place concrete construction is greatly enhanced when the only formwork which is required is flat deck forming and column forming with emphasis on keeping columns the same size as much as possible. The formwork cost increases significantly with the addition of concrete beams and shear walls. As a result it has been proven to be quite economical to use slab-column frames as the systems for buildings of moderate height (up to 12-14 levels) and in areas of low seismic risk.

This type of system works very well in hotel room towers as it does for office buildings. Some of the same reasons such as a desire to maintain a minimal floor to floor height make the slab-column frame an ideal solution for hotel towers up to approximately 12 floors. The normal gravity load system is a post tensioned flat plate with a thickness of 6 1/2" or 7". When the moment transfer requirements in the slab at the lower floors become a very large magnitude it is necessary to go to another lateral load resisting system. Normally this would occur at around 12 levels and would require the use of a shear wall system for heights greater than that.

2. DESIGN BASIS

2.1 Gravity Load Design

The gravity load design of slab-column frames is commonly accomplished utilizing the equivalent frame method or some PC based software. PCA's ADOSS is the program commonly used for mild reinforced systems and our office uses the post tensioning program developed and marketed by Structural Data, Inc. for the design of post tensioned floor systems. The normal procedure is to design the floor system for gravity loads and then to check it for the combination of lateral loads and gravity loads. In most cases this will require the addition of small amounts of bonded reinforcing which should be concentrated in the area over the column and immediately adjacent to each side of the column.

2.1 Lateral Load Design

Although the gravity load design of slab-column frames is similar to other systems, the design for lateral loads places some added constraints on the designer. The slab-column frame is a very flexible system so that drift or lateral deflections are of primary importance. The calculation of lateral deflections are greatly affected by the assumptions.

Our office practice is as follows:

1. All buildings are designed for strength as per the appropriate building code. This is normally the Building Officials & Code Administrators (BOCA Code) in the Washington, D.C. area. The design wind speed is generally 80 or 90 mph.

2. The normal criteria which we use for wind drift is h/500 or h/400 where h is the height of the building under design. THIS IS NOT A CODE REQUIREMENT.

3. The wind load used for drift calculations is related to the highest recorded wind speed in the area. In the Washington area we would generally use 60 mph for our drift calculations. Our theory is that in most buildings discomfort due to movement should be avoided for normal or probable loadings. These are not necessarily the same as CODE loadings. It is easy to see that the calculated drift is less than half if 60 mph is used in lieu of 90 mph.

4. Reduced stiffnesses are used for the slab-column frames. The slab stiffness is based on 35% of the total bay width and the columns on 100% of their gross stiffness.

5. The lateral load analysis is accomplished with either ETABS, a program developed at the University of California and marketed by Computers & Structures, Inc., or one of several plane frame programs utilizing various modeling techniques.

A similar procedure is used for consideration of Zone 1 earthquake loadings. We are presently doing our first project in a Zone 2 area utilizing a slab-band system and the provisions of Chapter 21 in ACI 318-89 and the 1985 Uniform Building Code (UBC) allowing the use of two-way slab systems in zones of moderate seismic risk.

2.3 Column Design

Utilizing the information from the gravity load design of the slab system and the lateral load analysis of the slab-column frame our office uses a simplified moment magnification approach as proposed by MacGregor for medium height structures. A more exact method would be required for tall structures. This approach is valid when the stability index Q is between 0.0475 and 0.20. Q is defined as $\Sigma P_u \Delta_1 / H_u h_u$. P_u is the factored load of the entire story, Δ_1 is the first order story deflection. H_u is the total lateral load for this story and the stories above, and h_u is the unsupported clear height of the column.

The method is described in STABILITY ANALYSIS AND DESIGN OF CONCRETE FRAMES, James G. MacGregor and Sven E. Hage, ASCE Structural Journal, October 1977.

The structural magnified moments which will normally be significantly less than those utilizing the CODE equations are then combined as appropriate with the factored loads and moments from the gravity load analysis.

2.4 Shear Design

Typical two-way slab systems utilize a "shear cap" to increase the shear capacity of the slab system in the critical area surrounding the column and to allow the subsequent use of a thinner slab controlled by flexure and deflection considerations rather than shear.

The 1983 ACI 318 basically did not allow for the contribution of a column capital or bracket which lay outside a 45° tapered wedge. Consequently if the horizontal

extension of a "shear cap" was greater than the vertical depth of the "shear cap", the added horizontal concrete was of no value in calculating the shear capacity of the slab system. This meant that if a 4'-0" square "shear cap" that was 6" deeper than the slab was used with a 24" square column only the first 6" projection contributed to the shear capacity of the system and the second 6" projection did not affect the capacity. Obviously, this was not correct and a subsequent change in the 1989 CODE gives a basis for utilizing that capacity.

The 1989 ACI 318 requirement requires a gradual decrease in v_c from $4\sqrt{f'_c}$ to $2\sqrt{f'_c}$ as the ratio of the critical perimeter b_o, to the critical depth, d, increases. The requirement will mean that at the edge of a 4'-0" square "shear cap" with an 8" slab such as might be used on an office building, the allowable v_c would be $3.32\sqrt{f'_c}$ in lieu of $4\sqrt{f'_c}$ as might have been assumed for an interior column.

ACI-ASCE Committee 352 also has a recommendation in their "Tentative Recommendation for Design of Slab Column Connections in Monolithic Reinforced Concrete Structures". Their requirement is based on just two adjustments. If the ratio of the maximum perimeter of the slab critical section to slab effective depth is less than 20, the allowable $v_c = 4\sqrt{f'_c}$. If the value is between 20 and 40, v_c is modified to $3\sqrt{f'_c}$ and if it is over 40 v_c becomes $2\sqrt{f'_c}$. Our sample from above would have a ratio of 4(48+d) over d. If we assume that d is 7 than 212/7 = 30.3 so $v_c = 3\sqrt{f'_c}$. Obviously, all of these values in any case would need to be adjusted as appropriate for other factors such as the aspect ratio of the column.

3. TEST PROGRAM

A small test program involving eight specimens was accomplished at the University of California at Berkeley in 1988 and '89 under the direction of Dr. Jack Moehle. The purpose of the program was to attempt to determine the effectiveness of a "shear cap" in increasing the shear capacity of a slab-column joint. The results of the testing were the confirmation of the allowable shear values indicated in both ACI-318-89 and the ACI-ASCE 352 report. The values are apparently conservative, but the failure mode is not as anticipated. The "shear caps" do not act as an extension of the column area but are much more flexible and actually tend to fall off the bottom of the slab. As previously noted, the allowables as proposed are appropriate.

4. DETAILING

Both the ACI-ASCE Committee 352 recommendations and the 1989 ACI 318 CODE require that some minimum amount of positive (bottom) reinforcing be continuous through the joint.

In slab-column frames there is often a requirement at the lower floors for continuous bottom reinforcing through the joint for strength considerations.

ACI-ASCE 352 and ACI 318-89 require some continuous bottom reinforcing in two-way slab systems at the supports regardless of the lateral load resisting system utilized for the building.

5. CONCLUSIONS

Slab-column frames have proved to be a viable, economical solution for many building projects in the Washington, D.C. area as well as other parts of the United States. In the last 3 or 4 years our office has designed at least 6 million square feet of construction utilizing this system. The system allows construction of large bay (30' x 30') or medium bay (20' x 20') office buildings with minimal floor to floor heights, since the effective structural depth is often no more than 8".

Although the system has limitations particularly for heavy seismic areas, it is a good solution for buildings in a concrete town like Washington, D.C. or any area of low-seismic risk.

Behaviour of Waffle Flat Slabs under Horizontal Load

Comportement des dalles nervurées soumises à des charges horizontales

Verhalten der Rippen-Flachdecken unter Horizontal-Belastung

Valter J.G. LUCIO
Res. Assist.
Techn. Univ.
Lisbon, Portugal

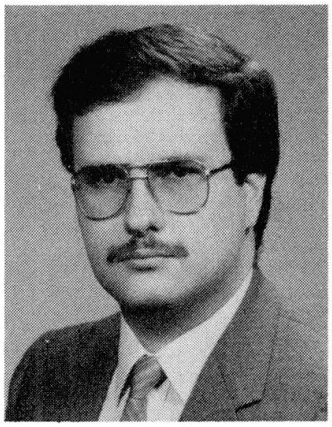

Valter Lucio has been a research assistant at UTL Lisbon since 1980 and has been preparing his Ph.D. thesis on waffle slabs for the last 4 years, 3 of them at the PCL.

Paul E. REGAN
Dr. Eng.
Polytechn. Central London
London, UK

Paul Regan has been at PCL since 1972 and has been active in research on flat slabs and particularly shear for many years.

SUMMARY

This paper presents a model of the behaviour of column-supported slabs under lateral actions. A method is proposed for quantifiying the rotational stiffness of slab-column connections for both solid and waffle slabs. The method takes account of the cracking of the slab. The results obtained from the model are compared with those from tests of reinforced concrete slabs.

RÉSUMÉ

Cet article présente un modèle destiné à étudier le comportement de dalles sur colonnes soumises à des actions latérales. Une méthode est proposée afin de quantifier la rigidité de rotation des joints dalle-colonne pour des dalles pleines et nervurées tout en tenant compte de la fissuration des dalles. Les résultats du modèle sont comparés avec ceux provenant d'essais effectués sur des dalles en béton armé.

ZUSAMMENFASSUNG

Der Artikel stellt ein Modell für das Tragverhalten von punktgestützten Platten unter Horizontallasten vor. Es wird ein Berechnungsverfahren für die Steifigkeiten des Stützen-Platten-Knotens bei Kassettendecken und massiven Decken vorgeschlagen. Dabei wird auf den Einfluss der Rissbildung unter Eigenlasten und Horizontallasten berücksichtigt. Die Berechnungsergebnisse wurden mit Versuchswerten verglichen.

1. INTRODUCTION

Equivalent frame methods offer an understandable and reasonable modelling of flat slab structures. In their usual forms they do however have problems in respresenting the behaviour of slab-column connections. These problems arise from geometry and from the effects of cracking.

2. EXPERIMENTAL STUDIES

Experimental data from realistic models subjected to lateral loading is available for tests by Lucio [1,2] on a waffle slab and by Long and Kirk [3] on solid slabs.

2.1 Waffle slab model

A column-supported waffle slab with 9 panels (Fig. 1) was tested at the Polytechnic of Central London. The slab, which represented typical prototypes to a scale of about 1 in 3.5, was supported on 16 columns and had solid infill panels with plan dimensions equal to 3/8 times the spans.

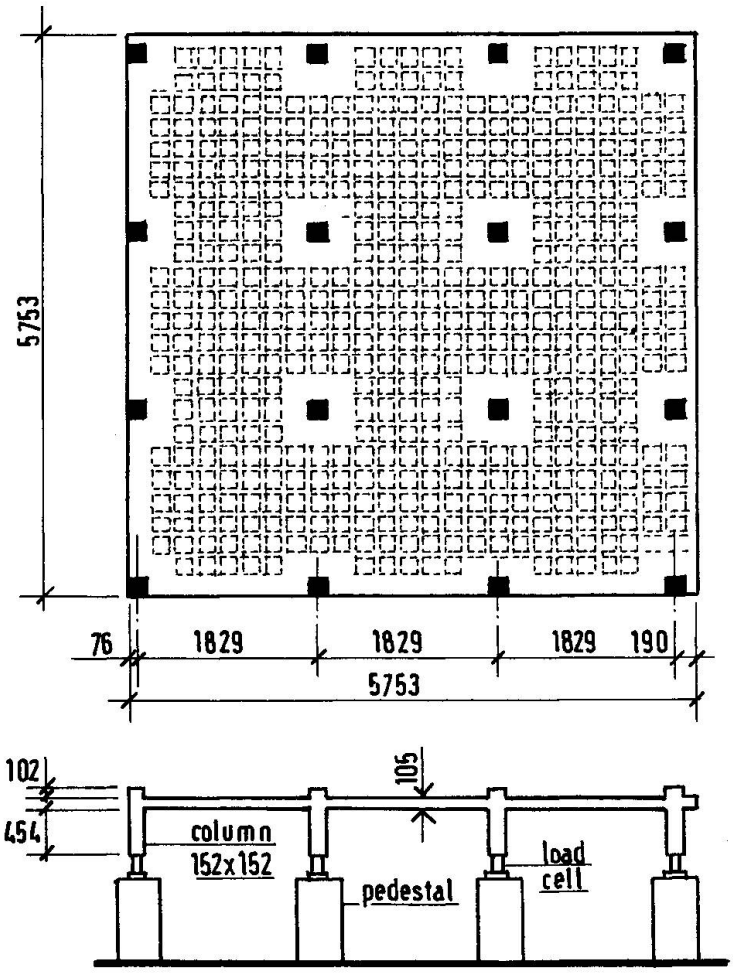

Fig. 1 Waffle slab tested by Lucio

The slab was subjected to various levels of vertical and horizontal loading to study its behaviour under lateral load with different amounts of cracking caused primarily by uniform vertical loading. The rotations at the column heads and the reactions at their bases were measured with inclinometers and triaxial load cells [4]. The base measurements allowed the moments at the slab-column joints to be determined.

Fig. 2 shows the rotations of an interior column head as functions of lateral load for various levels of prior vertical loading. The vertical loads during the lateral load tests were about 0.8 times the previous maxima.

Table 1 gives the stiffnesses of the structure at maximum horizontal loads in terms of H/a, where H is the total horizontal load and a is the lateral displacement at the level of the slab.

Prior Vert. Load (kN/m^2)	H (kN)	H/a (kN/mm)
9.4	40	176
12.0	50	147
17.0	80	97

Table 1. Stiffness from lateral load tests

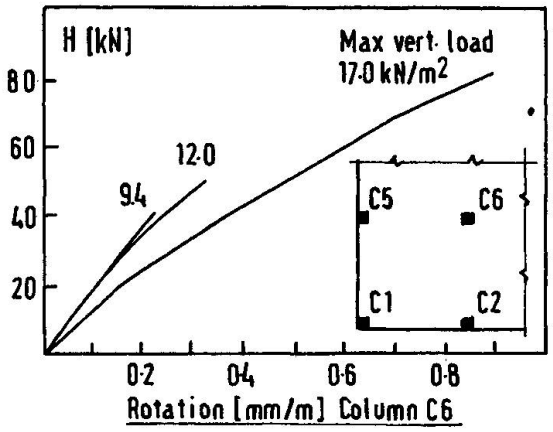

Fig. 2 Results of lateral load tests

2.2 Solid slab models

Long and Kirk tested three models representing parts of flat slab structures (Fig. 3). The supports were two columns and one line support. The long edges of the models represented mid-panel lines and rotations at and normal to these edges were prevented by the application of moments.

Model 2 included an edge beam and is not considered here. The other two differed in terms of column dimensions. For slab 1, the edge column was 100 x 150mm and the internal column was 150mm square. In model 3 the corresponding dimensions were 150 x 225mm and 225mm square.

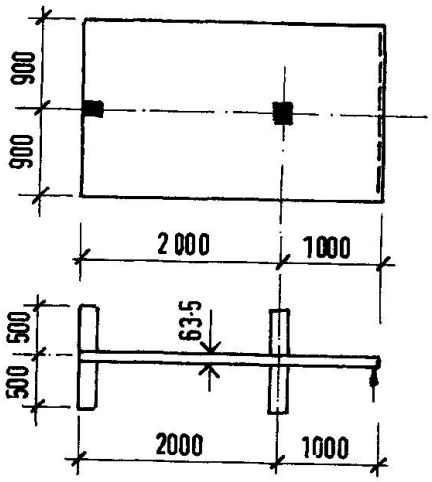

Fig. 3 Models of Long and Kirk

Displacements of 3mm were applied at the tops of the columns and horizontal reactions were measured at their bases During horizontal loading, the vertical load represented the dead load of a prototype 3 times the model size, but the slabs had been preloaded to the prototype service load.

3. FRAME ANALYSIS

3.1 General

Equivalent frame methods for the analysis of flat slabs include those of ACI 318-89 [5], BS 8110 [6] and the flexible joint method (FJM) proposed by Regan [7]. In the code methods, vertical and horizontal loadings are treated by different models. For vertical loading the properties of the members may be directly those of the structure, ie. $I = bh^3/12$ [6], in which case no allowance is made for the flexibility of the connections. Alternatively the column stiffnesses may be reduced to take account of this flexibility [5]. For horizontal loading the slab stiffness is reduced by considering an effective

breadth less than the full width between panel centre lines.

The FJM uses a torsional spring (Fig. 4c) to simulate the flexibility of a slab-column joint. This allows the same model to be used for any loading. All three methods are based on uncracked elastic theory.

3.2 Elastic behaviour

If the column of Fig. 4a has the same stiffness as the wall of Fig. 4b and the slabs are similar, the application of equal moments will produce a greater rotation in the former case. For elastic conditions the stiffnesses (M/θ) for both cases can be calculated by the Finite Element Method. The results depend somewhat on details but published data [8-11] for solid slabs is quite consistent.

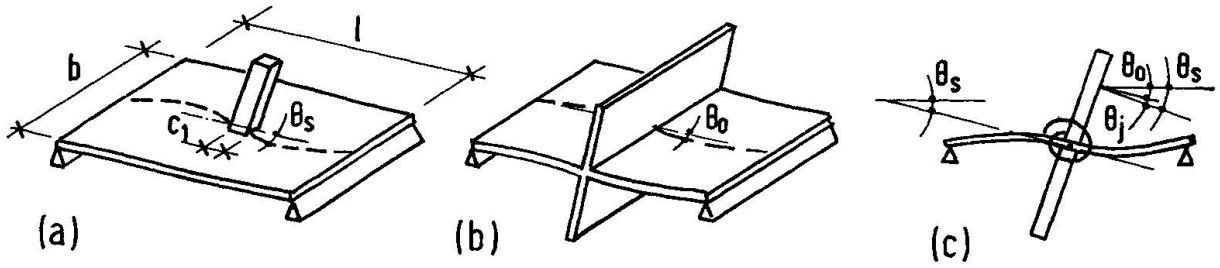

Fig. 4 Models for horizontal loading

The data can be presented in a form in which the slab rotation θ_s of Fig. 4a is the sum of θ_o (Fig. 4b) and a joint rotation θ_j. Each rotation is equal to the applied moment divided by the relevant stiffness (K_s, K_o, K_j).

$$\theta_s = \theta_o + \theta_j \qquad .....(1)$$

$$\frac{1}{K_s} = \frac{1}{K_o} + \frac{1}{K_j} \qquad .....(2)$$

where $K_o/D = 12(b/l)\ (1-c_1/l)^{-3}$ and D is the flexural stiffness per unit width of slab.

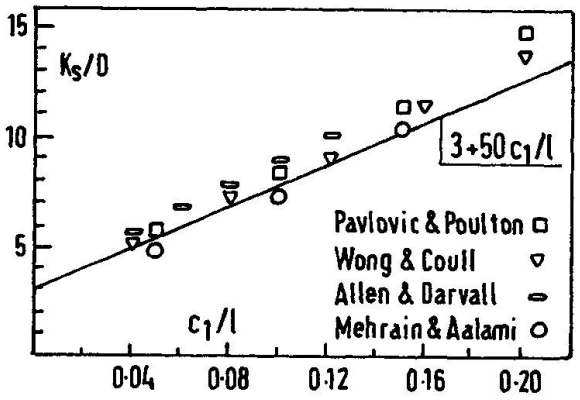

Fig. 5 Comparison of eqn. (3) with FEM results

Fig. 5 shows that FEM results for square columns ($c_1 = c_2$) and square panels (b=l) can be approximated by

$$K_s/D = 3 + 50(c_1/l) \qquad .....(3)$$

Moderate variations of c_1/c_2 have litte effect on stiffness. Expression (3) can be used directly for square panels. For rectangular ones K_j can be calculated from equation (2) and combined with the appropriate K_o.

Fig. 6 shows the model used to analyse waffle slabs by the Finite Element Method. For the coffers available on the market, the

ratio between the flexural stiffnesses of the solid and waffle zones varies only in the range from 3 to 4. Equation (4) is proposed [12] to approximate elastic analysis of square waffle slabs and Fig. 7 compares it with FEM results.

$$K_s/D = (6.25 + 50c_1/l)\,(l_s/l + b_{ss}/l)^{0.75}\,(b_s/l)^{0.25} \quad \ldots\ldots(4)$$

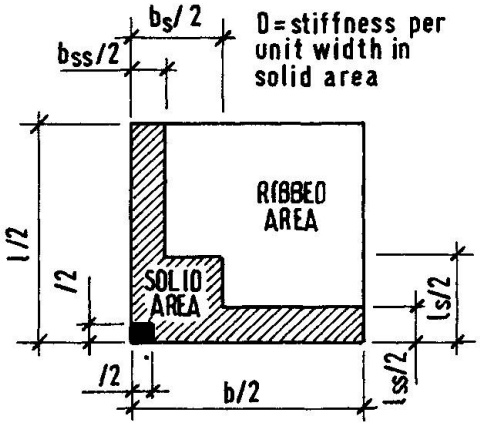

Fig. 6 Waffle slab model

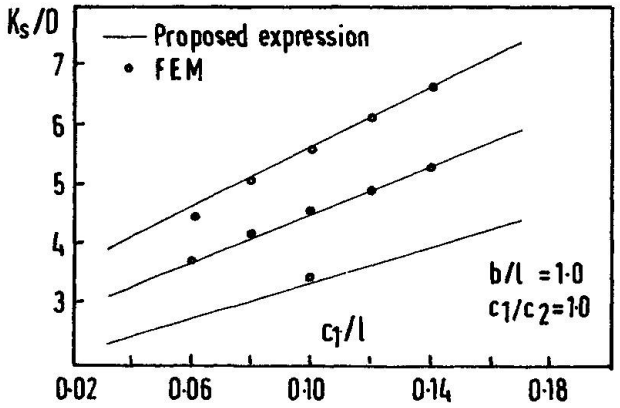

Fig. 7 Eqn. (4) compared with FEM data

3.3 Influence of cracking

The effect of vertical loading can be accounted for by a reduction of K_j to K_{jv}.

$$1/K_{jv} = \beta_1\beta_2\,(m_{cr}/m)^2(1/K_j) + [1 - \beta_1\beta_2(m_{cr}/m)^2]\,[D/K_jD_{cr}] \quad \ldots(5)$$

where $\beta_1 = 1.0$ for high bond bars and 0.5 for plain bars and $\beta_2 = 1.0$ for first loading and 0.5 for long term or repeated loading. m_{cr} is the cracking moment and m the applied moment at the column line and both of them may be averaged for the width of the column strip. For practical design the value of m should be that for the full service load. It is here taken as that for the maximum prior load. D is the uncracked and D_{cr} the fully cracked (bare steel) stiffness again averaged for the width of the column strip. K_o can be taken to retain its uncracked value.

As shown in Fig. 2 the influence of horizontal loading itself is a further reduction of stiffness which can be accounted for by reducing K_{sv} to K_{sh} where

$$K_{sh} = K_{sv}/(1 + M/M_r) \quad \ldots\ldots(6)$$

where M is moment acting between the column and the slab and M_r is the calculated resistance moment corresponding to flexural failure.

4. COMPARISON WITH TEST RESULTS

Table 2 presents the results of a comparison between the experimental stiffnesses of the three slabs discussed with values calculated by the method proposed. The agreement between the two sets of values can be seen to be very good.

	H/a(kN/mm)	
Slab	Test	Calc
Waffle	97	89
Long 1	1.66	1.66
Long 3	2.12	2.11

Table 2 Experimental and calculated stiffnesses

5. CONCLUSION

If the lateral load responses of flat slab structures are to be assessed realistically the models used in analysis must take account of the limited connections between the slabs and columns and also of the effects of cracking in the slabs.

There is no unique moment/rotation response for a slab-column connection as the local stiffness is greatly influenced by cracking produced by vertical loading, even if this involves no transfer of moment between the slab and column.

The model proposed provides a method of estimating joint stiffnesses and thence slab and column rotations, by accounting for geometric factors within an elastic approach and then modifying the results to allow for cracking.

REFERENCES

[1] Lucio V.J.G., An experimental model of a waffle slab with 9 panels, CMEST Report Ai10, Lisbon, March 1990.

[2] Lucio V.J.G., Description of the test of a waffle slab model with 9 panels, CMEST Report Ai11, Lisbon, March 1990.

[3] Long A.E. and Kirk D.W., Lateral load stiffness of slab-column structures, Reinforced Concrete Structures Subjected to Wind and Earthquake Forces, ACI Publication SP-63, Detroit 1980, pp 197-220

[4] Lucio V.J.G. and Regan P.E., Triaxial load cells for the tests of a waffle slab supported by 16 columns, 9th International Conference on Experimental Mechanics, Copenhagen, 1990

[5] ACI 318-89, Building code requirments for reinforced concrete, American Concrete Institute, Detroit, 1989

[6] BS8110 - Structural use of concrete, British Standards Institution, London 1985.

[7] Regan P.E., Behaviour of reinforced concrete flat slabs, Construction Industry Research and Information Association, Report 89, Feb. 1981

[8] Wong Y.C. and Coull A., Effective slab stiffness in flat plate structures, Proc. Inst. Civil Engrs. Part 2, 68. Sept 1980 pp 721-735.

[9] Allen F. and Darvall P. Lateral load equivalent frame, ACI Journal, No. 74-32, July 1977 pp 294-299

[10] Pavlovic M.N. and Poulton S.M., On the computation of slab effective widths, ASCE Journal of Structural Engineering, Vol. 111 No. 2, Feb 1985 pp 363-377.

[11] Mehrain M. and Aalami B., Rotational stiffness of concrete slabs, ACI Journal No. 71-29, Sept. 1974, pp 429-435

[12] Lucio V.J.G. Frame analysis of column supported slab structures, with special regard to waffle slabs. CMEST Report, Ai15, Lisbon 1990.

Sustained Tensile Strength of Concrete

Résistance à la traction du béton sous charge de longue durée

Betonzugfestigkeit unter Dauerlast

Hisham SHKOUKANI
Civil Eng.
Technische Hochschule
Darmstadt, Germany

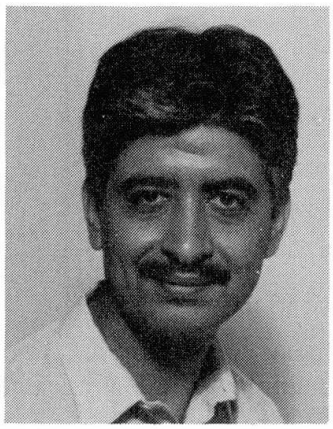

Hisham Shkoukani, born 1955, received his civil engineering degree at the Wayne State University, Detroit, Mich. In 1990 het received his Ph. D. at the TU Darmstadt.

Joost WALRAVEN
Prof. Dr.
Delft Univ. of Technol.
Delft, The Netherlands

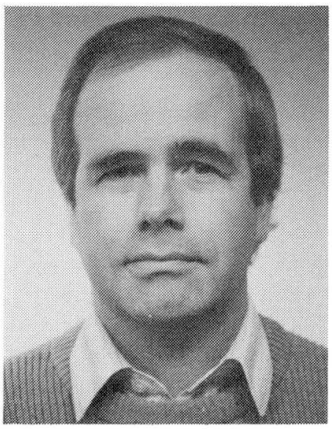

Joost Walraven, born in 1947, received his Ph. D. in Delft. After a period of consulting he became professor at the TU Darmstadt from 1985 – 1989, and at the TU Delft since 1989.

SUMMARY

Tests have been carried out in order to study the behaviour of concrete under concentric and eccentric sustained tensile loading. Variables were the eccentricity of the load, the shape of the concrete cross-section and the loading rate. Realistic values for the sustained tensile strength were determined, depending on the load level and the loading rate.

RÉSUMÉ

Des expériences ont été menées afin d'étudier le comportement du béton sous charge de traction centrée et excentrée. Les variables étudiées ont été l'excentricité de la charge, la forme de la section en béton et le temps de chargement; ceci aboutit à la détermination de la résistance à la traction, qui dépend du niveau de sollicitation et du temps de mise en charge.

ZUSAMMENFASSUNG

Es wurden Versuche zur Beschreibung des Verhaltens von Beton unter zentrischer und exzentrischer Dauerzugbeanspruchung durchgeführt. Dabei wurden unterschiedliche Exzentrizitäten sowie unterschiedliche Betonquerschnitte untersucht. Eine realistische Grösse der Zugfestigkeit des Betons unter Dauerbeanspruchung wurde in Abhängigkeit von Belastungsniveau und Belastungsgeschwindigkeit ermittelt.

1. INTRODUCTION

Nowadays the significant role of the tensile strength in the design of concrete structures begins to be reckognized. In the introductory lectures by Hillerborg and Duda/König many factors, influencing the concrete tensile strength and the post-cracking ductility, were discussed. However, hardly any attention has been devoted to the role of the so-called sustained loading effect. Nevertheless, if results of various authors may be believed, the sustained tensile strength is considerably lower than the tensile strength, obtained in a short term test. The ratio sustained to short term tensile strength is reported to be about 70%, see Fig. 1.

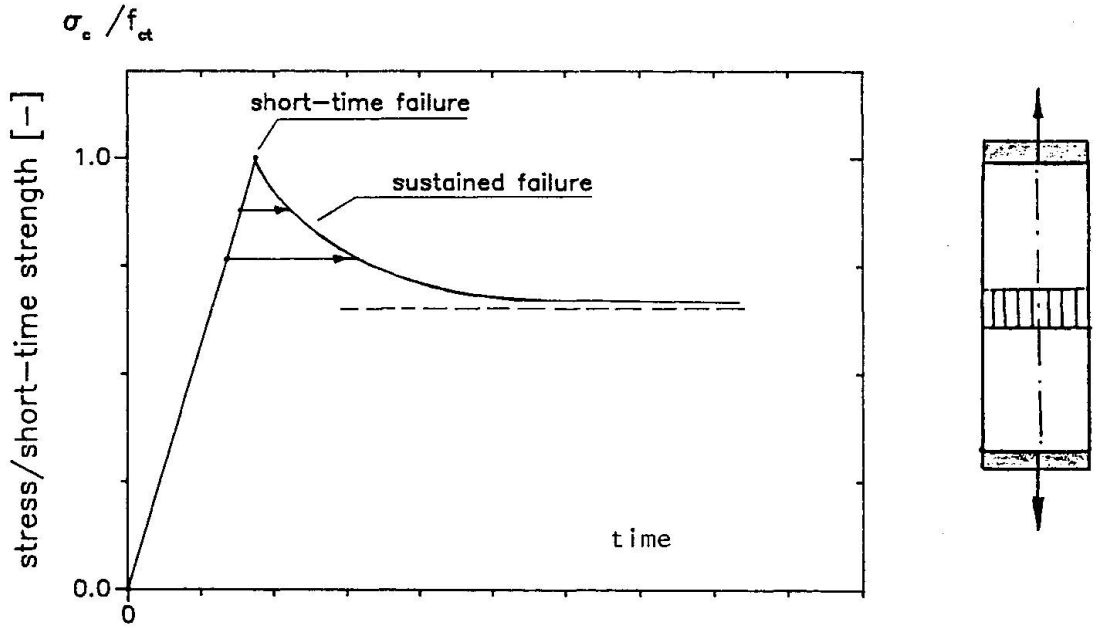

Fig. 1 Principle of sustained tensile test

An important observation is that this sustained strength-limit is reached after a relatively short period. A few days of sustained loading are sufficient to reach the 70% limit. This phenomenon may have important consequences, both in a favourable and in an unfavourable way. With regard to strength considerations, such as the shear capacity of members not reinforced in shear, a reduction of the capacity seems mandatory. On the other hand, a reduction of the tensile strength by sustained loading would have a positive effect in cases where minimum reinforcement is required due to the effect of imposed deformations. In this case the reduction of the tensile strength leads to a proportional reduction of the required amount of minimum reinforcement.

This shows that it is worthwhile to consider the influence of the strain rate more in detail. A number of questions can be raised, f.i.

- To what extend does the sustained strength-limit depend on the definition of the short term tensile strength? If the loading rate of the short-term test is not the same in all the tests, the sustained strength-limits $f_{ct,\infty}/f_{ct,o}$ as reported by various authors in the literature, are not comparable.
- Up to now only concentric sustained tensile tests have been reported. Many structural actions, however, lead to stress gradients. It is questionable if the results of concentric tensile tests can be applied to eccentric load application, or to flexure.
- Furthermore it may be wondered if the classical sustained loading test is representative for any loading case. If imposed deformations are concerned, the tensile stresses develop slowly in time and reach the cracking level within a period which may vary between hours and days.

In order to generate answers on these questions a number of tests has been carried out.

2. EXPERIMENTS

2.1 Sustained concentric tensile loading tests

The classical concept of a sustained loading test is as follows. The short term tensile strength (rapid test) is determined with a certain loading rate: subsequently, concrete with the same properties and storage conditions are loaded to a certain fractile of the previously determined short-term tensile strength. At this loading level the stress is kept constant. For high levels ($\frac{\sigma_c}{f_{ct}} > 0,7$), the concrete is observed to fail after a certain period.
This principle of testing was adopted for the first series of tests. The tests were carried out on cylindrical (ϕ 150 x 300 mm) and rectangular (150 x 150 x 300 mm) specimens, casted vertically in steel moulds. In order to prevent the development of internal stresses by shrinkage, the specimens were sealed before and during testing with plastic sheets. The average cube strength was 32 N/mm^2.

The short-term tensile strength was determined by testing specimens with such a loading rate that failure occured after about 10 seconds. In the sustained loading tests, the sustained load level was reached within one minute. Then the load was kept constant until failure occurred. The results of these tests are shown in Fig. 2.

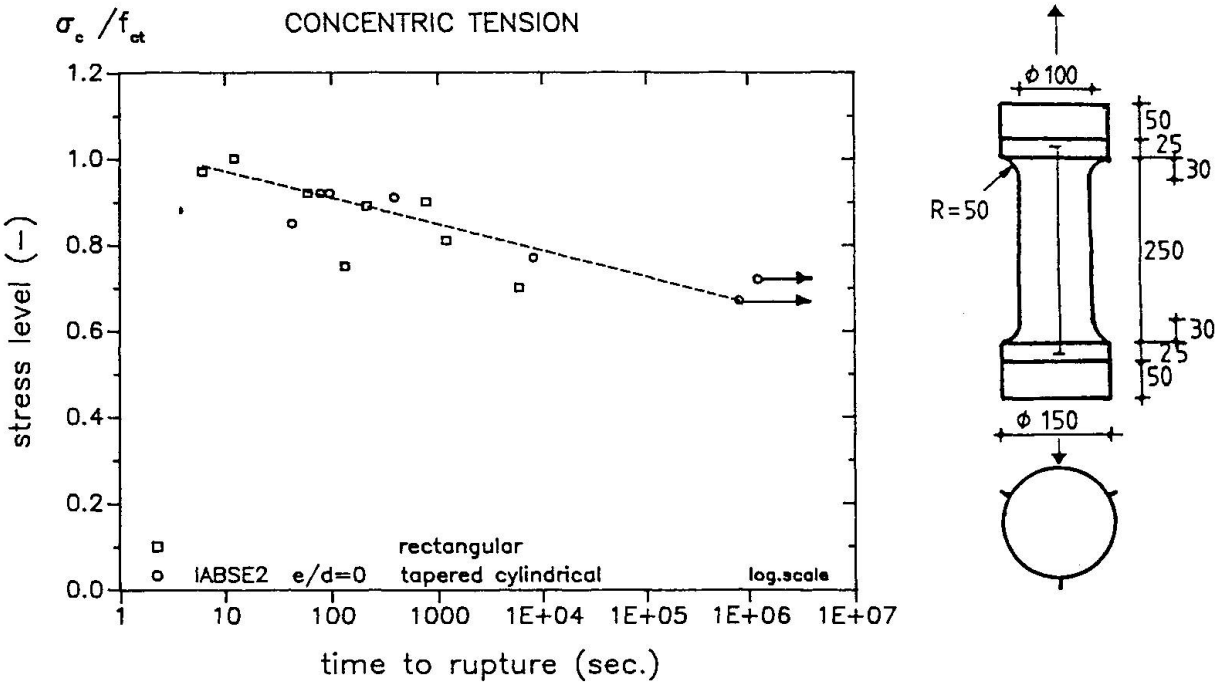

Fig. 2 Relationship between relative sustained stress level and time to failure for the concentric tensile tests

It can be seen that time to rupture increases with decreasing stress level σ_c/f_{ct}. It was found that, if a specimen did not fail within the first three hours, no failure at all occurred (the maximum loading time was two weeks). The lower limit of σ_c/f_{ct}, as observed, was 0.7. The specimens which did not fail after a period of sustained loading were subsequently loaded to failure in a rapid tests. Surprisingly, the strength obtained after this procedure was significantly higher than the strength obtained in a short term test on virgin specimens! This cannot be explained by the effect of continuing hydration, since an increase in strength was also observed after a sustained load of only a few hours. This might be explained by relaxation of the cement matrix during sustained loading, which could lead to a relaxation of stresses at the tip of the micro-cracks.

2.2 Sustained eccentric tensile loading tests

After the concentric tensile loading tests, a series of experiments was carried out on specimens, subjected to an eccentric tensile load. The relative load-eccentricities adopted in

the tests were e/d = 0.167 and 0.5.

Figs. 3a and b show, that the decrease of the strength by sustained loading, is smaller, the larger is the eccentricity of the load. For e/d = 0.167 no failure was observed to values of σ_c/f_{ct} smaller than 0.75. For e/d = 0.50 the lower limit was even about 0.9.

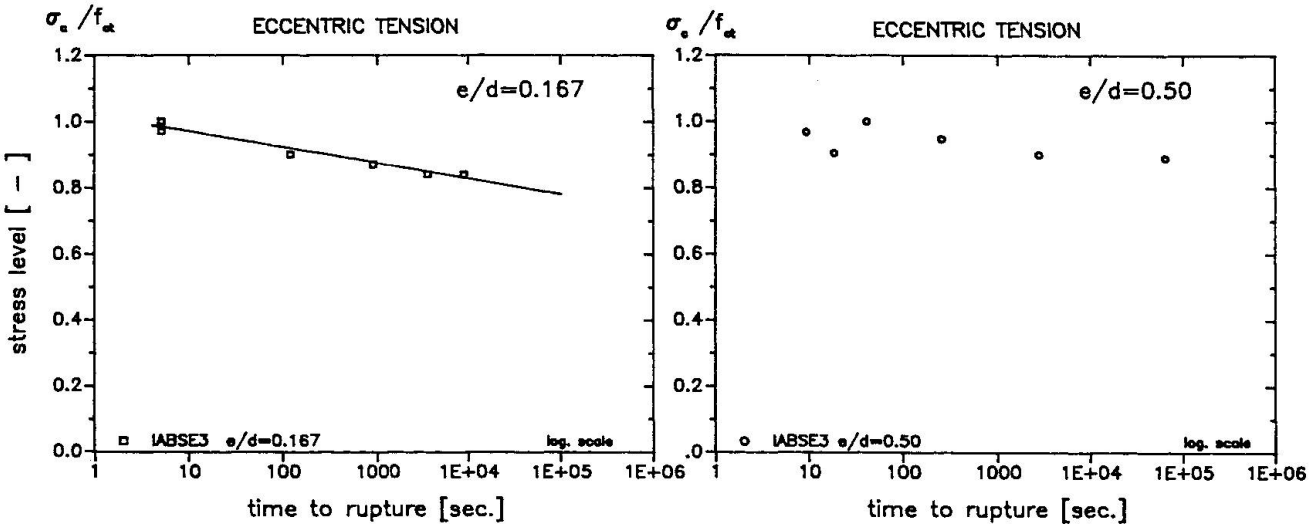

Fig. 3 Relation between relative stress level and time to rupture by eccentric tensile loading, with e/d = 0.167 and e/d = 0.50.

Also here the specimens which did not fail during sustained loading where loaded to failure in a short term test, and also here an increase of the strength was observed.

Obviously the sustained loading effect consists of two mechanisms, a damaging one and a hardening one. If the damaging mechanism is not strong enough to cause failure, the hardening mechanism starts to dominate, which results in a higher strength than the original one.

2.3 Eccentric tensile tests with different loading rates

If the previous conclusions, concerning damaging and hardening, were true, this would mean that, in case of a constant loading rate, a reduction of this loading rate could possibly lead to an increase of the strength. In order to examine this phenomenon, cylindrical specimens were loaded up to failure with different loading rates. The failure occurred after about 6 seconds, 2 minutes, 20 minutes, 1 hour and 2,5 hours. Fig. 4 shows the relationship between the failure load after the loading rate.

In Fig. 4 the loading rate is represented along the horizontal axis. The highest loading rate was such, that failure occurred in about 6 seconds (righthand side of the diagram). If the loading rate is decreased (passing from right to left), the strength decreases too. However, further lowering the loading rate leads to an increase of the strength.

This is remarkable because in such a situation, which reflects f.i. the case of stresses by imposed deformations (such as solar radiation), the lowest strength is obtained for a loading rate, which is generally considered as belonging to a short term test. Tensile splitting tests, carried out on control specimens, as usual in practice, do generally not require more than 2 minutes, so that application of a strength reduction factor to consider a sustained loading effect in practical situations seems to be unjustified.

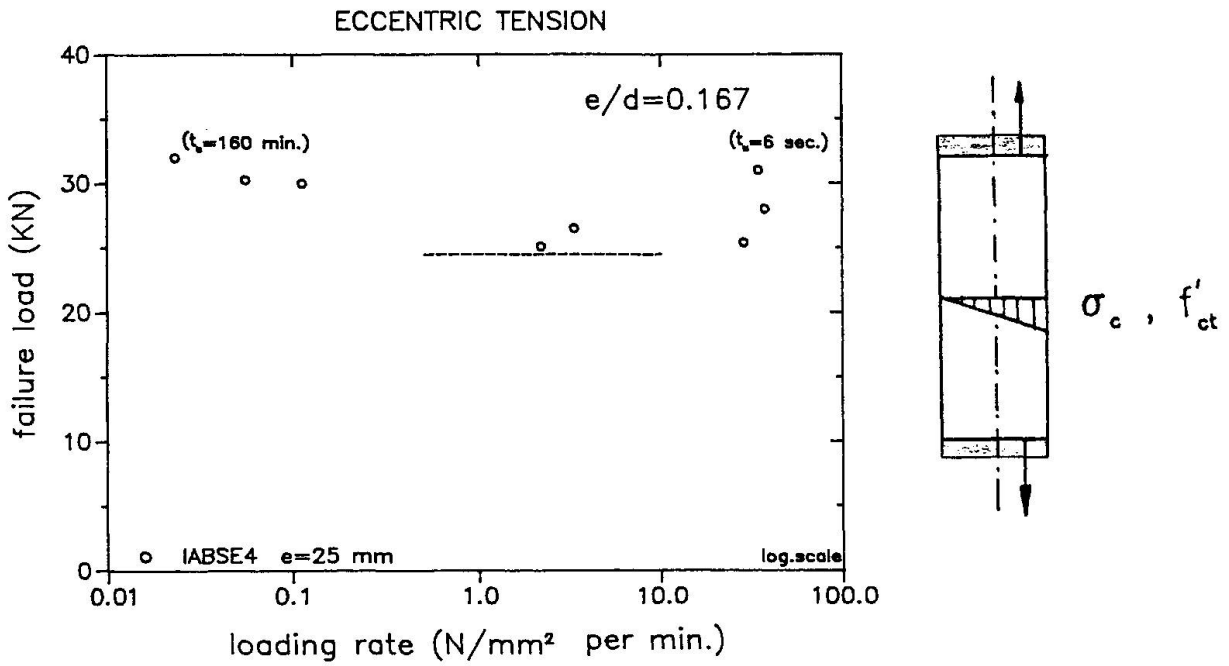

Fig. 4 Relationship between failure tensile load and loading rate for an eccentricity of e/d = 0.167

3. CONCLUSIONS

- In concentric tensile tests the strength under sustained loading is smaller than under short-term loading. In order to determine the sustained strength limit, a clear definition of the short-term strength is necessary. If the short-term strength is determined within a failure time of 10 seconds, the sustained tensile strength is about 70% of the short-term strength, whereas in the case of 100 seconds failure time, the sustained tensile strength is about 85% of the short-term strength.
- The sustained tensile strength increases with increasing eccentricity: i.e. if a stress gradient is available over a cross-section, and the short term strength is defined as that strength, which is obtained in 100 seconds, the sustained loading effect can be neglected.
- In addition to the damaging effect there is also a hardening effect, which can probably be explained by the reduction of the peak stresses by relaxation. This is most effective if the loading rate is relatively small.

REFERENCES

1. Reinhardt, H.W., Cornelissen, H.A.W., Sustained Tensile Tests on Concrete. Baustoffe '85, Bauverlag, Wiesbaden, 1985, pp. 162-167.
2. Shkoukani, H., Beton unter Dauerzugbeanspruchung. Tagungsband zum Darmstädter Massivbau-Seminar, Band 1, Rissbreitenbeschränkung und Mindestbewehrung, THD, 1989.

Leere Seite
Blank page
Page vide

Use of the Tensile Strength in Anchorage to Concrete

Emploi de la résistance à la traction lors d'ancrages dans le béton

Rechnerische Erfassung der Bauteilbeanspruchungen durch Befestigungen

Rolf ELIGEHAUSEN
Prof. Dr.
Univ. Stuttgart
Stuttgart, Germany

Rolf Eligehausen, born 1942, received his Dipl. Ing. in 1968 at the Technical University Braunschweig and Dr. Ing. in 1979 at the University of Stuttgart. From 1979 – 1981 he was research engineer at the University of California at Berkeley. Since 1984 he is Professor for fastening technology at the Institute für Werkstoffe im Bauwesen, Stuttgart.

Josko OZBOLT
Dr. Ing.
Univ. Stuttgart
Stuttgart, Germany

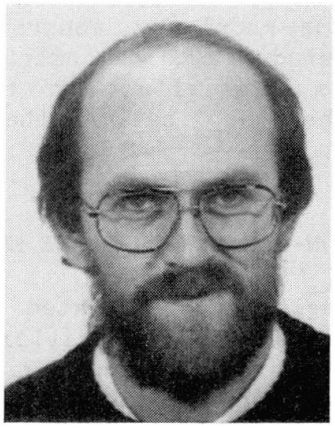

Josko Ozbolt, born 1955, received his Dipl. Ing. in 1978 and Dr. Ing. in 1982 at the University of Zagreb. In 1980 he performed a post-graduate study at the TNO Institute in Delft, and from 1987 – 1988 a postdoctoral study at Northwestern University. Since 1989 Research Engineer at Institut für Werkstoffe im Bauwesen, Stuttgart.

SUMMARY

Anchoring elements, such as headed studs, are used to transfer concentrated loads into reinforced concrete members. From experimental evidence it is known that, provided the steel strength of the stud is high enough, failure occurs by pulling out a concrete cone formed by circumferential crack growth in the so-called mixed mode, with significant size effect. Numerical analyses indicate that the dominant influence factor on the failure load is the concrete fracture energy. It is shown that in such applications, the load transfer from the anchor into the concrete may safely be done by using the concrete tensile strength.

RÉSUMÉ

Des éléments d'ancrage tels que les boulons sont utilisés pour transmettre localement des charges dans une structure en béton armé. Selon l'évidence expérimentale, il est clair que si la résistance de l'acier du boulon est suffisante, la ruine est atteinte par arrachement d'un cône en béton: une fissure circulaire se développe, accompagnée d'un effet de taille significatif dans ce qu'on appelle un «mode mixte». Les analyses numériques indiquent que l'influence dominante sur la charge ultime a l'énergie de fracture du béton. Il est très intéressant que dans ce type de structures, le béton puisse transmettre des charges de l'ancrage à la masse enserrante sans l'aide de l'armature, et ceci grace à la mobilisation de sa résistance à la traction.

ZUSAMMENFASSUNG

Befestigungselemente wie Kopfbolzen werden häufig eingesetzt, um Lasten in Stahlbetontragwerke einzuleiten. Versuche zeigen, dass das Versagen bei ausreichend hoher Stahltragfähigkeit durch die Ausbildung eines Betonausbruchkegels hervorgerufen wird. Die Bruchlast hängt nach den Ergebnissen der numerischen Untersuchungen hauptsächlich von der Betonbruchenergie ab. Es wird diskutiert, dass in diesen Anwendungsfällen die Betonzugfestigkeit in Anspruch genommen werden kann, ohne dass ein Sicherheitsrisiko besteht.

1. INTRODUCTION

In engineering practice, headed anchors are often used to transfer loads into concrete structures. From experimental evidence it is known that, provided the steel strength of the anchor is high enough, headed anchors fail by pulling a concrete cone. The failure is due to the failure of concrete in tension by forming a circumferential crack growing in the so-called mixed mode [1]. In recent years several attempts have been made to understand this growth and to predict the failure load of headed studs [1] - [4]. Summarizing these activities, it can be said that material models based on plasticity and on stress-strain relationships together with stress failure criteria are not capable of predicting the behavior of anchors as observed in experiments [1], [5]. Furthermore, the predicted failure load depends on the element size and load step size. A better explanation of anchorage behavior can be expected using more general material models based on fracture mechanics. Some recent results of the numerical analysis using axissymmetric finite elements and a non-local microplane model for concrete are shown and discussed. The main objective of this study is to demonstrate the influence of different concrete properties and the size effect on the failure load. Furthermore, it is discussed why in these applications the concrete tensile strength can be used without safety risk.

2. REVIEW OF THE NON-LOCAL MICROPLANE MODEL

The microplane models were initiated by G.I.Taylor [6], who suggested the principle for the modeling of plasticity of polycrystaline metals. Recently [7], this approach has been extended to include strain softening of concrete, and has been renamed more generally the "microplane model", in recognition of the fact that the approach is not limited to plastic slip but can equally well describe cracking and strain softening damage.
Basically, on the material level one may distinguish two types of interactions among particles or damage sites in the microstructures, which must be somehow manifested in the continuum model: (1) Interaction at a **distance** among various sites (e.g., between A and B, in Fig. 1); and (2) interaction **among various orientations** (see angle α in Fig. 1).
The interactions at a distance control the localization of damage. They are ignored in the classical, local continuum models, but are reflected in non-local models [8]. According to the non-local strain concept, the stress at a point depends not only on the strain at that point but also on the strain field within a certain region around the point. In the current study, an effective form of the non-local concept is used in which all variables that are associated with strain softening are non-local and all other variables are local [9]. The key parameter in the non-local concept employed is the characteristic length l_c over which the strains are averaged. However, it is still not clear how to correlate the characteristic length with concrete properties in general 3D stress-strain states. In a preceding paper [9] the non-local microplane model as well as an effective numerical iterative algorithm for the loading steps used in the finite element code are described in detail.

3. REVIEW OF THE NUMERICAL STUDIES ON THE BEHAVIOR OF ANCHORAGES

The behavior of headed studs embedded in reinforced concrete blocks is studied in [10] - [12]. In these studies, the influence of the different material and geometrical parameters on the concrete cone failure is investigated. The concrete
tensile and compression strength, fracture energy, initial Young's modulus and

the size of the stud are varied. To demonstrate the size effect, the influence of the embedment depth on the failure load is studied.
The analysis is performed using axissymmetric four-node finite elements and the non-local microplane model. A typical finite element mesh employed in the analysis is shown in Fig. 2. Fig. 3 shows a comparison between test results and results of the numerical analysis and demonstrates that the non-local microplane model can correctly predict the concrete cone failure load.
Fig. 4 demonstrates the influence of the concrete fracture energy G_F on the failure load. In these studies, the concrete tensile strength was kept constant. According to the Fig. 4, the failure load is roughly proportional to the square root of G_F. The influence of the tensile strength, for a constant value of G_F, on failure load is shown in Fig. 5. It indicates that the concrete tensile strength has a small influence on the concrete cone failure load. Both results are also confirmed by Sawade [5]. Concrete compression strength and the size of the head have a significant influence on the displacement field, but a relatively little influence on the failure load [11].
Because the analysis shows the dominant role of the concrete fracture energy on the anchor behavior a large size effect on the failure load must be expected. Indeed, results of numerical analyses obtained in [11] and [12], as well as test results indicate a significant size effect that is close to that predicted by linear elastic fracture mechanics (Fig.6).
In spite of the fact that the G_F value has a dominant influence on the concrete cone failure load, the design of fastenings should be based on the concrete compression strength, since this concrete property can easily be measured and is known to the designer.

4. USE OF THE TENSILE STRENGTH IN ANCHORAGES

In many applications, no reinforcement can be provided in the region of headed anchors that could take up the load transferred by the anchor into the structure. Therefore, these forces must be resisted by the concrete tensile strength. In contrast to that, generally in reinforced concrete design, the concrete tensile strength is neglected and any tensile stresses in the concrete are taken up by reinforcement. This approach is justified by the fact that tensile stresses may be induced in the concrete by the restraint of imposed deformations i.e. due to creep, shrinkage, temperature variations or support settlements, which may reach the concrete tensile strength and cause cracks in the concrete. These stresses are parallel to the tension stresses (i.e. bending stresses) induced by loads. Therefore, failure of the structure may be caused by the restraint of imposed deformations if no reinforcement is present to take up the tensile forces due to loads.
In the case of headed studs embedded in concrete, the situation is somewhat different. The failure surface is not perpendicular to the load directions and the tensile stresses on the failure plane are inclined to the concrete surface (Fig. 7). Therefore, the tensile stresses induced by the anchor load intersect with additional tensile stresses generated in the concrete and due to the restraint of imposed deformations, which are parallel to the concrete surface over a small part of the failure area only. Furthermore, the fracture process is very stable up to peak load because the circumferential crack forms a cone and the crack tip has to penetrate a larger area the move it grows. Therefore, if the additional stresses cause locally the formation or widening of a microcrack, stable stress redistribution is possible. According to rough theoretical investigations a reduction of the concrete cone failure load by about 20% can be expected if the additional tensile stresses σ_{add} reach the concrete tensile strength [13]. This possible reduction of the failure load is smaller than the reduction which must be expected if the anchor is located in a crack [14]. It should be taken into account in the design of the

fastening. Naturally, reinforcement must be present to prevent failure of the structure serving as anchor ground.

5. CONCLUSIONS

The numerical results as well as experimental observations indicate that the failure of headed studs embedded in plain concrete is due to failure of concrete in tension (circumferential cracking) rather than in compression. The failure load is mainly influenced by the concrete fracture energy G_F. However, the design of fastenings should be based on the concrete compression strength, since that value is known to the designer.
In spite of the fact that the concrete cone failure load is governed by the tensile properties of concrete, no reinforcement is necessary to take up the concrete tensile stresses induced by the anchor. This can be explained by the fact that the tensile stresses induced in the concrete by other external loads or by restraint of imposed deformations , e.g. due to temperature variations, intersect hardly with the tensile stresses induced by the anchor. Furthermore, the fracture process is very stable so that a stable stress redistribution is possible if local cracks are caused in the concrete by these additional tensile stresses. However, reinforcement may be provided to increase the anchor strength.

6. REFERENCES

1. ELIGEHAUSEN, R. and SAWADE, G. - 'Analysis of Anchoring Behavior (Literature Review)', Fracture Mechanics of Concrete Structures - RILEM Report, Ed. L.Elfgren, Chapman and Hall, 1989, pp.263-280.

2. OTTOSEN, N. S. - Nonlinear Finite Element Analysis of Pull-Out Tests. Journal of Structural Division, Vol. 107, No. ST4, pp. 591-603, 1981.

3. ELIGEHAUSEN, R. and SAWADE, G. - Behavior of Concrete in Tension. Betonwerk + Fertigteil Technik, No. 5 and 6, 1985.

4. KRENCHEL, H. and SHAH, S. - Fracture Analysis of the Pull-Out Tests. Material and Structures, Vol. 18, No. 108, pp. 439-446, 1985.

5. SAWADE, G. - Ein Beitrag zum Verhalten von zugbeanspruchtem Beton (A contribution to the behavior of concrete in tension). Thesis in preparation, Stuttgart University, in German.

6. TAYLOR, G.I., Plastic strain in metals. J. of Inst. of Metals, 62, 1983, pp. 307-324.

7. BAZANT, Z.P., and PRAT, P.C., Microplane model for brittle-plastic material - parts I and II. J. of Eng. Mech., ASCE, 114 (10), 1988, pp. 1672-1702.

8. BAZANT, Z.P., and PIJAUDIER-CABOT, G., Nonlocal continuum damage, localization instability and convergence. J. of Appl. Mech., ASME, 55, 1988, pp. 287-293.

9. BAZANT, Z.P., and OZBOLT, J., Nonlocal microplane model for fracture, damage and size effect in structures. J. of Eng. Mech., ASCE, 116, (11), 1990, pp. 2485-2505.

10. OZBOLT, J. and ELIGEHAUSEN, R., Numerical Analysis Of Headed Studs Embedded in Large Plain Concrete Blocks, Proceedings of the 2nd International Conference of Computer Aided Analysis and Design of Concrete Structures, Zell am See, Austria, April 1990, pp. 465 - 656.

11. OZBOLT, J. and ELIGEHAUSEN, R., Numerical Analysis of Headed Studs Embedded in Large Plain Concrete Blocks, Report Nr. 4/10 - 90/9, IWB, Stuttgart University, Oct. 1990.

12. ELIGEHAUSEN, R. and OZBOLT, J., Size effect in Anchorage Behavior, Proceedings of the Eight European Conference on Fracture - Fracture Behavior and Design of Materials and Structures, Torino, Italy, 1-5 October 1990.

13. Rehm, G., Eligehausen, R. and Silva, J., Dübel in der aus Lastspannungen erzeugten Zugzone von Stahlbetonbauteilen. Report No. 1/1-82/1 of the Institut für Werkstoffe im Bauwesen, Universität Stuttgart, June 1982.

14. Rehm, G., Eligehausen, R. and Mallie, R., Befestigungstechnik, Betonkalender 1988, Teil 2, Wiehelm Ernst & Sohn, berlin, 1988.

7. FIGURES

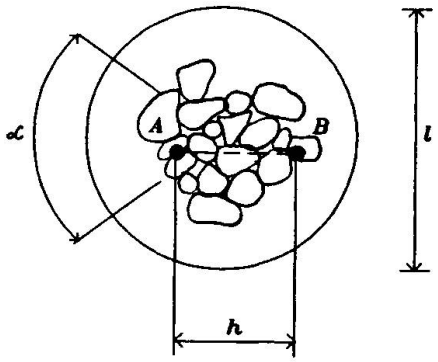

Fig. 1 Interaction among the various orientations and at distance

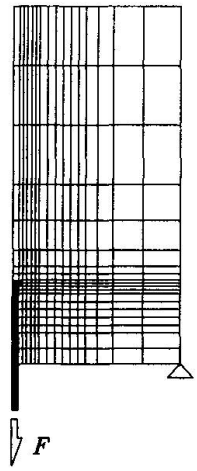

Fig. 2 Typical finite element mesh used in the analysis

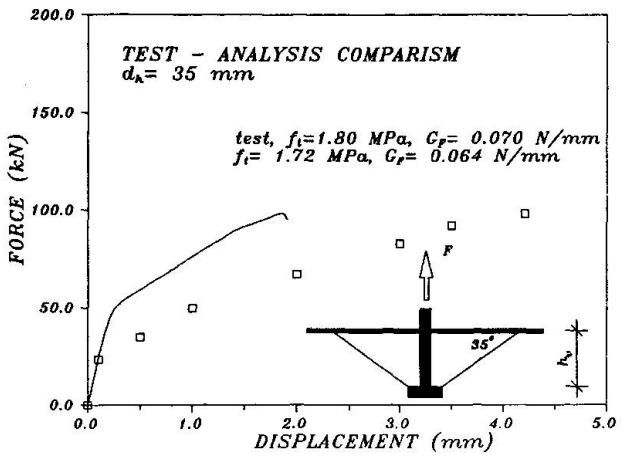

Fig. 3 Experiment-analysis comparison

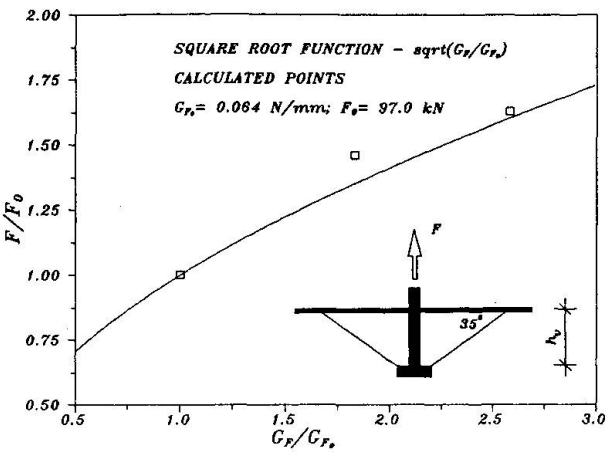

Fig. 4 Influence of the fracture energy on the failure load

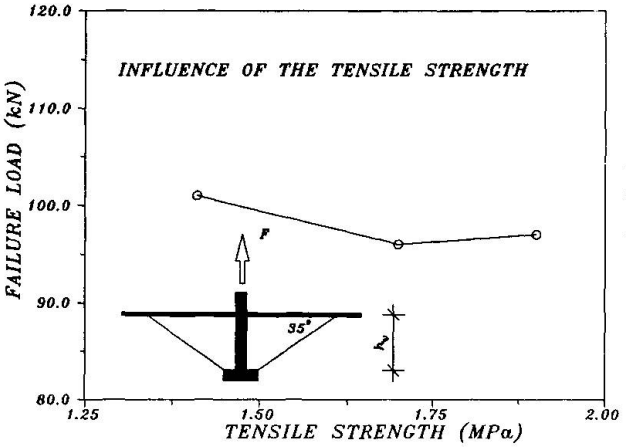

Fig. 5 Influence of the tensile strength on the failure load

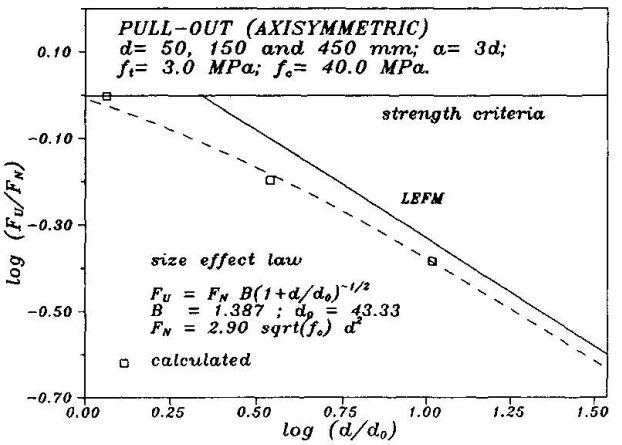

Fig. 6 Size effect on the pull-out load

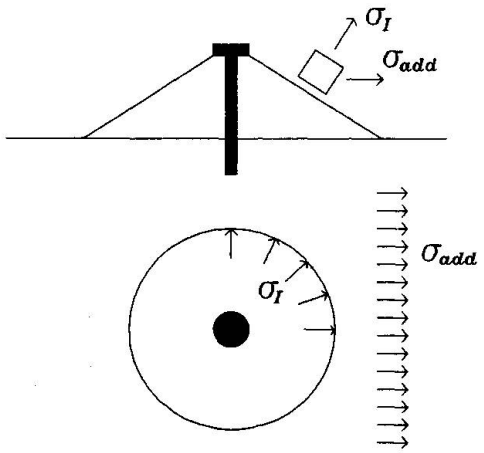

Fig. 7 3D stress state along the concrete cone failure surface and additional tensile stresses

Numerical Analysis of Anchoring Effects in Structures

Analyse numérique des effets d'ancrage dans les structures

Nutzung der Betonzugfestigkeit in der Befestigungstechnik

Rolf ELIGEHAUSEN
Prof. Dr.
Univ. Stuttgart
Stuttgart, Germany

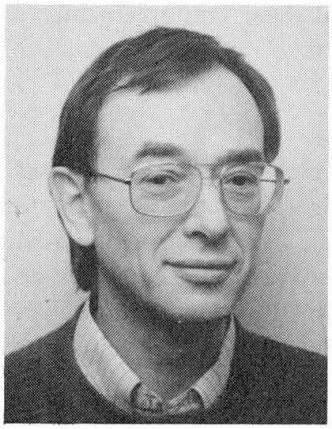

Rolf Eligehausen, born 1942, received his Dr. Ing. in 1979 at Univ. of Stuttgart. 1979 – 1981 Research Engineer at Univ. of California at Berkeley. Since 1984 Professor for fastening technology at the Inst. für Werkstoffe im Bauwesen, University Stuttgart.

Mihajlo KAZIC
Res. Eng.
Univ. Stuttgart
Stuttgart, Germany

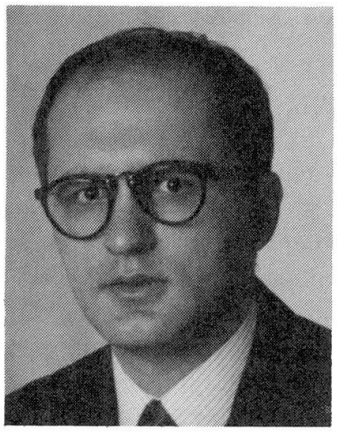

Mihajlo Kazic, born 1960, obtained his B.S. degree in 1983 in Novi Sad YU, M.S. and Ph.D. in 1986 and 1988 at Univ. of California Los Angeles. Senior Consultant at Pavlovich & Assoc. in L.A. and Teaching Assoc. at UCLA. Since 1989 Research Eng. at IWB, University Stuttgart.

SUMMARY

The shear behaviour of reinforced concrete beams with various types of vertical shear reinforcements and for different load arrangements, modelling the action of headed anchors installed in the tension zone, is numerically analysed by a non-linear finite element program based on a smeared crack approach taking into account non-linear fracture mechanics. Factors affecting the ultimate shear strength are discussed with respect to the numerical analysis and the overall structural response.

RÉSUMÉ

Le modèle mécanique d'affaiblissement de contrainte après fissuration du béton en traction, ainsi que la résistance-même en traction de ce matériau constituent le base du modèle de discrétisation des fissures dans une analyse par éléments finis. Ce concept est ultilisé dans l'analyse du problème du cisaillement de poutres en béton armé sous différentes positions de la charge, celle-ci cheminant dans la matière au moyen des éléments d'armature ancrés dans le béton et les étriers. Les facteurs qui influent sur la résistance ultime à l'effort tranchant sont discutés à la lumière du respect des dispositions énoncées par la Norme au sujet des techniques d'ancrage.

ZUSAMMENFASSUNG

Es wird der Einfluss von durch Kopfbolzen in die Betonzugzone eingeleiteten Lasten auf das Schubtragverhalten von Stahlbetonbalken mit unterschiedlichen Schubbewehrungen untersucht. Die Studien werden mit einem nichtlinearen FE-Programm durchgeführt, das auf dem Konzept der verschmierten Risse unter Berücksichtigung der nichtlinearen Bruchmechanik beruht. Die das Schubtragverhalten beeinflussenden Faktoren werden diskutiert.

1. INTRODUCTION

The shear strength of reinforced concrete beams is almost exclusively studied for the cases where the loads are applied through plates directly onto the top beam surface. However, in modern structures the loads may partly be applied by means of high-tech metal anchoring elements placed in the bottom part of the beam. The influence of this load application by means of anchoring elements on the shear strength of beams without shear reinforcement has been extensively studied by Eligehausen et al. [3]. Their principal conclusion was that on an average the shear failure load is reduced by 10% when the entire load is applied by means of anchoring elements placed in the bottom, tensile zone. The same conclusion was verified by Cervenka et al. [2] in a finite element analysis of reinforced concrete beams with no shear reinforcement.

The present analysis is accomplished by the FE program AXIS, developed at the Institut für Werkstoffe im Bauwesen, University of Stuttgart. The goal was to study the influence of loads introduced into the bottom zone on the shear strength of beams with different vertical shear reinforcements.

2. SCOPE OF ANALYSIS

The analysis concerns reinforced concrete beams failing in shear. The dimensions of the T-beam (Fig. 1) and the shear span ratio $\lambda = a/d = 2.8$ are chosen in order to ensure a shear-tension failure and to avoid a shear-compression (for small λ) and bending failure (for large λ). The principal goal is to investigate the influence of different load arrangements for various stirrups cross-sections on the shear strength. Three different loading cases may be distinguished from Fig. 2, in which load case *a* represents a beam with concentrated loads applied on the top surface. Load case *b* represents the application of 20% of the total loads by means of anchoring elements placed in the bottom zone. Load case *c* is analysed for the sake of direct comparison with load case *b*, with the same shear span ratio and load proportions, but with loads placed on the top surface. Each of this three loading cases was applied on a beam with five different stirrups configurations (no stirrups; two-legged $\phi 6$, $\phi 8$, $\phi 10$ and four-legged $\phi 8$ stirrups, each at a spacing $s = 0.15m$). The longitudinal reinforcement ratio $\rho_w = 2.38\%$ is taken as constant in order to preclude the influence of its variability on the results. Yielding point for all stirrups is $f_{sy} = 350MPa$ and for bending reinforcement $f_y = 450MPa$.

In the bottom part of the web, headed studs with anchoring length $h_v = 100mm$ are located. The stud spacing $s = 0.30m$ is chosen in order to avoid mutual effects of neighbouring studs [3]. The loads applied on the studs are proportional to the loads applied on the top surface, and are smaller than the concrete cone failure load of $55.0kN$ (according to [3]).

Only the effects of static loading are considered. The loads are increased gradually. Load increments are not equal, and depend on the employed arc length iterative procedure, which is a displacement controlled analysis. Effects of repeated, dynamic or reversed loading were not studied.

3. FE ANALYSIS: MATERIAL MODEL

3.1 Concrete Parameters

Reinforced concrete is a highly nonlinear structural material. Prior to crushing or tensile failure, in the FE program AXIS, concrete is considered as a hyperelastic material, for which the stress-strain relations are of the form:

$$\sigma_{ij} = F(I_1, J_2, J_3)\epsilon_{ij} \tag{1}$$

where the initial elastic constants are replaced by scalar functions $F(I_1, J_2, J_3)$ associated with the first invariant I_1 of the stress tensor and the second and third invariants J_2, J_3 of the deviatoric

stress tensor. The nonlinear isotropic elastic stress-strain relation prior to crushing or tensile failure is modelled by a quadratic parabola in compression and by linear loading in tension. A linear strain softening is assumed after crushing and after tensile failure (Fig. 3). The scalar functions $F(I_1, J_2, J_3)$, developed from Kupfer's biaxial experimental data are established to include the variable peak strengths in compression or tension, depending on the total state of stress. The crack is initiated after the principal stress exceeds the tensile strength. The softening modulus in tension E_T is based on nonlinear fracture mechanics and calculated according to the crack band theory of Bazant and Oh [1] :

$$E_T = \frac{E}{1 - \frac{L_{ch}}{L_e}} \qquad L_{ch} = \frac{2G_f E}{f_{ct}^2} \tag{2}$$

in which L_e is the width of an element, or the square root of the area assigned to an integration point. The value L_{ch}, called characteristic length is assumed to be a material property dependant on the fracture energy G_f, modulus of elasticity E and the direct tensile strength f_{ct}.

In the present analysis, the material properties are characterized by only three material parameters, with the following values: uniaxial compressive strength $f_c = 30MPa$, Poisson ratio $\nu = 0.17$ and fracture energy $G_f = 66N/m$. The direct tensile strength f_{ct} is assumed to be a function of the compressive strength:

$$f_{ct} = 0.269 f_c^{0.666} \implies f_{ct} = 0.269(30.0)^{0.666} = 2.60MPa \tag{3}$$

The values of the initial tangent modulus and softening modulus in compression are assumed as:

$$E = 5015\sqrt{f_c} \quad [MPa] \implies E = 27500MPa \tag{4}$$

$$E_{cc} = -E_c/8.0 \implies E_{cc} = -3500MPa \tag{5}$$

3.2 Shear transfer across the crack

Employing a smeared crack approach, the FE program AXIS has the options for both the fixed crack model based on orthotropic concepts and the rotating crack model based on nonlinear elasticity relations in principal coordinates. In the fixed crack model, the mechanisms of shear transfer accross the crack due to aggregate interlock or dowel action is simulated by reducing the value of the shear modulus corresponding to the crack plane according to the following expression:

$$G = \beta G_{initial} = \beta \frac{E}{2(1+\nu)} \tag{6}$$

In the program, the shear retention factor β can be assumed as constant or variable. For a variable β value the following expression derived by Kolmar [5] is utilised:

$$\beta = -\frac{ln\frac{\epsilon_m}{c_1}}{c_2} \qquad c_1 = 7.0 + 5.0\left(\frac{\mu - 0.005}{0.015}\right) \qquad c_2 = 10.0 - 2.5\left(\frac{\mu - 0.005}{0.015}\right) \tag{7}$$

in which ϵ_m (given in $^o/_{oo}$) is the strain perpendicular to the crack and $\mu \leq 0.02$ is the reinforcement ratio related to the considered finite element.

4. RESULTS OF THE NUMERICAL ANALYSIS

The influence of different crack models on the load displacement behavior of one analysed beam (load case a, stirrups $\phi 10$) is shown in Fig. 4. When using a fixed crack model in connection with variable shear retention factor according to Eq. 7, the beam fails in shear. However, the use of a fixed crack

model with constant shear retention factor, or a rotating crack model will result in a completely different behavior, namely a bending failure with considerably higher ultimate loads. Therefore, the fixed crack model with shear retention factor by Kolmar is used for the entire analysis.

The ultimate stage is reached after extensive diagonal cracking and after yielding of stirrups in case of beams with shear reinforcement. The ultimate shear forces P_u for all analysed cases are listed in Table 1. The ultimate shear stresses, computed by $v_u = P_u/(7bd/8)$, are shown in Fig. 5. A comparison of the results for load case a with empirical formulas by Kordina and Blume [6], Mallèe [7] and Specht [8] is presented in Fig. 6 (see [4] for details). For lower shear reinforcement ratios, the FE analysis gives higher ultimate shear stresses than the empirical formulas. This can be explained by the fact that with the FE analysis a T-beam was considered, while the empirical formulas are valid for beams with rectangular cross section. Test results prove that the shear strength of T-beams is about 20% higher than for beams with rectangular cross-section. Numerically obtained rate of shear strength increase with increasing shear reinforcement ratio ρ_s is somewhat lower than in empirical formulas, but matches well the prediction by the exact truss analogy for which the shear carried by stirrups is equal to: $v_s = \rho_s f_{sy} ctg\alpha$. The angle of major inclined crack α increases (and $ctg\alpha$ decreases) with increasing reinforcement ratios. However, in most code provisions and empirical formulas it is assumed that $v_s = \rho_s f_{sy} K$ in which the constant multiplyer K does not depend on ρ_s. The consequence is a steeper increase of the ultimate shear stress then in the case with $K = ctg\alpha$.

		no stirrups	$\phi 6mm$	$\phi 8mm$	$\phi 10mm$	$2\phi 8mm$
A_s	$[mm^2]$	-	56.5	100.5	157.1	201.1
Load	a	259	291	320	345	384
Case	b	282	308	330	381	428
	c	306	338	375	427	485

Table 1. Ultimate Force P_u (Reaction at the Support) in $[kN]$

The values of ultimate shear force in Table 1, and ultimate shear stresses in Fig. 5 reveal higher shear strengths for load cases b and c than for load case a. The reason is a shift from a concentrated load (load case a) towards a more uniformly distributed load (load cases b, c). According to test results, under otherwise constant conditions, the shear strength of a beam with distributed loads is higher than for concentrated loads. This change of loading arrangement represents a change of the shear span ratio and precludes the direct comparison between load case a and load cases b, c.

To study the influence of anchor loads on the shear strength of beams, load cases b and c which have the same shear span ratio are compared. The placement of anchoring elements in the bottom zone (load case b) results in a lower shear strength than for the beam where all loads are applied on the top surface (load case c). The measure of decrease is obtained from a comparison of the ultimate loads by:

$$\Delta P = \frac{P^c - P^b}{P^c} \tag{8}$$

in which superscripts denote load cases. Obtained values are presented in Fig. 7. The results show that the difference of shear strength is within the range of 8 - 11%. The higher shear strength for load case c is explaned in Fig. 8, where from the free body diagram follows that a part of the top load is directly transferred to the support. In contrast to that, the bottom load must be transferred to the top zone by stirrups before being transferred to the support by diagonal struts. Details concerning the decrease of shear strength are discussed in [4]. In the present analysis, the decrease of shear strength for the beam without shear reinforcement is about 8%. This is somewhat higher than found in a similar analysis performed by Cervenka et al. [2] for beams without shear reinforcement where 100% of the load is applied in the bottom zone and a decrease of 8-10% is obtained.

5. CONCLUSIONS

The performed analysis gives an insight into the behavior of reinforced concrete beams which are loaded by a concentrated load on the top surface and by equally distributed loads over the top or bottom zones. The analysis shows that loads introduced into the bottom zone by headed anchors might negatively influence the shear carrying capacity. The effects of different load arrangements are outlined.

References

[1] Bazant, Z. P. and Oh, B. H., "Crack Band Width Theory for Fracture of Concrete", *Materiaux et Constructions,* Vol. 16, 1983, pp.155-177.

[2] Cervenka, V., Pukl, R. and Eligehausen, R., "Computer Simulation of Anchoring Technique in Reinforced Concrete Beams". *Proceedings,* Second International Conference Computer Aided Analysis and Design of Concrete Structures, Zell am See, Austria, April 1990, Pineridge Press.

[3] Eligehausen, R., Fuchs, W., Lotze. D. and Reuter, M., "Befestigungen in der Betonzugzone", *Beton und Stahlbetonbau,* Vol. 84, 1989, pp.27-32. and 71-74.

[4] Kazic, M. and Eligehausen, R., "Numerical Simulation of Shear Problems of Reinforced Concrete Beams", Report in preparation, Institut für Werkstoffe im Bauwesen, Universität Stuttgart, 1990.

[5] Kolmar, W., "Beschreibung der Kraftübertragung über Risse in Nichtlinearen Finite Element Berechnungen von Stahlbetontragwerken", Dissertation, T.H. Darmstadt, 1985, 94 p.

[6] Kordina, K. and Blume, F., "Empirische Zusammenhänge zur Ermittlung der Schubtragfähigkeit stabförmiger Stahlbetonelemente", Deutsche Ausschuss für Stahlbeton, Heft 364, Berlin 1985.

[7] Mallèe, R., "Zum Schubtragverhalten stabförmiger Stahlbetonelemente", Deutsche Ausschuss für Stahlbeton, Heft 323, Berlin 1981.

[8] Specht, M., "Zur Querkraft Tragfähigkeit im Stahlbetonbau", *Beton und Stahlbetonbau,* Vol. 84, 1989, pp.193-198.

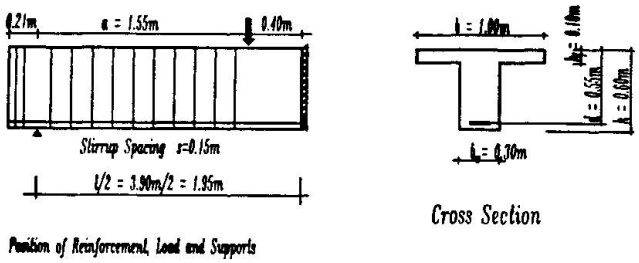

Fig.1 Dimensions of the Analysed Beam

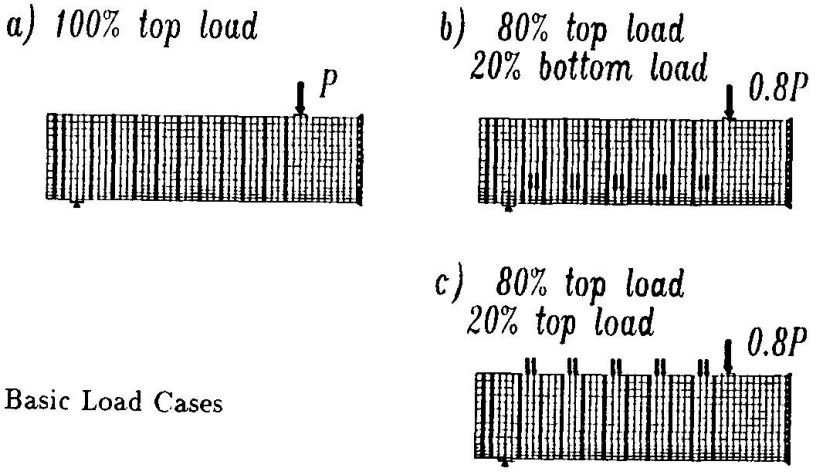

Fig.2 Basic Load Cases

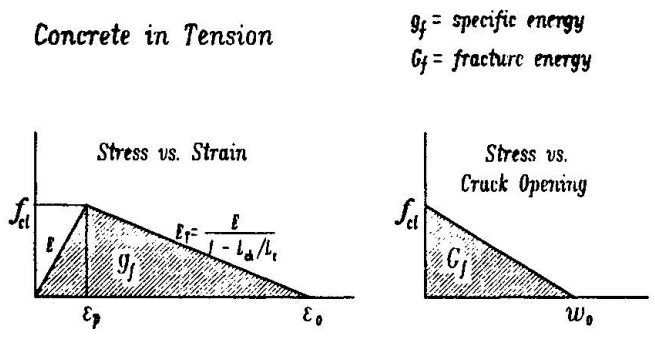

Fig.3 Concrete in Tension

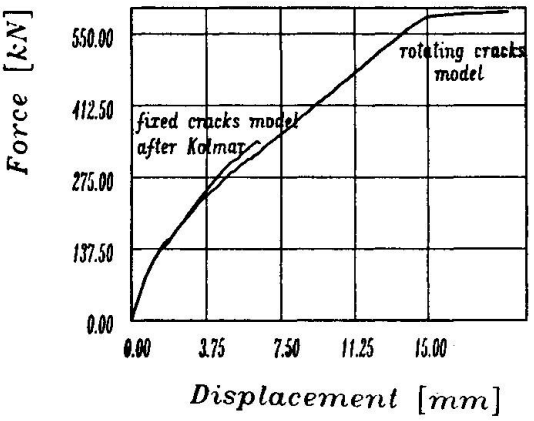

Fig.4 Influence of Crack Model

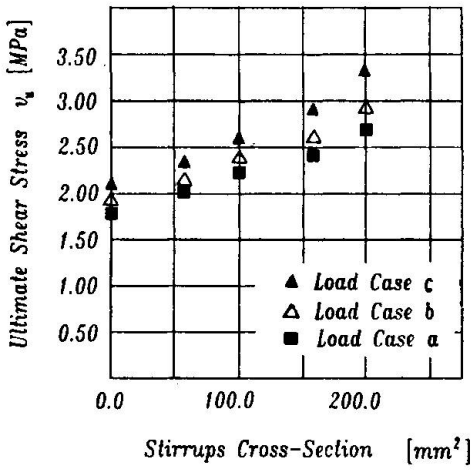

Fig.5 Ultimate Shear Stresses

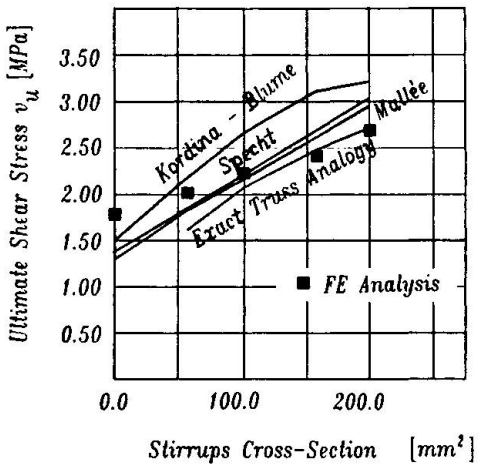

Fig.6 Results vs. Empirical Formulas

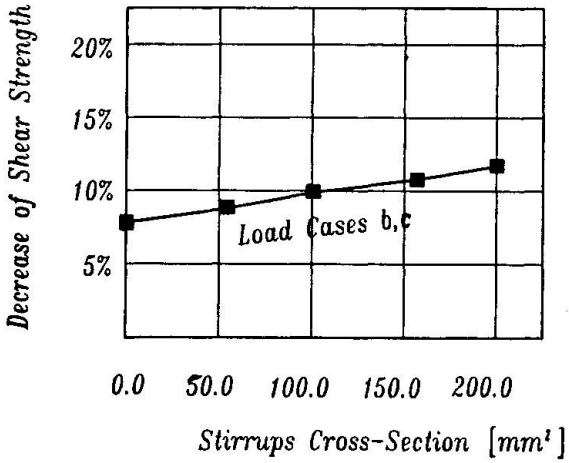

Fig.7 Decrease of Shear Strength

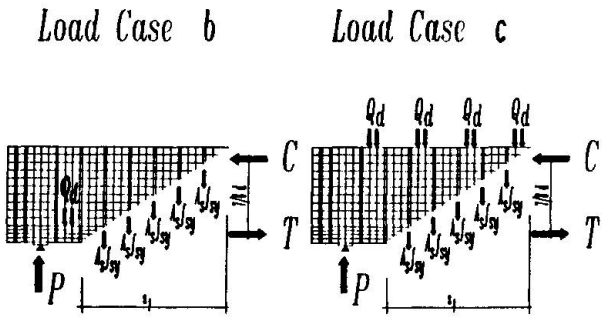

Fig.8 Free Body Diagrams

Load Carrying Mechanism of Anchor Bolt

Résistance d'un boulon d'ancrage chargé

Tragfähigkeit von Ankerbolzen

Kyuichi MARUYAMA
Assoc. Prof.
Nagaoka Univ. of Technology
Nagaoka, Japan

Kyuichi Maruyama, born 1948, received Ph.D. from the University of Texas at Austin in 1979. His research interests include durability of reinforced concrete structures.

Keiji SHIMIZU
Prof.
Nagaoka Univ. of Technology
Nagaoka, Japan

Keiji Shimizu, born 1928, received Doctor of Agriculture from the Univ. of Tokyo in 1971. He has extensive experience in railroad engineering.

Mitsuhiro MOMOSE
Civil Engineer
Nagano Pref. Office
Nagano, Japan

Mitsuhiro Momose, born 1966, received Master of Engineering from Nagaoka University of Technology in 1990.

SUMMARY
It is discussed in this paper how an anchor bolt, embedded in concrete, carries the applied load under static and fatigue loadings. An experimental test was conducted using anchor bolts of relatively small size in diameter and length. Examining the failure mode of concrete in detail, a mechanical model is developed in terms of an angle of crack propagation, stress distribution and the tensile strength of concrete.

RÉSUMÉ
Ce rapport décrit la façon dont un boulon d'ancrage dans le béton supporte l'application d'une charge statique et endure la fatigue. L'expérience a été menée sur des boulons d'ancrage relativement de petite taille (longueur et diamètre). Après observation du mode de rupture du béton environnant, un modèle mécanique est développé en fonction de l'angle de propagation de la fissure, de la distribution des contraintes et de la résistance du béton à la traction.

ZUSAMMENFASSUNG
In diesem Aufsatz wird erörtert, wie ein im Beton eingebetteter Ankerbolzen die Last unter statischen und ermüdenden Belastungen trägt. Der Versuch wurde mit in Durchmesser und Länge relativ kleinen Ankerbolzen durchgeführt. Nach sorgfältiger Prüfung des Betonbruchs wurde ein mechanisches Modell unter Berücksichtigung des Winkels des Rissfortschritts, der Verteilung der Spannung und der Zugfestigkeit des Betons entwickelt.

1. INTRODUCTION

The authors have reported the characteristics of the newly developed fixings (undercut type fixings) in terms of the static and fatigue strength, the applicability near the edge or the corner of concrete structures [1]. In the paper the empirical formulas were proposed for estimating the static and fatigue strength of such type fixings based on the experimental results. However, the formulas were limited to the fixings having 40 mm embedment length because of the limited range of test data. It was necessary to extend the study on the load carrying mechanism of the fixings from the low load level up to the failure stage with variations of embedment length and dimension of bolt.

In order to develop a general model of load carrying mechanism of the fixings, the static pull-out test was first conducted varying both the embedment length of bolt and the location of bolt from the edge of concrete block specimen. Referring to the study on application of acoustic emission to the pull-out test of anchor bolt [2], the discussion was extended to how the concrete carried the applied load, and what was the rational expression for the load carrying capacity of the undercut type fixings. The study should be applicable to the load carrying mechanism of ordinary anchor bolt because the load transfer point from the bolt to the surrounding concrete of this fixings is similar to that of ordinary anchor bolt.

2. EXPERIMENT

2.1 Bolts

The main parameters in the experiment were the size (diameter) and the embedment length of bolt. The shape of bolt is shown in Fig.1 and the dimension is summarized in Table 1. The tensile strength of bolt was 800 MPa. In order to assure the anchorage of bolt, the torque listed in Table 1 was applied to a bolt in advance of the pull-out test.

Concrete Block (cm)	Size of bolt (mm) d le	Φ	D	Torque (KN·cm)
50x50x20	14x40	M10	18	2.35
60x60x30	14x60	M10	18	3.53
	18x80	M12	24	6.76
120x60x30	22x100	M16	28	11.8

Table 1 Dimension of bolt

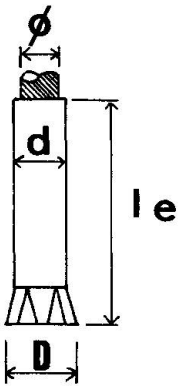

Fig.1 Shape of bolt

2.2 Test Setup

Fig.2 shows the test setup. The load was applied to a bolt by a center hole type oil jack, and was measured by a load cell of 50 KN or 200 KN capacity. The displacement was measured by LVDT-'s. In order to avoid the confinement effect due to the reaction supports, the supports were placed 3 times of embedment length (3·le) away from the bolt.

All the data were recorded and stored in a microcomputer through a dynamic strain meter and an A/D converter. The similar system was used for the fatigue test. The strength of concrete block specimen was evaluated by the compressive strength test using a cylindrical specimen of Φ10x20 cm.

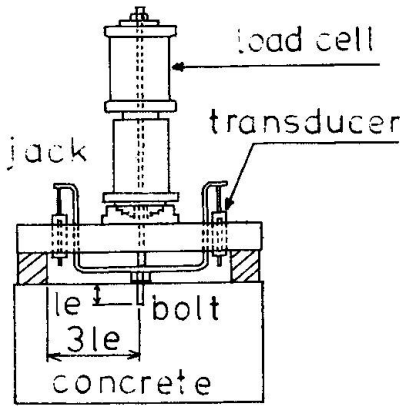

Fig.2 Test setup

3. TEST RESULTS AND DISCUSSION

After the pull-out test, the failure mode of the specimen was examined concerning with the shape of ruptured cone of concrete. A typical projection of cone is shown in Fig.3. The failure surface can be simplified as a tri-linear line as shown in Fig.4. Near the bottom end of bolt the concrete was splitted, and the crack developed at an angle of Φ from the horizontal. At a certain point the angle of crack propagation turned to θ. Finally, the ruptured cone was pulled out with the skirt of shallow angle near the surface of concrete.

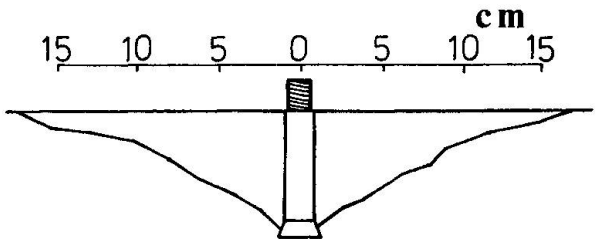

Fig.3 Ruptured cone

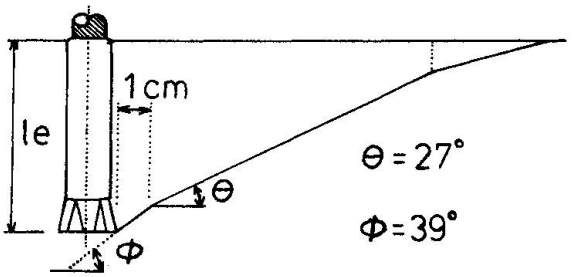

Fig.4 Simplified cone

Since the measurement of cone depth was done in the four directions, Table 2 shows four values of Φ and θ. The shallow angle of the skirt of cone was not shown because it was less important in the load carrying mechanism as will be discussed in the next section. The first angle (Φ) ranged from 26 to 50 degree, and the second one (θ) from 20 to 40 degree. There observed little influence of the diameter and the embedment length of bolt, and of the concrete strength on the angles. The mean values were 39 and 27 degree for Φ and θ, respectively. Some data of Φ are not shown because too much rupture of concrete made the measurement of angle impossible. The location of turning point of the crack angle from Φ to θ was observed scarcely influenced by the embedment length of bolt and the concrete strength. In the test it was about 1 cm away from the center of bolt (Fig.4). The examination was extended to the mortar block. The results were similar to those of concrete block, showing Φ=36 and θ=24 degree.

Bolt d le Φ	f'_c MPa	f_t MPa	Φ (degree)	θ (degree)	P_{max} KN
14x40 M10	19.2	1.75	41 34 48 -- 36 43 27 --	28 20 48 25 24 30 27 27	20.7 20.8
14x60 M10	38.7	2.84	-- -- -- -- 47 42 46 -- 37 45 48 35	26 20 27 45 29 27 27 25 15 18 21 25	44.1 55.0 38.4
18x80 M12	31.4 38.7 37.3	2.24 2.84 2.52	45 38 -- -- 29 32 53 45 49 41 -- --	30 30 25 30 24 35 21 29 21 26 23 22	61.9 65.7 55.0
22x100 M16	37.3	2.52	37 26 41 30 35 30 36 -- 38 54 -- --	37 28 24 38 30 30 31 16 34 32 -- --	90.6 86.2 109
14x40 M10	37.4*	2.39	42 33 51 20	27 24 26 20	22.3
Mean Value Standard Deviation Coeff. of Variation			39.2 8.2 20.8 %	27.1 6.5 24.0 %	

* : Block was made of mortar.

Table 2 Test results

4. MODELLING OF LOAD CARRYING MECHANISM

Before constructing a mechanical model, the pertinent researches were surveyed. Rokugo et al [2] reported that up to the maximum load level the acoustic emission in the pull-out test generated within the circle area having the radius of 1.6 times of embedment length (1.6·le; Figs.5,6). On the other hand, the finite element analyses done by Kamimura [3] and Kosaka [4] showed that the principal tensile stress became to zero at the location of (1.7-1.8)·le away from the center of bolt. The similar results were obtained by the other series of test which examined how the pull-out resistance of anchor bolt was influenced by varying the bolt location from the edge of concrete block.

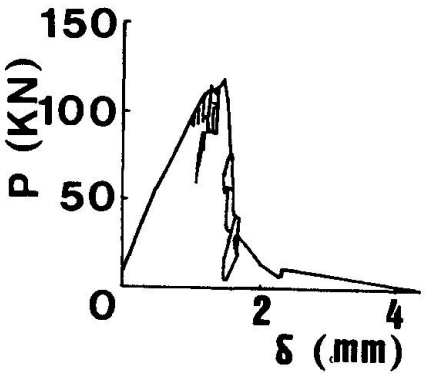

Fig.5 Load-displacement [2]

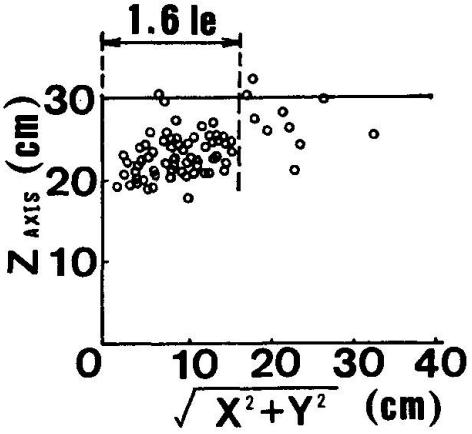

Fig.6 Acoustic emission [2]

Taking these results into account, the load carrying mechanism of anchor bolt was modelled on the following assumptions (See Fig.7).

(1) Crack initiates and propagates along the assumed cone line as shown in Fig.4.
(2) At the tip of crack (distance of x from the bolt center in Fig.7), the applied load is resisted by both the splitting strength of uncracked portion of concrete (outside the tip of crack) and the frictional resistance of cracked portion (inside the tip of crack). The distribution of resistant stress is assumed to be an isosceles triangle.
(3) Crack begins to propagate when the stress at the tip of crack exceeds the modulus of rupture of concrete (f_{tx}).
(4) The modulus of rupture of concrete depends upon the confinement condition of concrete. As shown in Fig.7 the modulus of rupture near the bottom end of bolt is assumed to be 1.2 times of (f_t) which is given by the standard test [5]. The confinement effect decreases and fades out at the location of 1.7·le away from the center of bolt.
(5) The fraction of resisting stress is neglected near the bottom of bolt where the concrete was splitted, and is neglected outside the projected circle range of 1.7·le radius.

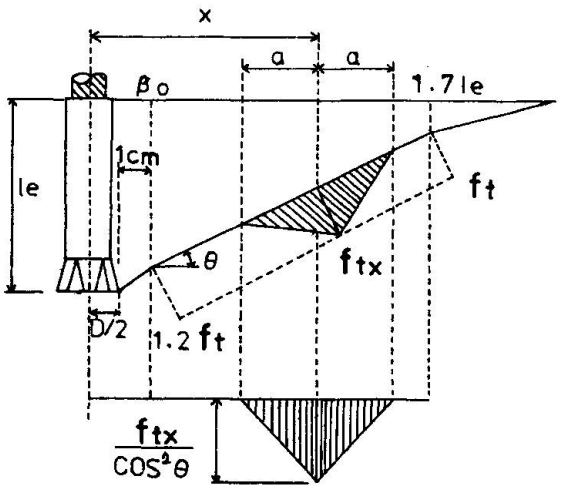

Fig.7 Proposed load carrying mechanism

The load corresponding to a given resistant stress distribution is, then, calculated as follows:

$$P = \frac{\pi \cdot f_{tx}}{\cos^2\theta} \cdot (2 \cdot a \cdot X) - A \qquad (1)$$

where, A :modification factor due to imperfect shape of stress distribution.

The ultimate capacity of fixings is, then, calculated so as to find the maximum value of P in Eq.(1) in the supposed failure surface. In addition, the resistant stress conditions could be correlated to the load-displacement curve in Fig.8. For example, at stage 1 , the deformation is mainly attributed to the elastic deflection of bolt. During stages 2 through 3, crack propagates at an angle of θ and the cracked portion of concrete is lifted up. The displacement may be due to the flexural deflection of cracked portion.

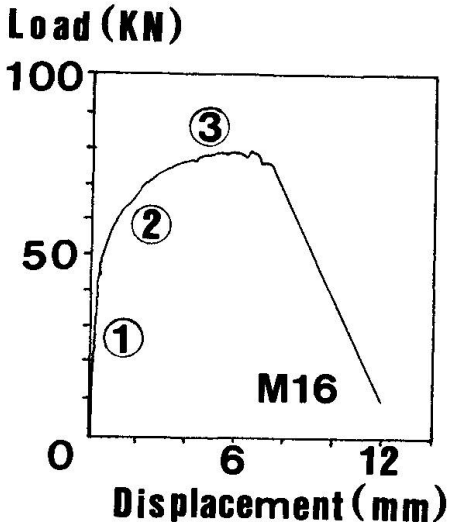

Fig.8 Load-displacement

5. COMPARISON OF CALCULATION WITH TEST

5.1 In general

For calculation by the model, it is necessary to determine the angle of θ and the base length (a) of the shape of stress distribution in advance. In this study the angle of θ was fixed as 27 degree which was the mean value of the experimental results. On the contrary, there was not any rational method to determine the length (a) at this moment. Then, the length (a) was chosen as 2.7 cm which was the best fit value to the test results after several trial and error calculations. Fig.9 shows the comparison of calculated results with test results having the factor of correlation of 97.5 %.

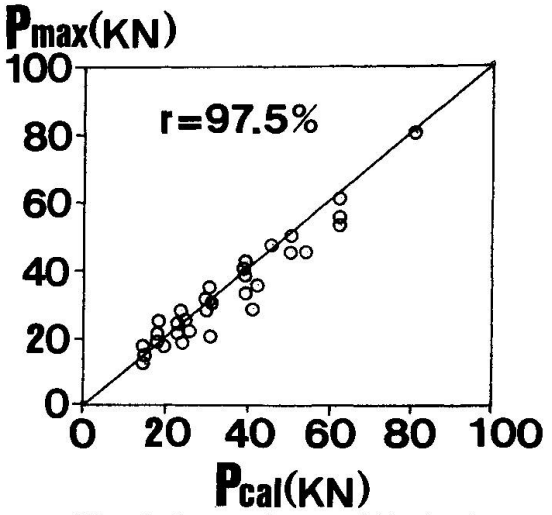

Fig.9 Comparison with test

5.2 Near Edge

The model with the same values of θ and (a) was applied to the case in which the bolts were mounted near the edge of concrete block. The resistant stress outside the edge was naturally neglected as shown in Fig.10. The comparison is shown in Fig.11. The factor of correlation was 91.9 % which was slightly less than that of general cases. This may be attributed to (1) the less confinement effect near the edge of concrete block, and (2) the difference of the failure pattern from the assumed one. However, the value of 91.9 % might not be so bad in prediction.

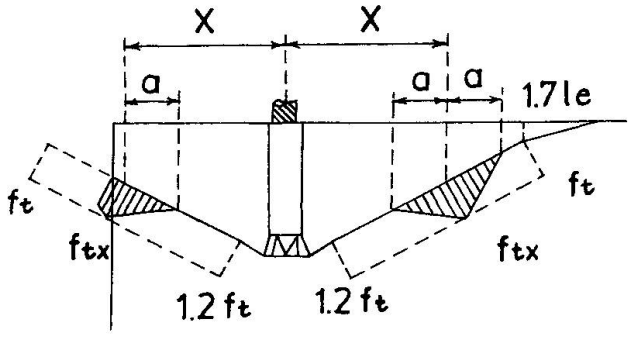

Fig.10 Stress distribution near edge

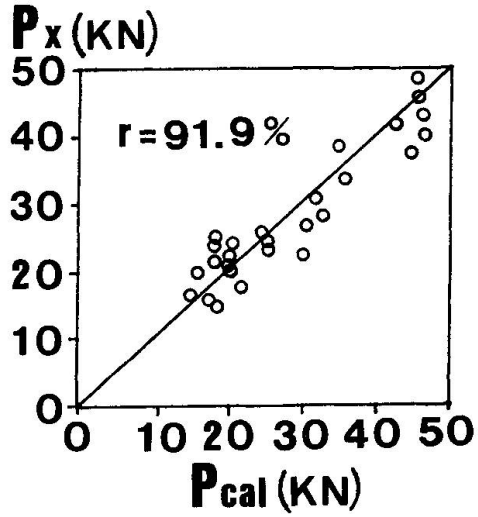

Fig.11 Comparison with test

6. FATIGUE CAPACITY OF FIXINGS

Varying the applied cyclic load level, the fatigue life of fixings was examined. The test results are plotted in Fig.12, where the solid circles represent the cases of bolt fracture and the open circles are those of concrete rupture in a conical shape. The solid line is drawn from the equation for the fatigue life of bolt (Eq.2), and the broken lines are from the equation for concrete (Eq.3). Both equations are proposed by the Japan Society of Civil Engineers [6].

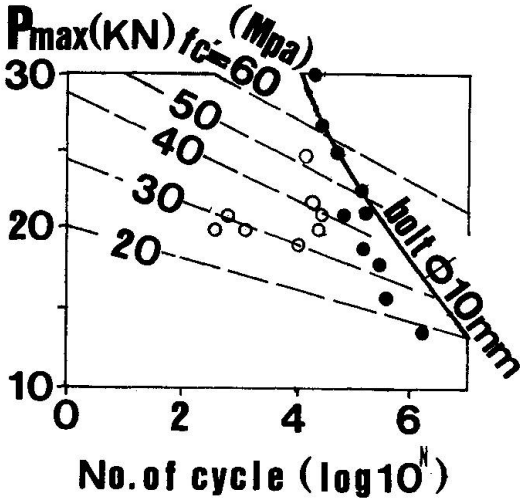

Fig.12 Fatigue Capacity

$$f_{srd} = 1900 \cdot (10^{\alpha}/N^{k}) \cdot (1-\sigma_{sp}/f_{ud}) \qquad (2)$$

where, $\alpha = 0.82-0.003\Phi$, $k = 0.12$,
Φ = diameter of bolt (mm).

$$\log N = 17 \cdot \{1-(\sigma_{max}-\sigma_{min})/(f_u-\sigma_{min})\} \qquad (3)$$

where, σ_{max} = maximum stress in concrete due to the model, σ_{min} = minimum stress and f_u = static strength.

7. CONCLUSIONS

The followings were concluded from this study.

(1) The resistance of concrete against the pull-out force of bolt may be attributed to the area within the projected circle with a radius of 1.7 times of the embedment length of bolt.
(2) The pull-out resistant capacity of the fixings can be predicted by the proposed model. The model is also applicable to the fixings used near the edge of concrete structures.

REFERENCE

[1] MARUYAMA, K., MOMOSE, M. and SHIMIZU, K., Mechanical Behavior of Undercut Type Fixings. Transactions of the JCI, Vol.11, 1989, pp.531-538.
[2] ROKUGO, K. and et al,Pull-out test of anchor bolts and examination of failure processing by means of acoustic emission. Proceedings of the JSCE 43rd annual meeting, Part 5, 1988, pp.418-419. (in Japanese)
[3] KAMIMURA, K. and et al, Influence of Concrete Properties upon Pull-out Strength of Mechanical Anchor Embedded in Concrete Members. Proceedings of JCI, Vol.8, 1986, pp.405-408. (in Japanese)
[4] KOSAKA, Y. and et al, Effects of Various Factors on Pull-out Strength of Hole-in Anchors Embedded into Hardened Concrete. Proceedings of CAJ 36th General Meeting, 1982, pp.195-198. (in Japanese)
[5] OHTANI, Y. and et al, Failure mechanism of stud anchor in tension. Proceedings of the JSCE 43rd annual meeting, Part 1, 1988, pp.372-373. (in Japanese)
[6] JAPAN SOCIETY OF CIVIL ENGINEERS, Standard Specification for Design and Construction of Concrete Structures - 1986, Part I (Design). 1986, p.244.

Pull-Out Test of Anchor Bolts Embedded in Concrete

Test d'arrachement du boulon d'ancrage dans le béton

Ausziehversuche von Ankerbolzen im Beton

Gianfranco VALENTE
Assoc. Professor
Univ. de l'Aquila
L'Aquila, Italy

Gianfranco Valente, born 1943, received his civil engineering degree at the University of Rome in 1967 Assistant Research in Rome until 1986.

SUMMARY

An incremental-iterative procedure for the nonlinear finite element analysis of reinforced concrete structures is adopted here. Solid concrete is modelled as a hypoelastic material, whilst cracked concrete (including fracture and aggregate interlock) is modelled with crack bands, according to the smeared crack approach. The proposed approach is applied to the analysis proposed by RILEM TC-90 FMA regarding pull-out tests of anchor bolts in concrete. Only the plane stress condition is considered in this paper.

RÉSUMÉ

On adopte ici une procédure itérative et incrémentale dans le cas de l'analyse non-linéaire de structures en béton armé. Le béton sain est modélisé par un matériau hypoélastique, tandis que le béton fissuré (includant fractures et déchaussements des agrégats) est modélisé par des «bandes de fissuration», ceci en accord avec l'aspect-même des fissures apparues. Cette approche est appliquée à l'analyse proposée par RILEM TC-90 FMA, concernant le test d'arrachement d'un boulon ancré dans le béton. On ne considére dans cet article que l'état de contrainte bidimensionnel.

ZUSAMMENFASSUNG

Ein inkrementelles Iterationsverfahren wurde für eine nichtlineare Finite-Element-Analysis von Stahlbetonbauten verwendet. Beton wird als ein hypoelastischer Werkstoff dargestellt, hingegen wird gerissener Beton (Bruchmechanik und Kornverzahnung) mit Rissbändern, nach dem «smeared crack»-Verfahren dargestellt. Das vorgeschlagene Verfahren wird für die vom RILEM TC-90 FMA vorgeschlagenen Analysis, Ausziehungsversuchen von Betonankerschrauben angewendet. Es wird nur ein ebener Spannungszustand berücksichtigt.

1. INTRODUCTION

Tensile failure in concrete occurs when the tensile stress in one principal direction exceeds the tensile strength. In this case the usual assumption that a plane of failure develops at right angle to the previous principal direction is introduced. Tensile cracking is identified using failure surfaces fixed at the onset of the cracking. The smeared crack concept for fracture and aggregate interlock is adopted . As regards fracture, it is easier to use compliance rather than stiffness matrices, and it suffices to adjust some terms of the compliance matrix. Instead, for aggregate interlock it is easier to use a stiffness matrix approach and it suffices to adjust four terms of this matrix, which is nonsymmetric and does not yield coincident principal axes for stress and strain increments because shear and normal components are coupled. As a general rule, in concrete models, after tensile cracking, the normal stress is released completely (ADINA [1]) and some coefficients of the concrete stiffness matrix are reduced with two constant factors (ADINA, DIANA [1], [5]). Isoparametric elements with a maximum of eight nodes and four integration Gauss points in each direction are used. For concrete, we must take into account three different angles at each integration point for: failure plane, principal strains, principal stresses [9]. The tangent stiffness matrix is referred to:

- principal stress directions, before tensile failure;
- failure coordinate system (axes parallel and transverse to the crack planes) after tensile failure.

The tensile failure envelope given in Fig.1 is employed. It may be observed that compressive stress change this tensile strength. The nominal stress at failure decreases as the size increases. This is caused by the fact that in the presence of the softening the failure cannot be simultaneous but must occur through propagation of a failure across the structure. In a larger structure, this nonsimultaneous nature of failure is more pronounced. In pullout failure, the existence of the size effect must clearly be expected, due to the brittle nature of these failures.

2. RELATIONSHIP BETWEEN THE STRESSES AND THE CRACK OPENING IN FRACTURE

The simplifing assumption that the descending branch is a straight line is adopted here. The analytical curve is shown in Fig.2a). The material behaves in the nonlinear way shown in Fig 2b), where:

- E_0 is the Young's modulus of concrete;
- the quantity of energy absorbed per unit crack area when the crack widens from zero up to or beyond δ_0 is represented by the area lying between the curve and the ϵ axis:

$$w \int \sigma(\epsilon) d\epsilon = G_F \tag{1}$$

Then, from Fig.2b:

$$\epsilon_1 = \sigma/E_0 + \delta/w \tag{2}$$

$$\epsilon_p = \sigma_t/E_0 \tag{3}$$

$$1/C_f + 1/E_0 = 1/E_t \tag{4}$$

$$G_F = (2.72 + 3.10\ \sigma_t)\ \sigma_t^2\ d_a/E_0 \qquad \text{(from [2])} \tag{5}$$

3. AGGREGATE INTERLOCK CONSTITUTIVE LAWS

The "Rough Crack Model" initially proposed by Bažant and Gambarova [3], and later improved ([4], [8], [9], [10]), is here adopted:

$$\sigma_{nn} = a_{12} r \sqrt{\delta_n}\ \sigma_{nt}/h \tag{6}$$

$$\sigma_{nt} = \tau_0 \left(1 - \sqrt{2\,\delta_n/d_a}\right) r\,(f/g) \quad (7)$$

where:

$$f = a_3 + a_4 |r^3| \quad (8)$$

$$g = 1 + a_4 r^4 \quad (9)$$

$$h = (1+r^2)^{1/4} \quad (10)$$

$r = \delta_t/\delta_n$, $a_{12}=0.62$, $a_3 = 2.45/\tau_0$, $a_4 = 2.44(1-4/\tau_0)$, $\tau_0 = 0.25\,\tilde{\sigma}_c$,

d_a = maximum aggregate size (3.5mm in the present paper), from (5).

FIG.1-Plane Tensile failure Envelope of Model.(——)Code,(---)Kupfer et al.

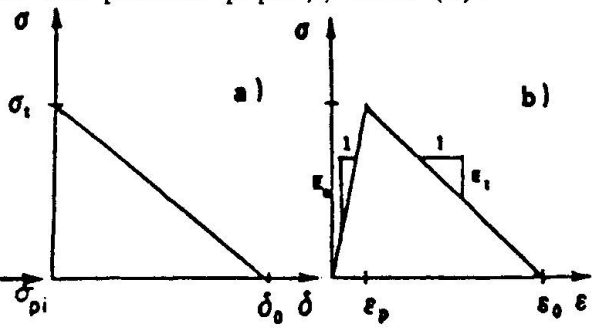

FIG.2-Stress-Strain Diagrams for Fracture.

4. ANALYSIS OF ANCHOR BOLTS IN CONCRETE

The material properties are as follows:

E_0 = 30000 N/mm^2 initial tangent modulus;

ν = 0.2 Poisson's ratio;

$\tilde{\sigma}_t$ = 3.0 N/mm^2 uniaxial tensile strength;

$\tilde{\sigma}_c$ = -40.0 N/mm^2 uniaxial compressive strength;

ϵ_c = -.0022 uniaxial crushing strain;

ϵ_u = -.0031 uniaxial ultimate strain;

β = 0.6 stress ratio for failure surface input;

γ = 1.0 strain scaling factor for multiaxiality;

k = 0.6 control for iso/orthotropic material law;

α = .01 control for loading/unloading chriterion;

$l_{ch} = E_0 G_F/\sigma_t$ = 333.3mm characteristic length.

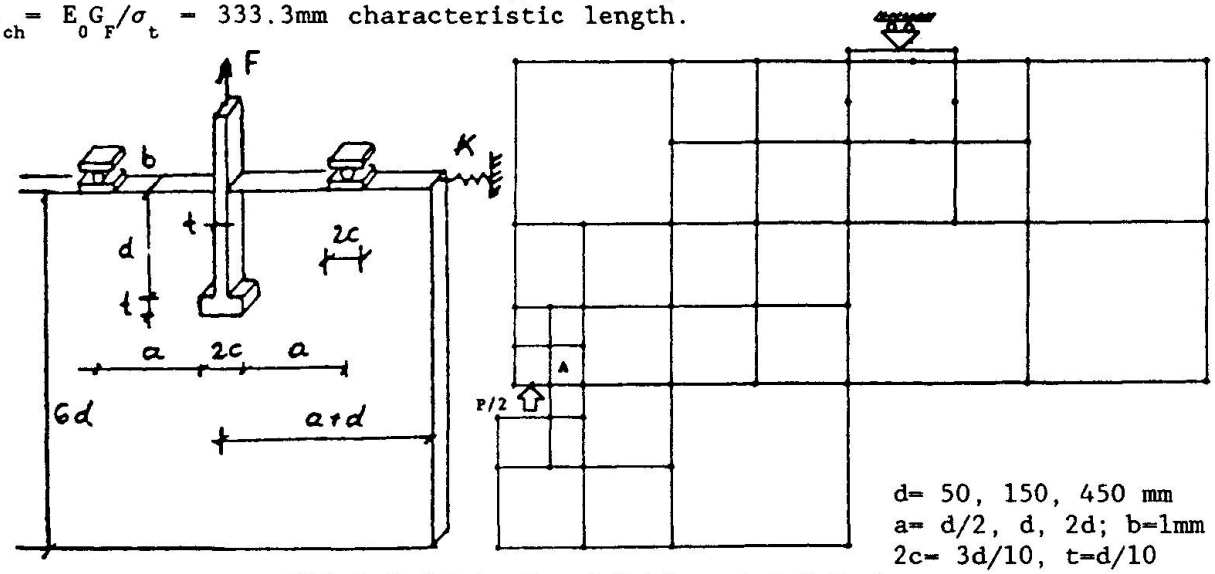

FIG.3-Model by Round Robin and F.E.Mesh.

The finite element mesh is shown in Fig.3. The load is applied at point A. For the unit width b=1.mm, the load-displacement curves of the full slab are shown in Fig.4 and have the maximum values P_u, δ_u as in Table I. Within the deadline of the Round Robin [11], the Author performed a case alone for d=150mm, a=d, K=0. But the final results gathered in [11] compelled himself to extend the analysis to all the six cases for a=d in order to complete the comparisons, expecially with Cervenka and Ozbolt.

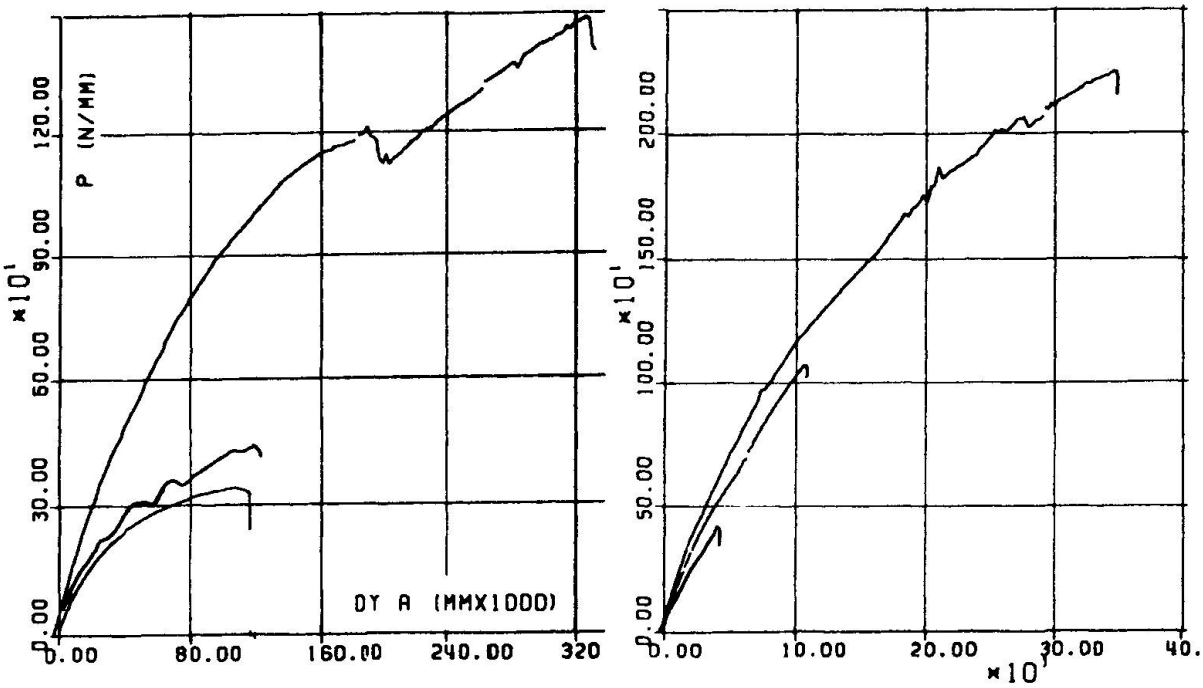

K=0 FIG.4- Load-Displacement Curves. K=∞

TABLE I-Maximum Loads and Displacements P_u/δ_u [N/μ], ([11]).

K=	0			∞		
d [mm]	50	150	450	50	150	450
Ozbolt	175/35	427/90	934/185	328/60	804/200	1790/400
Author	338/107	440/116	1469/327	414/40	1063/110	2232/346
Cervenka(f)	318/100	472/115	1090/340	690/120	1307/310	2549/600

Some of the features of the solution process are:
- both material and geometrical nonlinearities are considered;
- only prescribed displacemets are used;
- the load steps are performed in such a way that the peaks of the stress-strain curves for tensile stresses are matched within +2% (Fig.2b);
- the strain-softening range runs for at least 2 steps;
- the stiffness matrix is updated at each step;
- the equilibrium iterations are performed during each step, with the following tolerance on convergence:

  ($0.5\%P_u$) maximum allowed unbalanced load norm,

  1% for the norm of unbalanced incremental energy.

5. BAŽANT-SIZE-EFFECT-LAW

In concrete structures, the size effect [6] is intermediate between the linear elastic fracture mechanics, for which is much too strong, and the plastic

limit analysis, for which it is absent. These laws are represented in Fig.5. B is the negative slope of the tangent to the curve in Figs.5c,d. This slope approaches that of linear fracture mechanics for increasing d. In terms of sensitivity, it seems that in these cases the value of B is close to 0.5. One consequence of this is also that the formal stress associated with pull out of a bolt is very size-dependent.

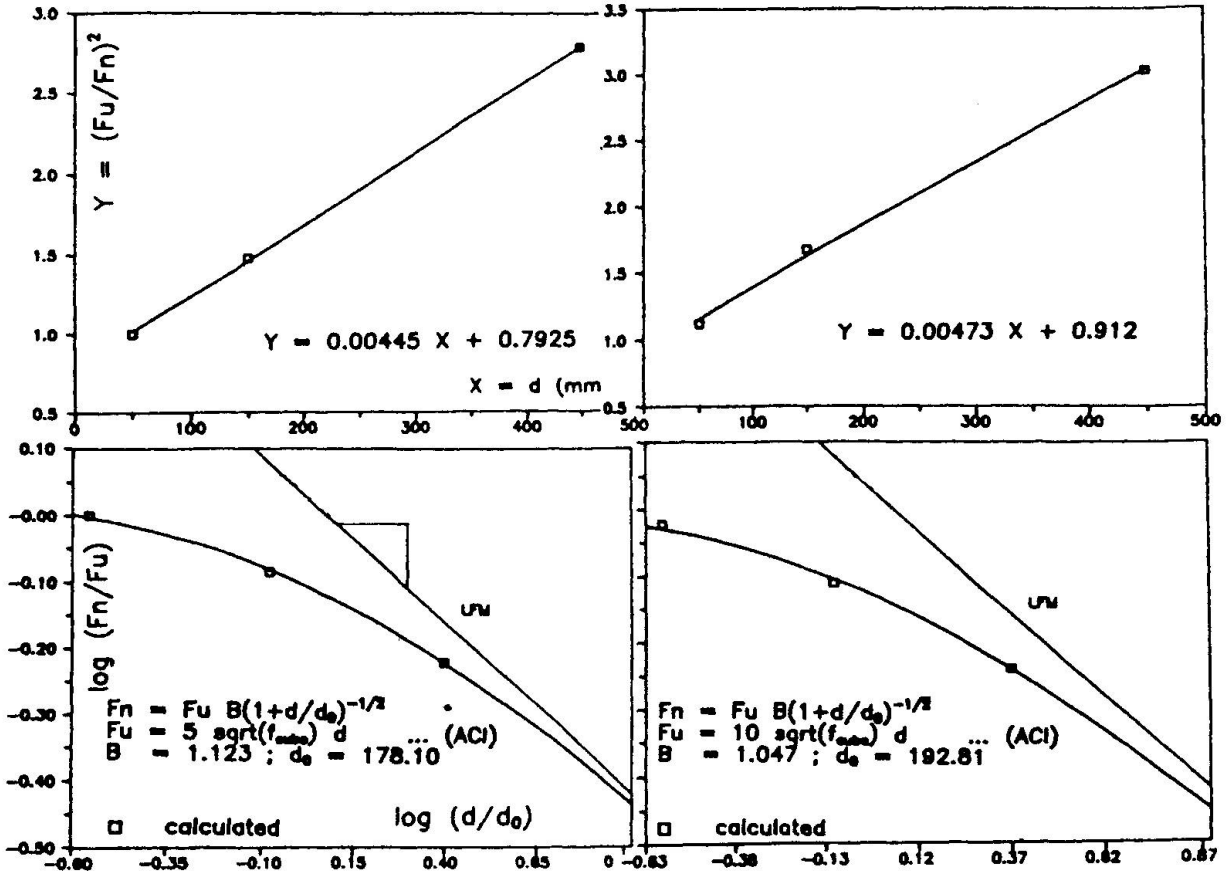

K=0 FIG.5-Bažant-Size-Effect-Laws [6](Figs.by Ozbolt[11]). K=∞

6. CONCLUDING REMARKS

Within this research project, a pre-existing F.E.program for the nonlinear analysis of R.C.elements has been implemented with suitable models for concrete fracture and aggregate interlock.

In principle, the model for tensile fracture can be applied in analysing all the cases where we need to rely on the tensile strength of concrete . We are still far from a sufficient understanding of all types of tensile-induced structural failures. Some of them are very complicated to analyse. A major research effort is needed within this area in order to achieve better guidelines for design rules. Such a research effort may be expected to lead a more even safety factor and large savings. The anchorage of bolts is a case which can be teoretically analysed , although it is rather complicated, because not only tension, but also shear stresses act in the fracture zone, and several fracture zones may have to be taken into account. In order to compare different analytical methods,an invitation was given to a round robin of this common structural detail. Here, comparison with more test results was done. The Code proposed by Cervenka [11] (with fixed cracks) seems very close to that one of the Author. Instead, Ozbolt [11] use a refined nonlocal microplane model. Some of the features of this comparison are:

- the shapes of the load-displacement curve are very similar;

- there is a certain scatter for the values P_u/δ_u that can be ascribed to different meshes, different constraint, different shear reduction factors.

For the Bažant-Size-Effect-Law, it may be conclude that:

1. The present analysis results confirm that a size effect is present, i.e. the nominal shear bond stress at failure decreases as the specimen increases.
2. It appears rhat the results are consistent with Bazant's approximate size effect law for failures due to distributed cracking, as should be theoretically expected according to the known failure mechanism.
3. The analyses indicate that larger specimens tend to fail in a more brittle mode, while smaller specimens tend to fail in a less brittle mode or more plastic shear-pullout mode. This transition in the type of failure as a function of specimen size is in agreement with the physical implications of the size effect law and supports its applicability.

ACKNOWLEDGEMENTS

This research is a part of a comprehensive project on the mechanical behavior of concrete elements, which was supported from the Italian Ministry of Education (M.U.R.S.T. 40% 1989).

REFERENCES

1. K.J. Bathe and S. Ramaswamy, On Three Dimensional Nonlinear Analysis of Concrete Structures, Nuclear Engineering and Design, Vol.52, 1979, pp.385-409.
2. Z.P. Bažant and B.H. Oh, Crack Theory for Fracture of Concrete,Vol.16,n.93, Materiaux et Constructions.
3. Z.P. Bažant and P.G. Gambarova, Rough Cracks in Reinforced Concrete, Jrn.of the Structural Division, ASCE, Vol.106, No.4, April 1980, pp.819-842.
4. S. Dei Poli, P.G. Gambarova and C. Karacoç Aggregate Interlock Role in R/C Thin-Webbed Beams in Shear, Journal of Structural Engineering, ASCE,Vol.113 No.1, January 1987, pp.1-19.
5. J.G.M.Van Mier, "Examples of non-linear analysis of reinforced concrete structures with DIANA", Heron, Vol.32, 1987, no.3.
6. Z.P.Bažant, S.Şener,"Size Effect in Pull Out Test", ACI Materials Journal, Sep-Oct 1988.
7. L.Elfgren,"Fracture Mechanics of Concrete Structures.From Theory to Applications", a RILEM Report prepared by TC 90-FMA, edited by Elfgren Chapman & Hall, 1989.
8. P.G.Gambarova, G.Valente,"Fracture and Aggregate Interlock Mechanism in R/C SMiRT 10, Div.Q, August 1989, Ca, USA.
9. P.G.Gambarova. G.Valente,"Smeared Crack Analysis for Fracture and Aggregate Interlock in Concrete", Engineering Fracture Mechanics, Vol.35, No.4/5,pp. 651-663, 1990.
10. M.Di Prisco, P.G.Gambarova, G.Valente, "Evolutive vs Limit Analysis in Modelling R/C Thin Webbed Beams failing in Shear", 2nd Int.Conf.on Computer Aided Analysis and Design of Concrete Structures, Austria, April 1990.
11. L.Elfgren, "Round Robin Analysis of Anchor Bolts", RILEM TC-90 FMA, Preliminary Report, September 1990.

Stresses and Strains in a Model Ring under Internal Radial Pressure

Contraintes et déformations dans un anneau soumis à une pression radiale intérieure

Spannungen und Verformungen im Betonring-Modell unter Radialdruck

Juraj BILČÍK
Civil Eng.
Techn. Univ.
Bratislava, Czechoslovakia

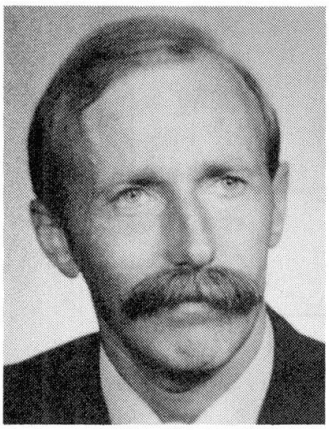

Juraj Bilčík, born 1947, obtained his civil engineering degree at the Slovak Technical University Bratislava, where, he is currently working as a reader at the Department of Concrete Construction and Bridges.

Vladimír PRIECHODSKÝ
Civil Eng.
Techn. Univ.
Bratislava, Czechoslovakia

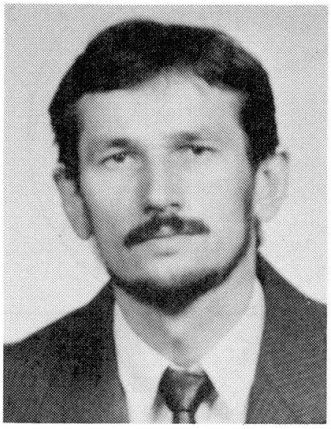

Vladimír Preichodský, born 1953, obtained his civil engineering degree at the Slovak Technical University Bratislava, where, he is currently working as a researcher at the Department of Concrete Construction and Bridges.

SUMMARY

A thick-walled concrete ring model is presented to analyze the state of stresses in the anchored zone of ordinary reinforcement and prestressing steel. The stress-strain diagram of concrete with an ascending and descending branch was used to describe the measured, large, relative strains. A gradual plastification starting from the internal surface of the ring towards the external one was observed.

RÉSUMÉ

Un modèle d'anneau en béton à parois épaisses est étudié en vue d'analyser l'état de contrainte régnant dans la zone d'ancrage d'armatures ordinaires et des aciers de précontrainte. Le diagramme contrainte-déformation du béton présentant une branche croissante et décroissante a été pris en compte lors de la description des déformations relatives élevées obtenues. Les résultats montrèrent une plastification progressive s'étendant de la face intérieure de l'anneau jusqu'à sa face extérieure.

ZUSAMMENFASSUNG

Es wird ein dickwandiges Betonring-Modell vorgestellt und zur Analyse der Spannungen im Eintragungsbereich der Bewehrungsstäbe und Spanndrahtlitzen herangezogen. Für die Beschreibung der gemessenen grossen örtlichen Dehnungen wird ein Kraft-Verformungs-Diagramm mit einem steigenden und einem fallenden Ast benützt. Es wurde eine kontinuierliche Plastifizierung des Querschnitts vom inneren zum äusseren Rand des Betonrings festgestellt.

1. INTRODUCTION

Anchorage of deformed bars and strands by bond causes relatively large radial compressive stresses at the interface between steel and concrete. A thick-walled concrete ring model has been considered to analyse the influence of radial compressive stress on the state of tensile stresses in the anchored area. The concrete ring approximates the effect of the surrounding concrete. The cylinder can be located in the beam section as shown in Fig. 1.

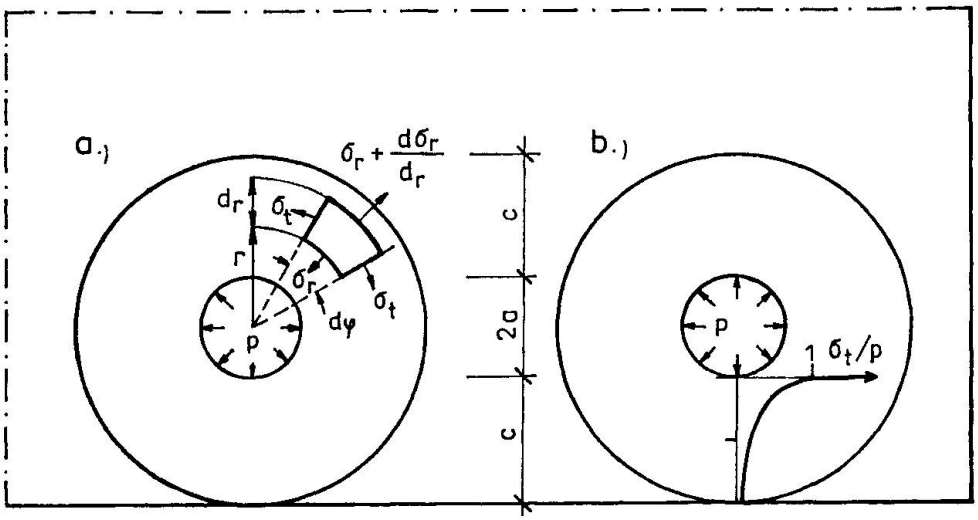

Fig. 1: a/ Location and geometry of the ring model in the section and stresses on an element.
b/ The variation in tangential tensile stresses in the ring model at the elastic stage.

The stresses are mostly calculated for an elastic or plastic stage:

- a solution for the stresses in a thick-walled ring subjected to internal pressure at the elastic stage is given by Timoshenko [1],
- the concrete is assumed to act plastically, that is the ring will not break until the stresses in the tangential direction at every part of the ring section have reached the ultimate tensile concrete stress [2].

2. EXPERIMENTAL TESTS FOR EVALUATION OF STRAINS

The variation in tangential and radial strains were investigated on thick-walled concrete rings with inner radius a = 9 mm, outer radius b = 50, 100, 150 mm and a height of 30 mm. The test rings concrete mix was of the following properties:

- the aggregate was a washed river sand with a maximum size of 4 mm,
- compressive cube strength $f_c = 37,9\ N.mm^{-2}$,
- tensile strength $f_t = 2,8\ N.mm^{-2}$,
- modulus of elasticity $E = 28\ 125\ N.mm^{-2}$ and Poissons ratio $\nu = 0,134$ at stress level of about 40 % of ultimate strength.

The rings were subjected to hydraulic pressure on the inner surface. The deformations of the rings were monitored with electric resistance strain gauges (length 8 mm) in the radial and tangential direction - see Fig. 2. The observed relative tangential strains ε_t and relative radial strains ε_r in the ring model for the increasing internal radial pressure p_i are plotted in the Fig. 2. In order to show the ability of the model to carry large strains it was importante to measure also the strains in the fracture zone, i. e. where the final failure occurs due to a crack.

3. TEST RESULTS AND DISCUSION

Fig. 2 shows that the tangential strains measured in the fracture zone are much higher (Fig. 2b) than that observed outside this zone (Fig. 2c, d, e).
Before the ring fails due to a crack in the fracture zone, under increasing radial pressure, a strain decrease was registrated outside the fracture zone. The following general conclusions regarding the experminental tests may be drawn:

1. The measured tangential strains in the fracture zone reached the maximal value $\varepsilon_t = 2,4.10^{-3}$ which many times exceeds the ultimate strain recorded at the centric tension test $\varepsilon_t = 0,12.10^{-3}$.
2. The test indicate that the observed maximum carrying capacity of the rings, exposed to internal radial pressure are lower than the theoretically carrying capacity at the plastic stage. These informations indicate that the intensity of tangential stress is considerably lower if the strain in the fracture zone exceeds a certain critical value. This fact shows that the fictitious crack model [3] gives a realistic description of tensile stresses in the tested rings. Based on the fictitious crack model it was possible to describe the state of tensile stresses in the ring.

The ascending branch of the stress-strain diagram was determined by means of the tensile test. The descending branch have been determined from the strains measured just before the final failure occurs and from the observed carrying capacity of the rings.
The carrying capacity is given by

$$\int_a^b \sigma \, dr = p.a \qquad (1)$$

The stress-strain diagrams of concrete for various inner radius are shown in Fig. 3.

Fig. 4 shows the variation in the tangential tensile stresses according to the stress-strain diagrams in Fig. 3.
It can be seen a continual transmission from elastic to elastoplastic stage starting from the internal surface of the ring towards the external one. From the distribution of the stresses it is evident that it is not possible to consider the ultimate tensile strength evenly distributed over the cross section.
The measured load capaties of the tested concrete rings, at the time cracks first appear, are plotted in Fig. 5. The experimental values occur just where expected, i. e. between the elastic and plastic stages.

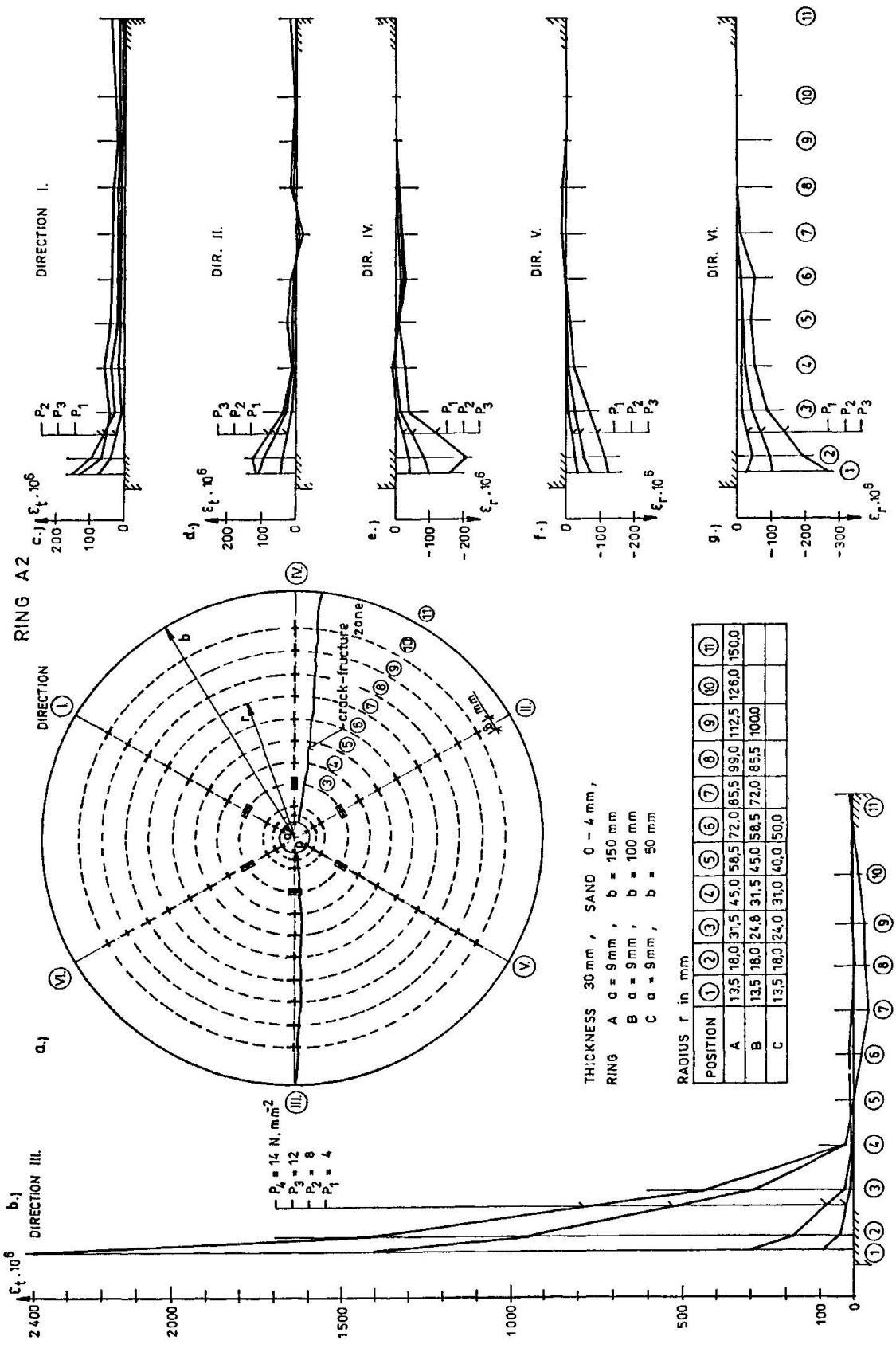

POSITION	①	②	③	④	⑤	⑥	⑦	⑧	⑨	⑩	⑪
A	13,5	18,0	31,5	45,0	58,5	72,0	85,5	99,0	112,5	126,0	150,0
B	13,5	18,0	24,8	31,5	45,0	58,5	72,0	85,5	100,0		
C	13,5	18,0	24,0	31,0	40,0	50,0					

Fig. 2: The variation in the relative strains ε_t and ε_r in the ring model

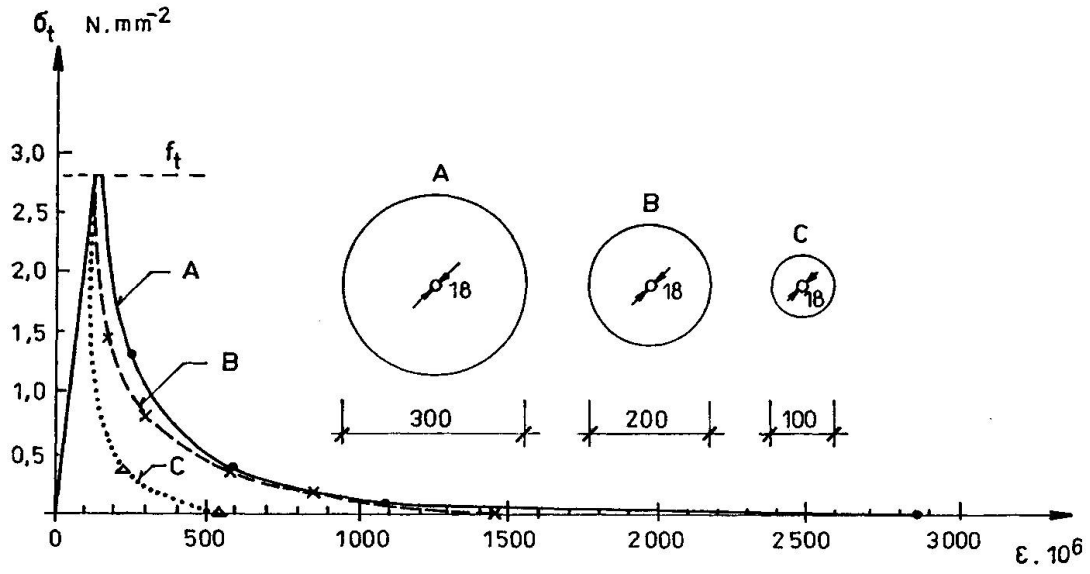

Fig. 3: Stress-strain diagrams of concrete in tension

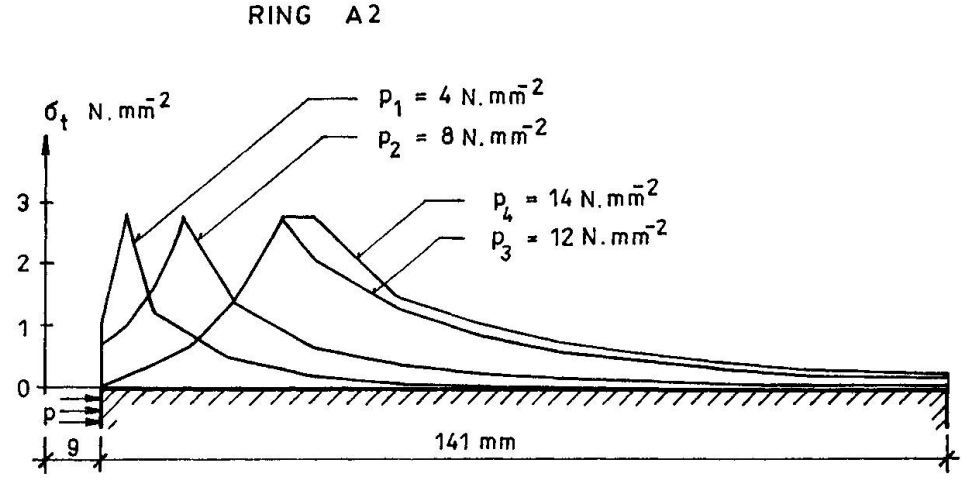

Fig. 4: The variation in the tangential tensile stresses for the increasing internal pressure

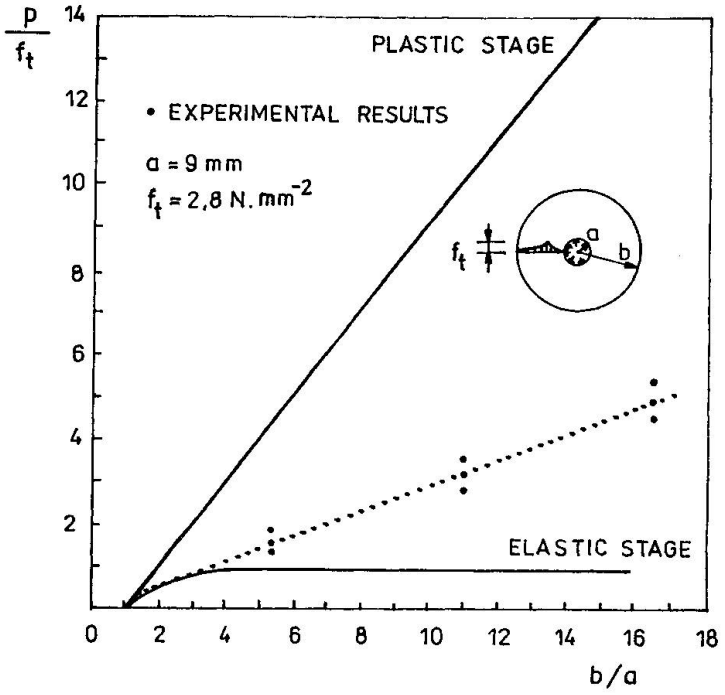

Fig. 5: Load carrying capacities of the rings on occurrence of cracking.

4. CONCLUSIONS

Realized tests confirm that by means of the elastoplastic ring model, based on the stress-strain diagram with an ascending and descending branch, it is possible to analyse the state of the tensile stresses in the transmission zone of prestressed or non-prestressed reinforcement. Futher tests based on the same approach are recomended in order to obtain valid results for practical design purposes.

REFERENCES

1. TIMOSHENKO S., Strength of materials Part II: Advanced theory and problems. Princeton, N.J.,D van Nostrand Company Inc. 1956. pp. 205-210.

2. TEPFERS R., A theory of bond applied to overlapped tensile reinforcement splices for deformed bars. Gothenburg, Chalmers University of Technology, Division of Concrete Structures, 1973, Publication 73:2.

3. HILLERBORG A., Reliance upon concrete tensile strength. IABSE Colloquium "Structural concrete", Stuttgart, April 1991.

4. KÖNIG G., DUDA H., Basic Concept for Using Concrete Tensile Strength, ibid.

5. KÖNIG G., SCHEIDLER D., FEHLING E., Grundlagen zur Traglast-ermittlung unbewehrter Betonbauteile unter Zugbeanspruchung, Beton und Stahlbetonbau, November 1986. pp. 292-296, December

Transverse Tension Decisive for Compressive Resistance of Concrete Cover

Importance de la tension transversale pour le résistance en compression du recouvrement de béton

Querzug massgebend für Mitwirkung der Betondeckung in der Druckzone

Walter STREIT
Res. Assist.
Techn. Univ. Munich
Munich, Germany

W. Streit, born in 1956, received his civil engineering degree at the University of Munich in 1981. For two years he was research assistant of Professor E. Grasser. After that he worked for one year at the construction company DYWIDAG. Since 1985 he is assistant of Professor Kupfer.

Jürgen FEIX
Res. Assist.
Techn. Univ. Munich
Munich, Germany

J. Feix, born in 1961, received his civil engineering degree at the University of Munich in 1986. After that he worked for one year at the construction company DYWIDAG. Since 1987 he his assistant of Professor Kupfer.

Herbert KUPFER
Prof. for Struct. Eng.
Techn. Univ. Munich
Munich, Germany

H. Kupfer, born in 1927, received his civil engineering degree at the University of Munich in 1949. For six years he was an assistant of Professor Rüsch. After that he worked at the construction company DYWIDAG, lattely as chief engineer. Since 1967 he is Full Professor for structural engineering at the above-mentioned university.

SUMMARY
To ensure the durability of reinforced concrete members, concrete cover has been increased lately. This paper shows that the strength of members may be reduced by an increasing concrete cover because this often leads to a higher transverse tension in the concrete cover of the compression zone, for example in frame corners subjected to positive moments and in beams subjected to shear and bending.

RÉSUMÉ
On montre qu'un accroissement du recouvrement de béton – pour des raisons de durabilité – peut entrainer une réduction de la résistance de certains membres du fait d'une augmentation de la tension transversale dans la zone de béton en compression. Cela peut ainsi réduire de façon notable la résistance à la rupture dans des angles soumis à des moments positifs.

ZUSAMMENFASSUNG
In diesem Beitrag wird aufgezeigt, dass die aus Gründen der Dauerhaftigkeit erhöhten Betondeckungen die Tragfähigkeit von Bauteilen negativ beeinflussen können, da die Vergrösserung der Betondeckung in vielen Fällen höhere Querzugbeanspruchungen in Betondruckzonen hervorruft. Dies gilt z.B. bei Rahmenecken mit an der Innenseite Zug erzeugender Biegebeanspruchung und bei Balken, die auf Schub und Biegung beansprucht sind.

1. INTRODUCTION

Concrete cover is usually regarded today as a perfect part of the compression zone. In general a sufficient tensile strength of concrete must be presupposed to do so.

A change of direction of the compressive stresses in frame corners subjected to positive moments as well as a change of magnitude of the compression force in beams with acting shear reinforcement causes tensile stresses in the concrete cover of the compression zone.

But all common codes allow omission of these tensile forces.

In the cases mentioned before a biaxial stress state exists. It must be considered that with increasing longitudinal compressive stress the transverse tensile strength is decreasing /1/. Our design rules were derived from laboratory tests, which were carried out with preciseness avoiding temperature shocks; therefore it is to be expected that in these tests the tensile strength was much higher than in practice. Furthermore most of these tests were made with a very thin concrete cover (1.0 - 2.5 cm), which is smaller than the concrete cover claimed by codes to ensure durability (Table 1).

Member	Exposure Class	DIN 1045 59	DIN 1045 72/78	DIN 1045 88	MC 78	MC 90	EC2 90	
Slabs	interior	10	10	20	15	20	20	[mm]
	humid	15	20	30	20	35	25	[mm]
	humid de-icing	<40	30	50	30	50	40	[mm]
Beams	interior	15	15	20	15	20	20	[mm]
	humid	20	25	35	25	35	30	[mm]
	humid de-icing	<40	35	50	35	50	45	[mm]

Table 1 Comparison of the concrete cover for different codes (nominal values)

In this paper some examples will show that the influences mentioned above can lead to safety risks even when the requirements of the codes are fulfilled.

2. FRAME CORNERS WITHOUT INCLINED REINFORCEMENT

Extensive laboratory tests of frame corners without inclined reinforcement subjected to positive moments were performed by Nilsson /2/ and Kordina /3,4/. Especially in cases of higher reinforcement ratios failure occured far below the calculated ultimate moment. The calculated ultimate moment was determined at an even beam for the same reinforcement. The reason for failure is generally a spalling of concrete cover or of the outer part of the compression zone in that area, where the compression force is being diverted. Afterwards the resisting

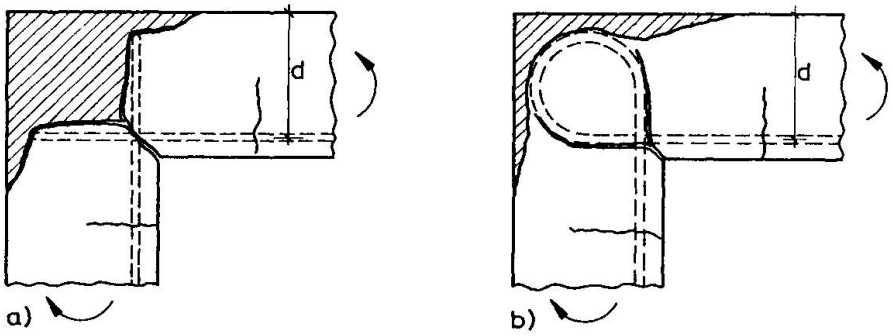

Fig. 1 Graphical illustration of the failure for two different tests of corners subjected to positive bending moments (and two different types of reinforcement)

moment decreases abruptly. Already under a small load a crack begins to form at the inside of the corner. Under higher load the crack divides into two cracks which approximately follow the reinforcement until the tensile force, which is necessary for diverting the compression force, cannot be carried any more and failure occurs. For example see the two crack patterns in Fig.1.

The force distribution in the corner can be described simplified by means of a strut and tie model /5/, which takes into account the failure mechanism and therefore separates the forces in the concrete cover /6/. See Fig.2.

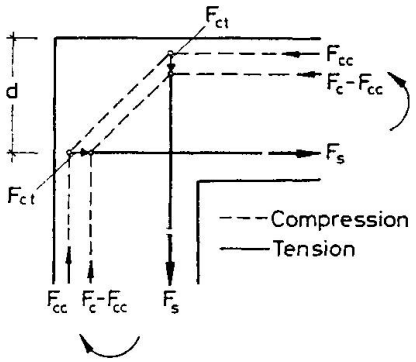

Fig. 2 Strut and tie model illustrating the failure mechanism.

This simple model shows that the compressive force F_{cc} of the concrete cover can only be diverted by the tensile Force F_{ct} resulting from concrete tensile stresses. The compressive force F_{cc} has to be determined with an area A_c, the height of which must exceed the concrete cover c, because the crack area between the reinforcement bars is curved (Fig.3). In this paper the area A_c is determined simplified by $A_c = b \cdot c' = b \cdot (c+s/4)$ with c = concrete cover and s = distance of the bars. The approximation s/4 means that the crack area assumed to be a parabolic area with a maximum inclination of 1.5:1.

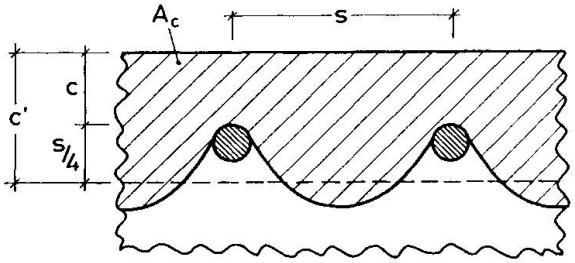

Fig. 3 Area A_c for the determination of the compression force F_{cc} of the concrete cover.

Taking into account the fast increasing of F_{cc} with increasing concrete cover for a given bending moment it is evident that also the tensile stresses which are decisive for the failure, grow fast. If in case of a small concrete cover the tensile strength is already utilized, it is obvious that in case of a larger concrete cover an equilibrium is only possible if a reduction of the bending moment occurs.

The German code DIN 1045 allows the design of frame corners subjected to positive bending moments without inclined reinforcement up to a reinforcement ratio $\mu = 0.4$ %. It must be pointed out, that a limitation of μ is not a good criterion but that a limitation of $\omega = \mu \cdot f_s/f_{ct}$ (a mechanical reinforcement ratio referred to the tensile strength of concrete) would be more precise.

In case of reinforcement ratios $\mu < 0.4$ % and normal concrete strength the influence of the concrete cover in the range of $2cm \leq c \leq 5cm$ at the compression

zone is without much importance for members with small depth ($d \leq 20$ cm), because the neutral axis depth x for the calculated ultimate moment is not much higher than c'(for c = 2 cm). But in case of members of intermediate height (d ~ 50 cm)the influence of the concrete cover (at the compression zone) on the resistance may be great.

Taking, for example, a member with μ = 0.4 %, B 35 (DIN 1045)$\cong$ C 30/37 (EC2), d = 40 cm and s = 8 cm, an increase of the concrete cover from c = 2 cm to c = 5 cm causes an increase of F_{cc} of about 25 %. Assuming that for a concrete cover c = 2 cm the resistance due to the transverse tension is already met, so that no greater F_{cc} can be carried, the failure moment is about 17.5 % lower. Taking into account the influence of the longitudinal compressive stress on the transverse tensile strength acc. to /1/ the failure moment is still about 10 % lower, because the longitudinal stress at the distance c' from the edge is decreasing with increasing c' (in case of a depth of d = 60 cm the failure moment is for c = 5 cm about 14 % lower than for c = 2 cm, taking the changing tensile strength into account). The ultimate moments calculated from a regular design for bending of the cross section remaining after spalling is for d = 40 cm lower than, and for d = 60 cm almost equal to the failure moment in case of the spalling of the concrete cover. That means that in cases of higher cross-sections the calculated ultimate moment at the face of the corner for the cross-section remaining after spalling is higher than the moment when the concrete cover spalls. But it is possible, too, that for high cross-sections the failure moment is lower than the calculated one of the remaining cross-section in the face of the corner, because of excessive damage of the corner area during spalling of the concrete cover (compare Fig.1a).

3. FRAME CORNERS WITH INCLINED REINFORCEMENT

Tests showed that the failure of frame corners with inclined reinforcement occurs in a different way from the failure of corners without inclined reinforcement /2,3/. Fig. 4 presents examples for typical failure in case of additional inclined reinforcement. Failure does not start anymore at the face of the corner as shown in Fig.1 but at the area of the anchoring of the inclined reinforcement. The reorientation of the compression force of the concrete cover already takes place in this area and the resulting transverse tension leads to failure. In cases of corners with inclined reinforcement the failure moment was usually greater than the calculated ultimate moment in the face of the corner (neglecting the inclined reinforcement). Tests were carried out only up to rein-

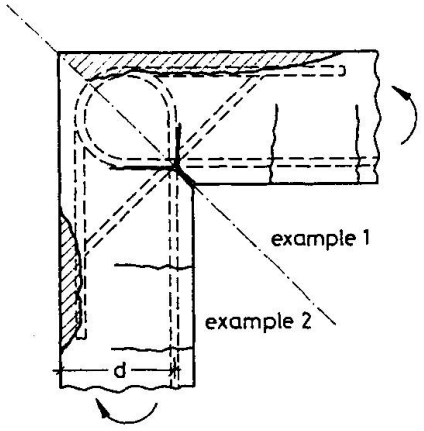

Fig. 4 Graphical illustration of failure of corners with inclined reinforcement subjected to positive bending moments

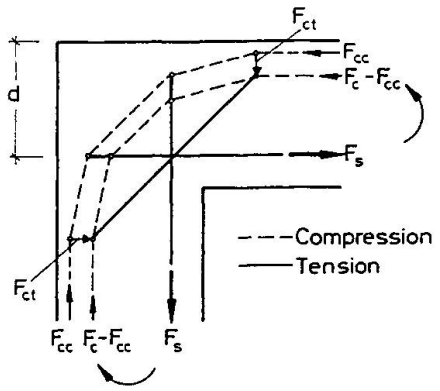

Fig.5 Strut and tie model, illustrating the failure mechanism

forcement ratios of μ = 1.1 %. All test specimen were reinforced in a way that failure should be initiated by flow of the reinforcement but it was observed in all tests that the failure was caused by spalling of the concrete cover in the area of the anchoring of the inclined reinforcement. The strain of the longitudinal reinforcement at failure amounted to about 2 ‰

A simplified strut and tie model presented in Fig.5 clearly shows the failure mechanism. The compression force F_{cc} of the concrete cover is already diverted in the area of the anchoring of the inclined reinforcement (activated for the sake of compatibility). The area of the face of the corner which is decisive for the failure of corners without inclined reinforcement, is relieved.

In the following the test V4 of Kordina is used as an example. The ratio of the failure moment to the calculated ultimate moment for pure bending was 1.0 (due to a normal force in tests the failure moment related to the axis of the tension reinforcement must be used). In the test specimen concrete cover was 2 cm. In case of a concrete cover of 5 cm the failure moment was calculated in accordance with chapter 2 by comparing the forces F_{cc}, in view of the influence of the compressive stress on the transverse tensile strength. The calculated ultimate load for the cross section remaining after spalling is of about the same size as the moment when the concrete cover spalls. The reinforcement ratio ot the test V4 was μ = 0.86 %. But the decisive value of μ corresponding to the compressive force $F_c < F_s$ is only μ = 0.76 %, because a tensile axial force was acting on the cross-section. When the reinforcement ratio is related to the tensile strength of concrete, it becomes evident that this test in relation to all other tests of /2,3/ is among the most reinforced ones.

Taking into account that the tensile strength in practice is usually lower than in laboratory tests it is to be expected that in practice failure moments are lower, too. In corners with inclined reinforcement failure moment will increase moderately with increasing reinforcement ratio, because the cross section, which remains after spalling of the concrete cover will become decisive provided that the compression zone in the corner is not damaged too much.

4. BEAMS SUBJECTED TO BENDING AND SHEAR

Along a beams with high shear there is a rapid change of the compressive force. This means that there is also a rapid change of the compressive force F_{cc} in concrete cover; for example see the area close to the point of zero moments (Fig. 6).

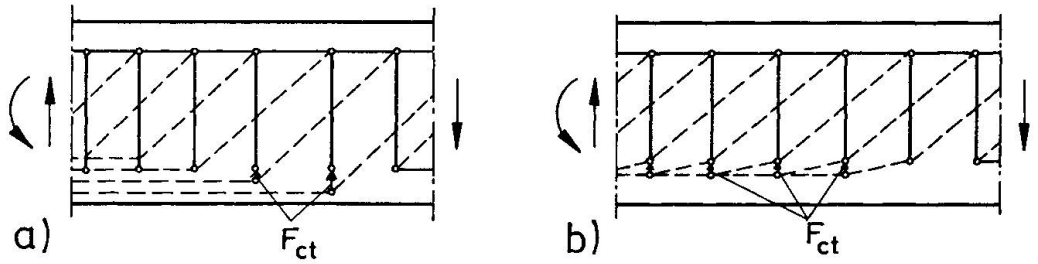

Fig. 6 Two Models illustrating a possible force distributions in a beam under high shear in the area close to the point of zero moments.

The model in Fig. 6a produces in case of thick concrete cover average transverse tensile stresses $\sigma_{ct} = \tau$. Further on it will be shown that the model in Fig.6b causes smaller tensile stresses.

The force distribution in the compression zone for model Fig. 6b was examined for different concrete covers computing the compression zone as a wall. The influence of the thickness of the concrete cover was examined for the most unfavourable case of a beam with a overall depth of 30 cm (effective depth of 25 cm) and with a compression zone heigth of 10 cm. The compression field was

supposed to act under an angle of 45^0 and to be uniformly distributed along the upper rim of the wall. The spacing of the stirrups was assumed to be 10 cm. Furthermore it was supposed that the transmission of the stirrup force into the wall-segment should cause constant forces along the length x-c", where c" = c + ϕ_s = c + 1 cm. Linear and constant distribution of the compressive stresses were examined, the resulting transverse tensile stresses differed only slightly. All calculations are based on a linear elastic behaviour of the material. For a concrete cover of c = 1 cm (c"= 2 cm) the average tensile stress amounts to about 9 % of the assumed acting shear stress τ. For a thick concrete cover c = 5 cm (c" = 6 cm) the calculation showed destinctly higher average tensile stresses of even more than 40 % of τ. Localized tensile stresses are even considerable higher.

This simplifying analysis shows that beams with a thick concrete cover which are substantially subjected to shear may reach an ultimate limit state by a spalling of the concrete cover. To what extent these theoretical results are representing the actual behaviour in the concrete cover should be checked by future tests.

5. SUMMARY

This paper deals with the negative influence of the increase of concrete cover upon the resistance of reinforced concrete. In codes the concrete cover was enlarged in the sake of the durability of concrete structures.

The influence of an increase of concrete cover on the transverse tensile stresses was examined in the case of a corner (with and without inclined reinforcement) subjected to positive bending moments. It was shown theoretically that an increase of concrete cover often leads to a substantial increase of the transverse tensile stresses in concrete. This causes also a substantial decrease of the failure moment compared with members with smaller concrete cover.

Also in cases of beams with high shear the transverse tensile stresses in the concrete cover of the compression zone increases considerably with increasing concrete cover.

The authors think that experimental research is urgently necessary to clarify the negative influence of an increasing concrete cover on the resistance of reinforced concrete.

REFERENCES

1. Kupfer H.B., Das Verhalten des Betons unter mehrachsiger Kurzzeitbelastung unter besonderer Berücksichtigung der zweiachsigen Beanspruchung. Deutscher Ausschuß für Stahlbeton, Heft 229, Verlag Ernst & Sohn, Berlin 1973

2. Nilsson I.H.E., Reinforced concrete corners and joints subjected to bendcing moments. Document D7, 1973, National Swedish Building Research, Stockholm 1973

3. Kordina K., Bewehrungsführung in Ecken und Rahmenknoten. Deutscher Ausschuß für Stahlbeton, Heft 354, Verlag Ernst & Sohn, Berlin 1984

4. Kordina K., Fuchs G., Untersuchungen zur Anwendung von hakenförmigen Übergreifungsstößen in Rahmenecken. Vorläufiger Abschlußbericht, Technische Universität Braunschweig 1970

5. Schlaich G., Schäfer K., Konstruieren im Stahlbetonbau. In: Beton-Kalender 1989, Teil 2, Verlag Ernst & Sohn, Berlin 1989

6. Breen J.E., Why structural concrete. Introductors Report, IABSE Colloquium "Structural Concrete" 1991 Stuttgart

Dimensioning of Elements with Built Up Steel Corbel at the End

Dimensionnement d'éléments en béton munis de cornières métalliques à leur extrémité

Bemessung am Auflager als Stahlkonsole ausgebildeter Elementen

József ALMÁSI
Assoc. Prof.
Techn. Univ.
Budapest, Hungary

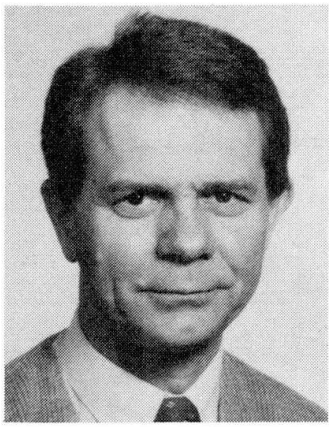

József Almási, born 1940, received his civil engineering degree at the University of Budapest in 1964, and Ph.D. degree in 1972. The focus of his work nowadays is plasticity and detailing.

SUMMARY

The paper reviews experimental work on specially supported elements, where there is discontinuity in geometry and load. It proposes three calculation models: crack free state, cracked state, and strut-and-tie. The determined tensile forces can be followed with a good detailed reinforcement fulfilling the serviceability limit state requirements.

RÉSUMÉ

L'article présente le travail expérimental effectué sur des éléments sur appuis spéciaux, où l'on a constaté des discontinuités dans la charge et la géométrie. Trois méthodes de calcul sont proposées: état non-fissuré, fissuré et analogie du treillis. Les forces de traction calculées peuvent être requises par une armature détaillée assurant les conditions de l'état limite de service.

ZUSAMMENFASSUNG

Der Aufsatz gibt einen Überblick über Versuche besonders gelagerter Träger, bei denen in Geometrie- und Belastung-Diskontinuitäten vorkommen. Drei Berechnungs-Methoden werden vorgeschlagen: Rissefreier Zustand, Riss-Zustand, und Stabwerk-Modell. Die berechneten Zugkräfte können mit Bewehrung abgedeckt werden, die die geforderten Ansprüche hinsichtlich Gebrauchstauglichkeit erfüllt.

1. INTRODUCTION

Structural elements can be used for various purposes if their supporting is solved in an "adjustable" way at the butt end. This is shown in Fig.1 e.g. on a floor-plate element, where on the left side the built up steel corbel has a lower- and on the right side an upper position.

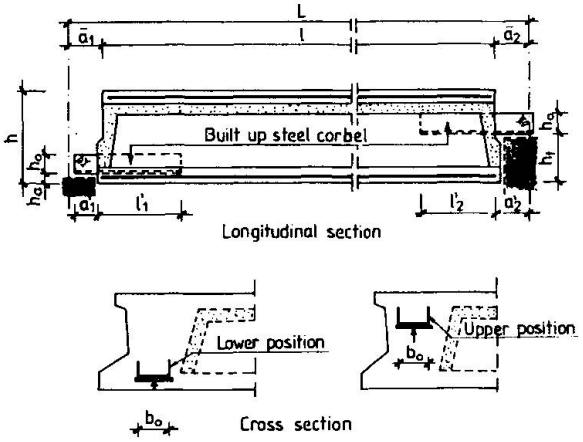

Fig.1 Floor plate element with built up steel corbel at the end

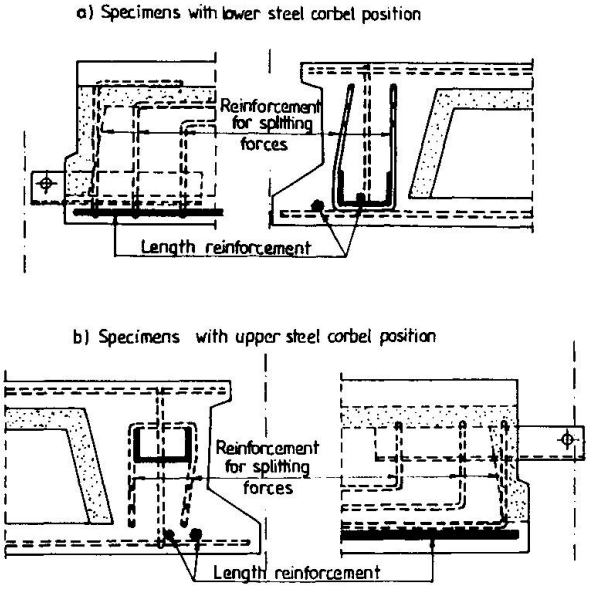

Fig.2 Reinforcement at the support for the specimens

The paper reviews some dimensioning methods which can be used at the support, considering concrete tensile strength 1,2 .

2. RESULTS FROM THE EXPERIMENTAL WORK 7

The reinforcement of specimens for the test is shown in Fig.2. During the step-by-step loading we measured the concrete surface strains and crack width. The typical crack patterns are shown in Fig.3 and 4.

With the steel corbel in the lower position it was found that the concrete surface around the corbel was crack free until 75% of the ultimate load. The cracks started from the inside-end of steel corbel. These craks can be regarded as splitting craks. Generally at the same load level bending cracks can also be found.

In the specimens where the steel corbel was in upper position we found crack free state until 60% of the ultimate load. The cracks started from the butt-surface, from the corner of steel corbel ascend.

In both cases the failure was caused by the yielding of vertical reinforcement.

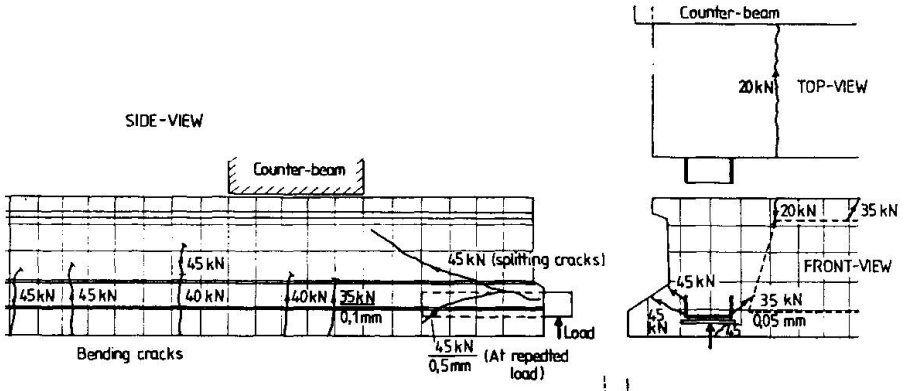

Crack patterns at „lower" position of built up steel corbel

Fig. 3.

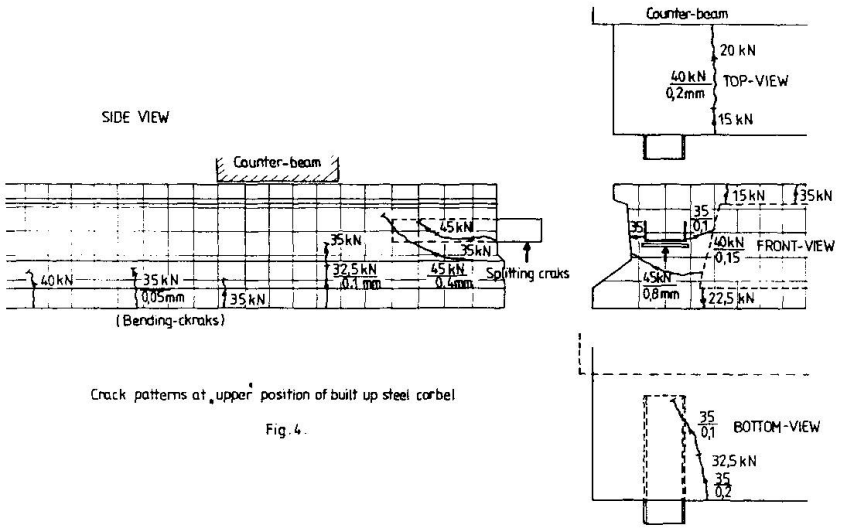

Crack patterns at „upper" position of built up steel corbel

Fig. 4.

3. POINT OF VIEWS OF DIMENSIONING

Besides providing ultimate limit state and serviceability limit state requirements during the dimensioning we have to take into account the following:

The steeel corbel outstanding from the concrete should be stiff in order to have a very small deflection. The sufficient built up length l_1, l_2 Fig.1 of steel corbel has to be provided.

A possible failure can cause a large economic damage and has a significant danger for the human life, therefore at the dimensioning we cannot take directly into account the tensile strength of concrete, because of brittleness 1,2 . Splitting forces arising around the steel corbel can be counterbalanced with vertically placed reinforcement Fig.2, where we can use one admissible value of tensile strength for concrete at the anchorages.

At the detailing we have to be ensure the connection between the steel corbel and the longitudinal reinforcement of the element, and to enlarge the redistribution zone by use of vertical reinforcement 2 . For the calculation of forces around the steel corbel we can use different types of models.

4. MODELS FOR CALCULATION

In this chapter we suggest some calculation models. We assume according Sant-Venant principle that part of the whole element near the support can be regarded like an independent structure.

4.1 Crack free state

Based on the experimental results 7 we assumed three typical, crack patterns Fig.5. where cracks are concentrated in one place. Along the fully developed cracks the tension stress distribution was taken from fracture mechanics approaches. The failure occurs if tensile stresses in concrete arrive the tensile strength f_t. The calculated tensile force is $F_{cr} = b \cdot \sum A_\sigma$. Reinforcement calculated from the vertical component helps to avoid brittle fracture. If the steel stress is reduced appropriately (exp. $\sigma_s = 0{,}4 \cdot f_{sy}$) the crack width can be controlled. By distributing reinforcement according to the tensile stresses, we can fulfilled the requirements (s.Ch.3.).

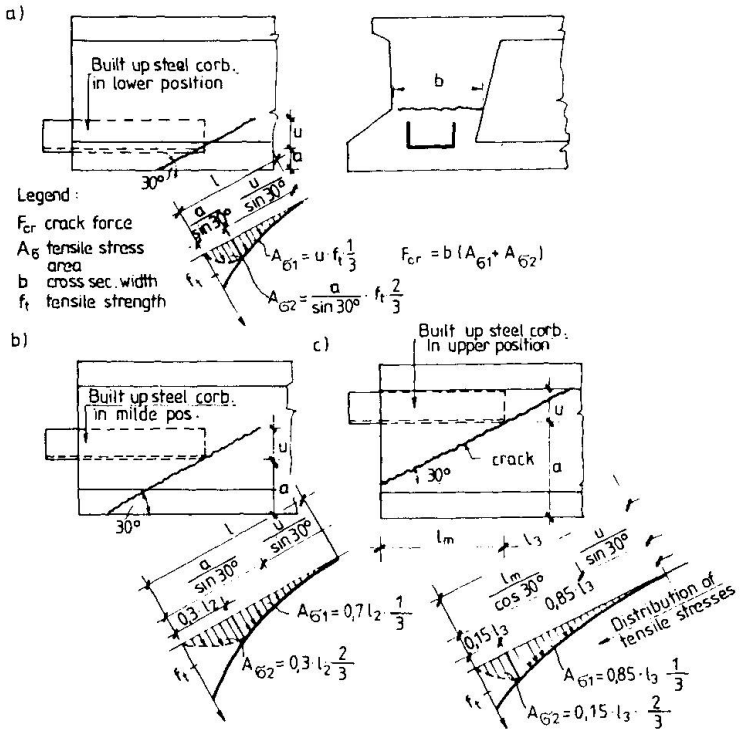

Fig.5 Calculation models in crack free state

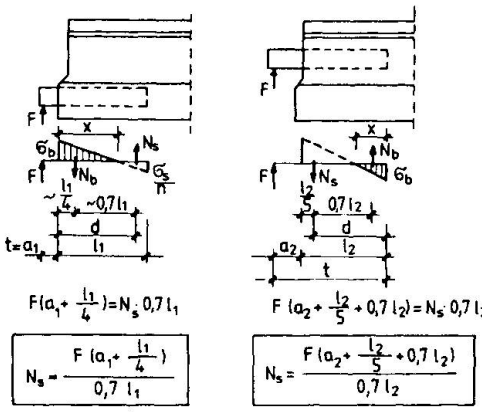

Simplified calculation of the tensile forces

Fig.6

4.2 Cracked state

In the cracked state the equilibrium is arrived through reinforcement. A simplified calculation model is shown in Fig.6 . To use the moment equilibrium we have to choose some geometrical dates in the right way, or to make the traditional calculation. To fulfill the serviceability limit state requirements controll of the crack width, through the stresses in the tensioned members N_s has to be carried out.

4.3 Strut-and-tie models

To have clear "detailing" rules we need a more accurate model like strut-and-tie 5 . Depending on the position of the steel corbel we can develop three typical strut-and-tie models Fig.7 which follow the force paths indicated by the theory of elasticity. Controll calculation showed that strut-and-tie elements can be built up from concrete combining them with elements from the steel corbel, instead of using the steel corbel as a stiff body in this system. The results of an elastic calculation are given in Fig.7. The bearing capacity of concrete compression struts are shownd in 3. Tie forces are counterbalanced with reinforcement Fig.2.

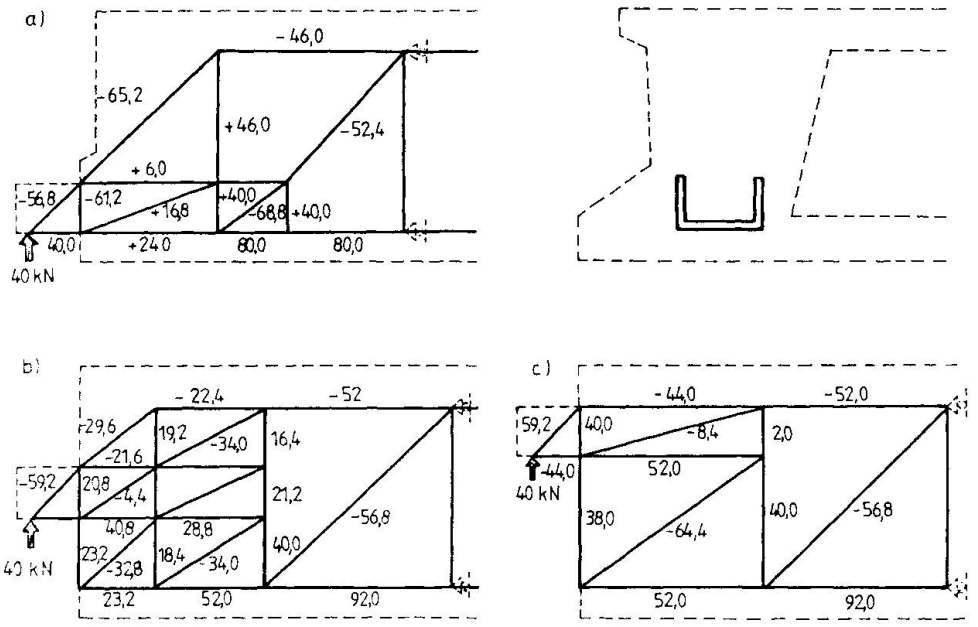

Fig.7 Strut-and-tie forces calculated on truss-construction

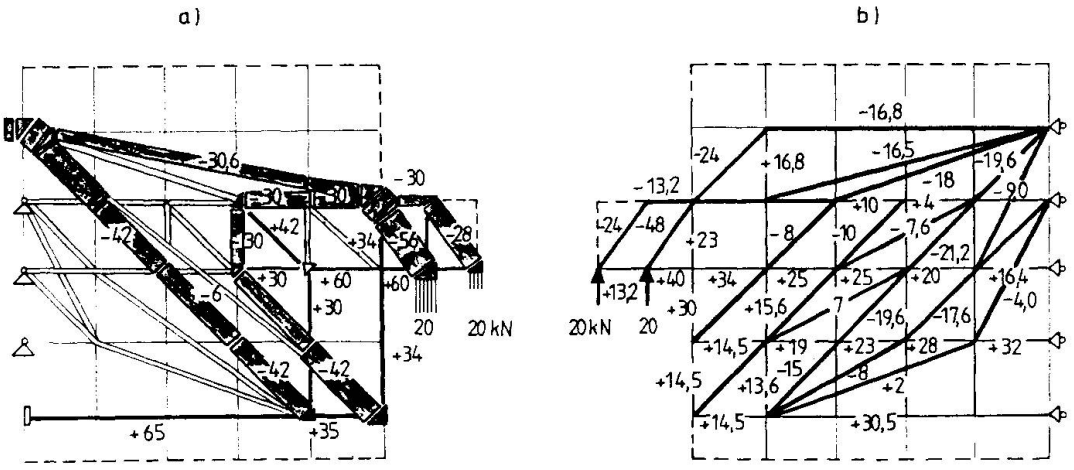

Calculation with stress fields

Fig.8

Calculation on detailed truss

If we chose a more detailed strut-and-tie model Fig.8b we get a finer force-distribution. Comparing these results with a more sophisticated calculation Fig.8a (statically admissible stress-field 6), we can find some differences in the forces. The clearly determined tensile forces followed with a proper detailed reinforcement, using one admissible tensile strength at the anchorages, secure us a good result.

References

1. HILLEBORG A., Reliance upon concrete tensile strength. In this report, IABSE Colloq. Stuttgart 1991.
2. KÖNIG G., DUDA H., Basic concept for using concrete tensile strength. In this report, IABSE Colloq. Stuttgart 1991.
3. WALRAVEN J.C., LEHWALTER N., Die Tragfähigkeit von Betondruckstreben in Fachwerkmodellen am Beispielen von gedrungenen Balken. Bet.u. Stahl. 84 (1989), H.4.
4. CLARK L.A., THOROGOOD P., Serviceability behaviour of reinforced concrete half joints. The Struc.Eng.No 18/20 Sept. 1988.
5. SCHLAICH J. Non-linear design on the basis of strut-and-tie models, FIP Symp. Israel, 1988.
6. SCHLAICH M., Computerunterstuzte Bemessung von Stahlbeton-scheiben mit Fachwerkmodellen. Professur für Informatik, ETH ZÜRICH, Bericht Nr. 1., 1989.
7. ALMÁSI. J. The behaviour of prefabricated elements with built up steel corbel at the end. Research Report VI.Techn. Uni. Budapest, Dep. of R.C., 1987 (in Hungarian)

Tensile Strength Concrete: Prodigal Son or Primary Source?

Résistance à la traction du béton: qu'en est-il?

Die Zugfestigkeit des Betons: verlorener Sohn oder Urquelle?

Andor WINDISCH
Civil Engineer
Dyckerhoff & Widmann AG
Munich, Germany

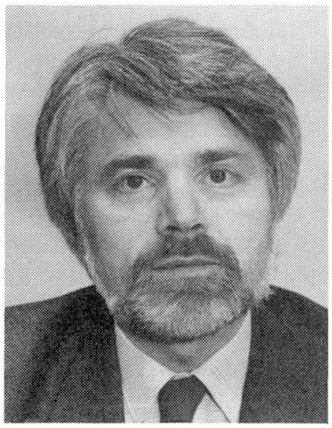

Andor Windisch, born 1942, obtained his Dr. techn. degree at the TU Budapest, Hungary in 1975. He served there as Assistant Professor for reinforced concrete structures until 1983. For 3 years he was Research Assistant at TU Stuttgart. He joined the R & D Department of a building company in 1987.

SUMMARY

Based on results of fracture mechanics and numerical modelling of concrete, the important role of the tensile strength as material property is discussed. The contribution shows that a) contrary to popular opinion high-strength concretes have a relatively high compressive strength compared to their tensile strength, b) the conditions in a structural concrete structure can be better characterized with a tension rather than a compression field, c) tensile strength of concrete must become an integral part of any physical model, d) tensile tests and not compressive tests should be applied in Quality Assurance.

RÉSUMÉ

Tout en se référant aux résultats donnés par la mécanique de la rupture et à la simulation numérique du béton, on discute du rôle primondial de la résistance à la traction du béton par rapport à la résistance en compression. Ce rapport met en valeur quatre aspects: a) Contrairement à ce que l'on pourrait penser, dans un béton à haute résistance, la forte résistance en compression ne va pas de pair avec la résistance en traction mobilisable. b) Les conditions régnant dans une structure en béton armé peuvent mieux être caractérisées par un champ de tractions que par un champ de compressions. c) Le résistance à la traction du béton doit devenir partie intégrante de tout modèle physique. d) Dans tout contôle de qualité, on devrait donner la priorité au test de résistance à la traction par rapport au test de résistance en compression.

ZUSAMMENFASSUNG

Bezugnehmend auf Ergebnisse, die bei Anwendung der Bruchmechanik und numerischen Modellierung zur Erforschung des Betons entstanden, wird die zentrale Bedeutung der Betonfestigkeit hervorgehoben. Der Beitrag zeigt, dass a) im Gegensatz zur allgemeinen Auffassung, die hochfesten Betone eine höhere Druckfestigkeit in bezug auf ihre Zugfestigkeit aufweisen, b) der Beanspruchungszustand eines Tragwerks aus konstruktivem Beton kann besser mit einem Zugfeld als mit einem Druckfeld beschrieben werden, c) die Zugfestigkeit muss als ein wichtiger Bestandteil aller physikalisch integeren Modelle betrachtet werden, d) die Qualitätskontrolle sollte statt die Druckfestigkeit, die Zugfestigkeit des Betons prüfen.

1. INTRODUCTION

Concrete is a inhomogeneous building material. It has a considerable and reliable compressive strength and a relative law tensile strength which can be even exhausted locally under unfortunate conditions, e.g. due to the hydration heat of cement or to its plastic shrinkage. It is quite obvious that the concrete tensile strength was always reprehended as the most unreliable concrete property.

As the compressive strength of the conventional test specimens (200 mm cubes or 150/300 mm cylinders) was rather insensitive to most of the aforementioned influences and it was convenient to be measured, it became accepted by the material science, the design office and the construction site as the fundamental mechanical property of concrete.

Several other properties were deduced empirically by the help of best–fit formulas using the compressive strength as basic variable.

The mean and fractile values of the different tensile strengths too became a function of compressive strength [1]. The degressive character (e. g. the fractional exponent) of this function reflects that high strength concretes have a relative lower tensile strength compared to low strength concretes. Obviously high strength concretes has been always treated as less perfect concretes.

According to a sad terminology, students learn to neglect the concrete tensile strength at dimensioning any s. c. member. Even the CEB–FIP Model Code [2] uses this verb, in EC 2 [3] the tensile strength will be ignored. (As a matter of fact, this applies to dimension the flexural reinforcement only.) In dimensioning of watertight or prestressed concrete members the tensile strength will be relied on with a shy consciousness of guilt.

Even quite recent engineering models for s. c. try to circumscribe those phenomena (e. g. bond) where the tensile strength is the main influencing factor. Thus the modeling of a slab without shear reinforcement became a quite unsolvable problem.

All these problems could be easily removed if we realize that the tensile strength is a more fundamental mechanical property of concrete as the compressive strength is.

The introduction of fracture mechanics and numerical modeling to describe the fundamental behaviour of concrete provides the chance to understand it and to rectify the hierarchy between tensile and compressive strength.

This paper intends to contribute to the acceptance of the tensile strength as a more fundamental concrete property.

2. COMPRESSIVE STRENGTH VS. TENSILE STRENGTH OR VICE VERSA

At the early seventies texture–oriented material models were developed to investigate the mechanism of the internal load bearing system of the two–phase composite material concrete [4], [5]. These models yielded qualitative and partly quantitative predictions on the load bearing and failure mechanisms as function of the rigidity– and strength–relationships between the cement matrix and aggregates. It was concluded that the characteristics of the interface between matrix and aggregate are the primary source of the mechanical properties. Depending on the differences in the rigidities of matrix and aggregates resp. the load trajectories are forced to local deviations in their course shich cause tensile stresses in the matrix and on the interface. These result in microcracks and inelastic response of the concrete. The microcracks were detected during compression tests [6].

During development of their model for "numerical concrete" Wittmann et al. [7] too realized the important influence of the interface on behaviour of concrete, the "mesolevel model" has been introduced.

The texture–oriented and the numerical models resp. showed that both, the compressive and tensile strength have the same origin: the adhesion of the matrix to the aggregates. Under tensile conditions the interface is stressed directly, under compressive conditions indirectly. In this latter case some internal redistribution in the load bearing system is possible, this is the source of the toughness of concrete under compression.

As methods of fracture mechanics had been applied to investigate concrete, it was not by chance that tensile and flexural tests were applied to determine the fracture energy, e. g. the fundamental characteristic of the material concrete, and not any compression test.

Thus we may hope that the traditional empirical way, how to deduce the tensile strength from the compressive strength will be converted to a physically right relationship: the compressive strength will be deduced from the tensile strength and the fractional exponent will disappear as well.

This would become an important step towards more reliance upon concrete tensile strength.

3. COMMENTS ON THE RELATIVE LOW TENSILE STRENGTH OF HIGH STRENGTH CONCRETES

The most important differences between the texture of a high strength concrete and a low strength concrete resp. are the higher stiffness and strength of the cement matrix and its higher adhesive strength to the aggregates in high strength concretes. Due to the quite similar stiffnesses of matrix and aggregate in high strength concretes the inner trajectories under compressive loading conditions are not forced to stronger local deviations, hence the induced stresses along the interface remain relative small. This results in a higher compressive strength compared to the given adhesive strength of the interface.

Thus a high strength concrete must not be reprehended any more for its relative low tensile strength but should be praised for its relative high compressive strength.

This would be an other step to recognition of the tensile strength.

4. COMPRESSION FIELD OR TENSION FIELD?

Soil has, similar to concrete, a low tensile strength compared to its compressive strength. The experts of soil mechanics continued to check form, position and load bearing capacity of sliding surfaces in soil structures even after introduction of the theory of plasticity.

Similar to soil structures, the condition of s. c. members can be better described with a tension field than with a compression field, unless the member will become over–reinforced,

The condition in different parts of a s. c. member can be characterized in relation to the probability of exceeding a certain fractile value of the tensile strength (f_{ctk}) in serviceability and ultimate limit states resp. This probability determines the necessary steps of dimensioning and the type of reinforcement to be applied:

- regions which probably remain free of cracks in ULS get minimum reinforcement
- regions where f_{ctk} will be exceeded in ULS, but probably not in SLS, must be reinforced without fulfilling the requirements in SLS. (As upto the ULS the tensile strength has been already exhausted, it can not be taken into account – instead of to be neglected or ignored – at fulfilling of equilibrium conditions. The usage of the verbs "neglect" or "ignore" is not correct.)
- regions where f_{ctk} has been exceeded already in SLS, the requirements both in ULS and SLS must be fulfilled as well.

This classification can not be achieved with any classes of effective compressive strengths of any compression field theory. Here once more the superiority of the tensile strength over compressive strength is highlighted.

5. BIAXIAL STRENGTH OF COMPRESSIVE STRUTS

Theory, experiments and practice prove that the concrete can be loaded bi– and triaxially, it has strengths in all directions [8].

The rapid decrease of the compressive strength under influence of transversal tensile stresses should not merely be considered at reduction of the axial strength of some compression elements in engineering models, but even the transversal tensile load bearing capacity of those compression elements which are not stressed upto the uniaxial prism strength should be realized as well.

According to the assumed strain distribution in the compression zone at ULS in flexure, only the most exterior concrete fiber reaches the compressive failure strain, all others have $\epsilon_c < \epsilon_{cu}$. This means that the load bearing capacity of any compression zone has a reliable transversal component as well, which is, as a matter of fact, the main part of the V_c term [9].

In ULS each fiber of the compression zone in a s. c. member with bending and shear, will fulfil the failure criterion simultaneously, the whole compression zone will fail at the same time. This was experienced and interpreted as the brittle character of the compression zone's failure under shear loading. The transversal stresses in the compression zone can be decreased with a transversal (shear) reinforcement but they can not be eliminated. Compatibility conditions will determine the effective ratio between V_c and V_s.

Accepting the biaxial strength of concrete some interpretation problems of recent engineering models [10], e. g.

- the shear strength of shear–unreinforced slabs
- the increase of the shear strength due to prestressing

would vanish immediately.

6. QUALITY ASSURANCE WITH TENSILE TESTS ON SITE

Performance and durability aspects have revealed the importance of concrete curing. The tensile strength is more sensitive to mistakes during curing as the compressive strength is.

In previous clauses the central part of tensile strength as concrete property has been discussed.

All these circumstances can leed to the conclusion that the quality control of s. c. structures should be performed with tension tests on the structure on site and not with compression tests on cubes or cylinders in the laboratory.

7. SOME COMMENTS ON THE INVITED LECTURES

7.1 Comments on the Test Setups

It is beyond any dispute that the uniaxial tension test is the most direct way to determine a strain–softening diagram. As it is difficult to carry out uniaxial tension tests on concrete under strain–controlled conditions, simpler test setups have been looked for and applied.

In order to achieve simply interpretable test results, test specimens with predetermined failure surfaces, e. g. notched beams in three point bending tests have been proposed as RILEM Recommandation [11]. It must be kept in mind that the predetermined failure surfaces do not yield that fractile value of G_F, which will govern the failure characteristics of a given

test specimen, as it will fail along its "weakest" surface, with the lowest G_F.

The specimen's form and the boundary conditions of that test, shich should yield more understanding about the fundamental properties of concrete need and must not be the simplest one, otherwise we shall have the same situation as with the compressive strength: we shall order and evaluate using an argument only for the reason that it is simple to be determined. It must be cleared up, which of the properties belong to the test setup, the specimen's behaviour and the material behaviour resp. as proposed in [13].

7.2 Comments on the Properties of the Fracture Energy

Fracture energy must be unique and independent of specimen type, size and shape. Size effect laws are felt to be created using the nominal stress

$$\sigma_N = P / (b \cdot d)$$

at evaluation of test results. These laws could be eliminated if the effective depth d_{ef} would be applied at evaluation of test results. The effective depth is that part of the specimen's depth, which is activated when the fictitious crack has first even came up to its maximum width (w_2). It is felt, that even the apparent dependence of the specific fracture energy with increasing ligament length could be eliminated using d_{ef}.

If it is true, that fracture energy is a material property, which has no direct connection with other material properties, such as the compressive strength [12], then we should look for more fundamental material properties, as after all, concrete is a quite simple composite, consisting of a porous matrix, aggregates and an interface between them. Nevertheless, as the influencing factors are the same as for the other mechanical properties [13], we will soon have a quite complete and coherent understanding for these properties and their relations.

REFERENCES

1. RÜSCH H., Die Ableitung der charakteristischen Werte der Betonzugfestigkeit. Beton 1955
2. CEB–FIP Model Code for concrete structures, 1978
3. Eurocode No. 2 Design of Concrete Structures. Final Draft 1989
4. WISCHERS G., LUSCHE M., Einfluß der inneren Spannungsverteilung auf das Tragverhalten von druckbeanspruchtem Normal– und Leichtbeton. Beton 1972
5. MODEER M., A Fracture Mechanics Approach to Failure of Concrete Material. Lund 1979
6. RÜSCH H., Physikalische Fragen der Betonprüfung. Zement–Kalk–Gips. 1959 Heft 1
7. WITTMANN F.H., ROELFSTRA P.E., KAMP C.L., Drying of Concrete – An Application of the 3L–Approach. Nuclear Engineering and Design. 1987
8. KUPFER H., Das Verhalten des Betons unter mehrachsiger Kurzzeitbelastung unter besonderer Berücksichtigung der zweiachsigen Beanspruchung. DAfStb. Heft 229, 1973
9. WALTHER R., Über die Berechnung der Schubtragfähigkeit...Beton– und Stahlb. 1962
10. MACGREGOR J.G., Dimensioning and Detailing. Invited Lecture Sub–theme 2.4
11. RILEM, Determination of the Fracture Energy of Mortar and Concrete by Means of Three–Point Bend Tests on Notched Beams. Materials and Structures 1985
12. HILLERBORG A., Reliance upon Concrete Tensile Strength. Invited Lecture 2.5
13. KÖNIG G., DUDA H., Basic Concept for Using Concrete Tensile Strength. Invited Lecture Sub–theme 2.5

Leere Seite
Blank page
Page vide

Design of Vertical Joints in Precast Reinforced Concrete Shear Walls

Dimensionnement de joints à cisaillement vertical dans le cas de parois préfabriquées en béton

Bemessung von Fugen zwischen vorgefertigten Wänden

Gheorghe CIUHANDU
Dr. Eng.
INCERC
Timisoara, Romania

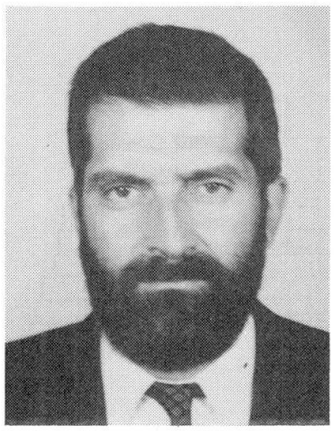

Gheorghe Ciuhandu, born 1947, received his civil engineering degree at the Polytechnical Institute of Timisoara, Romania, in 1970. For five years he worked in designing. From 1975, in Building Research Institute INCERC, Timisoara. He got his Ph. D. degree in 1986. Now as senior researcher at INCERC Timisoara, he is responsible for problems concerning structural concrete.

Valeriu STOIAN
Dr. Eng.
Polytechn. Inst.
Timisoara, Romania

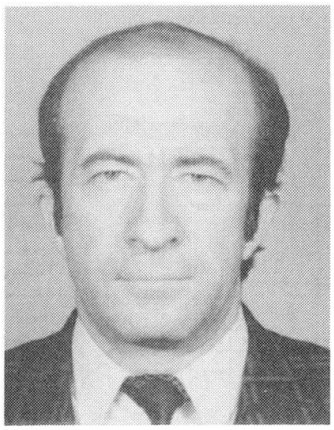

Valeriu Stoian, born 1949, received his civil engineering degrees at the Polytechnical of Timisoara, Romania, in 1972, and his Ph. D. degree in 1982. He is now professor of Civil Engineering at Building Construction Faculty, Polytechnical Institute of Timisoara, Romania.

SUMMARY

For vertical shear joints, new design formulae are presented in order to establish the most appropriate design requirements describing the real behaviour of these structural elements. The theoretical values evaluated using different formulae, are compared with the experimental shear forces. Numerical analyses were performed in order to complete the experimental tests and to offer adequate numerical procedures vs, simpler hand calculations for the shear force resistance of the vertical joints.

RÉSUMÉ

Pour ce type de joints, de nouvelles formules de dimensionnement sont présentées; les autres, déjà consacrées, sont rappelées en vue d'établir les meilleures recommendations possibles pour le projet de tels éléments de structure et d'en illustrer le comportement réel. Les valeurs théoriques calculées selon les différentes formules sont comparées avec des cisaillements expérimentaux. Des analyses numériques ont complété ces essais et permettent donc d'offrir les procédures numériques et manuelles les plus simples pour le calcul de la résistance au cisaillement des joints verticaux.

ZUSAMMENFASSUNG

Es werden Formeln für die Bemessung der auf Schub beanspruchten Vertikalfugen von Wandscheiben vorgestellt, die das reale Verhalten dieser Strukturelemente genauer veranschaulichen sollen. Die mit verschiedenen Formeln berechneten theoretischen Werte der Schubkräfte werden mit den Versuchsergebnissen verglichen. Diese Versuchsergebnisse wurden durch numerische Analysen ergänzt, um Berechnungsformeln für die auf Schub beanspruchten Vertikalfugen aufzustellen.

1. FORCE DISTRIBUTION IN VERTICAL SHEAR JOINTS

Known the shear force distribution in the vertical shear joints of the reinforced concrete shear walls assembled from large precast panels is a major task in the designing of these structural elements. In a shear wall or a floor assembled from large precast panels the joints are, in general, the weakest link within the system. Therefore an elastic material behaviour can be assumed for the panels, since cracks and shear deformations only appear in the joints.

In accordance with the above mentioned facts, in structural systems composed of rectangular subunits the panels can be discretized with rectangular elastic finite elements in the plane state of stress. The reinforcement can be introduced aproximately through modified modulus of elasticity for the concrete. As proposed in [1] the behaviour of the finite elements for the joints can be simulated by a pair of orthogonal springs at each end. Their characteristics diagram are coupled through an interaction diagram P_N-P_T as in fig.1. This characteristic and interaction diagram are based on a nonlinear incremental analysis or on results from suitable experiments. The latter procedure gives more realistic values, but is more expensive.

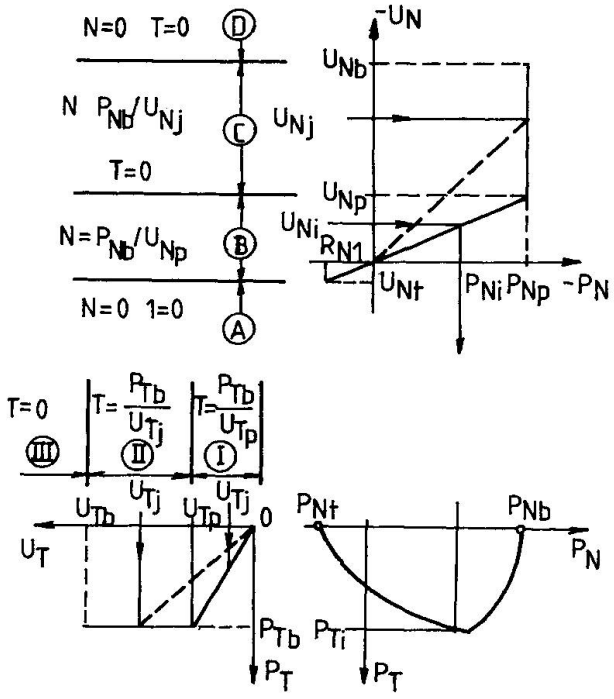

Fig.1 Interaction diagram P_N-P_T

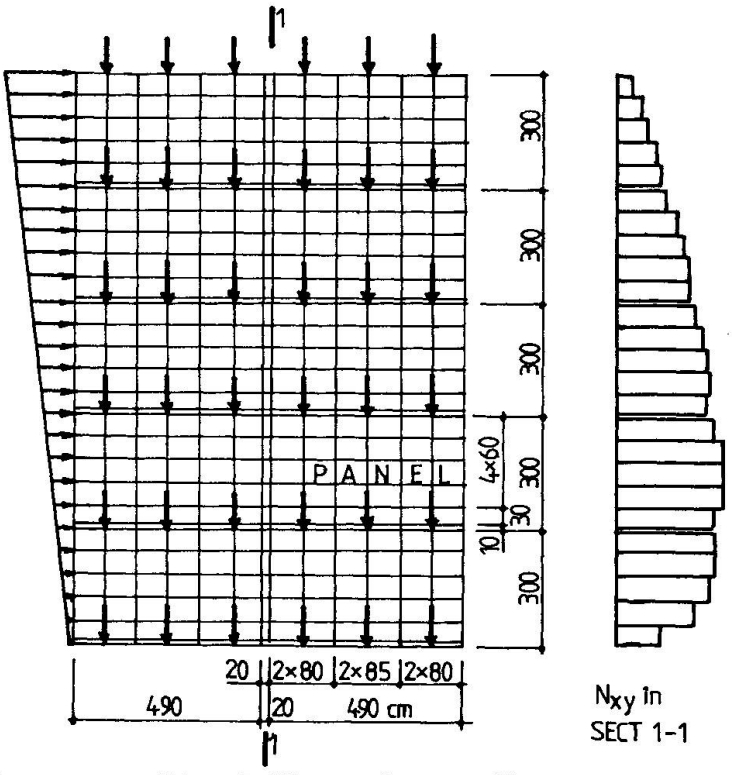

Fig. 2 Plane shear wall

The nonlinear analysis of the behaviour of the joints takes place iteratively, wereby within the succesive iteration steps, each step is calculated linearly-elastic. For the mean value of the normal and tangential displacements in a joint finite element, U_{Ni} and U_{Ti}, Fig.1 allows to obtain the updated rigidities N and T of the springs. It can be seen that the nonelastic behaviour is described by secant rigidities.

In order to establish the force distribution in the vertical shear joint, the plane shear wall in Fig.2, composed from ten large precast panels was analysed under given vertical and horizontal loads. It was found that all joints remain in the elastic range for a given combination of the horizontal and vertical forces which are applied on the shear wall in an structure analysis. For this reason the results for the vertical joint are comparable with results obtained with the approximative method for the analysis of shear walls with holes. Yet, the latter method cannot be applied for a nonlinear analysis of the

coupling beams in shear walls. These conclusions are the basis for the new design formulae of the vertical shear joints.

2. NUMERICAL ANALYSIS OF THE SHEAR FRACTURE PROCESS

Experimental and numerical analysis of the shear fracture shows important features about the contribution of the tensile strenght in this process. Therefore, the authors developed experimental and theoretical research programms aimed to establish the contribution of the tensile strenght to the total amount of the shear strenght in the shear structural elements.

The numerical analysis is performed with anisotropic reinforced concrete elements [3]. This modell was adopted because of his well known performancies in modelling plain and reinforced concrete.

The nonlinear process hich may be developed in the structure after reaching the elastic limit are: crack formation, crack closing, crack reopening, plasticity of uncracked or cracked concrete, crushing of the compressed concrete.

Element stiffness D_{RC} is formed for every physical state of the material by superposing concrete stiffness D_C and reinforcement stiffness D_R, taking into account the reinforcement ratio μ:

$$D_{RC} = D_C + \mu D_R \qquad (1)$$

Reinforcement is assumed to be uniformly distributed over the finite element, with perfect and continuously adherence to the concrete. Cracks are considered as smeared cracks. For the concrete a combined v.Mises-Navier behaviour criterion is considered, while for the reinforcement an elastic-plastic bilinear behaviour is assumed [2].

In [4] a set of 22 experimental models were analysed. The model is presented in Fig.3. An typical representation of the shear and tensile strenght in the critical section of the element is illustrated in fig.4.

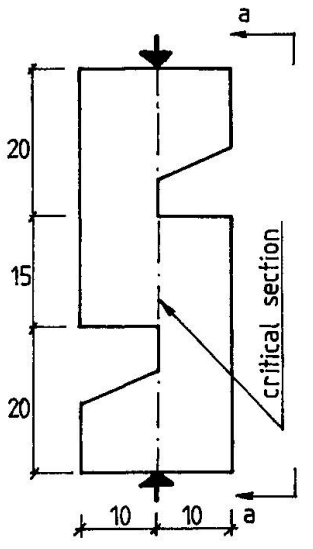

Fig.3 Shear modell

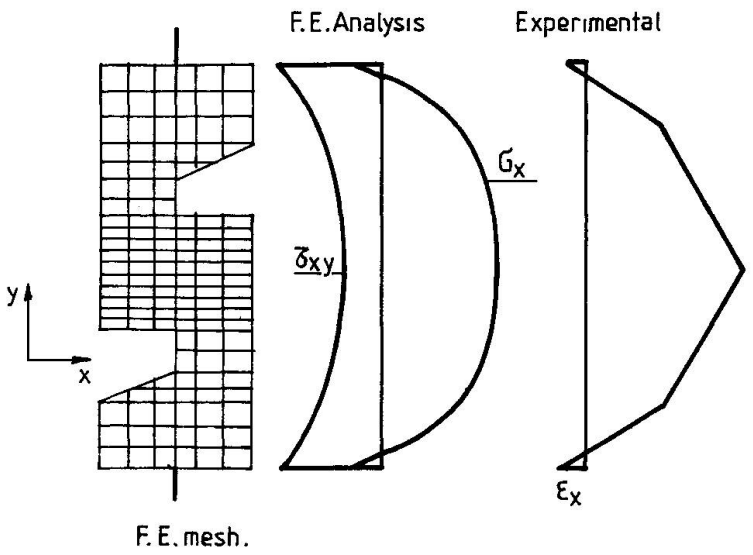

Fig.4 Strenght in the critical section

The main conclusion of these analyses taking into account also the experimental results is that between the shear strenght f_v and the tensile strenght of the concrete f_{ct} there is the following relation:

$$f_v = 1.5 f_{ct} \qquad (2)$$

The propoesed value $f_{ss} = 1.5f_{ct}$ can be adopted for the design of plain or reinforced concrete structural elements in shear.

3. EXPERIMENTAL PROGRAMME

The accomplished researches were meant to observe the hysteretic behaviour of vertical joints under cyclic - alternating loads, their capacity to absorb and dissipate energy, the cracking and collapse mechanism. The experimental shear forces were compared to theoretical values calculated with various formulae, including the relation proposed in the new version of the Romanian technical instructions concerning the design of building with large, precast panel structures [5].

Four models of the same vertical joint were tested. The geometrical scale used was that of 1:1 (M1-M4). The experimental model shaped of two panel parts and the one-storey high vertical joint is given in fig.5.

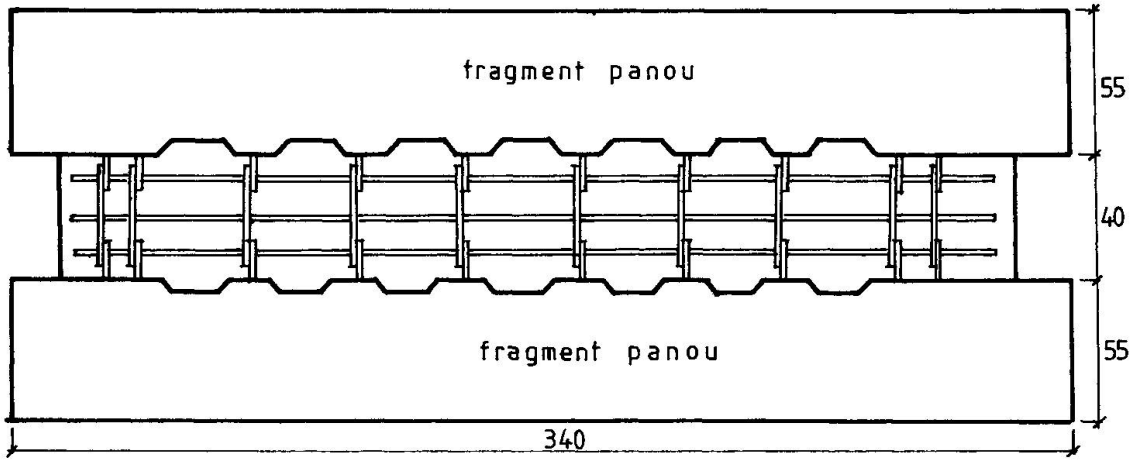

Fig. 5 Experimental model

The joint was tested in turned down position, on the narrow side, the model being inserted into the testing device schematically rendered in fig.6.

The testing methodology applied in the mentioned experiments was taken from the RILEM specifications concerning cyclic load testing. The monotonous M1 model testing served to establish the reference data required in the testing of the other three models under cyclic-alternating loads, according to the imposed deformation methodology [6].

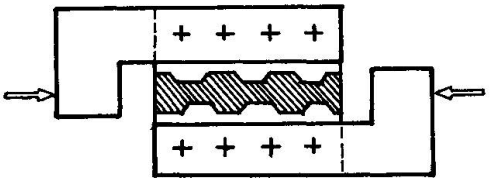

Fig. 6 Testing device

4. EXPERIMENTAL MODEL BEHAVIOUR

Generally, the behaviour of the experimental models points out cracks at the interfaces panels-joint, followed by the cracking of the joint in-situ concrete. The collapse results from shear failures of the keys in the joint. Consequently, the contribution of the in-situ concrete to the resistance of keyed joints is more dependent upon the resistance of cconcrete to tension than upon its resistance to compression.

At collapse, the cracking image typical for the tested models is that shown in fig.7.

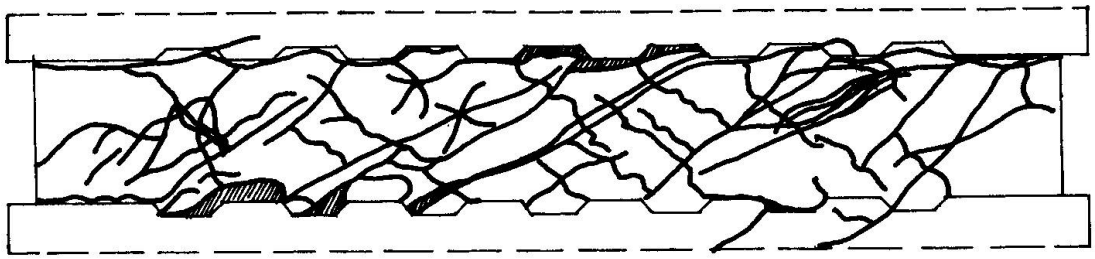

Fig.7 Cracking at collapse

The ultimate loads (capable shears) of the experimental vertical joints were calculated in view of comparing them to the experimental results.

Characteristics of the materials used (f_c, f_{ct}, f_y), the geometrical (Akey, A_{crush}) and reinforcement (A_s) features have been considered in this respect.

Four estimating relations were used:

- the relation proposed by CEB [7]

$$R_{jv} = \beta_1 A_{key} f_c + \beta_2 A_s f_y \tag{3}$$

- the relation proposed by P101-78 [5]

$$R_{jv} = A_{crush} f_c + 0.8 A_s f_y \tag{4}$$

- the relations proposed by Tassios and Tsoukantas [8],[9]:

$$R_{jv} = A_j \tau_u = A_j (0.15\lambda f_c + \mu\rho f_y + 1.8\rho f_{ct} f_y) \tag{5}$$

- the relation proposed in the new version of P101, as a result of the experimental behaviour of the joints in conjunction with relation (2):

$$R_{jv} = \min \left\{ \begin{matrix} 1.5 A_{key} f_{ct} \\ A_{crush} f_c \end{matrix} \right. + 0.8 A_s f_y \tag{6}$$

The estimated collapse force values compared to the experimental ones are given in Table 1:

Exp. mod.	f_c (MPa)	f_{ct} (MPa)	f_y (MPa)	A_{key} (cm^2)	A_{crush} (cm^2)	A_s (cm^2)	R_{jv} [kN] rel.(3)	calc.with rel.(4)	rel.(5)	rel.(6)	Exp.val. R_{jv} [kN]
M1	23.54	2.17	360	1904	336	11.3	680	1116.5	1168.7	946	1150
M2	21.27	2.04	360	1904	336	11.3	650	1000	1103.7	905	1070
M3	30.53	2.58	360	1904	336	11.3	773	1351	1368.2	1064	1170
M4	29.96	2.55	360	1904	336	11.3	765.5	1332	1352	1054	1110

Table 1 Experimental and theoretical results.

The notations of the material characteristics used in Table 1 are those from the CEB Draft Guide [7].

5. CONCLUSIONS

As far as the possible shears in the joint are concerned, relations (5) and (6) offer values closer to the experiment. It is obviously that the relation (6) gives values under the experimental ones.

The experimental behaviour of the models shows that the contribution of the in-situ concrete to the resistance of keyed joints is more dependent upon the strength of concrete to tension than upon its strength to compression.

The joint behaves well with cyclic-alternating loads, since the joint resists without cracking to larger shear effort values as compared to the maximum shears that might occur in the joint in case of an earthkuake.

The adequate joint behaviour to cyclic-alternating loads is confirmed by the curve position in fig.8 as well

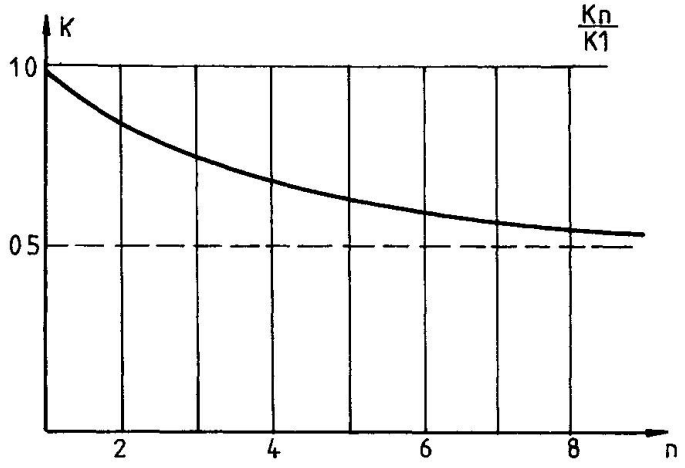

Fig.8 Stiffness decrease

REFERENCES

1. MEHLHORN G., SCHWING H., Tragverhalten von aus Fertigteilen zusammengesetzten Scheiben, DAS, H.288, W.Ernst u.Sohn, Berlin, 1977.
2. CERVENKA V., GERSTLE K.H., Inelastic Analysis of RC Panels Under In-Plane Loads, Inelasticity and Non-Linearity in Structural Concrete, University of Waterloo Press, 1972.
3. AVRAM C., BOB C., FRIEDRICH R., STOIAN V., Reinforced Concrete Structures. Finite Element Method. Theory of Equivaleces. (in Romanian), Editura Academiei, Bucuresti, 1984.
4. ABDUL R., Shear Strenght in Concrete Fracture (in romanian), Dissertation, Polytechnical Institute Timsoara, 1990.
5. "Technical Instructions for Designing Building of Large Panel Structures P101-78" (in Romanian), Bucharest, 1978
6. TSOUKANTAS S., MACCHI G., Proposals on Test-Prosedures under Cyclic-Loading, RILEM Committee 81-LCP, 1985
7. CEB, Draft Guide for the Design of Precast Wall Connections, Bulletin d'information, 169(1985)
8. TASSIOS T.P., TSOUKANTAS S.G., Serviceability and Ultimate Limit States of Large Panels Connections under Static and Dynamic Loading, Proceedings RILEM-CEB-CIB Symposium on Mechanical and Insulating Properties, Vol.1 Athens, 1978
9. TASSIOS T.P., TSOUKANTAS S.G., Reinforced Concrete Precast Panel Connections under Cyclic Actions. Proceedings of 7th European Conference on Earthkuake Engineering, Vol.5, Athens, 1982

Influence of Contact Surface Problems on Design Practice

Influence de problème des joints de contact sur le dimensionnement

Einfluss von Kontaktflächenproblemen auf die Bemessungspraxis

Jürgen RUTH
Civil Eng.
Univ. of Stuttgart
Stuttgart, Germany

Jürgen Ruth, born 1957, obtained his civil engineering degree in 1983 at the Technical University Darmstadt, Germany. For three years he worked with a consultant, where he was especially involved in the design of railroad bridges. Since 1987 he is a Research Assistant.

SUMMARY

Large buildings contain construction joints which may have a great influence on the loadbearing capacity of the structure. The design concepts of various standards for concrete structures will be presented and discussed briefly. Unfortunately, these design concepts treat the same problem in different ways. Based on a failure criteria of Mohr-Coulomb it will be shown how joints can be treated consistently in the design concept of strut-and-tie-models.

RÉSUMÉ

Les grands bâtiments comportent des joints qui influencent beaucoup la capacité portante de la structure; des concepts divers de dimensionnement sont brièvement présentés puis discutés. Le critère de rupture de Mohr-Coulomb constitue la base d'une démonstration décrivant comment les joints sont considérés dans le cadre d'un dimensionnement utilisant le modèle des bielles (analogie du treillis).

ZUSAMMENFASSUNG

Grössere Bauwerke beinhalten Fugen, die einen grossen Einfluss auf die Tragfähigkeit der Konstruktion ausüben können. Für Betonbauwerke werden Bemessungskonzepte verschiedener Normen vorgestellt und kurz diskutiert. Leider wird das gleiche Problem in diesen Bemessungskonzepten unterschiedlich behandelt. Auf der Grundlage eines Mohr'schen Versagenskriteriums wird aufgezeigt, wie Fugen in dem Bemessungskonzept der Stabwerkmodelle einheitlich behandelt werden.

1. DESCRIPTION OF THE PROBLEM

There are many structures where forces have to cross contact surfaces. In concrete structures this occurs for example at cracks or at construction joints between cast in situ or precast elements. The behaviour of the contact surfaces cannot solely be described by well-known material characteristics like the tensile and compressive strength, but also the surface condition (like smooth or rough) must be considered. Therefore an additional failure criterion for the contact surface must be defined.

In the following an attempt is made how the contact surface problems in connection with construction joints are treated in the consistent and translucent dimensioning concept of strut-and-tie-models according to Breen /B2/ and Schlaich /S1,S2/. This is desirable because contact surface problems may have an important effect on the structural behaviour. Up to now they are dealt with not systematically and partly unsufficiantly in the design practice.

2. PRESENT DESIGN PRACTICE AND EXISTING CODES FOR CONCRETE STRUCTURES

In codes for concrete structures these problems are so far treated either as dimensioning problems for shear and normal stress in the contact surface or/and in terms of construction requirements.

2.1 German Standards

The German Standards /D2/ require a sufficient roughness for longitudinal joints between prefabricated parts and concrete cast in situ. The description of the appropriate surface condition is only given in a comment upon the Standards /E1/. An increased transverse reinforcement is needed, apart from a few exceptions, and the permissible shear stress is limited to 60 % of the regular value. The specialities of construction joints transverse to the loadbearing direction are specified only for prestressed structural members. Thereby a rough (or keyed) surface is a precondition, too. Additionally a value for the compression strength for the joint section is given.

2.2 ACI Standard 318-77

In the ACI Standard 318-77, section 11.7 /A1/ the dimensioning of construction joints is described on the basis of the shear-friction-theory which was originally developed by Birkeland /B2/ and Mast /M1/. An ultimate shear force V_u is defined for rough surfaces.

$V_u = 1.0\, A_s\, f_y <$ $0.2 f'_c A_c$ [N] or $5.5\, A_c$ [N]

A_s : total crossectional area of reinforcement across interface
f_y : yield strength of reinforcement < 420 N/mm^2

Thereby rough means a clean interface which is free of laitance and roughened to a full amplitude of approximately 5 mm.

2.3 SIA-Standard 162

The SIA-Standard 162 /S3/ section 4 45 limits the concrete strength and steel strength of the prefabricated and connected parts.

Concrete: $f_{c,red} = 0.35\, f_{cw,min}$ Steel: $f_{y,red} = 0.80\, f_y$

According to section 6 06 2 only rough or keyed joints are permissible preferably perpendicular to the direction of the compression field. The rough joint should be realized by removing the cement-sand grout from the concrete surface.

3. A CONSISTENT DIMENSIONING-CONCEPT USING STRUT-AND-TIE-MODELS

3.1 Mathematical Description of the Loadbearing Capacity of Joints

The mathematical description of the loadbearing capacity of joints is based on the extended shear-friction-theory of Mattock /M1,M2/. It is drawn from a proposal by a FIP-Commission /F1/ supplemented by Walraven /W1/. The results are shown graphically in fig. 1.

$\tau_u = K1\,(f_y + \sigma_N) + K2\, f_{ctk} \leq 0.25\, f_{ck}$

μ : A_s/A_c
f_y : yield strength of reinforcement <400 N/mm^2
σ_N : normal stress
f_{ctk} = $0.25\,\sqrt{f_{ck}}$

surf.cond.	K1	K2
very smooth	0.6	0.1
smooth	0.6	0.2
rough	0.9	0.4

Table I

The coefficient K1 is equivalent to a frictional coefficient and the term K2 f_{ctk} corresponds to the so-called cohesion, which here is proportional to the tensile strength of the concrete. Both coefficients depend on exactly described surface conditions which are subdivided in three categories (Tab. I). By comparison with an extensive series of experiments carried out by Daschner /D1/ Walraven found out that the concept is on the safe side, if the steel strength is limited to $f_y < 400$ N/mm^2. For comparison, the parabolic description of the joint behaviour according to Tassios /T1/ is shown in fig. 2.

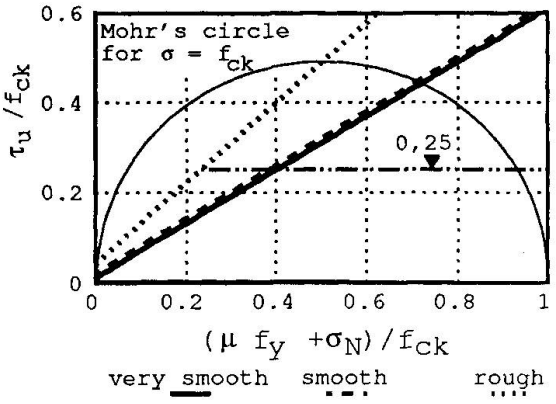

Fig. 1: acc. to FIP

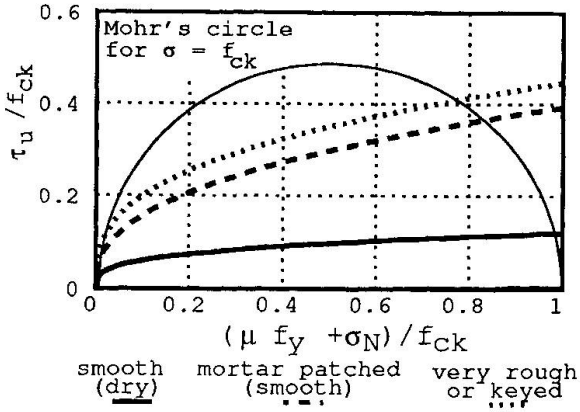

Fig. 2: acc. to Tassios

3.2 The Influence of a Joint on the effective Strength of a Prism

With the above given proposals the loadbearing capacity of a prism with a joint (fig. 3) is given according to Zelger and Rüsch /Z1/ and can be seen in fig. 4 and fig. 5. The diagrams clearly show that the capacity of the prism is only reduced by the joint, if the inclination of the joint exceeds a critical angle α_{crit}. If the inclination is smaller than α_{crit} the prism fails in concrete-compression. These dependencies can also be shown in a different way using Mohr's circle (see: Guckenberger /G1/ and Basler /B1/).

according to FIP /F1/:

$$\frac{\sigma_u}{f_c} = \frac{K2\ f_{ctk}}{f_c} \cdot \frac{1 + \tan^2 \alpha}{\tan \alpha - K1} \leq 1$$

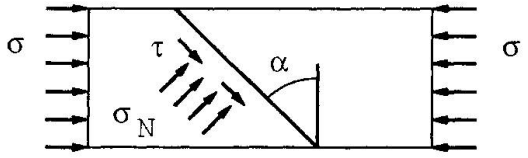

Fig. 3: prism with a joint

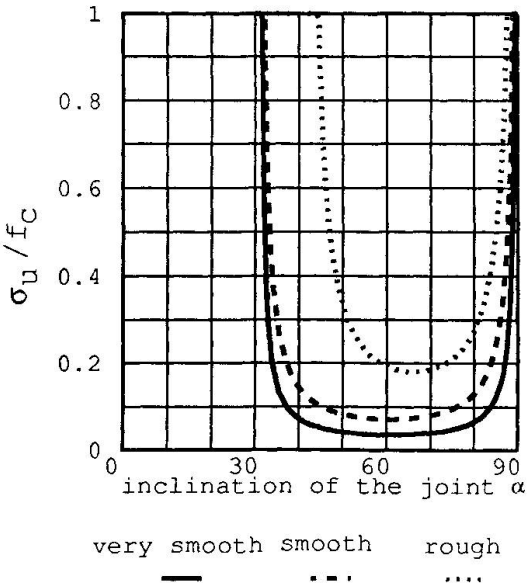

Fig. 4: acc, to FIP

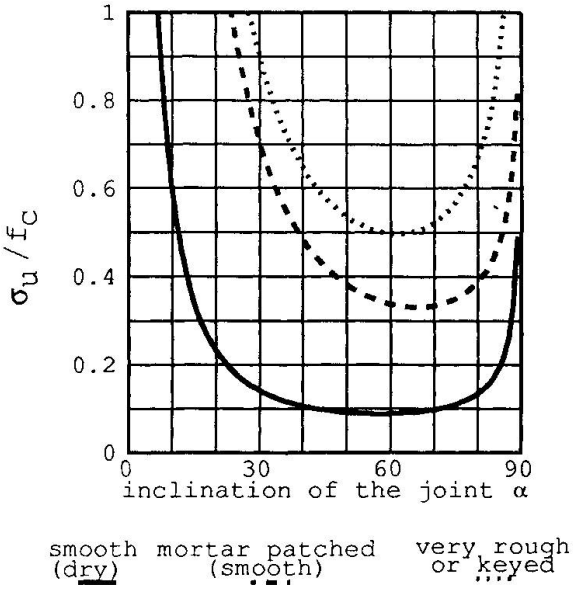

Fig. 5: acc. to Tassios

The following diagrams show in a different way some characteristics of the loadbearing behaviour of the prism. They are based on the FIP proposal, because it satisfies the demands of the structural engineer better than other proposals. Fig. 6 shows the dependence of the critical inclination on K1 and K2 f_{ckt}. It is remarkable that the critical inclination of the joint is almost totaly independent of the term K2 f_{ckt} (cohesion). Fig. 7 shows the dependence of the minimal effective strength on K1 and K2 f_{ckt}.

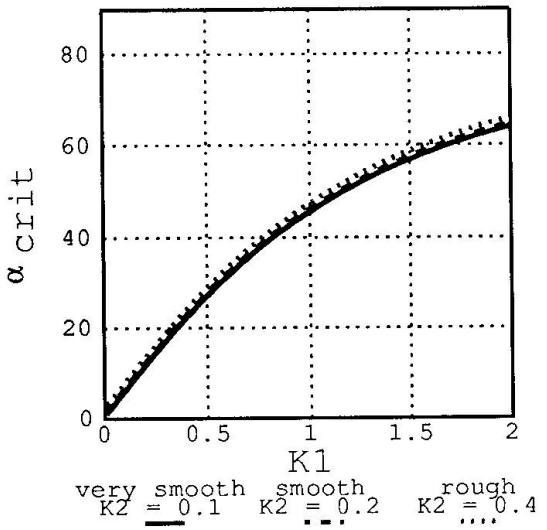

Fig. 6: crit. inclination

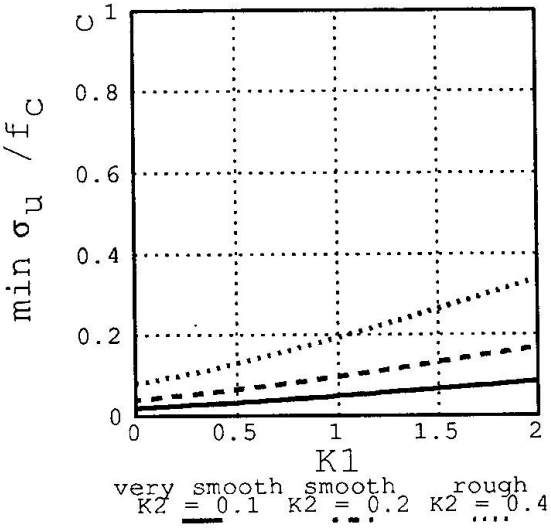

Fig. 7: minimal effective prism strength

With the above diagrams some problems of dimensioning structural members with joints can be solved directly, as e.g. for a joint in an arch bridge between the bottom edge of a column and the supporting arch.

3.3 Joints in the web of a Beam

In the following the influence of the joint on the ultimate shear force of a beam is explained. Two cases are considered either a longitudinal joint between a precast part and a layer of cast in situ concrete or a transverse construction joints between two stages of construction or precast elements (fig. 8). The loadbearing behaviour of the beam is described with a strut-and-tie-model. Thereby the joint influences essentially the effective strength of the compression strut. It is assumed that the effective strengths of the chords are not reduced. This leads to the conclusion that the reduction of the ultimate shear force depends mainly on the inclination of the strut - and accordingly on the transverse reinforcement - and the roughness of the joint.

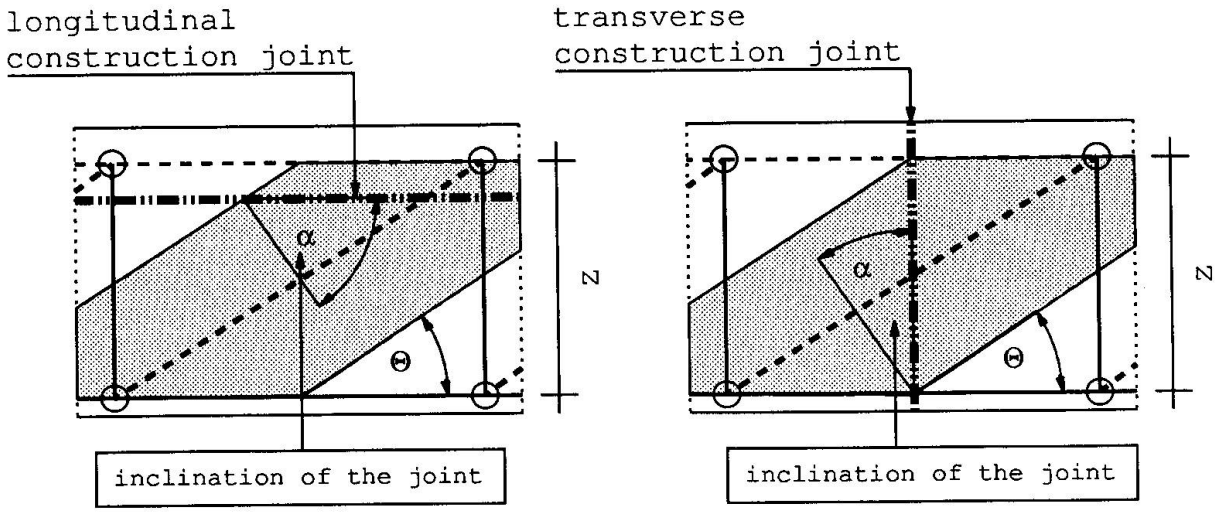

Fig. 8: strut-and-tie-model of a beam

The reduced ultimate shear force due to joint failure can be calculated as follows:

$$\frac{V_u}{b\,z\,\sigma_{cw,u}} = \frac{K2\,\sin\Theta\,\cos\Theta(1+\tan^2\alpha)}{\tan\alpha - K1}\,\frac{f_{ctk}}{\sigma_{cw,u}} \le 1 \qquad \text{for } \alpha > \alpha_{crit}$$

Considering $\alpha = 90° - \Theta$ in case of a longitudinal joint and $\alpha = \Theta$ in case of a transverse joint yields the curves shown in fig. 9 and fig. 10. In both cases the ultimate shear force of a beam without joints can be reached nearly if the surface is rough. However for a longitudinal joint an inclination 45° for the compression field and an accordingly increased tie reinforcement is required. For a transverse joint the inclination of the compression field varies between 30° and 45° as usually.

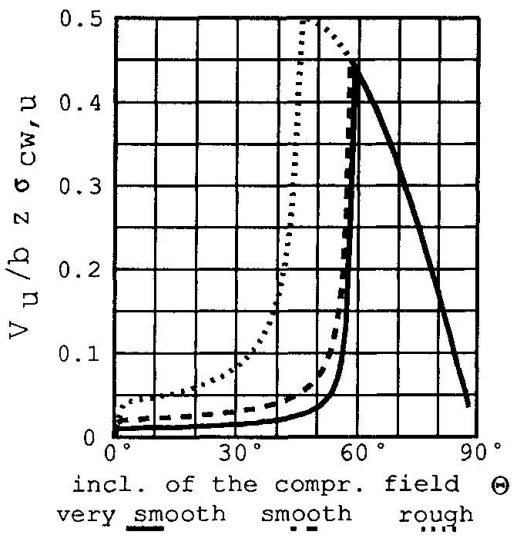

Fig. 9: Longitudinal joint

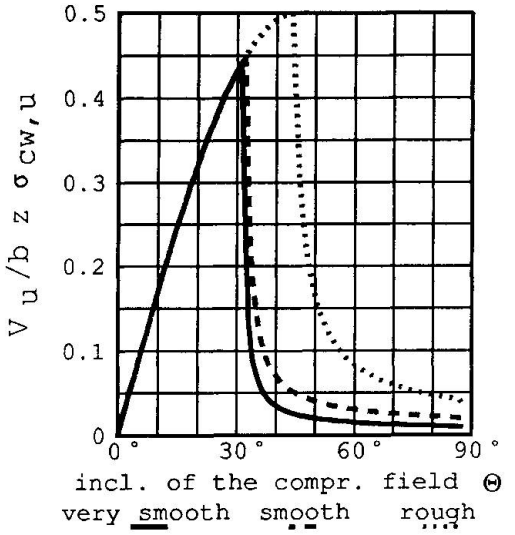

Fig. 10: Transverse joint

Fig. 12 and fig. 13 show diagrams for the necessary vertical shear reinforcement. For longitudinal joints highly increased reinforcement is required even if the joint is rough. For rough transverse joints only the maximum value for the ultimate shear force is reduced by the joint.

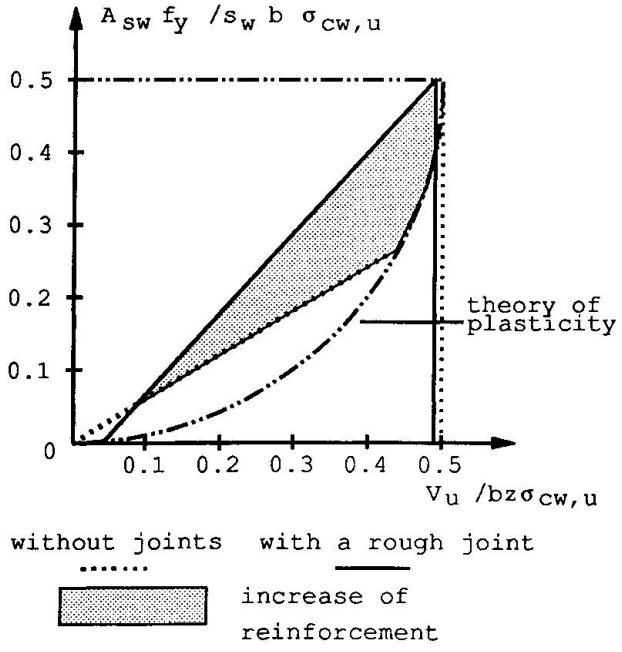

Fig. 11: Longitudinal joint

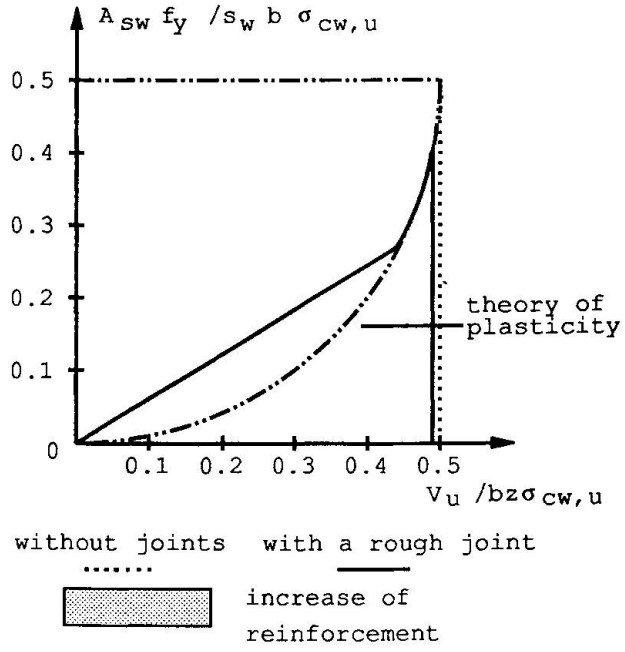

Fig. 12: Transverse joint

4. SUMMARY AND PROSPECTS

It was shown that the influence of a joint on a structural concrete member can be expressed by an reduced effective strength of the struts in a strut-and-tie-model. Therefore the normally given relation between the normal stress and the ultimate shear stress of a joint must be transformed into a relation between the inclination of the joint in a strut and of its effective compressive strength. This relation depends on the roughness of the contact surface, which has to be described exactly. Reineck shows a similar approach in /R1/ concerning the influence of friction mechanisms in cracks on the ultimate strength of the web compression field. The advantage of these methods is that it becomes more obvious how a structural member with a joint or cracks works and which element will fail under ultimate load.

Prospective efforts should aim in the direction of integrating composite structures with contact surface problems between their different materials in a consistent dimensioning concept. At the moment this is unfortunately complicated by the splitting of codes according to materials which leads to different approaches for the same problem. Further types of contact surface problems will arise in future, when the advantages of combining new or unusual materials will be used to realize new kinds of structures with different and novel qualities.

REFERENCES:

/A1/ ACI Standard 318-77: Building Code Requirements for Reinforced Concrete.

/B1/ Basler, E., Witta, E.: Grundlagen für kraftschlüssige Verbindungen in der Vorfabrikation. Beton-Verlag GmbH, 2. Auflage, Düsseldorf 1967

/B2/ Birkeland, P.W., Birkeland, H.W.: Connections in precast concrete constructions. ACI-Journal V.63, March 1966, pp.345-368

/B3/ Breen, J.E.: Why Structural Concrete. Introductory Report, IABSE Colloquium "Structural Concrete", Stuttgart, April 1991

/D1/ Daschner, F.,: Versuche zur notwendigen Schubbewehrung zwischen Betonfertigteilen und Ortbeton. DafStb Heft 372, Berlin 1986

/D2/ DIN-Normen 1045 und 4227 Teil1 und Teil3

/E1/ Erläuterungen zu DIN 1045 Beton- und Stahlbeton Ausgabe Juli 1988, DafStb, Heft 400, Berlin 1989

/F1/ FIP-Commission on Prefabrication: Shear at the interface of precast and in situ concrete. FIP-Report, Jan. 1982

/G1/ Guckenberger, K., Daschner, F., Kupfer, H.: Segmentäre Spannbetonträger im Brückenbau. DAfStb, Heft 311, Berlin 1980

/M1/ Mast,R.F.: Auxiliary reinforcement in concrete connections. Journal of the Structural Division, ASCE, V. 94, ST6, June 1968, p. 55-75

/M2/ Mattock, A.H., Hawkins, N.M.: Research on shear transfer in reinforced concrete. PCI-Journal, V. 17,No.2, March-April 1972, pp. 55-75

/M3/ Mattock, A.H.: Shear transfer in concrete having reinforcement at an angle to the shear plane. ACI-Special Publication 42, Detroit, Michigan, 1974, pp. 17-42

/R1/ Reineck, K.H.: Consistent Modelling of Structural Concrete Members with Transverse Reinforcement Considering Strains and Cracks. IABSE Colloquium "Structural Concrete", Stuttgart, April 1991

/S1/ Schlaich, J.: The need of consistent and translucent models. Introductory Report, IABSE Colloquium "Structural Concrete", Stuttgart, April 1991

/S2/ Schlaich, J., Schäfer, K., Jennewein, M.: Toward a Consistent Design of Structural Concrete. PCI-Journal Vol.32, No.3, May/June 1987

/S3/ SIA-Norm 162: Betonbauten. Ausgabe 1989

/T1/ Tassios, T.P.: Physical and mathematical Models for RE-Design of repaired Structures

/W1/ Walraven, J.,: Über den kraftschlüssigen Verbund von Betonen unterschiedlichen Alters und unterschiedlicher Oberflächenbeschaffenheit der Verbundfuge. VDI Berichte Nr. 840, Oktober 1990

/Z1/ Zelger, C.,Rüsch, H.: Der Einfluß von Fugen auf die Festigkeit von Fertigteilschalen. Beton- und Stahlbetonbau (1961), Heft 10, S.234-237

Reliance on Tensile Strength for Cast-in-Situ Wall-to-Wall Joints

Résistance à la traction des joints clavés de parois coulées sur place

Tragfähigkeit von Fugen in Ortbetonwänden

Antanas KUDZYS
Prof. Dr.
Lithuanian Academy
Vilnius, USSR

Antanas Kudzys, Prof. Dr. Sc. Member of Lithuanian Academy, Head of Reinforced Concrete Department Vilnius Technical University. He is noted for his design projects and researches in the fields of reinforced concrete and reliability theories.

Vytautas PAPINIGIS
Assoc. Prof.
Vilnius Techn. Univ.
Vilnius, USSR

Vytautas Papinigis, Associate Professor at Vilnius Technical University. He is involved in research problems of concrete strength under short-term and long-term tension. Probationer of Hannover Technical University.

Vladimir POPOV
Assist. Prof.
Vilnius Techn. Univ.
Vilnius, USSR

Vladimir Popov, Assistant Professor at Vilnius Technical University. His research field belongs to problems of concrete and reinforced concrete joints and modelling in structural mechanics.

SUMMARY
The paper considers theoretical and practical problems concerning an estimation of the complete concrete tensile deformation diagram in the analysis of the load bearing capacity of keyed joints of cast-in-situ exterior and interior walls.

RÉSUMÉ
Cet article prend en considération les problèmes théoriques et pratiques d'une appréciation concernant le diagramme complet traction-déformation du béton, et ceci, dans le contexte de l'analyse de la capacité portante de joints clavés, appartenant à des parois intérieures et extérieures coulées sur place.

ZUSAMMENFASSUNG
Im Aufsatz wird das theoretische und praktische Problem der Bewertung des vollständigen Dehnungsdiagramms des Betons in der Tragfähigkeitsberechnung der Monolithverzahnung der Aussen- und Innenwände besprochen.

The connections of intersection walls constructed both of cast-in-situ concrete of different nature and class (Fig. 1) and of precast concrete members can be provided by using keyed joints. The cross-shaped and wavy dividing closures of asbestos cement sheets provided a rational solution ensuring technologically simple connections between walls of buildings and constructions. A remarkable cohesion of these sheets with concrete is characteristic. Therefore it is expedient to use new types of joints for connections of cast-in-situ exterior lightweigt and interior heavy concrete walls of buildings.

The experimental laboratory and site data indicate the necessity of new types joints with the division closures. The keyed joints of concrete walls lead to the economy and increase in both tolerable rigidity of the connections and stiffness of multi-storey buildings subjected to shear forces. Such forces are generated by horizontal wind or seismic actions, non-symmetrical vertical loading, shrinkage deformations, temperature gradient etc.

Shear carrying capacity of keyed joints depends on mechanical properties of wall concrete in tension. The shear strength of a key system belonging to one of wall connection members is closely related to the possibility of a redistribution of shear stresses both in a single key and among the connection keys.

Twenty four full-scale specimens of exterior and interior wall connections were tested to investigate the behavior of concrete keys and to establish a cracking resistance (a load rating) and a failure strength of keyed joints.

The shear capacity of keyed wall-to-wall joints can be determined by the following equation derived from a test analysis and modelling data

$$R = nR_1 (1 - tg\alpha / tg\beta) + A_s f_y tg\alpha . \qquad (1)$$

Here n - the number of keys in weaker wall member; R_1 - shear strength of a single key; $tg\alpha$ - coefficient taking into account the shape of a crack surface and the position of a crack direction angle; $tg\beta$ - coefficient characterizing the key slope angle and the contract surface between asbestos cement sheet and concrete; A_s - cross-sectional area of horizontal reinforcing bars; f_y - steel yield strength.

The shear strength of a concrete key

$$R_1 = \varkappa A_c f_v , \qquad (2)$$

where $\varkappa$ - coefficient which helps to evaluate the influence of crack location on the cross-sectional area A_c of shear key; f_v - concrete shear strength.

The value of the strength f_v can be calculated on the basis of the empirical equation

$$f_v = \xi_v \sqrt{f_c f_{ct}} , \qquad (3)$$

where ξ_v = 0,7 for heavy and ξ_v = 0,5 for lightweight concrete;

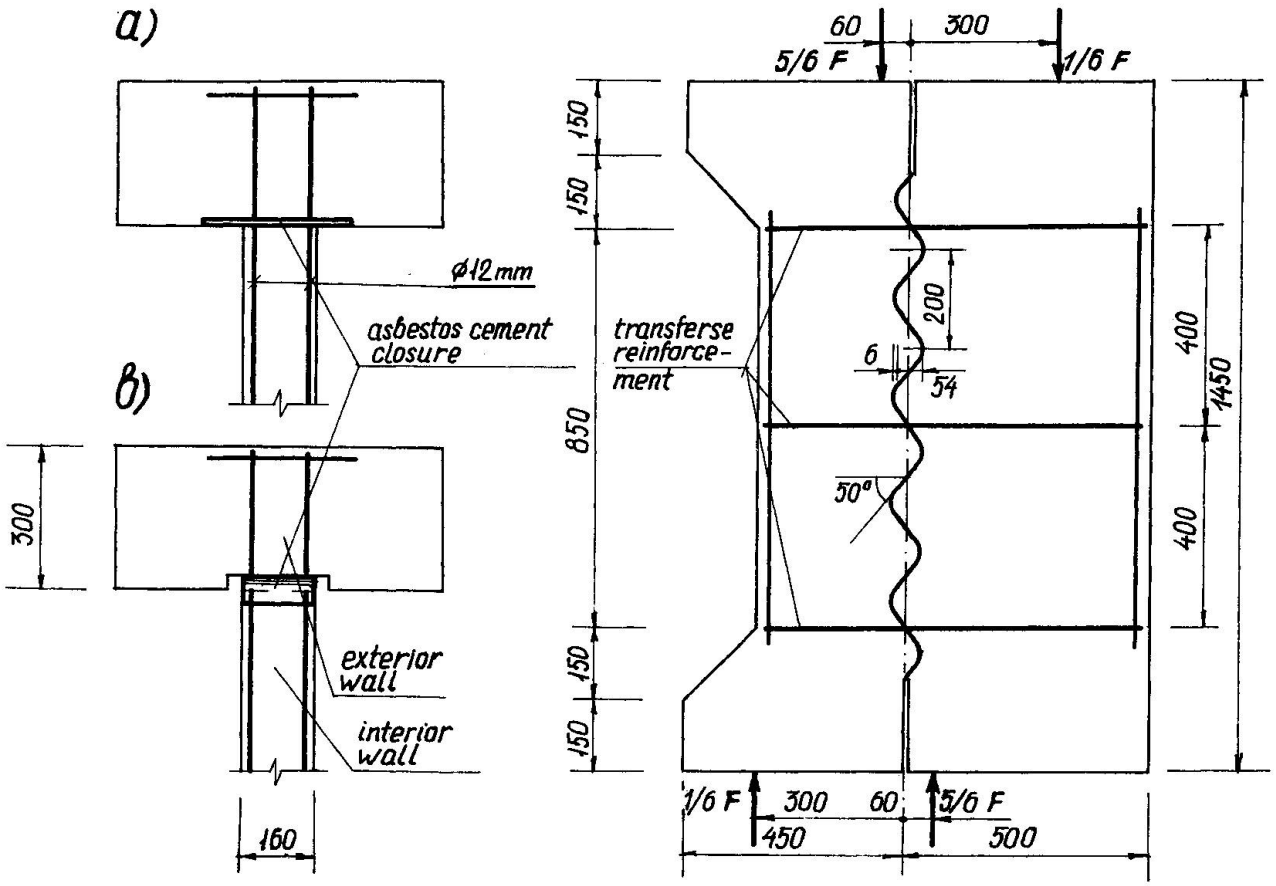

Fig. 1. Test specimens and test loading diagram of plain (a) and keyed (b) joints (dimensions in mm)

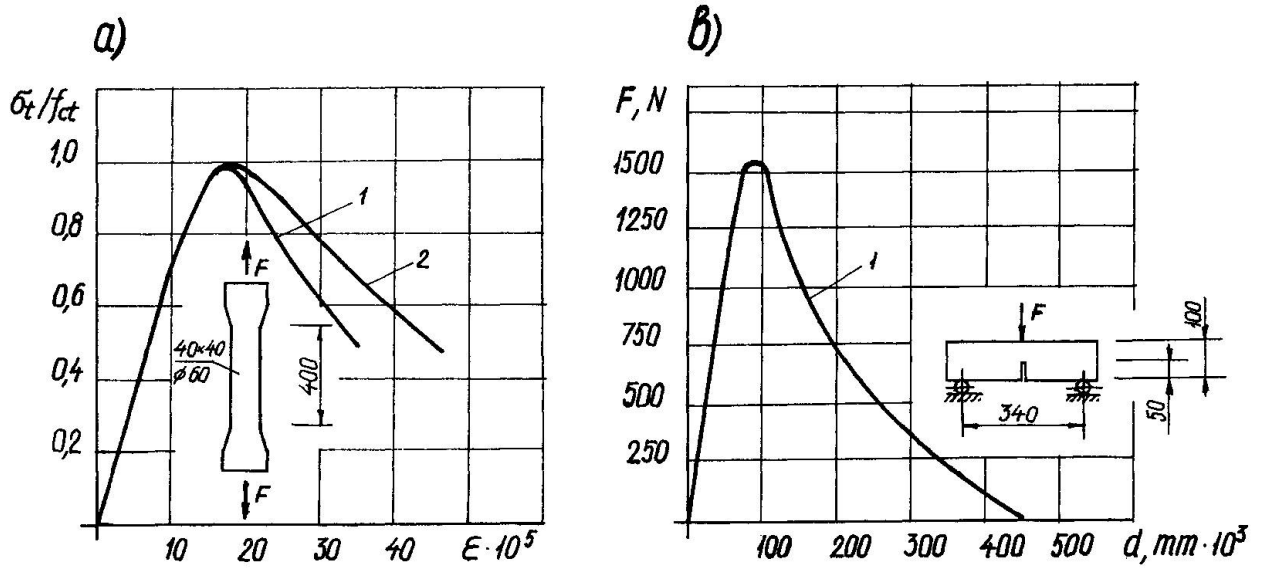

Fig. 2. A tensile (a) and a stable bending (b) tests of concrete (1) and reinforced concrete (2) specimens

f_c and f_{ct} - concrete compressive and tensile strength, respectively.

According to the theory of plasticity [1] the shear strength of concrete can be assumed as

$$f_v = \sqrt{\frac{\nu_{ct}}{\nu_c} f_c f_{ct} \left(\nu_c - 4 \frac{\nu_{ct}}{\nu_c} \frac{f_{ct}}{f_c}\right)} \quad , \tag{4}$$

where ν_{ct} and ν_c - are the so called effectiveness factors for concrete in tension and compression, respectively.

The values of factors ν_{ct} and ν_c can be obtained by using the stress-deformation curves not only with ascending but also with descending branches, i.e. with the help of intensity of released energy of tensile concrete in fracture G_1 .

A non-linearity of the post-peak curve contributes substantially to the toughness and ductility of tensile concrete. An investigation of fracture mechanism of tensile concrete gives a possibility to understand the behavior of keyed joints in shear. Moreover, it helps to conceive the indispensable conditions leading to instantaneous cracking and collapsing of the keyed joints.

A tensile stress concentration in concrete due to internal cracking is noticed. If concrete is a sufficiently tough material the stress concentration does not lead to a sudden brittle failure of a single key and to a decrease of carrying capacity of wall-to-wall joints. It may be explained by the fact that the toughness property helps to absorb the released energy of cracking concrete. Owing to it a distribution of load effects occurs in the key system.

Twenty test sets were used to investigate the main mechanical and energetical properties of tensile loaded concrete C15...C20. Both notched and un-notched tensile and bending specimens were tested to study the tension behavior of concrete (Fig. 2).

According to the recommendation [2] the failure mechanism of tensile concrete may be described by two parameters (Table 1). The critical coefficient of stress intensity

$$k_1 = \sqrt{\pi \ell} \, f(\zeta) \quad , \tag{5}$$

where $f(\zeta)$ - function, characterizing a specimen configuration and loading technique.

The intensity of released energy may be evaluated by the equation

$$G_1 = k_1^2 / E_c \quad , \tag{6}$$

where k_1 - coefficient by (5); E_c - modulus of elasticity of concrete. The intensity G_1 by (6) allows to calculate the values of factors ν_{ct} , ν_c and concrete shear strength f_v by (4) more accurately.

Table 1

Parameters of fracture criterion of concrete in tension

Loading technique	Loading diagram	k_1, $MN/m^{3/2}$	G_1, N/m
Centric tension	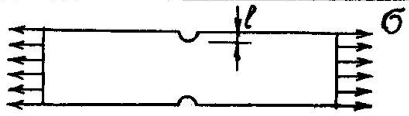	1,02	52
Centric tension	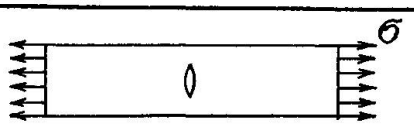	1,19	62,8
Three point bending	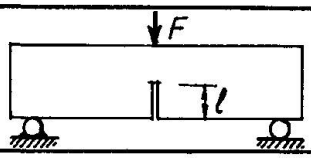	1,08	51,6

REFERENCES

1. Nielsen M.P. Limit Analysis and Concrete Plasticity. Prentice-Hall, Inc., Englewood Cliffs. New Jersey, 07632. 1982. 420 pp.

2. Siratory M., Miosy T., Macusita Ch., Vytchislitelnaia technika razrushenia. Moskva. Mir. 1986. 336 pp.

Leere Seite
Blank page
Page vide